Gene expression in trabecular meshwork and cornea: Control mechanisms and microarray studies

DISSERTATION ZUR ERLANGUNG DES DOKTORGRADES DER NATURWISSENSCHAFTEN (DR. RER. NAT.) DER NATURWISSENSCHAFTLICHEN FAKULTÄT III – BIOLOGIE UND VORKLINISCHE MEDIZIN – DER UNIVERSITÄT REGENSBURG

vorgelegt von

Annika Irene Pienimäki-Römer, geb. Pienimäki

aus Hanko, Finnland

im Jahr 2010

Das Promotionsgesuch wurde eingereicht am: 15.04.2010

Die Arbeit wurde angeleitet von: Prof. Dr. med. Ernst R. Tamm

Abbreviations

aa	amino acid(s)
abs.	absolute
ad	fill up to
AH	aqueous humour
AP	activator protein
as	antisense
ASD	anterior segment dysgenesis
ATP	adenosine triphosphate
BM	basement membrane
BMP	bone morphogenetic protein
bp	base pair(s)
BSA	bovine serum albumin
C_T	cycle threshold
CB	ciliary body
cDNA	complementary DNA
Ci	Curie
CM	ciliary muscle
CNS	central nervous system
CP	choroid plexus
Cre	Cre recombinase
CSF	cerebrospinal fluid
CTM	corneoscleral meshwork
d	days
Δ	Delta
DAPI	4'-6-diamidine-2-phenyl indole
DCRi	intronic distal control region
Dkk2	dickkopf homolog 2
DMEM	Dulbecco´s Modified Eagle Medium
DMSO	dimethyl sulfoxide
DNA	deoxyribonucleic acid
dNTP	deoxyribonucleotide triphosphate
ds	double-stranded
E-box	enhancer box
ECM	extracellular matrix
E. coli	*Escherichia coli*

EDTA	ethylene diamine tetraacetic acid
eGFP	enhanced green fluorescent protein
Egr2	early growth response 2
EGTA	ethylene glycol tetraacetic acid
ER	endoplasmic reticulum
ESC	embryonic stem cell
EtBr	ethidium bromide
FCS	fetal calf serum
FGF	fibroblast growth factor
FOX	forkhead box
Fst	follistatin
fw	forward
g	relative centrifugal force
GC	glucocorticoid
Gjb2	gap junction membrane channel protein beta 2
GRE	glucocorticoid response element
H	region of Homology
HEK	human embryonic kidney
HTM-N	immortalized human trabecular meshwork cell line
IF	intermediate filament
IGF	insulin-like growth factor
Igfbp6	insulin-like growth factor binding protein 6
IOP	intraocular pressure
IPTG	isopropyl-ß-D-thiogalactopyranoside
IRES	internal ribosomal entry site
JCT	juxtacanalicular tissue
JNK	c-Jun N-terminal kinase
kb	kilobase(s)
Krt14	keratin complex 1, acidic, gene 14
KSPG	keratan sulphate proteoglycan
Lama3	laminin, alpha 3
Lamb3	laminin, beta 3
LB	lysogeny broth
LPR6	LDL-receptor related protein 6
MAPK	mitogen-activated protein kinase
MCS	multiple cloning site
miRNA	microRNA
MITF	micropthalmia-associated transcription factor

MM	master mix
Mmp13	matrix metallopeptidase 13
MPI	Max Planck Institute
MW	molecular weight
MYOC/*myoc*	human/mouse myocilin gene
nc	non-coding
NC	neural crest
Neo	neomycin resistance gene
NF-κB	nuclear factor κ light-chain enhancer of activated B cells
NLS	nuclear localization signal
NTC	no template control
OAG	open-angle glaucoma
Oca2	oculocutaneous albinism II
ON	optic nerve
O/N	over night
ONH	optic nerve head
ORF	open reading frame
P	postnatal day
p313+67	human myocilin basal promoter
PACG	primary acute closed angle glaucoma
PAX6	paired box 6
PBS	phosphate buffered saline
PCG	primary congenital glaucoma
PCR	polymerase chain reaction
PFA	paraformaldehyde
PGD2	prostaglandin D2
PGH2	prostaglandin H2
PITX	paired-like homeodomain transcription factor
PNK	polynucleotide kinase
POAG	primary open-angle glaucoma
POM	periocular mesenchyme
Ptgds	prostaglandin D2 synthase
PVP	polyvinylpyrrolidon
PVZ	periventricular zone
RA	retinoic acid
RAR	retinoic acid receptor
RARE	retinoic acid response element
rev.	reverse

RLU	relative light unit
RNA	ribonucleic acid
rpm	rounds per minute
RT	room temperature/reverse transcriptase
SC	Schlemm´s canal
± SD	standard deviation
SDS	sodium dodecyl sulphate
Sg	SYBR-Green I
SgMM	SYBR-Green I master mix
α-SMA	α-smooth muscle actin
ss	single-stranded
SS	scleral spur
SSC	saline-sodium citrate
SV40	simian virus 40
SVZ	subventricular zone
TAE	Tris-acetate-EDTA
TBE	Tris-borate-EDTA
TG	transgenic
TGF	transforming growth factor
TIGR	trabecular meshwork induced glucocorticoid response
TIMP	tissue inhibitor of matrix metalloproteinase
TK	thymidine kinase
TM	trabecular meshwork
Trpm1	transient receptor potential cation channel, subfamily M, member 1
U	unit(s)
USF	upstream stimulatory factor
UTM	uveal meshwork
UTR	untranslated region
vol.	volume(s)
WT	wild-type
w/v	weight per volume
X-gal	5-bromo-4-chloro-3-indolyl-β-D-galactopyranoside

1. Introduction

1.1. Anatomy and function of the human eye

Normal vision is pivotal in the full perception of the surroundings and indispensable in the practical every day life. The anterior eye, together with the retina, a part of the brain, enables us to experience the life as a visual scene. The incoming light is correctly focused by the transparent cornea and the lens onto the retina that by means of photoreceptor cells convert the perceived light into nerve signals that are transmitted through the optic nerve (ON) to the brain (Fig. 1.1).

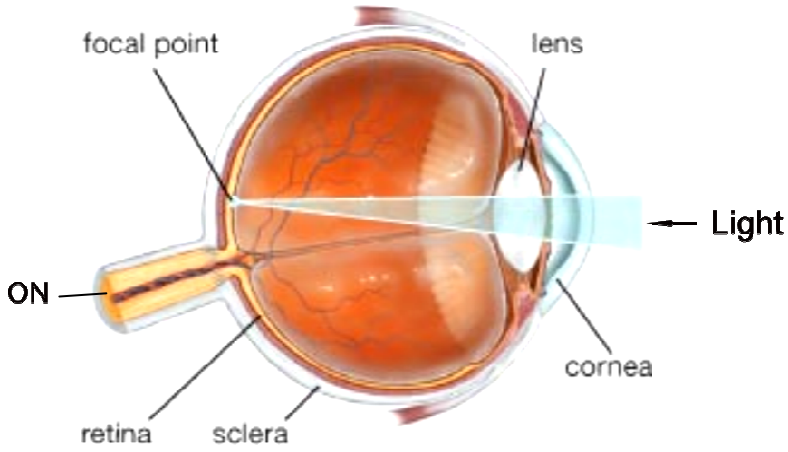

Figure 1.1: Sagittal model of the human eye. Incoming light is focused by the cornea and the lens onto the photoreceptors of the retina. The rods and cones convert the photons into nerve signals that are transmitted along the optic nerve (ON) to the brain. The focal point, the *fovea centralis*, is the region of the retina with the highest density of cone cells, thus confering the sharpest visual acuity. Adapted from ©2008 Encyclopædia Britannica, Inc.

1.2. Anterior eye development

1.2.1. Morphological development

During vertebrate gastrulation, the endoderm and mesoderm interact with and destine overlying ectoderm to become head ectoderm with lens-forming bias (Saha et al., 1989). The optic vesicle, an evagination of the brain, activates this bias and induces the head ectoderm to become a lens placode. The lens placode invaginates to form the lens, whereas the optic vesicle forms the optic cup that will develop into the retinal layers, including the ON. Lens-derived signals induce overlying ectoderm to become corneal ectoderm that rests on a basal lamina and that secretes multple layers of collagen (Gilbert, 2006).

At the 6th week of gestation mesenchymal cells of both ocular neural crest (NC), as well as of paraxial mesoderm origin, migrate along the collagen matrix to fill the space between corneal ectoderm and the lens. Most of the cells form several layers of loosely aggregated cells that condense and differentiate into corneal endothelium (reviewed by Cvekl and Tamm, 2004). The differentiation of the corneal endothelium is critical for the separation of the lens from the cornea and subsequent anterior chamber formation (Reneker et al., 2000; Flügel-Koch et al., 2002). New mesenchymal cells continue to migrate to the future corneal stroma. By the 12th week of gestation, glycosaminoglycan and collagen fibril secreting fibroblasts appear (reviewed by Qazi et al., 2009). Glycosaminoglycans are the ground substance of the cornea, whereas the small in diameter and spatially highly ordered collagen fibrils confer corneal transparency (Maurice, 1957; Benedek, 1971). A new group of mesenchyme cells invade the future anterior chamber angle and differentiate into stroma of the iris and ciliary body (CB). Beginning from weeks 15 - 20 of gestation until birth, anterior chamber or iridocorneal angle invading mesenchyme cells develop into the trabecular meshwork (TM) and Schlemm´s canal (SC) (reviewed by Cvekl and Tamm, 2004), the structures that build up the aqueous humour (AH) outflow pathway. The above described key anterior eye development steps can also be found in mouse embryos between E12.5 and E19.5 as illustrated in Fig. 1.2.

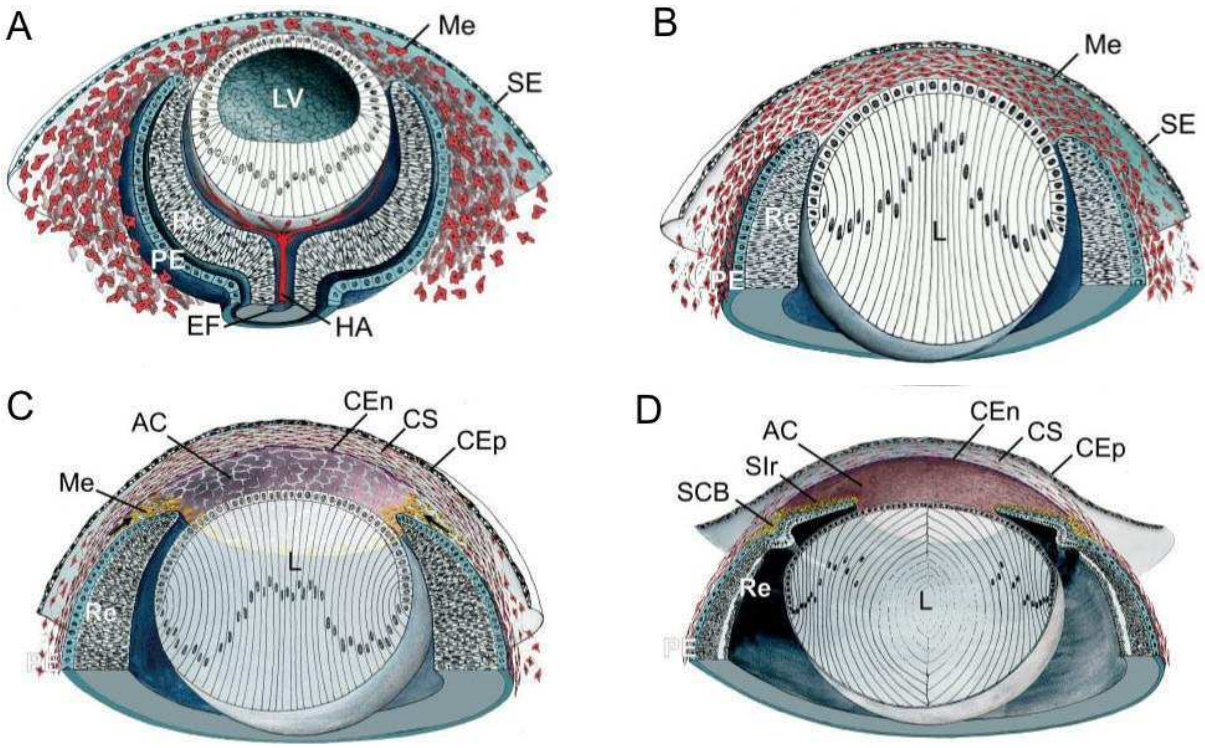

Figure 1.2: Illustration of mouse anterior eye development. A) After the lens has detached from the corneal ectoderm/surface epithelium (SE) at E12.5 - E13.5 (at 6th week of gestation in human), mesenchymal cells (Me) of both ocular NC, as well as of paraxial mesoderm origin, migrate along a collagen matrix into the space between the corneal ectoderm and the lens (L). B) At E13.5 – 14.5 the mesenchymal cells condense to several flat layers separated by extracellular matrix. In human, the mesenchymal cells condense and differentiate into corneal endothelium already at this stage. C) At E14.5 – E15.5 all layers of the cornea (corneal epithelium (CEp), corneal stroma (CS) and corneal endothelium (CEn)) have formed, allowing the separation of the lens and the formation of an anterior chamber (AC). New mesenchyme cells migrate into the future anterior chamber angle (black arrows). D) At E15.5 the anterior edges of the optic cup extend to form the iris and CB. Invading mesenchyme cells form the stroma of these structures (SIr and SCB). The last vawe of mesenchymal cells migrate into the anterior chamber angle between E17 and E19 (between 15th and 20th week of gestation in human), resulting in the formation of the TM and SC. LV = lens vesicle, Re = neural retina, PE = pigmented epithelium, EF = embryonic fissure, HA = hyaloid artery. Adapted from Cvekl and Tamm, 2004.

1.2.2. Signalling molecules

The mature anterior eye is made up of tissues originating from the four embryonic lineages neural ectoderm (epithelial layers of CB and iris), ocular surface ectoderm (lens, corneal epithelium, limbus, conjunctiva, harderian and lacrimal glands, eyelid epidermis), NC (corneal stroma and endothelium, conjunctival and eyelid mesenchyme, stroma of iris and CB) and mesoderm (SC and blood vessel endothelium), that interact in a complex way during morphogenesis. These mechanisms are strictly controlled by spatial and temporal regulation of the expression of various transcription factors, as well as by integration of different signalling pathways. The transcription factor paired box 6 (PAX6/Pax6 in human/mouse) is a key transcription factor in the synchronization of eye development in vertebrates. Its restricted spatial expression in the head ectoderm confers bias for the invagination and formation of the lens (Li et al., 1994). Spatial and temporal regulation of Pax6 expression in widespread regions of the eye regulates the spatial and temporal expression of downstream key transcription factors. In addition, Pax6 has cell-autonomous roles in migration and differentiation of NC-derived cells of the cornea (stroma, endothelium) and TM (Baulmann et al., 2002; Collinson et al., 2003).

The lens-derived transcription factors MAF (v-maf musculoaponeurotic fibrosarcoma oncogene homolog), FOX (forkhead box) E3 and PITX (paired-like homeodomain) 3, as well as the transcription factors PITX2 and FOXC1 that are expressed in the anterior eye ocular mesenchyme cells themselves, are crucial controllers of normal anterior eye development. Mutations in their genes are known to cause different subtypes of anterior segment dysgenesis (ASD) including Peters´ anomaly, Axenfeld-Rieger´s syndrome, aniridia and embryotoxon. ASD phenotypes show anomalities in anterior mesenchyme-derived structures like iris, cornea and the anterior chamber angle, which may result in the absence of an anterior chamber, corneal opacity or, due to dysgenesis of the AH outflow tissues in the anterior chamber angle, an elevated intraocular pressure (IOP) (reviewed by Cvekl and Tamm, 2004). It has been proposed that ASD relys on defects in the migration and differentiation of mesenchymal NC cells (Kupfer and Kaiser-Kupfer, 1978). The fact that phenotypes of different ASD subtypes may be overlapping and that the same mutation may show different phenotypes, shows the complexity of ASD. Mouse models have shown that some secreted signaling molecules

transforming growth factor-ß (TGF-ß) and bone morphogenetic protein 4 (BMP4) lead to defects that closely resemble those seen in ASD (Chang et al., 2001; Sanford et al., 1997; Flügel-Koch et al., 2002), which raises the possibility that their expression may be controlled by above described key transcription factors.

Since *Pax6*-mutant mice have a defect retinoic acid (RA) signaling (Enwright and Grainger, 2000), there have been speculations about to what extent the effect of PAX6 on eye development is modified via retinoids. It is well established that vitamin A (retinol) is indispensable for eye development (Hale, 1933). RA is synthesized in the retina and the corneal ectoderm, though it signals via retinoic-acid receptor (RAR) heterodimers in the periocular mesenchyme and NC-derived mesenchyme to affect the gene expression of key transcription factors involved in anterior eye morphogenesis (Matt et al., 2005). Experiments with *Pitx2*- and *Dkk2*-mutant mice showed that the RA signalling in the NC mesenchyme was able to control Wnt signalling of the NC, as well as that of the overlying corneal ectoderm (Gage et al., 2008).

1.3. The TM

1.3.1. AH outflow

AH drainage through the anterior eye produces an IOP of 16 - 17 mm Hg that is optimal for maintaining shape and thus optical properties of the eye. AH transports oxygen and nutrients to, as well as waste products from, the avascular lens, cornea and TM. AH is thought to have a role in the delivery of antioxidants, as well as in the immune response (reviewed in Civan, 2008). AH is produced by the ciliary body in the posterior chamber and flows through the pupil into the anterior chamber. From here, most of AH is drained through the conventional or the trabecular outflow pathway, whereas the rest of AH is conducted through the unconventional or uveoscleral outflow pathway with a negligible contribution to the IOP

(Johnson and Erickson, 2000). The conventional pathway includes the TM and SC, from where the AH is drained into the episcleral venous system (Fig. 1.3A, B).

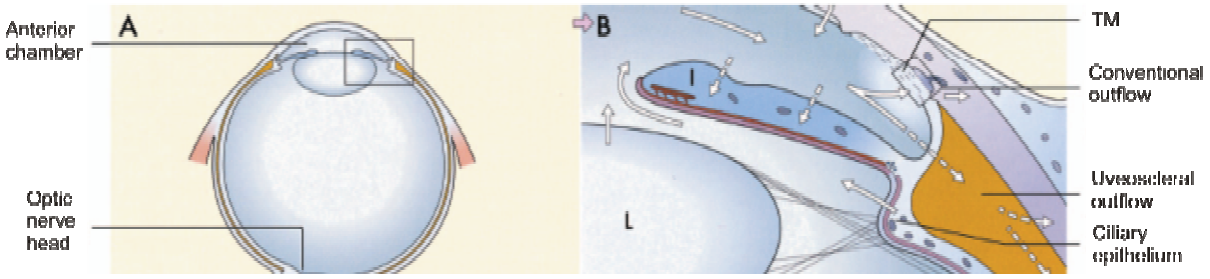

Figure 1.3: Diagramm showing the conventional or trabecular, as well as the unconventional or uveoscleral AH outflow pathways. AH is produced in the CB epithelium in the posterior chamber and flows through the pupil into the anterior chamber. A part of the AH escapes through the uveoscleral pathway with a negligible contribution to the IOP. The bulk of the AH is drained through the TM, the tissue that builds up an outflow resistance and thus is responsible for the build-up of IOP. The AH from both pathways flows into the episcleral venous system. B) is a magnification of the squared area in A). Adapted from Lütjen-Drecoll, 2000.

1.3.2. TM architecture

AH is drained through the TM by a pressure gradient. Beginning from the anterior chamber, the TM is made up of the uveal and corneoscleral meshworks (UTM and CTM, respectively) and the juxtacanalicular tissue (JCT) (Fig. 1.4B).

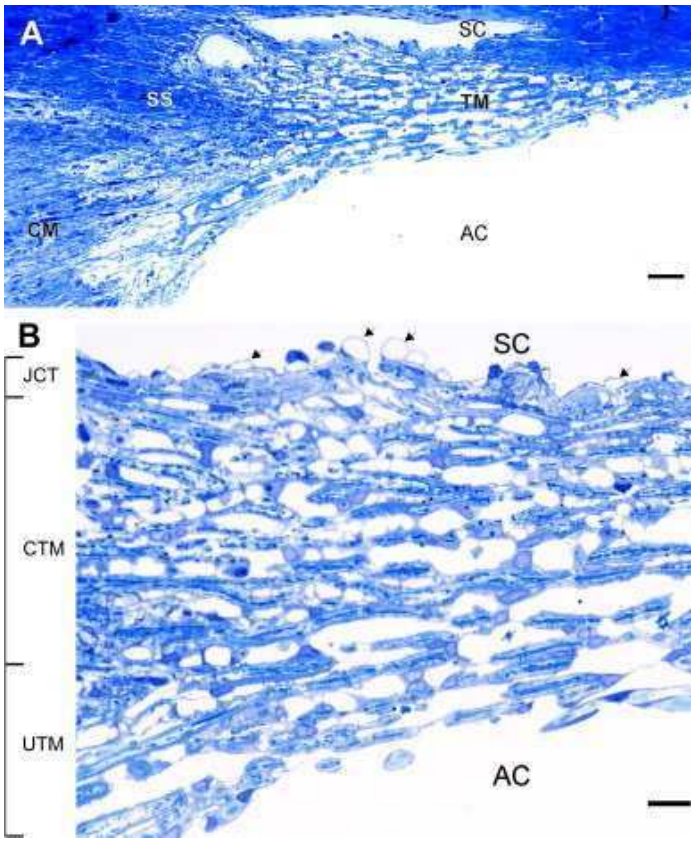

Figure 1.4: A) The conventional AH outflow pathway is made up of the TM between the anterior chamber and the SC. B) Beginning from the anterior chamber, the TM is made up of the uveal and corneoscleral meshworks (UTM and CTM, respectively) and the juxtacanalicular tissue (JCT). The JCT, as well as the lining between the JCT and the inner wall endothelium of SC are thought to be the sites that generate outflow resistance. The fluid flow into SC is controlled by pouchings and pores of the inner wall endothelium of SC (small arrows). SS = scleral spur, CM = ciliary muscle. Magnification bars: 20 µm (A), 5 µm (B). Light micrograph of a meridional section through the TM as presented in Tamm, 2009.

UTM and CTM are made up of layers of trabeculaer lamellae. The core of the lamellae contain dense elastic fibers that are surrounded by a sheath of flat trabecular cells that resides on a basal lamina and that thickens with age. The cells can phagocytize dispensable material like iris-derived pigment particles and extracellular material (reviewed by Tamm, 2009; Acott, 1994). The lamellae of the UTM and CTM show a relatively ordered spatial organization with numerous open spaces between the lamellae. This gives the UTM and the

CTM a highly porous structure with a negligible contribution to fluid flow resistance (reviewed by Johnson, 2006).

In contrast, the cells of the JCT are organized more irregularly and are attached to each other, to extracellular matrix (ECM) or to the SC endothelium. Structural elements of the ECM are a network of elastic fibers and fibronectin-based cell-matrix connections between the ECM and SC endothelium. Matricellular proteins of the JCT ECM that are involved in structural ECM modulation are thrombospondin-1 (Flügel-Koch et al., 2004) and SPARC (secreted protein, acidic and rich in cysteine) (Rhee et al., 2003). The POAG associated myocilin, one of the most highly expressed proteins in the TM (Tomarev et al., 2003) can associate with fibrillar elements of the JCT ECM (Ueda et al., 2000).

1.3.3. Generation of outflow resistance

The JCT and the inner wall endothelium of SC have proven to be the sites of build up of AH outflow resistance. Since the spaces between the cells and the ECM are the route for AH outflow through the JCT, the amount and quality of the ECM are crucial regulators of the resistance (reviewed by Acott and Kelley, 2008). JCT ECM turnover is controlled by the growth factors TGF-ß2, CTGF (connective tissue growth factor), BMP4 and BMP7 (Fuchsofer and Tamm, 2009), as well as by glucocorticoid (GC) and prostaglandin derivatives (Johnson et al., 1990; Bahler et al., 2008). It is thought that AH flow into the SC is controlled by emerging outpouchings (giant vacuoles) and pores of the SC inner endothelium (Figs. 1.4B and 1.5), whereas the flow resistance itself is generated in the JCT ECM or the SC basement membrane (BM) (reviewed by Johnson, 2006).

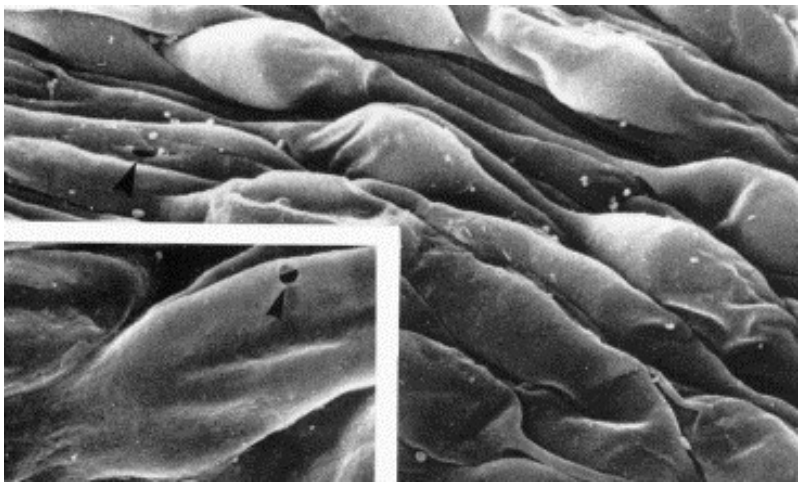

Figure 1.5: AH flow into the SC is controlled by emerging outpouchings (giant vacuoles) and pores (arrows) of the SC inner endothelium. Scanning electron micrograph as presented by Johnson, 2006.

Tendons and elastic fibers structurally connect the ciliary muscle (CM) and the scleral spur (SS) with the TM ECM (Fig. 1.4A). The SS contains innervated myofibroblast-like cells (Tamm et al., 1995) that contain actin filaments (Tamm et al., 1992). Both CM and SS cell contraction affect TM architecture, probably in opposite directions (reviewed by Tamm, 2009).

1.3.4. Pathology

Glaucoma is the definition of a complex group of neurodegenerative disorders that are characterized by optic neuropathy leading to gradual visual loss, and that in its irreversible end phase is the second leading cause of blindness worldwide (reviewed by Leske, 2007). Classically, the optic neuropathy is thought to develop as a consequence of an elevated IOP due to an elevated AH outflow resistance through the TM. The fact that normal-tension glaucomas exist and that the inheritance of glaucoma is complex, show the complexity of the disease (reviewed by Armstrong and Smith, 2001).

Three main classes of glaucoma are primary open-angle glaucoma (POAG), primary acute closed angle glaucoma (PACG) and primary congenital glaucoma (PCG). In PACG and PCG an increased AH outflow resistance through the TM rely on defects in anterior chamber angle morphology (reviewed by Ray et al., 2003; Kupfer and Kaiser-Kupfer, 1979). Glaucoma can also be manifested as a symptom of other eye malformations like different forms of ASD (reviewed by Cvekl and Tamm, 2004).

1.3.4.1. POAG

Due to normal morphology of drainage structures in POAG, and since an elevated IOP due to increased AH outflow resistance through the TM is asymptomatic, the disease is not manifested until loss of visual fields, a timepoint where apoptosis of optic nerve head (ONH) cells already has begun. POAG is the most common form of glaucoma and can, dependent on the age of onset of the disease, be divided into the juvenile and adult forms. 13 - 25 % of POAG cases are inherited in an autosomal dominant or recessive pattern, though with varying clinical expression and penetrance of disease (Becker et al., 1960; Kellerman and Posner, 1955).

Age-related changes of the TM are the most important factors leading to POAG, which explains the fact that mostly elderly people are affected. An altered histological structure of the outflow pathway like a decrease in the number of cells, as well as an accumulation of ECM have been reported (reviewed by Armstrong and Smith, 2001). Electron microscopy has revealed an accumulation of collagen and fine fibrillar material. The fine fibrils, that are embedded in a glycosaminoglycan matrix, form sheaths around the elastic fibers of the JCT. The sheaths can thicken to form so called plaques (Lütjen-Drecoll and Rohen, 1981). Additional glaucomatous changes of the JCT are the presence of numerous large cells containing many mitochondria and lysosomes, but no endoplasmic reticulum (ER) or Golgi apparatus (Rohen et al., 1993).

1.3.4.2. Secondary forms of open-angle glaucoma (OAG)

OAG can develop secondary due to dysfunction of autoregulation of ocular blood flow, which affects IOP and normal metabolism in eye tissues, including ONH and TM (reviewed by Moore at la., 2008). Corticosteroid treatment (including the GC dexamethasone) of inflammatory and allergic eye conditions increase IOP to a degree that correlates with the patient´s steroid responsiveness (Armaly, 1965), a trait that in turn is inherited (Armaly, 1967). An established risk factor for developing OAG is a thinner than normal central corneal thickness (Gordon et al., 2002), an inheritable trait (reviewed by Dimasi et al., 2009). The mechanisms that link the secondary factors to OAG are far from clear.

1.3.5. Treatment of glaucoma

Since the molecular mechanisms that generate an elevated AH outflow resistance through the TM are to be unraveled, treatment of tension-glaucoma has focused on the symptom; i.e. in lowering IOP. Treatments include reduction of production of AH by the CB (e.g. carbonic anhydrase inhibitors) or facilitation of AH outflow through the anterior chamber angle. The latter can be achieved by stimulating a contraction of the parasympathetically innervated CM and subsequent relaxation of the TM (e.g. parasympathomimetics), or by enhancing the outflow through the uveoscleral route (e.g. prostaglandin F receptor agonists) (reviewed by Costagliola et al., 2009). The final alternative to cure raised IOP are surgical methods like laser trabeculoplasty (reviewed by Coakes, 1992), filtration surgery (Anand et al., 2007) or CB ablation (Mastrobattista and Luntz, 1996).

1.3.6. Glaucoma genetics

Chromosomal linkage analyzes of families affected by inherited forms of POAG have identified many disease-associated chromosomal loci. Mutated forms of the genes for myocilin (*MYOC*) and optineurin (*OPTN*) can act as causative (reviewed by Ray et al., 2003), whereas mutated forms of the genes for CYP1B1 (*CYP1B1*) (cytochrome P450, family 1, subfamily B, polypeptide 1) and WDR36 (*WDR36*) (WD repeat domain 36) can act mainly as modifying (reviewed by Vasiliou and Gonzalez, 2008; reviewed by Challa, 2008) genes in POAG etiology. The many involved loci and the different nature of involved proteins again demonstrate the complex nature of both the genetics, as well as the molecular mechanisms lying behind glaucoma.

1.4. Myocilin

1.4.1. History

The locus GLC1A (GLC, 1 and A stand for glaucoma, primary open angle and first linkage for POAG, respectively) in the region 1q21 - 31 on chromosome 1 was identified to be responsible for the juvenile form of OAG in 1993 (Sheffield et al., 1993). Since increased IOP had been recognized as being a consequence of GC treatment (Armaly, 1963; Becker, 1965), research now focused on the effects that GCs exerted on human TM cells in culture, a recognized good model in studying cellular *in vivo* processes (reviewed by Wordinger and Clark, 1999). Reported effects were alterations in ECM protein composition (Dickerson et al., 1998), cytoskeleton (Clark et al., 1994) and gene expression (Kawase et al., 1994). In 1997, Polansky et al. showed that prolonged GC-treatment of cultured human TM cells induced the expression of a new 57 kD protein, named trabecular meshwork induced GC response (TIGR) protein. In the same year *TIGR* was cloned from CB (Ortego et al., 1997) and retina (Kubota et al., 1997). As Stone et al. (1997) mapped *TIGR* to the region 1q23 - 24 within the GLC1A locus and showed that mutations within *TIGR* cause glaucoma in 3.9 % of POAG patients, as

well as in a fraction of juvenile OAG cases, the gene got its status as being a POAG causing gene. Later, mutations in *TIGR* have also been found in other forms of OAG, though not to such an extent as in POAG (Alward et al., 2002). Since TIGR is a myosin-like acidic protein it has been named myocilin (Kubota et al. 1997).

1.4.2. Transcript structure

The *MYOC* 5′ → 3′ coding sequence is found on the opposite chromosome at location 1q23 - 24. *MYOC* contains two possible start ATGs (Fig. 1.7), both of which can be used. The transcription starts 65 bp upstream of the first start ATG and produces a 17.25 kb transcript made up of three exons and two intervening introns. Exons 1, 2 and 3 have lengths of 664, 126 and 1293 bp, respectively, whereas the first and second intervening introns show respective lengths of 13 285 and 1 887 bp. Exon 3 contains a 509 bp long 3′-untranslated (UTR) region containing three possible polyadenylation signals, two of which are used (Nguyen at al., 1998) (Fig. 1.6).

Figure 1.6: The *MYOC* 5′ → 3′ coding sequence is found on the opposite chromosome at location 1q23 - 24. The MYOC transcript has a length of 17 250 bp and is made up of three exons and two intervening introns. Exons 1, 2 and 3 have lengths of 664, 126 and 1293 bp, respectively, whereas the first and second intervening introns have respective lengths of 13 285 and 1 887 bp. Exon 3 contains a 509 bp long 3′-UTR region composed of three possible polyadenylation signals, two of which are used (Source: NCBI: Entrez Gene).

1.4.3. Protein structure

MYOC mRNA shows sizes between 2.37 and 2.5 kb and is translated to the 504 bp glycoprotein myocilin (reviewed by Tamm 2002). The second ATG within exon 1 is followed by a hydrophobic signal sequence containing a cleavage site between amino acids (aa) 32 and 33 (Nguyen at al., 1998), as well as a myosin-like domain containing a leucine zipper coiled coil motif. The N-terminal myosin-like domain shows 25 - 29 % homology to the heavy chain of myosin, a muscle motor protein. Exon 3 contains a highly conserved C-terminal olfactomedin domain that shows 31 - 50 % conservation (reviewed by Tamm, 2002). Olfactomedin is an ECM protein that was originally discovered from frog olfactory neuroepithelium (Snyder et al., 1991). Exon 2 contains a cleavage site between aa 226 and 227, suggesting that this exon serves as a linker between the myosin-like and olfactomedin domains (Aroca-Aguilar et al., 2005). A tripeptide targeting signal for microbodies is located at the final C-terminus (Adam et al., 1997) (Fig. 1.7).

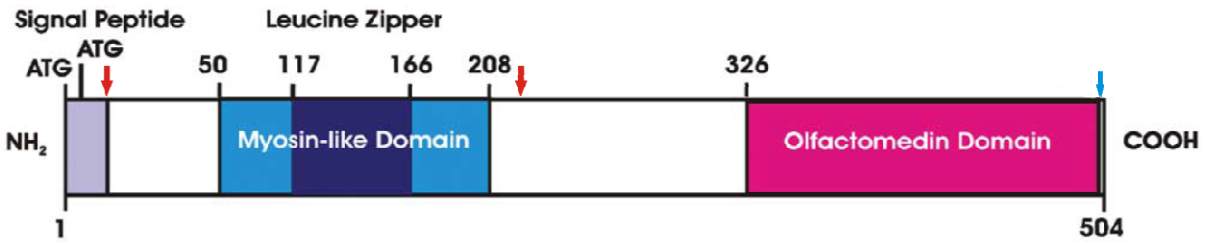

Figure 1.7: Structure of translated 504 bp myocilin polypeptide, beginning from the first possible start ATG. Exon 1 is built up of an N-terminal signal peptide and a conserved myosin-like domain. The signal peptide can be cleaved at aa position 32 (red arrow). The myosin-like domain contains a leucine zipper coiled coil motif. Exon 3 contains a highly conserved C-terminal olfactomedin domain, as well as a tripeptide targeting signal for microbodies (Adam et al., 1997) (blue small arrow). Exon 2 contains a cleavage site at aa position 226 (red arrow), suggesting that this exon serves as a linker between the myosin-like and olfactomedin domains (Aroca-Aguilar et al., 2005). Adpated from Tamm, 2002.

1.4.4. Myocilin protein forms

Myocilin contains many sites that confer the possibility for post-translational modification. The many *N*-glycosylation sites found within myocilin produce bands that vary in size from 53 – 57 kD (reviewed by Resch and Fautsch, 2009), and which also may be responsible for band sizes that reach MWs of up to 66 kDa. In addition to the many *N*-glycosylation sites, myocilin contains sites for *O*-glycosylation, glycosaminoglycan initiation, hyaluronan-binding, and phosphorylation (Nguyen at al., 1998; Fingert et al., 1998).

Myocilin is a hydrophobic protein that can be found in AH in larger than 250 kD aggregates (Russell et al., 2001), probably composed of myocilin aggregating with itself and other proteins. Leucine zipper motifs are involved in homo- and heterodimerization of proteins (Hurst, 1996). *In vitro*, myocilin can dimerize and oligomerize through its leucine zipper domain (Fautsch and Johnson, 2001), as well as form intra- and intermolecular disulfide bonds through its five cystein residues (Fautsch et al., 2004).

1.4.5. mRNA expression pattern

Myocilin mRNA is found at high levels in most ocular tissues including TM, CB, sclera, choroid, cornea, iris, retina and ONH (reviewed by Tamm, 2002). Very high expression is seen within TM, sclera (Adam et al., 1997), CB and iris (Ortego et al., 1997). Mouse myocilin mRNA has a similar expression pattern, with very high expression within CB epithelium, anterior portion of sclera and TM (Takahashi et al., 1998), tissues that are involved in production and drainage of AH.

Outside the eye myocilin mRNA can be found in skeletal muscle, heart, small intestine, and to a lesser extent in mammary gland, thymus, prostate, testis, colon, stomach, thyroid, trachea and bone marrow (Ortego et al., 1997; Adam et al., 1997; Fingert et al., 1998). Tiny amounts

of myocilin mRNA has also been found within Schwannoma tumours that affect the myelin sheath of vestibular nerves of the brain (Ohlmann et al., 2003). The myocilin mRNA distribution pattern outside the eye is akin in mouse (reviewed by Tamm, 2002), with the addition that myocilin mRNA has been detected in adult mouse brain, including the ependymal lining of the ventricles and the choroid plexus (CP) (Swiderski et al., 1999). In rat, myocilin mRNA is abundantly expressed in the sciatic nerve (Ohlmann et al., 2003).

1.4.6. Protein expression and localization

Expression of myocilin protein correspond its mRNA distribution pattern. High amounts of myocilin are detected in all parts of the TM, Sclemm´s canal endothelium, CM, CB epithelium, in all layers of the cornea and corneal sclera, iris, vitreous humour, retina and ONH (Karali et al., 2000; Ueda et al., 2000). Within the JCT, the part of the TM with the highest AH outflow resistance, myocilin localizes to the ECM space, and to a lesser extent to the cytoplasm of TM cells (Konz et al., 2009). Within the JCT ECM, myocilin associates with the fine fibrils and associated glycoprotein matrix that surround the elastic fibers, and which are able to thicken and form plaques (Ueda et al., 2002). Myocilin also associates with the elastic fibers themselves (Ueda et al., 2000) and collagen (Tawara et al., 2000) and is, in its secreted glycosylated and aggregated form, a major constituent of AH (Russell et al., 2001). Intracellularly, myocilin is reported to localize to intermediate filaments (IFs), mitochondria, and intracellular vesicles (Ueda et al., 2000), and after dexamethasone-treatment to the ER (Wentz-Hunter et al., 2002), the Golgi apparatus and the microtubule motor protein kinesin (Clark et al., 2001) of cultured human TM cells.

The expression of myocilin in the mouse eye correspond the expression pattern in the human eye. During development, expression of myocilin is first detected in the axons of the retinal ganglion cells at E17.5, whereas expression in the anterior eye is not visible until postnatal day (P) 10. TM, CB epithelium, iris with stroma, as well as corneal endothelium and stroma are positive for myocilin staining at P12 - P14. Thus, in the eye, myocilin expression

commence with the time of the morphological maturation of respective tissue (Knaupp et al., 2004).

Outside the eye, myocilin is expressed in the sciatic nerve. In rat, the site of expression within the sciatic nerve was shown to be the myelin sheath (Ohlmann et al., 2003). Myocilin has been detected within fibroblast-like cells of the outer fibrocartilagenous annulus fibrosus of the intervertebral disc (Gruber et al., 2006), the ECM-rich joint ligament between adjacent vertebrae. Within rat kidney glomeruli, myocilin is found constitutively within podocytes, and during induced mesangioproliferative glomerulonephritis, a condition characterized by an excess production of ECM (Floege et al., 1991), in the cytoplasm and ECM of mesangial cells (Goldwich et al., 2005).

1.4.7. Function

70 different mutations in myocilin are responsible for 2 – 4 % of POAG cases, and in as many as 36 % of patients suffering from the juvenile onset OAG (Schimizu et al., 2000). Over 90 % of the mutations reside within exon 3, the rest are found within exon 1. Most of the mutations within exon 3 and 1 reside within the conserved olfactomedin and myosin-like domains, respectively (reviewed by Zachary and Fautsch, 2009). The majority of *MYOC* mutations are missense mutations, leading to an aa substitution that may affect protein structure and function, whereas the most frequently occurring single mutation is a nonsense mutation that results in a truncated 368 aa protein (reviewed by Tamm 2002). The single mutations usually show specific clinical features regarding IOP, frequency, age of onset and severity of disease (Alward et al., 1998). Since patients with only one copy (Wiggs and Vollrath, 2001) or homozygous deletion of > 90 % (Lam et al., 2000) of *MYOC* are healthy, and since myocilin knock-out mice have a normal phenotype (Kim et al., 2001), the function and the mechanism how mutated myocilin causes POAG is still a secret and suggests a gain of function or a dominant-negative effect theory. Even though myocilin is expressed in many organs and tissues (reviewed by Tamm, 2002; Ohlmann et al., 2003; Gruber et al., 2006), the only pathology that results from *MYOC* mutations is glaucoma. This suggests an important and

specific function for myocilin within the eye in the maintenance of an adequate AH outflow resistance.

1.4.7.1. Intracellular myocilin

Most data that confer myocilin an intracellular role are derived from *in vitro* biochemical and cell culture experiments. The N-terminal leucine zipper coiled coil motif targets cellular recombinant myocilin to intracellular membranes (Stamer et al., 2006). The fact that myocilin is found associated with ER (Sohn et al., 2002), the Golgi apparatus, (O´brien et al., 2000) and vesicles (Lütjen Drecoll et al., 1998) probably reflects its trafficking between ER and Golgi during post-translational modification. The finding that myocilin, vesicles and the motor protein kinesin all co-localize within TM cells (Clark et al., 2001), indicates that myocilin may be involved in vesicular transport. Myocilin has also been found within mitochondria and can, when mutated, disturb normal mitochondrial energy metabolism function, affecting cell viability (He et al., 2009).

Another theory gives myocilin a role in the regulation of cytoskeletal architecture, an interesting approach, since modulation of the cytoskeleton with various pharmacological agents have shown to decrease AH outflow resistancy in living monkey eyes, as well as to reduce IOP in human eyes (Tian et al., 2000). A role for myocilin within the actomyosin system of TM cells is corroborated by the facts that myocilin interacts with the myosin motor protein through its conserved leucine zipper domain, myocilin and myosin co-localize to actin stress fibers (Wentz-Hunter et al., 2002) and by the fact that myocilin associates with IFs like vimentin and actin (Ueda et al., 2000).

Optineurin is another leucine zipper containing protein found within TM, retina and the CB body epithelium, that in its mutated form cause POAG. As myocilin, it can also localize to the Golgi apparatus and vesicular structures (reviewed by Chalasani et al., 2008). Over-

expression of optineurin in TM cells leads to a stabilization of *MYOC* mRNA with subsequent up-regulation of myocilin protein expression (Park et al., 2007).

1.4.7.1.1. The olfactomedin domain and secretion

Olfactomedin domain containing proteins are secreted glycoproteins or membrane-bound receptors that are involved in neurogenesis, NC formation, dorsal ventral patterning, cell cycle regulation, tumorigenesis and cell signalling (Tomarev and Nakaya, 2009). Myocilin shares similarities in structure to these proteins regarding the secretory signal peptide, the leucine zipper coiled coil region and the C-terminal olfactomedin domain (Nagy et al., 2003). The fact that most of the OAG causing mutations reside within the conserved olfactomedin domain, indicates that this domain has an important function in OAG pathology. The olfactomedin domain of myocilin can form intra- (Nagy et al., 2003) and inter- (Fautsch et al., 2004) molecular disulphide bonds by Cys433, an aa that if substituted for Arg can cause OAG (de Vasconcellos et al., 2003).

The olfactomedin-domain is responsible for myocilin secretion (Sánchez-Sánchez et al., 2007). If mutated, folding of myocilin is impaired, leading to accumulation of aggregates of misfolded protein within the ER (Liu et al., 2004). This can lead to ER stress and subsequent cytotoxicity, affecting the morphology and viability of TM cells (Joe et al., 2003). The theory is supported by the facts that only wild-type (WT), but not mutant myocilin, is secreted from TM cells *in vitro*, and that mutated myocilin can not be detected in the AH of OAG patients. Mutated myocilin also has a dominant-negative effect in that it can suppress the secretion of WT myocilin (Jacobson et al., 2001).

Within the ER, myocilin can be proteolytically spliced at aa position 226 (Aroca-Aguilar et al., 2005) (Fig. 1.7) in a Ca^{2+}-dependent manner (Sánchez-Sánchez et al., 2007), the cleavage is inhibited by some mutations within the olfactomedin domain. The cleavage produces a 20 kD N-terminal myosin-like domain and a 35 kD C-terminal olfactomedin-domain containing

fragment (Aroca-Aguilar et al., 2005). Only the C-terminal part, along with full-length myocilin, was shown to be secreted from different cell types (Sánchez-Sánchez et al., 2007), whereas the N-terminal fragment has been shown to accumulate within the cell, reduce secretion of endogenous myocilin and affect outflow facility (Caballero et al., 2000). This may explain why perfusion with the olfactomedin-domain alone through human and porcine anterior eyes did not affect outflow facility (Goldwich et al., 2003).

Myocilin and αB-crystallin co-localize and are both up-regulated in the TM of glaucoma patients and elderly people (Lütjen-Drecoll et al., 1998). αB-crystallin is a molecular chaperone that promotes proper folding of and protects proteins from aggregation during stress (Horwitz, 1992). Treatment of TM cells with pharmacological agents that can act as chemical chaperones has been shown to restore normal folding and secretion of mutant myocilin, as well as to resolve myocilin aggregates. The increased secretion reduced ER stress and apoptosis (Yam et al., 2007).

1.4.7.2. Extracellular role

The up-regulation of myocilin in dexamethasone-treated perfused cultured human eyes, as well as in living monkey eyes, correlates with an increase in IOP in a dose-dependent manner (Clark et al., 2001). Immunostaining has shown that myocilin expression is elevated in the TM of glaucoma patients (Lütjen-Drecoll et al., 1998). These facts support a theory that an elevated amount of myocilin within the TM may lead to glaucoma. Since myocilin is found to be associated with ECM material of the TM (Ueda et al., 2000, 2002; Tawara et al., 2000), and since myocilin expression is seen to be elevated within the JCT ECM in POAG patients (Konz et al., 2009), the role of increased myocilin in causing glaucoma is thought to be extracellular. Perfusion of human anterior eye segments with recombinant myocilin increases outflow resistance and IOP (Fautsch et al., 2000), but the effect is only seen after complexing of myocilin with another unknown protein (Fautsch et al., 2006). Thus, the mechanism by which myocilin obstructs the AH outflow pathway is unclear and suggests that myocilin acts as a matricellular protein, i.e. a protein that does not itself have a specific function, but that is

able to modulate cell-matrix interactions by interacting with various ECM molecules like cell-surface receptors, cytokines, growth factors, proteases and structural proteins (reviewed by Bornstein et al., 2000).

The multi-domain character of myocilin suggests that it is able to form various interactions. In fact, myocilin seems to interact with proteins from different categories. Leucine zipper domains are known to dimerize into homo- and heterodimers (Hurst et al., 1996). Myocilin forms dimers and multimers through its leucine zipper domain in human AH (Fautsch and Johnson, 2001). In addition, biochemical *in vitro* studies have shown that the myocilin leucine zipper is capable of binding numerous other proteins (Wentz-Hunter et al., 2002).

In the human eye, myocilin co-localizes with fine fibrils of the sheath material that surround elastic fibers of the JCT. Myocilin overlaps with fibronectin, fibrillin-1, microfibril-associated glycoprotein, decorin and type VI collagen. *In vitro*, myocilin interacts physically with fibronectin, fibrillin-1, vitronectin, laminin, decorin, and laminins I, III, V and VI (Ueda et al., 2002). Cell culture experiments have shown that the coiled coil and leucine zipper motifs of myocilin are important in forming extracellular interactions that favour adhesion (Gobeil et al., 2005). Myocilin binds to the Heparin II domain of fibronectin (Filla et al., 2002). This domain mediates cell adhesion, organization of the cytoskeleton, signal transduction and phagocytosis (Hynes, 1990). In cell cultures, myocilin impairs fibronectin-mediated adhesion and cell spreading (Peters et al., 2005). Experiments using primary cell cultures of human TM showed that myocilin inhibits cell-matrix cohesiveness by modulation of cAMP/PKA signalling (Shen et al., 2008). cAMP/PKA signalling is known to be involved in cell-matrix adhesion and cytoskeletal reorganization, that in turn affect cell migration (reviewed by Howe, 2004). Other studies have shown an adhesion promoting effect of myocilin (Goldwich et al., 2009).

Via its olfactomedin domain, myocilin can physically interact with the olfactomedin domain of optimedin, a secreted candidate glaucoma glycoprotein expressed in the TM and retina (Torrado et al., 2002). Hevin is a secretory ECM glycoprotein with anti adhesive activity (Girard and Springer, 1996). In cell cultures, myocilin interacts with the C-terminus of hevin.

Myocilin co-localize with hevin in the CB epithelium of human eyes, as well as in the ER and Golgi apparatus of cultured cells. Myocilin impaired the secretion of hevin, the glaucoma causing mutation P370L still augmented the effect (Li et al., 2006). Myocilin has also been shown to interact physically with antagonists of the Wnt-pathway, as well as to bind Wnt-receptors, leading to Wnt-signalling and re-organization of the cytoskeleton in TM cells (Kwon et al., 2009).

In summary, myocilin seems to modulate cell adhesion, probably by modulating other cell-matrix interactions, or/and by changing gene expression of proteins involved in adhesion (Paper et al., 2008). This emphasizes its role as a matricellular protein. In addition to conferring stability to, the degree of glycosylation of a protein is important for its bioactivity (reviewed by Fares, 2006) and adhesive properties (Jones et al., 1986; Kaufmann et al., 2004). Thus, the different degree to which myocilin can be glycosylated may regulate its interaction with other ECM molecules and the impact it has on cell adhesion.

1.4.7.3. Theory for why mutated or an excess of myocilin leads to POAG

The various data of intra- and extracellular roles of myocilin can be summarized in the way that when mutated myocilin is retained within the ER (Liu et al., 2004) and thus not secreted, it can not fulfil its normal function as a glycosylated matricellular protein within the ECM. As a possible modulator of cell-matrix (and matrix-matrix) interactions and adhesion (Peters et al., 2005; Goldwich et al., 2009), a decreased amount of extracellular myocilin could impair normal interactions within the TM, resulting in morphology changes and alteration of cell signalling. In the same way, an excess of myocilin within the ECM would lead to a dysregulation of cell-matrix (and matrix-matrix) interactions. Thus, the altered amount of myocilin in the ECM could alter the effect it normally has on ECM molecules. This could influence normal morphology and resistance of the AH drainage route, resulting in an elevated outflow resistance and IOP. Thus, a tight regulation of the amount of extracellular myocilin seems to be important. Since glycosylation seems to be important for the function of

proteins (reviewed by Fares, 2006; Jones et al., 1986), a tight control of the level of glycosylation of myocilin within the Golgi apparatus is important.

The role of myocilin as a modulating matricellular protein may explain the fact that knocking out myocilin in mice is without phenotypic effect (Kim et al., 2001). Since matricellular proteins do not themselves act as specific structural or ligand-binding proteins, their absence may be compensated for by other matricellular proteins (reviewed by Bornstein et al., 2000). This possible complex role of myocilin may also explain the genetic complexity of OAG.

1.4.8. Inter-species conservation

The sequences of *MYOC* and myocilin orthologs from different species have been resolved and shows that the gene is well conserved both at the nucleotide and protein levels. Human myocilin shows a respective homology of 97 and 87 % to monkey (Fingert et al., 2001) and cat (Fautsch et al., 2006), a 85 % homology to rat (Taguchi et al., 2000) and rabbit (Shepard et al., 2003), a 83 % homology to pig (Obazawa et al., 2004), cow (Taniguchi et al., 2000) and mouse (Abderrahim et al., 1998), as well as 82.7 % homology to dog (Ricard et al., 2006) myocilins.

All orthologs contain 3 exons. The leucine zipper motif and the olfactomedin domain are well preserved, whereas differencies are seen concerning the signal peptide, glycosylation and phosphorylation sites as well as cysteine residues. Rat *Myoc* shares the two both possible start ATGs with the human gene (Taguchi et al., 2000) (Fig. 1.7), whereas the *MYOC* orthologs of the other mentioned species only contain the to the human gene corresponding second possible start ATG. The C-terminal tripeptide targeting signal for microbodies found within *MYOC* (Adam et al., 1997) (Fig. 1.7) can also be found within the rabbit ortholog (Shepard et al., 2003). The majority of the glaucoma causing mutations are conserved (Fautsch et al., 2006).

As the mouse has become the most frequently used animal model in glaucoma research, its *MYOC* ortholog *Myoc*, has been examined intensively. *Myoc* resides on chromosome one and the locus is surrounded by a genomic landscape that correspond that of the *MYOC* locus (Abderrahim et al., 1998). There is considerable conservation of the proximal 5´-UTR, and looking further upstream, there are several conserved putative promoter and enhancer binding sites (Fingert et al., 2007). The nucleotide sequence is 83 % identical to that of the human gene (Fingert et al., 2007). Exon-intron boundaries are conserved and exons show roughly the same size as those of *MYOC* (Abderrahim et al., 1998). The shorter transcript size of *Myoc* (10 530 bp compared to 17 250 bp for *MYOC* (Fig. 1.6)) is due to shorter introns. In addition to the leucine zipper and olfactomedin domain, the N-terminal signal peptide and many possible phosphorylation and glycosylation sites have been conserved in *Myoc*. Mouse myocilin has a length of 490 aa (compared to 504 aa in human) and a molecular weight of 55 kD.

1.4.9 Transcriptional regulation

Analyzes of 5 kb of the 5´-UTR region of *MYOC* have identified several possible regulatory motifs, including hormone response elements for GCs and estrogen, transcription factor binding sites for activator proteins (AP-1 and AP-2) and NF-κB (nuclear factor κ light-chain enhancer of activated B cells), as well as repeat elements like Alu and MIR (mammalian interspersed repetitive) (Nguyen et al., 1998). DNAse I footprinting experiments showed that there are many sites of protein binding within the proximal 370 bp *MYOC* 5´-UTR, some of these sites contain a putative NF-κB site, an E-box (enhancer box), a TATA-box, a Sac-box, as well as AP-1 and AP-2 like sequences. This proximal promoter confirms basal transcription of *MYOC* in cell cultures. Upstream stimulatory factor (USF) was shown to bind the E-box *in vitro* (Kirstein et al., 2000). It is well known that prolonged, up to 10 d, treatment of cultured TM cells with the GC dexamethasone induces the expression of *MYOC* (Nguyen et al., 1998). This, as well as the fact that none of the putative GREs within the analyzed 5´-UTR of *MYOC* confer any GC response (Kirstein et al., 2000; Shepard et al., 2001), has led to the hypothesis of a delayed secondary GC response for *MYOC* induction (Shepard et al., 2001). *MYOC* expression in cultured TM cells can also be induced by treatment with TGF-ß1,

H_20_2 and mechanical stretch (Polansky et al., 1997; Tamm et al., 1999). Fibroblast growth factor (FGF) and TGF-ß are able to counteract the induction of *MYOC* by GCs (Polansky et al., 1997). How these factors are linked to myocilin on the molecular level is not clear.

1.5. The cornea

The transparent avascular curved cornea transmit and bend incoming light properly to allow the likewise transparent and avascular lens to focus the light correctly onto the retina for subsequent visual processing. In addition to being responsible for two thirds of the refractive power, the cornea protects inner ocular tissues from pathogens and trauma (reviewed by Land and Fernald, 1992).

1.5.1. Architecture

Of the three corneal layers, the epithelium is the only one that is of ectodermal origin. The cornea consists of an outermost 5 – 7 layered stratified non-keratinized epithelium, whose undifferentiated dividing BM continously confer new daughter cells that differentiate and migrate upwards to replace outermost sloughed off epithelial cells. Barrier function is conferred by tight junctions, whereas the corneal reflex or blink reflex is evoked by a dense innervation. As an avascular tissue, the corneal epithelium is nourished by the tear film. The outermost cells also contribute to a minor outward fluid transport (reviewed by Lu et al., 2001).

The mesenchymal and/or NC-derived stroma is the thickest corneal layer. The highly ordered architecture of stromal keratocytes (differentiated fibroblasts) and ECM material, mainly collagens and proteoglycans, is crucial for corneal transparency and refractive power. The stroma is, due to the high abundance of proteoglycans, highly hydrated (reviewed by Qasi et

al., 2009). Another theory to explain corneal transparency is the assumption that the keratocytes express high amounts of water soluble proteins, so called corneal crystallins. These may be known abundantly occuring proteins/enzymes like aldehyde dehydrogenase that, in addition to their normal enzymatic function, serve to refract light (reviewed by Jester, 2008).

The single-layered squamous endothelium, also of mesenchymal and/or NC cell origin, has an important barrier function in that it actively and passively pumps solutes between the AH of the anterior chamber and the stroma (Fishbarg and Lim, 1974). The active fluid transport through the endothelium is necessary to prevent the stroma from swelling and loosing its transparency (Maurice, 1972).

The epithelium-stroma and stroma-endothelium interfaces are made up of the collagenous Bowman´s and Descemet´s membranes, respectively. Bowman´s membrane is an acellular extension of the epithelium BM that support in the maintenance of corneal shape, whereas the Descemet´s membrane is the BM of the endothelium (Fig. 1.9).

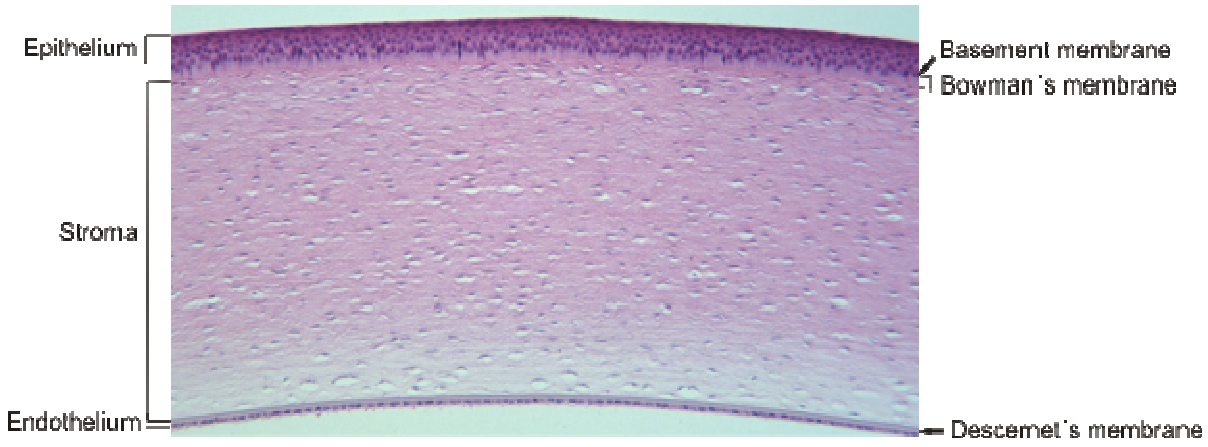

Figure 1.9: Hematoxylin-eosin stained section of normal dog cornea. The corneal stroma is bounded anteriorly by the collagenous Bowman´s membrane, an extension of the epithelial BM. Posteriorly, the stroma is confined

by the endothelial BM, the Descemet´s membrane. The well organized architecture of stromal keratocytes and ECM confer transparency and refractive power. Proper hydration and nutrition of the avascular stroma is conferred by solute transport through the epithelium and endothelium. Adapted image from http://www.vetmed.ucdavis.edu/courses/vet_eyes/images/archive/s_4015_a.jpg.

1.5.2. Fibrosis

As a protector of inner ocular tissues, a scarred cornea has rapidly to be renewed. Whereas corneal epithelium heals by upward migration, division and differentiation of basal cells (Krachmer et al., 2005), the stroma shows a fibrotic reaction characterized by keratocyte activation into myofibroblasts that recruit inflammatory cells (monocytes and macrophages), produce ECM and express α-smooth muscle actin (α-SMA). Fibrotic inflammation, excess ECM accumulation and α-SMA mediated contraction reduce corneal transparency and function, thus impairing vision (reviewed by Saika et al., 2008). Since corneal endothelial cell division *in vivo* is minimal, the endothelium heals through migration and enlargement of neighbouring healthy cells (reviewed by Qasi et al., 2009).

Fibrosis is mediated by growth factors and cytokines, most importantly by TGF-ß. Normally, TGF-ß is localized intracellularly within the corneal epithelium. Wounding up-regulates TGF-ß1 in the stroma, both intra- and extracellularly (reviewed by saika et al., 2008), and it is expressed by infiltrating inflammatory cells to be localized to fibrin clots (Stramer et al., 2003). Thus, TGF-ß1 is the isoform that induces an early fibrotic response, including keratocyte activation, myofibroblast transformation and the expression of the major isoform TGF-ß2 (Huh et al., 2009). In addition to inducing the expression of TGF-ß2, TGF-ß1 can auto-induce its own mRNA expression (Yokozeki et al., 1997), resulting in a positive fibrotic feedback loop. TGF-1 and 2 then act in concert with each other, as well as with other cytokines and growth factors, to maintain the fibrotic response. TGF-ß signals via the Smad2/3 pathway, as can mediators of the mitogen-activated protein kinase (MAPK), c-Jun N-terminal kinase (JNK) and p38 kinase pathways. Thus, the attempts to treat fibrosis thus far have focused on targeting the Smad2/3 pathway (reviewed by Saika et al., 2006, 2008).

2. Scientific objectives

The scientific objectives of the dissertation are various approaches that aim to give information that may help to better understand the molecular mechanisms of pathological processes in the anterior eye. The main focus was set on POAG, whereby the characterization of the myocilin gene, the attempt to create a TM specific promoter element and the creation of animal models are described. A part of the dissertation aimed to learn more about the molecular signalling mechanisms that are activated during wound healing in the cornea.

2.1. Characterization of *MYOC*

Despite over a decade of investigation about the normal, as well as the pathologic, function of myocilin in the eye, there is no definite consensus about how it exerts its pathologic function that leads to glaucoma. Most of the data that aim to clear the molecular mechanisms of myocilin within the TM come from *in vitro* studies, but only a few of these studies report the analysis of the transcriptional regulation of the myocilin gene.

A better understanding of the transcriptional regulation of myocilin is of clinical interest, since a proportion of glaucoma patients show an elevated expression of myocilin within the TM (Lütjen-Drecoll et al., 1998; Konz et al., 2009), and since myocilin accumulates within TM and elevates AH outflow resistance and IOP in anterior eye segments *in vitro* (Fautsch et al., 2000; 2006). In addition, since myocilin is known to behave as a matricellular protein (reviewed by Resch and Fautsch, 2009), regulating molecular interactions within the TM, a precise regulation of myocilin protein expression within this tissue is critical for optimal AH drainage capacity.

Even though it is known that expression can be regulated by far 5´- and 3´-UTRs, as well as by intronic regions (Plaza et al., 1995; Uchikawa et al., 2004*;* Kleinjan et al., 2006; Aruga et

al., 2007), available data from regulation studies only involve the close 5´-UTR of *MYOC*, including the known myocilin basal promoter (Kirstein et al., 2000; Shepard et al., 2001). Thus, we wanted to extend earlier regulation studies to encompass also far 5´- and 3´-UTRs, as well as intronic regions of *MYOC*, to find out if these regions contain elements that are responsible for up-regulation of myocilin expression over basal transcription level in the TM. By inter-species alignment we wanted to search for evolutionarily conserved regions within *MYOC* and to clone these into reporter constructs in front of a reporter gene. We then aimed to analyze if the cloned regions contain TM-specific enhancer elements by comparing the capacity of these regions to drive reporter gene expression over the *MYOC* basal promoter level in cultured TM cells.

It is known that the expression of myocilin is highly induced by GCs (Polansky et al., 1997; Tamm et al., 1999), but no functional GC response elements (GREs) have been found within the close 5´-UTR (Kirstein et al., 2000; Shepard et al., 2001). Thus, we also in this context wanted to extend available data by searching for TM-specific functional GREs outside the close 5´-UTR. We aimed to search for TM-specific functional GREs within our cloned far 5´- and 3´-UTRs, as well as within the cloned intronic *MYOC* regions, by treating transfected human TM cells with dexamethasone and by then analyzing and comparing the capacity of the cloned regions to drive reporter gene expression in treated vs. untreated cells.

2.2. Search for and analysis of an artificial enhancer element for TM directed overexpression of protein

To date, there is no data that describe specific targeting of protein expression exclusively to the TM. Available *in vivo* glaucoma animal models are restricted to overexpression models that make use of either the endogenous myocilin or lens-derived promoters (e.g. Gould et al., 2004; Zillig et al., 2005), targeting expression not only to the TM. In addition to being important for basic research, specific TM-directed expression would enable clinically relevant gene targeting approaches.

Thus, we wanted to create an artificial enhancer element that in combination with the *MYOC* basal promoter would target an overexpression specifically to the TM *in vivo*. We first wanted to analyze the capacity and specificity of cloned enhancer elements to drive reporter gene expression over *MYOC* basal promoter level in TM cells *in vitro*. Later, we aimed to prove the capacity and specificity of candidate elements to drive visible reporter gene expression *in vivo* in a mouse model. The dissertation describes the *in vitro* analysis of candidate elements, the cloning of a candidate enhancer element-driven ß-galactosidase overexpression construct, as well as the creation and analysis of an *in vivo* mouse model.

2.3. Creation of an animal model that would allow a TM directed conditional knock-out

The majority of available animal models relevant for POAG involve myocilin and are restricted to lines that either overexpress (e.g. Zillig et al., 2005), are stably deficient in (e.g. Kim et al., 2001), or show a mutation in one or both of the allelles (e.g. Gould et al., 2006). A conditional knock-out shows many advantages over a stable knock-out. It makes it unnecessary to create a new stable knock-out line for every gene of interest, and it makes it possible to study the effect of a deletion of a gene, that normally would be embryonic lethal, in the adult.

We wanted to create a mouse line that would allow a conditional knock-out in the TM by the Cre/*loxP* system (reviewed by Sauer, 1998) by homologous recombination. We wanted to design and clone a knock-in construct that would target the endogenous myocilin locus and which would allow the Cre recombinase (Cre) to be driven by the endogenous *Myoc* promoter in mouse embryonic stem cells (ESCs). Screening for correct targeting by Southern blot and injection of respective positive clone into blastocysts would then allow the screening for founder animals with a germ line knock-in and the establishment of a mouse line with endogenous *Myoc* promoter-directed expression of Cre. Analyses of spatial and temporal patterns of expression of Cre would then confirm the usefulness of the knock-in mouse line as

a tool for a myocilin expression pattern-like knock-out of any *loxP*-flanked gene of interest. The dissertation describes the design and cloning of the knock-in construct, as well as the screening of mouse ESCs for homologous recombination.

2.4. Analysis of gene expression during corneal fibrosis

Wounding and subsequent fibrosis (scar formation) of the cornea due to trauma, infection or complications during surgery may severely affect corneal transparency and vision. To date, there is no effective way to treat early wound healing in order to minimize scar formation. The main area of investigation has been early molecular and signalling events that evoke a fibrotic response. Experiments indicate that targeting the TGF-ß signalling pathway may be a solution to avert scar formation in the cornea (reviewed by Saika 2006; Saika et al., 2008). Against these facts we wanted to analyze which genes downstream of the TGF-ß signalling pathway are differentially regulated during fibrosis and that may be crucial regulators of corneal transparency.

Our lab earlier generated a transgenic mouse line that due to an overexpression of TGF-ß1 in the lens show a corneal phenotype that in many aspects resemble fibrosis (Flügel-Koch et al., 2002). By microarray analysis we earlier showed that the fibrotic corneas from transgenic animals have hundreds of differentially expressed genes when compared to normal WT corneas (not yet published). We now wanted to validate earlier microarray data for selected interesting genes by RT-real-time PCR. The dissertation describes the criteria for the selection of genes of interest, as well as the validation of these genes as downstream effector genes of TGF-ß1 in leading to the observed opaque fibrotic-like cornea in transgenic mice. Finding and validating downstream TGF-ß signalling targets are important in trying to understand how and through which signalling mechanisms TGF-ß1 evokes an early fibrotic response in the cornea, as well as in finding candidate genes that are responsible for corneal transparency. Studies like this are fundamental for future therapeutic targeting strategies in reducing corneal scar formation.

3. Materials and methods

Recipes for buffers, solutions and media, as well as used laboratory supplies are listed in Chapter 9: Appendix.

3.1. Molecular biology techniques

3.1.1. General cloning techniques

3.1.1.1. Polymerase chain reaction (PCR)

In vitro amplification of DNA was carried out by the PCR technology by using the GoTaq® Green Master Mix (MM) 2 X-Kit. The 2 X MM is an optimized mix containing Taq (from *Thermus aquaticus*) polymerase, 400 µM of each dNTP, 3 mM $MgCl_2$ and buffer. A 25 µl reaction volume was set up as follows (Table 3.1.):

2 X GoTaq® Green MM	12.5 µl
Primer: forward (fw)	0.4 µM
Primer: reverse (rev.)	0.4 µM
Template (plasmid/genomic DNA)	1 - 10 ng
H_20	ad 25 µl

Table 3.1: PCR reaction setup using the GoTaq® Green MM from Promega.

For colony PCR, a bacterial clone was picked with a sterile pipette tip and inserted into the 25 µl reaction mix. The following PCR program (Table 3.2) was modified to be optimal for each type of template, primer pair and amplicon:

Step:	Temperature:	Time:
Initial denaturation	95 °C	2 min
Denaturation	95 ° C	30 s - 1 min
Primer annealing	55 °C – 65.9 °C	30 s - 45 s
Elongation	72 °C	1 min/kb
Final elongation	72 °C	5 - 7 min

Table 3.2: For amplifications by GoTaq® Green MM, variations of the following PCR program were run to be optimal for each type of template, primer pair and amplicon.

30 - 35 cycles of denaturation, primer annealing and denaturation were carried out.

3.1.1.2. Agarose gel electrophoresis

For analysis and purification of DNA, fragments of different size were separated by agarose gel electrophoresis. Depending on expected fragment size, 0.7 – 2.0 % (w/v) agarose was dissolved in 100 - 150 ml of 1 X TBE or 1 X TAE by boiling. The solution was cooled down to ~ 60 °C and EtBr was added at a concentration of 0.1 µg/ml. The mix was poured into a gel rack for polymerization. The DNA samples were mixed with 6 X loading buffer, loaded into the wells of the gel and run for 15 min – 2 h in an electrical field of 120 - 140 V towards the cathode. For the evaluation of fragment size, 0.5 µg of an appropriate molecular weight marker was run in parallel. For the analysis of RNA, the gel chamber equipment was rinsed with 0.5 M NaOH before use to reduce the risk of RNAse contamination. The nucleic acids were visualized by UV-irradiation and subsequent fluorescence of the between the base pairs intercalated EtBr.

3.1.1.3. Extraction of DNA fragments from agarose gel

The extraction of DNA fragments from agarose gel for further cloning applications was achieved by cutting out the DNA fragment of interest with a scalpel under UV-light at low irradiation intensity. The gel slice was put into an Eppendorf tube and the DNA fragment was purified using the NucleoSpin® Extract II kit by following the instructions provided by the manufacturer.

3.1.1.4. Dephosphorylation of 5´-ends

To remove 5´-phosphoryl groups from linearised plasmids bearing equal restriction overhangs, the plasmid was dephosphorylated by treating it with 5 U of antarctic phosphatase per 1 mg of DNA and by adding 1/10 vol. of 10 X antarctic phosphatase reaction buffer. For 5´-extensions and blunt ends, the reaction was allowed to proceed at 37 °C for 15 min, whereas for 3´-extensions the reaction was run for 60 min. Antarctic phosphatase was inactivated for 5 min at 65 °C.

3.1.1.5. Ligation

Subcloning of amplified inserts bearing A-overhangs was carried out by ligation into the pDrive®-cloning vector (Fig. 3.1) by the QIAGEN PCR Cloning kit and the reaction setup in Table 3.3. For a clean PCR reaction, maximally 2 µl of PCR reaction was directly mixed into the ligation. In case of unspecific amplicons, the wanted PCR product was purified via agarose gel electrophoresis and then mixed with the ligation reaction at a volume of 1 - 4 µl. The reaction was allowed to proceed O/N at 4 - 16 °C.

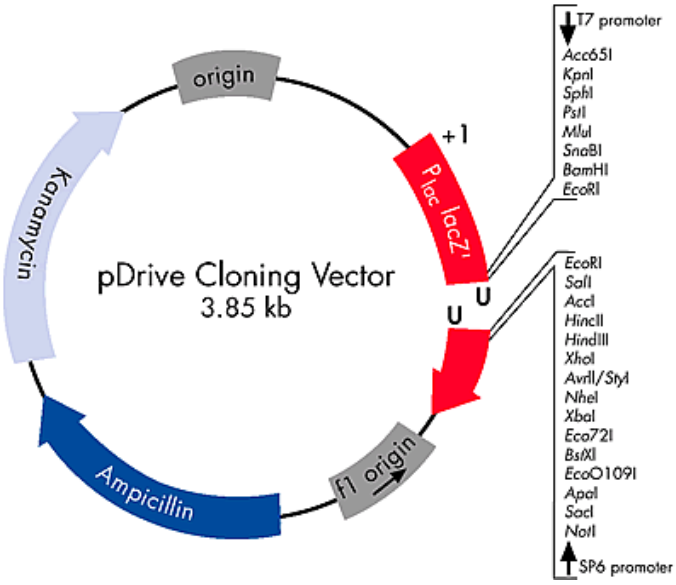

Figure 3.1: Amplified PCR products bearing A-overhangs were subcloned by ligation between the U´-overhangs in the multiple cloning site (MCS) of the pDrive® cloning vector. Positive colonies were selected by blue/white screening and by test cutting the isolated plasmids by one of the restriction enzymes that recognize a restriction site in the MCS. Positive clones were sequenced by using the primers M13 fw (-20) and M13 rev. (source: Qiagen).

pDrive®-vector	1 µl (= 50 ng)
PCR product	1 - 4 µl
2 X Ligation MM	5 µl
H_20	ad 10 µl

Table 3.3: Ligation setup for subcloning of A-overhanged PCR products into pDrive®-cloning vector.

The ligation of inserts bearing restriction overhangs was performed by adding an excess of insert compared to vector (equimolar insert:vector ratios ranging from 2:1 - 5:1) in the ligation reaction (Table 3.4). In parallell, a re-ligation control without insert was setup. The ligation was allowed to proceed at RT O/N. The recombinant plasmid, as well as the re-

ligation control, were directly transformed into competent *E. coli*, or stored at – 20 °C until use.

Insert	2:1 – 5:1 to ng vector
Vector	1:2 – 1:5 to ng insert
10 X T4-ligase buffer	2 µl
T4-ligase	1 µl (= 1 U)
H_20	ad 20 µl

Table 3.4: Ligation setup for inserts bearing restriction enzyme overhangs. In most cases the liagtion was performed in a reaction volume of 20 µl.

3.1.1.6. Transformation of *E. coli*

For the propagation of a recombinant plasmid it was transformed by a heat-chock into chemically competent one shot®TOP10 *E.coli* cells by following the instructions provided by the manufacturer. 20 - 300 µl of the propagated bacteria were plated onto agar plates containing the antibiotics to be selected for. For blue/white screening the bacteria were plated onto agar plates containing IPTG, X-gal and the antibiotic to be selected for. The plates were incubated upside down at 37 °C for 16 - 20 h.

3.1.1.7. Preparing and inoculating of bacterial glycerol stock

For long-term storage of a transformed bacterial culture, 850 µl of an O/N propagated culture was properly mixed with 150 µl sterile 100 % glycerol. The mix was snap-frozen in liquid nitrogen and stored at – 80 °C. If required, a scrape of a glycerol-stock was inoculated for propagation and plasmid isolation.

3.1.1.8. Preparation of plasmid DNA

To isolate and purify a plasmid, a bacterial colony was picked and inoculated to grow O/N in LB-medium containing ampicillin or kanamycin (dependent on plasmid resistance). For mini-preparation of plasmid DNA a volume of 2.5 - 5 ml of bacterial culture was propagated, whereas for midi- and maxi-preparations the volumes were 500 ml and 1 l, respectively. Mini- and midi-preparation of plasmid DNA was carried out by using the NucleoSpin® Plasmid-kit and PureYield™ Plasmid Midiprep System, respectively, by following the instructions provided by the manufacturer. Maxi-preparation of plasmid DNA was carried out by using the QIAfilter Plasmid Maxi Kit, or in the case of endotoxin-free preparations, the EndoFree Plasmid Maxi Kit by following the instructions provided by the manufacturer. For mini-preparations, the DNA was eluted in 50 - 100 µl of nuclease-free H_20. For midi- and maxi-preparations the DNA was, depending on pellet size, dissolved in 500 µl – 2 ml of (endo) nuclease-free H_20.

3.1.1.9. Quantification of nucleic acids

Spectrophotometric analysis of DNA and RNA was carried out by measuring the absorptions of UV-light at a wavelength of 260 nm by appropriate sample dilutions. The absorbance of a sample at a given wavelength is proportional to its optical density, and the concentration can be calculated by the formula:

c (µg/ml) = OD x V x Fm, where

OD = optical density

c = concentration

V = dilution factor

Fm = factor of multiplicity (= 50 for double-stranded (ds)DNA, 40 for RNA)

The purity of nucleic acids was measured by calculating the ratio of absorbance of nucleic acid at 260 nm to the absorbance of protein at 280 nm. For a pure DNA/RNA preparation this ratio is 1.8 - 2.0.

3.1.1.10. Restriction digestion

Depending on approach, 0.5 - 2 µg of plasmid DNA was digested in a volume of 10 - 50 µl by the restriction setup in Table 3.5. For double digests, equal amounts of U of enzyme were added.

DNA	0.5 – 2 µg
For the enzyme appropriate 10 X restriction buffer	1/10 vol.
10 X BSA (if required for the restriction enzyme)	1/10 vol.
Restriction enzyme	1 – 10 U/1 µg DNA
H_20	Ad to appropriate reaction volume

Table 3.5: Restriction setup for plasmid DNA. Depending on approach (test-cut or preparative cut), 0.5 – 2 µg of DNA was digested.

The reaction was allowed to proceed at 37 °C for 1 - 2 h. For direct use of a linearized plasmid in downstream cloning applications, the enzyme(s) were heat inactivated at their respective temperature for heat inactivation. In the case of equal restriction overhangs, the linearized plasmid was dephosphorylated to avoid re-ligation. The plasmid was purified with the NucleoSpin® Extract II kit by following the manufacturer´s instructions. To recover a released insert, the restriction reaction was resolved on an agarose gel and the insert was purified as described in section 3.1.1.3.

3.1.1.11. Sequencing of DNA

Plasmid DNA containing an insert to be sequenced was mixed at a concentration of 150 - 300 ng with 1.25 µM of primer and H_2O in a final volume of 8 µl and sent to GENEART AG. The sequences were analyzed by using the Vector NTI® Software from Invitrogen.

3.1.2. Molecular biology techniques specific for the creation of a ß-galactosidase overexpression mouse line

3.1.2.1. Cloning of ß-galactosidase overexpression construct

As backbone plasmid for cloning of a ß-galactosidase overexpression construct we used psD*LacZ*-pA, a gift from Prof. Wegner (Institute of Biochemistry, University of Erlangen-Nürnberg). psD*LacZ*-pA already contained the gene for ß-galactosidase, *LacZ*, as well as an SV late polyA signal (fig. 3.2). The function of the polyA signal is to confer stability to, and to assist in termination, export and translation of the mRNA (reviewed by Bernstein and Ross, 1989; reviewed by Sachs, 1990).

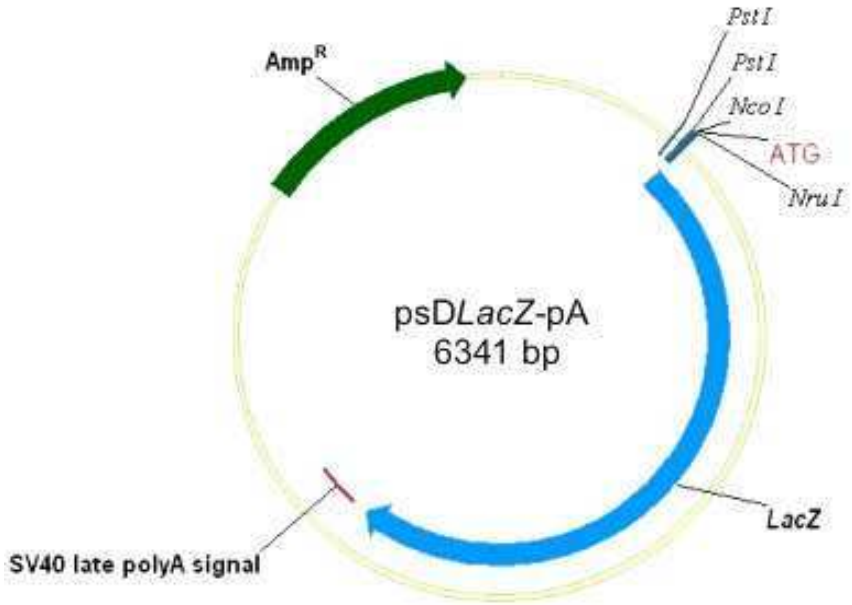

Figure 3.2: The plasmid psD*LacZ*-pA, a gift from Prof. Wegner, served as backbone for the ß-galactosidase overexpression construct. This plasmid already contained the gene for ß-galactosidase, *LacZ*, as well as an SV late polyA signal. For cloning, we used the restriction enzyme recognition sites *Pst*I, *Nco*I and *Nru*I.

We amplified the sequence containing the enhancer RAREß/PITX3/FOX and the human *MYOC* basal promoter p313+67 in one stretch from the Luciferase-reporter construct pGL3-RAREß/PITX3/FOX-p313+67 by the primer pairs *Pst*I-RAREß fw and *Nco*I-p313+67 rev. (Fig. 3.3).

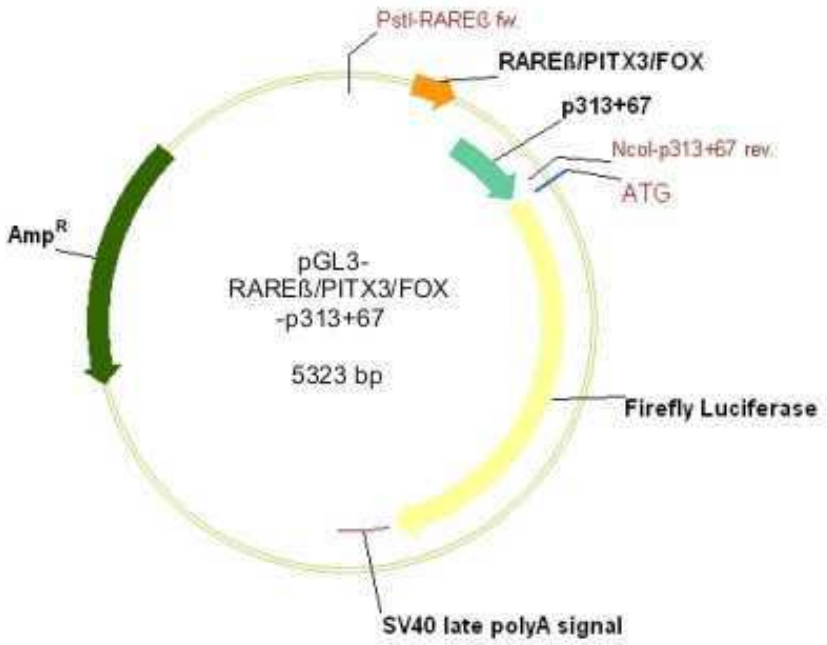

Figure 3.3: The artificial enhancer element RAREß/PITX3/FOX and the human *MYOC* basal promoter p313+67 were amplified in one 780 bp stretch by the primer pair *Pst*I-RAREß fw and *Nco*I-p313+67 rev. (depicted in red) from the Luciferase-reporter construct pGL3-RAREß/PITX3/FOX-p313+67. This construction had earlier been shown to confer high expression of reporter in cultured human TM cells (Results: Fig. 4.8). The primer pair had been designed to confer restriction enzyme recognition site overhangs that would able final cloning of the amplicon into psD*LacZ*-pA in front of the *LacZ* start ATG (Fig. 4.10).

The 780 bp RAREß/PTX3/FOX-p313+67 amplicon was subcloned into pDrive®-cloning vector and, to be sure that no nucleotide changes had occurred during amplification, sequenced. The product was further cloned into psD*LacZ*-pA between the restriction enzyme overhangs *Pst*I and *Nco*I (Fig. 4.10). When attached to its amino terminus, the short sequence Pro-Lys-Lys-Lys-Arg-Lys-Val derived from SV40 large T-antigen can act as a nuclear localization signal to direct mature ß-galactosidase into the nucleus of mammalian cells (Kalderon et al., 1984). A reiteration of this nuclear localization signal (NLS) significantly increases the efficiency of nuclear polypeptide transport in mammalian cells (Fischer-Fantuzzi and Vesco, 1988). To ensure that the mature ß-galactosidase would be effectively

imported into the nucleus, a repetitive NLS, 3 X NLS, was cloned in frame with the *LacZ* open reading frame (ORF), just behind the codon for the start ATG between the restriction enzyme overhangs *Nco*I and *Nru*I (Fig. 4.10). We created the ds3 X NLS by phosphorylating and annealing two long complementary oligonucleotides coding for this sequence. The oligos had been designed to create correct restriction enzyme half-sites for cloning at each end of the annealed duplex, as well as not to cause a frame-shift of the *LacZ* ORF after insertion (Fig 3.4).

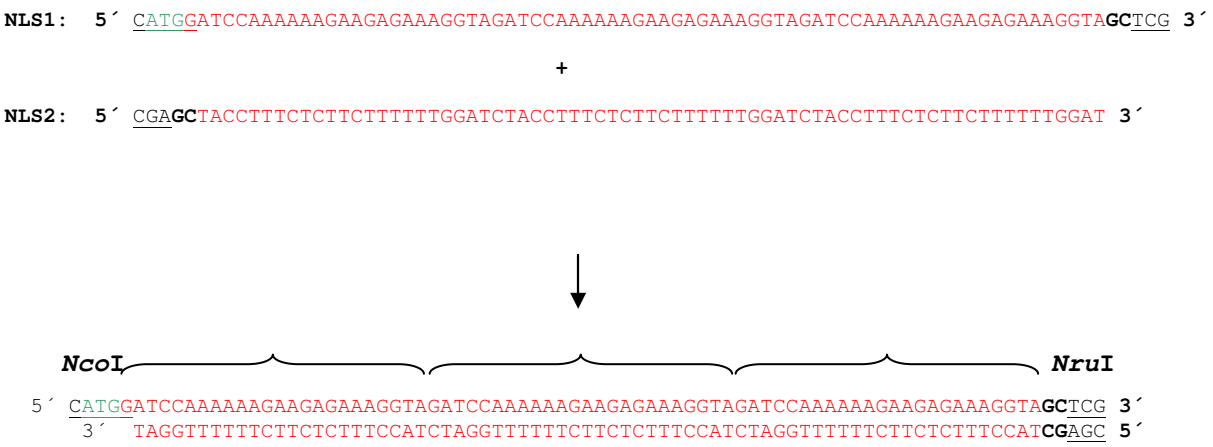

Figure 3.4: Complementary single-stranded long oligos NLS1 and NLS2 were phosphorylated and annealed to create a 72 bp 3 X NLS duplex that aimed to direct ß-galactosidase overexpression into the nucleus. The oligos had been designed to create correct restriction enzyme recognition half-sites for cloning at each end of the annealed duplex, as well as not to cause a frame-shift of the *LacZ* ORF after insertion. 3 X NLS is depicted in red, where the recurring NLS motif is marked with horizontal large curly brackets. Start ATG of *LacZ* is depicted in green and restriction enzyme recognition half-sites for *Nco*I and *Nru*I are underlined. After annealing, the phosphorylated duplex was immediately cloned into psD-*LacZ*-pA between the restriction enzyme recognition sites *Nco*I and *Nru*I (Fig. 4.10).

The phosphorylated 3 X NLS duplex was cloned into psD*LacZ*-pA between the restriction enzyme overhangs *Nco*I and *Nru*I in-frame with the *LacZ* ORF (Fig. 4.10). To be sure that the long oligos creating the 3 X NLS had annealed properly, the overexpression construct was sequenced over this region by the primer LacZ rev. 3. The construct was propagated in bacteria and extracted as an endonuclease-free maxi-preparation (section 3.1.1.8).

3.1.2.1.1. Phosphorylation of DNA 5´-OH ends

The phosphorylation of single-stranded (ss) DNA oligonucleotides at their 5´-OH overhangs was carried out by mixing 8 µl of substrate with 1 µl (= 10 U) of T4 polynucleotide kinase (PNK) and 1 µl of 10 X T4 ligase buffer containing ATP. The reaction was incubated at 37 °C for 30 min, followed by incubation at 65 °C for 20 min. The phosphorylated oligonucleotides were stored at + 4 °C until use, or directly used for annealing as described below.

3.1.2.1.2. Annealing of oligonucleotides

The annealing of phosphorylated DNA oligonucleotides to create an insert for ligation into a vector was carried out by mixing 8 µl of one PNK-reaction with 10 µl of the other PNK-reaction (described above). 2 µl of 10 X annealing buffer was added and the mixture was vortexed. The annealing reaction was allowed to proceed in a heat block at 95 °C for 3 min, after which it was slowly let to cool down to RT. The mixture was vortexed and subsequently ligated into an appropriate dephosphorylated vector.

3.1.2.2. Purification of DNA for pronuclear injection

To get a highly pure transgene for injection into a male pronucleus of a fertilized mouse oocyte, the transgene was cut out O/N from 50 µg endotoxin-free plasmid construct in a reaction volume of 400 µl. An aliquote of the reaction was proved for digestion by agarose gel electrophoresis. The reaction was dissolved by agarose gel electrophoresis on a 0.7 % agarose gel using a clean gel apparatus and sterile filtrated 1 X TAE buffer. No DNA standards were used because of the risk of contamination. The sample was run until the transgene had completely separated from the vector backbone. The transgene was cut out from the gel under UV-light of low intensity (320 nm wave length) and transferred into a dialysis bag. The bag was filled with fresh running buffer and closed with clamps. The dialysis bag was fixed across the electrical field in the running chamber and the transgene was electroeluted out from the gel into the buffer of the bag for ~ 1 h at 80 V. To force the transgene back from the dialysis bag wall into the solution, the polarity of the electrophoresis was changed by changing the orientation of the dialysis bag by 180 ° and by continuing the run for another 30 s at 80 V. The electroelution was controlled under UV-light of low intensity. The solution containing the transgene was transferred into a sterile Falcon tube with a syringe needle plunged through the wall of the dialysis bag. The DNA-solution was diluted 1:2 with sterile filtrated low-salt buffer. The mixture was slowly pressed through an equilibrated (equilibration was carried out as described by the manufacturer) elutip-D® column with a flow rate of 0.5 - 1.0 ml/min to adsorb the DNA to the column matrix. The column was washed twice with 5.0 ml of low-salt buffer. The transgene was eluted into an eppendorf tube with 400 µl of sterile filtrated high-salt buffer. 1.0 ml of EtOH abs. was added and the mixture was put into – 20 °C O/N to enhance the yield of precipitation. The transgene was precipitated by centrifugation at 12 300 rpm for 30 min at + 4 °C and washed three times with ice cold 70 % EtOH abs. The pellet was air-dried and dissolved into an appropriate volume of sterile filtrated injection buffer to give an endconcentration of 100 ng/µl. The purity and the spectrophotometrically measured concentration were verified by loading different concentrations of the transgene on an agarose gel and by comparing the band intensities with those of a reference DNA of known concentration.

3.1.3. Molecular biology techniques specific for the creation of a *myoc* knock-in mouse line

3.1.3.1. Cloning of *myoc* knock-in construct

A myocilin knock-in construct, which would allow the expression of Cre under the control of the endogenous *myoc* promoter, was designed in the way that aimed the construct to be integrated at the published mouse *myoc* translational start ATG (Tomarev et al., 1998) by homologous recombination (Tymms and Kola, 2001; Ch. 3). Published information about the transcriptional regulation of *myoc* is restricted to the 5´-UTR of the gene (Kirstein et al., 2000; Shepard et al., 2001). Our promoter studies corroborate a theory that some intragenic regions of *myoc* are able to drive expression above basal promoter level (Fig. 4.3). Consequently, the knock-in construct was designed in a way that would allow a homologous recombination without deletion of any intragenic regions (Fig. 4.22). As construct backbone vector, we chose pTV-0 (Fig. 3.5), a kind gift from Prof. Michael Wegner. pTV-0 contains two MCSs that were of advantage in the introduction of the two homologous flanks. The backbone carries genes for neomycine resistance (Neo), as well as for thymidine kinase (TK), which are required for positive and negative selection, respectively, of electroporated ESCs (Tymms and Kola, 2001; Ch. 3).

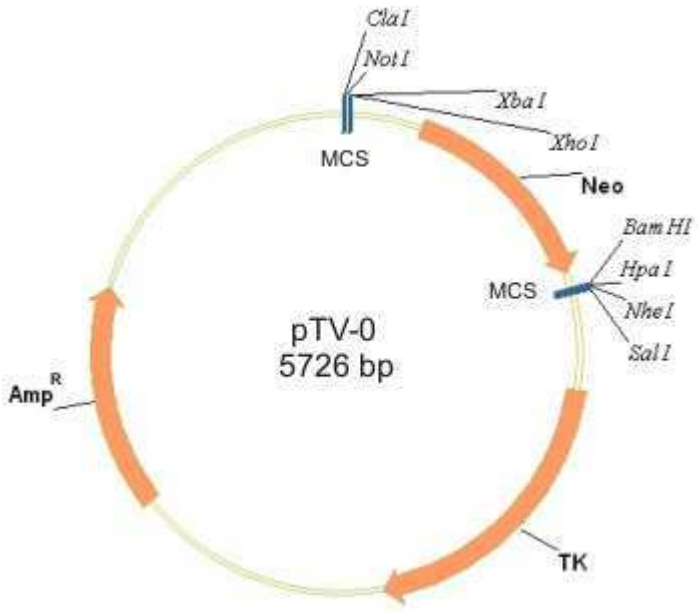

Fig. 3.5: pTV-0, a gift from Prof. Wegner, served as backbone vector for the *myoc* knock-in construct. The vector carries two MCSs that were of advantage in the introduction of the two homologous flanks. The genes for neomycin resistance, Neo, and thymidine kinase, TK, are required for positive and negative selection, respectively, of electroporated ESCs (Tymms and Kola, 2001; Ch. 3).

3.1.3.1.1. Cloning strategy and sequencing of NLS-Cre-IRES-eGFP

The plasmid pSL1180 bearing a 2484 bp long NLS-Cre-IRES-eGFP construction, followed by a 784 bp long rabbit ß-globin intron and an SV40 polyA tail, was a kind gift from Ruth Ashery-Padan (Dept. of Human Genetics, Tel Aviv University, Israel). In this construction Cre contains a NLS that assures that the synthesized protein will be translocated into the nucleus (Le et al., 1999). The gene for IRES (internal ribosomal entry site) enables 5´-cap independent translation of an mRNA-molecule (Pelletier and Sonenberg, 1988; Jang et al., 1988). This enables Cre and the gene for the visual marker eGFP (enhanced green fluorescent protein) (Goetz et al., 1997) to be translated polycistronically, i.e. as one polypeptide, from the same promoter.

Because the exact nucleotide sequence of the gift plasmid was unknown, and because we wanted to avoid any cloning problems arising from unknown restriction enzyme recognition sites within this construction, we first sequenced the plasmid through. We started the sequencing with primers that bind the backbone plasmid at the 5´- and 3´- ends of NLS-Cre-IRES-eGFP-intron-polyA (Cre fw 1 and Cre rev. 1, respectively). Based on these sequences, we designed the next primers (Cre fw 2 and Cre rev. 2) that allowed further inward sequencing of the construction. In this way, we sequentially sequenced a 4232 bp region of the plasmid beginning from the 5´- and 3´-end. By assembling the sequences by the Vector NTI® Software we got the whole 5´-NLS-Cre-IRES-eGFP-intron-polyA-3´ sequence (Fig. 3.6).

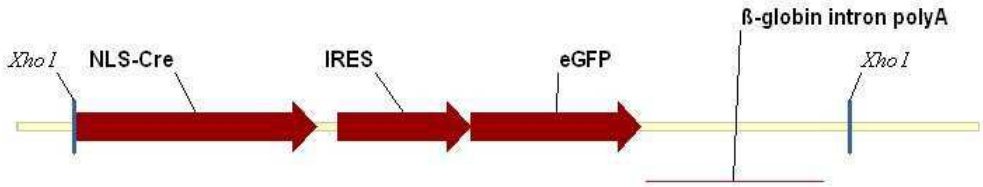

Fig. 3.6: Based on overlapping sequence data, the exact nucleotide sequence of NLS-Cre-IRES-eGFP with its ß-globin intron polyA-tail was reconstituted. Based on the data we made up a cloning strategy for the *myoc* knock-in construct. We aimed to release NLS-Cre-IRES-eGFP with its polyA-tail from the backbone by restriction with *Xho*I and ligate the 3416 bp fragment into pTV-0-5´-flank-3´-flank, just downstream of the 5´-flank.

Based on the sequence data we made up a cloning strategy that first aimed to introduce the homologous flanks into the pTV-0 backbone vector by the restriction enzyme overhangs *Not*I/*Xho*I for the 5´-flank, and *Nhe*I/*Sal*I for the 3´-flank. After that we aimed to release NLS-Cre-IRES-eGFP-intron-polyA from pSL1180 by restriction with *Xho*I and to clone the 3416 bp fragment in correct orientation downstream of the 5´-homologous flank (Fig. 4.22).

3.1.3.1.2. Amplification of the 5´-homologous flank

The 5´-flank is homologous to 3072 bp of the 5´-UTR of *myoc* and ends at the described start ATG of the mouse gene (Tomarev et al., 1998). It was amplified for 35 cycles from mouse ESC DNA by the primer pair *Not*I-5´-flank fw and *Xho*I-5´-flank rev. by the following reaction conditions (Table 3.6):

Step:	Temperature:	Time:
Initial denaturation	95 °C	2 min
Denaturation	95 °C	1 min
Primer annealing	65.9 °C	30 s
Elongation	72 °C	4 min
Final elongation	72 °C	7 min

Table 3.6: Reaction conditions for amplification of the 5´-homologous flank from mouse ESC DNA. 35 cycles of denaturation, primer annealing and elongation were performed.

The amplified 5´-flank was purified via agarose gel electrophoresis and subcloned into the pDrive®-cloning vector for sequencing.

3.1.3.1.3. Amplification of the 3´-homologous flank

The 3´-homologous flank is homologous to a 2268 bp stretch of exon 1 and intron 1 of mouse *myoc*. It was amplified for 35 cycles from mouse ESC DNA by the primer pairs *Nhe*I-3´-flank fw and *Sal*I–3´-flank rev. by the following reaction conditions (Table 3.7):

Step:	Temperature:	Time:
Initial denaturation	95 °C	2 min
Denaturation	95 °C	1 min
Primer annealing	59°C	45 s
Elongation	72 °C	2 min
Final elongation	72 °C	5 min

Table 3.7: Reaction conditions for amplification of the 3´-homologous flank from mouse ESC DNA. 35 cycles of denaturation, primer annealing and elongation were performed.

The amplified 3´-flank was purified via agarose gel electrophoresis and subcloned into the pDrive®-cloning vector for sequencing.

3.1.3.2. Purification of DNA for electroporation into mouse ESCs

To get highly pure DNA for the electroporation into mouse ESCs, 150 µg of endonuclease-free plasmid construct was linearized in a reaction volume of 500 µl O/N. The linearization was proved by running a small aliquote of the reaction on an agarose gel. 1 vol. of phenol/chloroform/isoamylalcohol (in the proportions 24:24:1, respectively) was added to the linearized plasmid, the mix was vortexed, and transferred to a pelleted Phase Lock Gel™ (preparation of the Phase Lock Gel™ tube was carried out as described by the manufacturer) tube. The sample was centrifuged at 12 000 g for 20 min at + 4 °C, whereby the organic phase and interface became trapped below the phase lock gel barrier and the aqueous phase containing the DNA was found above the gel. 500 µl phenol/chloroform (1:1) was added to the aqueous phase, the mixture was vortexed and centrifuged at 12 000g for 20 min at + 4 °C. The upper phase was transferred into a fresh eppendorf tube, followed by the addition of 1/10 vol. of sterile 1 M natrium acetate (pH 5.5) and 2.5 vol. of 95 % EtOH abs. The mix was vortexed and held on ice for 10 min. DNA was precipitated by centrifugation at 13 200 rpm for 10 min at + 4 °C. The pellet was washed with 500 µl 80 % EtOH abs. by mixing and centrifugation at 13 200 rpm for 5 min at + 4 °C. The pellet was air-dried and dissolved into an appropriate volume of sterile nuclease-free H_20 to give an endconcentration of 1 µg/µl.

3.1.3.3. Screening of ESC clones for homologous recombination

3.1.3.3.1. Amplification and cloning of 5´-flank and 3´-flank probes

DNA templates for radioactive probes for Southern blot were amplified from mouse ESC-DNA by the primer pair 5´-probe fw and 5´-probe rev. for the 5´-flank probe, and 3´-probe fw and 3´-probe rev. for the 3´-flank probe. The probes were designed to bind outside of the recombinated construct, but within the resulting restriction fragments (Fig. 4.23). The PCR-programs for the amplifications were as follows (Tables 3.8 and 3.9):

5´-flank probe (360 bp):

Step:	Temperature:	Time:
Initial denaturation	95 °C	2 min
Denaturation	95 °C	1 min
Primer annealing	61 °C	30 s
Elongation	72 °C	30 s
Final elongation	72 °C	5 min

Table 3.8: Reaction conditions for the amplification of the 360 bp template for the radioactive 5´-flank probe. 35 cycles of denaturation, primer annealing and elongation were performed.

3´-flank probe (729 bp):

Step:	Temperature:	Time:
Initial denaturation	95 °C	2 min
Denaturation	95 °C	1 min
Primer annealing	65.7 °C	30 s
Elongation	72 °C	1 min
Final elongation	72 °C	5 min

Table 3.9: Reaction conditions for the amplification of the 729 bp template for the radioactive 3´-flank probe. 35 cycles of denaturation, primer annealing and elongation were performed.

The amplified probes were cloned into the pDrive®-cloning vector and propagated for midipreparation of plasmid DNA. The pDrive-probe plasmids were stored at – 20 °C. For Southern blot, linear probe templates were amplified from the midipreps, purified from the agarose gel and used as templates for radioactive labelling. Purified linear probe templates were stored at – 20 °C.

3.1.3.3.2. Radioactive labelling of DNA probes

The radioactive labelling of DNA probes to be used in Southern blot was carried out by using the Random Primers DNA Labeling System by following the instructions provided by the manufacturer. The labelling system takes advantage of the Klenow fragment, the large protein subunit produced by the cleavage of *E. coli* DNA polymerase I (Klenow and Henningsen, 1970). The Klenow fragment possesses a 5′ → 3′ polymerase activity and thus fills up the gaps produced by bound hexamer random primers with labelled and unlabelled deoxynucleotides.

50 - 100 ng of linear dsDNA probe template was diluted in 23 µl of H_20. To separate the DNA double helix, the sample was boiled at 95 °C for 5 min and immediately put onto ice to avoid reannealing. 2 µl each of dATP, dGTP and dTTP, and 15 µl of Random Primers Buffer Mixture were added and the sample was mixed. The following steps were performed in an isotope laboratory: 5 µl of [α-^{32}P]-labeled dCTP (= 50 µCi) and 1 µl (3 U) of Klenow fragment were added and the total 50 µl reaction volume was mixed. The reaction was allowed to proceed for 1 h at RT. Mini Quick Spin™ Columns for the elimination of unincorporated nucleotides were prepared and the probe was purified according to the instructions provided by the manufacturer. The double-stranded labelled probe was denatured at 95 °C for 3 min and immediately put onto ice to avoid reannealing. Subsequently, the whole reaction volume (50 µl) was added to the hybridization solution (21.2 ml).

3.1.3.3.3. Southern blot

Electroporated ESC clones were screened for homologous recombination by Southern Blot (Southern, 1975). For each clone, the following restriction reaction was setup (Table 3.10) and allowed to proceed at 37 °C O/N.

Genomic DNA	41.5 µl
Restriction enzyme (20 U/µl)	2 µl
Appropriate 10 X restriction buffer	5 µl
RNAseA (10 µg/µl)	1 µl
100 X BSA	0.5 µl
Total volume	50 µl

Table 3.10: Restriction setup for each ESC clone to be screened for homologous recombination by Southern blot.

The reaction was resolved on a 0.7 % agarose gel in 1 X TAE for 2 h at 120 V. To prove for complete digestion, the resolved DNA was visualized under UV-light at low intensity and photographed. The DNA was prepared for membrane transfer by treating the gel as follows (Table 3.11).

Treatment:	**Solution:**	**Time:**
Depurination	0.25 M HCl	15 min
Rinsing of gel	H_20	15 min
Denaturation	Denaturation solution	2 X 15 min
Neutralization	Neutralization solution	2 X 15 min
Equillibration of gel	20 X SSC	10 min

Table 3.11: The following steps of gel treatments were performed to prepare the high molecular weight dsDNA for transfer to the blotting membrane. All incubations were carried out by gentle rocking.

The DNA was transferred to a positively charged nylon membrane by building up a capillary transfer assembly in a tray filled with 20 X SSC. Beginning from the bottom, the assembly was composed of saturated blotting filter papers, the gel, an equilibrated nitrocellulose membrane, saturated blotting filter papers and paper towels. A weight of 250 g was placed on top of the assembly and the DNA was let to transfer upwards O/N with the capillary force from the gel into the membrane. The membrane was air-dried and the DNA was cross-linked to the membrane in a UV-transilluminator by exposing it to 0.160 J of UV-light. The membrane was put into a hybridization vial filled with 20 ml of pre-hybridization solution. To prevent the probe from unspecific hybridization, the memrane was pre-hybridized in a hybridization oven at 42 °C for 1 h. The hybridization of radioactive probe to its complementary DNA fragment was carried out in an isotope laboratory. Dextransulphate and denatured [α-^{32}P]-labeled probe were added to the pre-hybridization solution. The hybridization was let to proceed in a hybridization oven at 42 °C O/N. The following steps of washing the membrane were performed (Table 3.12):

Step:	Solution:	Duration:	Temperature:
1.	2 X SSC + 0.5 % SDS	5 min	RT
2.	2 X SSC + 0.1 % SDS	15 min	RT
3.	0.1 X SSC + 0.1 % SDS	30 min	65 °C

Table 3.12: Steps for washing the radioactively labeled membrane.

The radioactive membrane was wrapped in thin plastic wrap and exposed to a phosphoimager screen in a dark cassette for 24 h. The hybridized [α-^{32}P]-labeled probes were visualized by reading the screen in a phosphoimager. The obtained data were analyzed by using the Aida Image Analyzer V.3.28 software.

3.1.4. Molecular biology techniques specific for the analysis of corneal gene expression in TGF-ß1 overexpression mice

3.1.4.1. Preparation of mouse corneas

Newborn WT and transgenic (TG) mice were sacrified for gene expression analysis by quickly cutting off their heads. The preparation of the corneas was carried out under a binocular by freeing the eye from overlying skin with scissors. The cornea was prepared *in situ* by making an incision through the cornea into the anterior chamber and by extending this incision along the corneal-conjunctival border. The cornea could then easily be lifted up by mini-forceps. The corneas from both eyes were put into a cooled eppendorf tube, immediately snap-freezed in liquid nitrogen and stored at – 80 °C until use.

3.1.4.2. RNA isolation

Stored corneas were thawed on ice. RNA was isolated by adding 500 µl of TRI reagent® and by incubating the sample for 5 min at RT. The tissues were homogenized with a tissue shredder and centrifuged at 12 000 for 10 min at + 4 °C to pellet cell debris and contaminants. The supernatant was transferred into a fresh eppendorf tube and 1/5 vol. of chloroform was added. The sample was mixed for 15 s, incubated for 2 - 3 min at RT and centrifuged at 12 000 g for 15 min at + 4 °C. The aqueous phase was carefully transferred into a fresh eppendorf tube and 350 µl isopropanol was added. The sample was vortexed and put into – 20 °C O/N to enhance the yield of precipitation. RNA was precipitated by centrifugation at 12 000 g for 10 min at + 4 °C. The pellet was washed twice by adding 700 µl of 75 % EtOH abs., by vortexing the mix, and by centrifugation at 7 500 g for 5 min at + 4 °C. The pellet was air-dried and dissolved in 20 µl of sterile nuclease-free H_20. The quantity and purity of RNA was analyzed spectrophotometrically in a dilution volume of 1:20. The integrity of RNA was analyzed by running 2 µl of RNA on an agarose gel. If the RNA is not degraded, most of the

sample should be visualized as two bands corresponding to the 28S and 18S spliced ribosomal RNA subunits (Farrell, 1993). RNA of good quality was stored at – 80 °C.

3.1.4.3. Preparation of cDNA (= complementary DNA)

RNA that had been stored at – 80 °C were transcribed into cDNA by using the iScript™ cDNA Synthesis Kit. The kit takes advantage of an RNAse inhibited RNAse H+ reverse transcriptase (RT), as well as a blend of oligo (dT) and random hexamer primers to initiate the transcription of mainly polyA-tailed mRNA. Per sample, 448.5 ng of RNA was transcribed into cDNA by adding 4 µl of 5 X iScript reaction mix, 1 µl of iScript RT and nuclease-free H_20 to fill up the volume to 20 µl. To prove the sample for any DNA contaminants, a control sample without RT (referred to as the - RT-reaction) was mixed in parallel. The reaction was allowed to proceed in a mastercycler by using the following steps of reaction conditions (Table 3.13):

Step:	Temperature:	Time:
1. Primer annealing	25 °C	5 min
2. Reverse transcription	42 °C	30 min
3. Inactivation of RT	85 °C	5 min
4. Cooling down reaction	4 °C	∞

Table 3.13: Reaction steps for preparation of cDNA by the iScript™ cDNA Synthesis Kit.

The cDNA was stored at – 20 °C until use.

3.1.4.4. Primer design

Primer pairs for quantitative RT-PCR that spanned intron boundaries of the mouse genome were designed by the Universal ProbeLibrary System from Roche (https://www.roche-applied-science.com/sis/rtpcr/upl/index.jsp?id=UP030000) for genes selected according to the criteria described in Results 4.5.1. Target gene names, primer sequences, positions of primer binding sites within mouse genome and product sizes are listed in Table 3.14.

Target gene:	Primer sequence:	Position in mouse genome:	Product size:
Egr2	fw: 5´-ctacccggtggaagacctc-3´ rev.: 5´-aatgttgatcatgccatctcc-3´	317 - 335 408 - 428	112 bp
Fst	fw: 5´-aagcattctggatcttgcaact-3´ rev.: 5´-gataggaaagctgtagtcctggtc-3´	928 - 949 988 - 1011	84 bp
Gjb2	fw: 5´-acccatttcggaccaacc-3´ rev.: 5´-aatccatcttgtcctctggatg-3´	94 - 111 217 - 238	145 bp
Krt14	fw: 5´-tcccaattctcctcatcctc-3´ rev.: 5´-atgaccttggtgcggatct-3´	1358 - 1377 1431 - 1449	92 bp
Lamb3	fw: 5´-agccagcaggcaatgaat-3´ rev.: 5´-gccggtccttcaactctgt-3	3338 - 3355 3392 - 3410	73 bp
Lama3	fw: 5´-ccaggagctgctgaaacc-3´ rev.: 5´-tggtgcctgtgtgaaacact-3´	8997 - 9014 9063 - 9082	86 bp
Mmp13	fw: 5´-cagtctccgaggagaaactatga-3´ rev.: 5´-ggactttgtcaaaaagagctcag-3´	895 - 917 966 - 988	94 bp
Igfbp6	fw: 5´-agagaccggcagaagaatcc-3´ rev.: 5´-gctgcagtactgaatccaagtg-3´	586 - 605 673 - 694	109 bp
Oca2	fw: 5´-gagcctagtgagatcgtcgaa-3´ rev.: 5´-gcaagcactttctccagca-3´	1733 - 1753 1839 - 1857	125 bp
Trpm1	fw: 5´-cctcatggcctgttatctcc-3´ rev.: 5´-acttgacttcaaagaaggtattgttg-3´	749 - 768 812 - 837	89 bp
Dkk2	fw: 5´-ctggtacccgctgcaataat-3´ rev.: 5´-catggttgcgatctctatgc-3´	1085 - 1104 1170 - 1189	105 bp
Ptgds	fw: 5´-ggctcctggacactacacct-3´ rev.: 5´-atagttggcctccaccactg-3´	360 - 379 416 - 435	76 bp

Table 3.14: Primer pairs for quantitative RT-PCR were designed for selected genes by the Universal ProbeLibrary System (Roche). The list summarizes target gene names, primer sequences, positions of primer binding sites within mouse genome and product sizes.

3.1.4.5. Quantitative real-time PCR

To analyze the differences in corneal gene expression between WT and TG mice, a quantitative real-time PCR was performed by using cDNA as a template. In an optimal RT-reaction the amount of a given transcribed cDNA corresponds to the amount of copies of its mRNA in the original RNA sample. Thus, the rate of amplification for a given gene from the cDNA template mix can be used to calculate the number of copies of its mRNA in the original sample. In practice, the PCR was carried out by using a combination of the multicolour iQ™5 RT-PCR Detection System and an iCycler® thermal cycler. The system takes advantage of SYBR-Green I, a fluorescent dye that binds non-specifically to dsDNA (Witzthum et al., 1999). As the amplification reaction proceeds into its exponential phase, the intensity of the fluorescence exceeds a background level. This time-point is called the cycle-threshold, C_T, for that gene. The more cDNA for a given gene in the template the less cycles the reaction has to proceed until it reaches its C_T. To get a relative quantification of the expression levels of tested genes, their C_T-values were compared with those of selected reference genes. Reference genes are referred to as genes that function as "house-keeping" genes in the investigated tissue and that, independent of treatment, show no transcriptional regulation between samples. Because of variance in composition, each amplicon has its individual melting temperature, resulting in an individual sharp melting curve. To avoid any false positive results caused by primer dimers or mis-priming, the melting curves for each sample product were analyzed for their purity.

To get reliable data, duplicates or triplicates of each sample were investigated. For each investigated gene, one – RT-reaction and one NTC (no template control) were run in parallel. Because of the huge amount of samples, two different master mixes for the reagents were

mixed. The 2 X MM was mixed first and was a part of the SYBR-Green I (Sg) MM (Tables 3.15 A and B).

A) 2 X MM:

10 X buffer	300 µl
$MgCl_2$ (25 mM)	120 µl
dNTPs (25 mM each)	24 µl
H_20	1006.5 µl
Total volume	1450.5 µl

B) SgMM (for one reaction):

2 X MM	7.24 µl
Taq Polymerase (5 U/µl)	0.06 µl
SYBR-Green I (7.4 % (w/v) in DMSO)	0.19 µl
Fluorescein (1:100 in H_20)	0.015 µl

Table 3.15: Master mix for 2 X MM (A) and one Sg (SYBR-Green I) MM (B). The 2 X MM was made up first and was then used as a component in the SgMM. The 2 X MM can be stored at - 20 ° for later use.

In the next step, master mixes for primers, cDNAs, RT-reactions and NTCs were setup (Tables 3.16 A, B and C).

A) cDNA/-RT mix (10 µl):

SgMM	7.5 µl
cDNA/-RT-reaction	0.7 µl
H_20	ad 10 µl

B) NTC-mix (10 µl):

SgMM	7.5 µl
H_20	2.5 µl
Total volume	10 µl

C) Primer mix (5 µl):

Primer fw (100 µM)	0.08 µl
Primer rev. (100 µM)	0.08 µl
H_20	ad 5 µl

Table 3.16: A) The cDNA/-RT-reaction mix (10 µl) for one reaction. The amount cDNA/-RT-reaction was taken directly from the RT/-RT-reaction volume of 20 µl. B) The NTC mix (10 µl) for one reaction. C) The primer mix (5 µl) for one reaction.

Finally, the cDNA/-RT-reaction/NTC-mix of 10 µl was added together with the 5 µl primer mix in a reaction well of a 96-well PCR plate to give a total reaction volume of 15 µl. The PCR-plate was covered with a sealing film and the samples were shortly centrifuged. The reactions were run by the following steps of reaction conditions (amplification + melting curve) (Table 3.17):

Step:	Temperature:	Time:
1. Taq polymerase activation	95 °C	15 min
2. Amplification 40 cycles	95 °C ↔ 60 °C	10 s ↔ 40 s
3. Final elongation	95 °C	1 min
4. Transit to melting cycles	55 °C	1 min
5. 81 cycles for melting curve	55 °C + 0.5 °C/cycle	6 s

Table 3.17: The quantitative real-time PCR by the iQ™5 RT-PCR Detection System and iCycler® thermal cycler was run by the following steps of reaction conditions. The program combines the amplification with the melting curve calculation.

The data were calculated and evaluated by using the iQ Optical System Software version 2.0 to give the relative expression values for each sample. The relative expression values are calculated by the comparative C_T- method, $\Delta\Delta C_T$, according to the formula

$$\Delta\Delta C_T = \Delta C_{T\,(sample)} - \Delta C_{T\,(reference\ gene)}$$ (Livak et al., 2001)

The relative expressions were graphically presented by transferring the obtained expression data into Microsoft® Excel. The statistical significance was calculated according to the student´s *t*-test by assessing a *p*-value of $p < 0.05$ as significant, and a *p*-value of $p < 0.02$ as highly significant.

3.2. Cell culture techniques

3.2.1. Description of cell lines

1. HTM-N (immortalized human trabecular meshwork cells)

HTM-N cells are adherent cells that grow as a monolayer culture. The cells are derived from the TM of a glaucoma patient. The cell line has been immortalized by transforming it with an origin defective mutant of SV40, which significantly increases its growth rate, whereas its cellular and extracellular composition, as well as its signalling mechanisms, correspond to those of non-transformed cells (Pang et al., 1994).

2. HEK (human embryonic kidney)-293 cells

HEK-293 cells are adherent cells that grow as a monolayer culture. The cells are derived from human embryonic kidney cells of a healthy aborted fetus. The cell line has been immortalized by transforming it with adenovirus type 5 DNA (Graham et al., 1977).

3.2.2. Storage and culturing

For long-term storage, cells were suspended in appropriate culture medium containing 10 % DMSO, and stored in a cryovial in liquid nitrogen. For culturing, a cryovial of cells were thawed in a water-bath. The cell suspension was transferred into 1 vol. of appropriate culture medium and the cells were pelleted by centrifugation at 1000 rpm for 5 min. The pellet was resuspended in 2 ml of culture medium and the suspension was transferred into a 75 cm^2 culture flask containing 11 ml of medium. The cells were grown in a cell culture incubator at

37 ° C with a CO_2-content of 7 %. At confluence, the cells were passaged by washing them twice in 2 ml of 1 X PBS, and by trypsinizing them in 2 ml of 0.05 % trypsin dissolved in EDTA. After detaching, the cells were transferred into a Falcon tube containing 2 vol. of culture medium. The cells were pelleted by centrifugation at 1000 rpm for 5 min and the pellet was resuspended in 1 - 5 ml of culture medium. An aliquote of the suspension was transferred into a new culture flask containing 12 ml culture medium.

3.2.3. Transient transfection

Transient transfection of cultured cells was carried out by lipofection. The technique takes advantage of cationic lipids that form a complex with the foreign DNA, and which then fuse with the plasma membrane to enter the cell (Felgner et al., 1987). The day before transfection cells were counted by using the Casy® Cell Counter system according to the instructions provided by the manufacturer. The cells were plated out at a density of 2 X 10^5 cells/well in a 24-well culture plate. On the day of transfection the cells had reached a confluence of 80 - 95 %. For transfection, 25 µl of culture medium without additives, 4 µl of Plus™ Reagent and 100 – 500 ng of plasmid were mixed and let to pre-complex for 15 min at RT. In case of co-transfection, 5 ng of plasmid expressing Renilla Luciferase was added to the pre-complexing mix. 1 µl Lipofectamine™ 2000 was diluted in 25 µl of culture medium without additives and the dilution was mixed with the pre-complexing mix. The complexing of DNA and lipofectamine was allowed to proceed for 20 min at RT. The cells were washed twice with 1 ml of culture medium without additives. 200 µl of culture medium without additives was added to the cells, after which the lipofectamine-DNA complexes were added. The plate was gently agitated to blend the complexes throughout the medium. The transfection was allowed to proceed at 37 °C, 7 % CO_2, for 6 h. The medium was changed to 1 ml culture medium with additives. 24 h after transfection the medium was changed once more, and the protein expression was allowed to proceed for an additional 48 h.

3.2.4. Dexamethasone treatment

Dexamethasone treatment of transfected cells was carried out 6 h or 24 h after transfection, concomitantly to culture medium exchange. Dexamethasone at a concentration of 10^{-5} M dissolved in EtOH was added to the fresh culture medium to give an endconcentration of 10^{-7} M. The treatment was continued until the cells were harvested.

3.2.5. Dual-Luciferase® Reporter assay

Promoter activity was analyzed by measuring the relative activities of the reporter genes firefly luciferase (*Photinus pyrialis*) (experimental reporter) to *Renilla* luciferase (*Renilla reniformis*) (control reporter) from the same sample by applying the Dual-Luciferase® Reporter Assay System according to the instructions provided by the manufacturer. The normalization of the activity of the experimental reporter to the activity of the control reporter minimizes experimental variability caused by differences in cell density, transfection efficiency or assay efficiency. Co-transfected cells were harvested 72 h after transfection by washing them with 1 X PBS and by rocking the plate in 150 µl/well 1 X PLB (passive lysis buffer) for 20 min at RT. The cell lysate was transferred to an Eppendorf tube and cell debris was pelleted by centrifugation for 5 min at 13 200 rpm. 20 µl of lysate was transferred to a luminometer vial and the activities of firefly luciferase and *Renilla* luciferase were subsequently measured in an AutoLumat LB953 luminometer according to the instructions provided by the manufacturer. 5 readings for 10 s were performed for each reporter gene. First, the activity of firefly luciferase was measured by injecting 100 µl Luciferase Assay Substrate II to the vial. In this reaction firefly luciferase converts beetle luciferin to oxyluciferin, which emits light (Lottspeich and Zorbas, 1998). Secondly, the activity of *Renilla* luciferase was measured by injecting 100 µl of Stop & Glo® buffer, which quenches the firefly luminescence and subsequently activates *Renilla* to convert coelenterazine to coelenteramide by the emission of light (Matthews et al., 1977). The activities of 5 readings were summarized, and the activity of firefly luciferase was divided by that of *Renilla* luciferase. The results were graphically presented by using the Microsoft® Excel software.

Because of ease in handling, we later went over to a more sophisticated luminometer system, the Centro XS^3 LB 960 microplate luminometer. In this system 10 µl of cell lysate was pipetted into the wells of a 96-well luminometer plate and the Dual-Luciferase® Reporter Assay was performed by injection of 50 µl LAR II, followed by injection of 50 µl Stop & Glo® buffer. The measurement and normalization of the values were performed as above by using the MicroWin 2000 software and the data were further exported to Microsoft® Excel for graphical presentation.

3.3. Mice

TG mice were generated in an inbred defined FVB/N genetic background. This mouse strain is characterized by a vigorous reproductive performance, large litters and pronuclei that are large and easy to microinject (Taketo et al., 1991). Two of the many characterized genetic markers described for this strain are the classical albino mutation (*c*) and the *Pdeb*^{rd1} retinal degeneration mutation (Gimenez and Montoliu, 2001).

3.3.1. Breeding of mice

Breeding of mice was carried out at the age of 5 - 6 weeks by crossing a TG mouse with a WT mouse of the same FVB/N genetic background. The offspring were separated from the parent animals at the age of 3 weeks, or as soon as a new litter was born. The litter was kept together until an age of 4 weeks, after which it was separated into females and males, and genotyped.

3.3.2. Isolation of genomic DNA from mouse tail biopsies

For genotyping of mice at the age of 4 weeks, the animals were etherized, pierced with an earmark and cut for a 0.5 cm tail biopsy. The fresh biopsy was lysed by adding 200 µl of Proteinase K lysis buffer and by shaking the sample at 55 °C at 1200 rpm O/N. Proteinase K was inactivated by incubation for 15 min at 95 °C. Cell debris was pelleted by centrifugation at 13 200 rpm for 10 min. The supernatant was spectrophotometrically measured for DNA concentration and purity, and the sample was diluted in H_20 to give an endconcentration of ~ 25 ng/µl. The mouse tail DNA was stored at + 4 °C.

3.3.3. Genotyping of transgenic mice

Screening of possible founder animals was carried out by PCR of genomic DNA isolated from tail biopsies. A primer pair was designed (LacZ fw and LacZ rev.) that binds within *LacZ* of the transgene, and which amplifies a sequence of 524 bp length (Fig. 4.10). For genotyping, the following reaction setup was mixed (Table 3.18).

Template	2 µl (~ 50 ng)
Primer fw	0.6 µl
Primer rev.	0.6 µl
2 X GoTaq® Green MM	7.5 µl
H_20	4.3 µl
Total volume	15 µl

Table 3.18: The reaction setup for genotyping of TG mice by PCR.

The PCR was carried out for 34 cycles by the following reaction conditions (Table 3.19).

Step:	Temperature:	Time:
Initial denaturation	95 °C	2 min
Denaturation	95 °C	30 s
Primer annealing	55 °C	30 s
Elongation	72 °C	30 s
Final elongation	72 °C	5 min

Table 3.19: PCR reaction conditions for genotyping of TG mice. 32 cycles of denaturation, primer annealing and elongation were carried out.

For routine genotyping during breeding of the lines, a new primer pair was designed, NLS fw and LacZ rev. 2, which binds within the sequence of 3 X NLS and *LacZ*, respectively, and which amplifies a sequence of 220 bp length (Fig. 4.10). Reaction setup and PCR conditions were as above (Tables 3.18 and 3.19), with the exception that the PCR was carried out for only 32 cycles.

3.4. Histological techniques

3.4.1. *LacZ*-staining of transfected cells

HTM-N cells were plated out at a density of 2 X 10^5 cells on a 1.8 cm^2 chamber slide and transiently transfected with cloned ß-galactosidase overexpression construct by lipofection as described in chapter 3.2.3. For staining, the cells were washed once with 0.1 M $NaPO_4$ buffer and fixed for 5 min at RT in *LacZ*-fixation buffer. The cells were washed 3 times for 5 min in *LacZ*-wash buffer and stained in *LacZ*-staining solution in a moist chamber at 37 °C for 1 - 3 d, or until blue colour was visible. The cells were washed 3 times for 5 min in *LacZ*-wash buffer, after which the object slide was released from the chamber rim. The slide was dehydrated by incubating it in a series of increasing ethanol concentrations and xylol (Table 3.20):

Step:	Solution:	Duration:
1.	70 % isopropanol	5 min.
2.	80 % isopropanol	5 min.
3.	96 % isopropanol	2 X 5 min.
4.	100 % isopropanol	2 X 5 min.
5.	xylol	2 X 10 min.

Table 3.20: Dehydration of *LacZ*-stained object slides was carried out by incubating them in a series of increasing ethanol concentrations and xylol.

The slides were mounted by coverslips with a few drops of Depex mounting medium and stored in dark at + 4 °C.

3.4.2. Fixation and *LacZ*-staining of adult mouse organs

Eyes, heart and sciatic nerves from adult TG mice were prepared for *LacZ*-staining as follows. The mouse was etherized and killed by cervical dislocation and the organs were removed by using scissors and forceps. The organs, whereby the heart was halved, were shortly washed in 0.1 M $NaPO_4$ buffer and fixed in 0.1 M $NaPO_4$ buffer with added 4 % PFA for 6 h at + 4 °C. The organs were washed twice in 0.1 M $NaPO_4$ buffer for 30 min and left in 0.1 M $NaPO_4$ with 0.02 % (w/v) added NaN_3 in dark at + 4 °C until cryoprotection and embedding in Tissue-Tek® (section 3.4.4). Alternatively, mouse adult organs were fixed, cryoprotected and embedded in Tissue-Tek® before *LacZ*-staining. Stored cryosections of organs were stained for *LacZ* as described in section 3.4.1 and, if required for a better recognition of fine structures, counterstained by haematoxylin-eosin staining by standard protocols before dehydration and mounting.

3.4.3. Fixation and *LacZ*-staining of embryos

For mouse embryo preparation at E12.5, TG and control females were superovulated by standard protocols (Nagy et al., 2003). On the morning after mating, the females were

checked for a copulation plug. The visible plug was considered as E0.5. The pregnant female was etherized and killed by cervical dislocation at E12.5. The embryos were recovered from the uterus and immediately washed in 0.1 M $NaPO_4$ buffer. Each embryo was separately prepared under a binocular. The embryo was freed from the amnion and a tail biopsy was taken for genotyping. To enable proper penetration of the fixation solution, an incision was made in the abdomen. The embryos were fixed in *LacZ*-fixation buffer for 30 min, washed 3 times for 15 min in *LacZ*-wash buffer and stained in *LacZ*-staining solution in dark at 37 °C for 1 - 2 d. After staining, the embryos were washed 3 times for 15 min in *LacZ*-wash buffer and once for 10 min in 0.1 M $NaPO_4$ buffer. The embryos were stored in 0.1 M $NaPO_4$ with 0.02 % (w/v) added NaN_3 in dark at + 4 °C until cryoprotection and embedding as described in section 3.4.4.

3.4.4. Cryoprotection and embedding of adult mouse organs and embryos

In order to protect organs and embryos from structural damage during freezing, they were cryoprotected by infiltrating them successively for 4 – 24 h in each 10 %, 20 % and 30 % sucrose in 0.1 M $NaPO_4$ buffer. The organs were embedded in Tissue-Tek®, snap-freezed in liquid nitrogen and stored at – 20 ° C until sectioning

3.4.5. Cryosectioning of embedded mouse organs and embryos

Embedded mouse organs and embryos were sectioned by cutting sagittal or transverse cryosections of 12 µm thickness in a Microcom HM 500 OM cryostat. For storing, the sections were placed on SuperFrost®Plus object-plates, wrapped in aluminium foil, and stored at - 20 °C until mounting and analysis by phase contrast microscopy. Sections of unstained adult organs were stored at - 20 °C until staining, dehydration and mounting as described in section 3.4.1.

3.4.6. Phase contrast microscopy

Active ß-galactosidase cleaves X-gal into a blue substrate (Pearson et al., 1963), which can be visualized by normal phase contrast microscopy. *LacZ*-stained adult organs and embryos were analyzed by a Zeiss Axioskop 40 microscope and observed blue staining was documented by making images by an Axio Imager Z1 microscope in a Carl Zeiss AxioVision format (.zvi) at different magnifications (5 X - 40 X). The data were converted into .tif-format and further edited by using the Adobe® Photoshop® CS3 Extended software.

3.4.7. Immunohistochemistry

The vascular system of the brain of a 6 week old rat of the strain Wistar was perfused with 4 % PFA by standard protocols to remove erythrocytes and thus to eliminate possible background labelling. The brain was fixed in 0.1 M $NaPO_4$ buffer with added 4 % PFA for 5 - 6 h, washed 3 times for 15 min in 0.1 M $NaPO_4$ buffer and left in this buffer O/N. The brain was sectioned, dehydrated and embedded in paraffin by standard protocols, or cryoprotected and embedded in Tissue-Tek® as described in section 3.4.4. Paraffin embedded brain was cut coronal by a microtome in 6 µm thin sections, put onto object slides and dried O/N in 37 °C. Slides were de-paraffinized and hydrated by standard protocols and incubated in 0.1 M boiling citrate buffer, which was then let to cool down to RT. Slides were incubated in H_20 for 5 min, in 0.1 M $NaPO_4$ buffer containing 0.05 % Tween-20 for 5 min, and blocked with 0.5 % BSA diluted in 0.1 M $NaPO_4$ buffer for 45 min. For detection of myocilin expression, slides were incubated with a rabbit-derived anti-myocilin antibody diluted 1:50 in 0.1 M $NaPO_4$ buffer containing 0.5 % BSA O/N in a moist chamber at + 4 °C. Control slides were incubated with 0.1 M $NaPO_4$ containing 0.5 % BSA alone. Slides were washed three times for 5 min in 0.1 M $NaPO_4$ and incubated with a green fluorescing goat-derived anti-rabbit secondary antibody diluted 1:1000 in 0.1 M $NaPO_4$ containing 0.5 % BSA in dark for 1 h at RT. Slides were washed 3 times for 5 min in 0.1 M $NaPO_4$ buffer and mounted by coverslips with a few drops of 1:10 DAPI (4'-6-diamidine-2-phenyl indole) mounting medium. The slides were stored in dark at + 4.

3.4.8. Fluorescence microscopy

DAPI stained nuclei and GFP-labelled myocilin were analyzed by UV-light and appropriate filter systems in an Axio Imager Z1 fluorescence microscope. Images were documented in a Carl Zeiss AxioVision format (.zvi) at 20 and 40 X magnifications. The data were converted into .tif-format and further edited by using the Corel PHOTO-PAINT® software.

4. Results

4.1. Characterization of *MYOC*

4.1.1. Search and analysis of conserved genomic regions

4.1.1.1. Functional analysis of conserved intronic and 3´-UTR regions

Since only the basal *MYOC* promoter has been characterized (Kirstein et al., 2000), and since a better understanding of the regulation of *MYOC* would be of importance to better understand the role of myocilin in glaucoma, we analyzed the capacity of different regions of human *MYOC* to drive reporter gene expression. It is known that non-coding (nc) parts of a gene like introns, or even more distal regions lying tens of kb up- or downstream of the translated part, can contain important transcriptional enhancers (Plaza et al., 1995; Uchikawa et al., 2004; Kleinjan et al., 2006; Aruga et al., 2007). A search for evolutionary conserved regions by inter-species comparison of orthologous sequences can reveal distal enhancers even within gene-sparse regions, so called gene deserts (Nobrega et al., 2003). VISTA is a computational tool for comparative genomics aimed to identify functional elements (Frazer et al., 2004). To find regions within *MYOC* that have been conserved between species throughout evolution, and that may serve a regulatory role in the transcription process, we used the VISTA Browser 2.0 software (http://pipeline.lbl.gov/cgi-bin/gateway2) that is based on pre-computed alignments, and that offers a graphical view of conserved areas. By comparing the human and mouse *MYOC*/*myoc* locus, we identified several intronic conserved regions, as well as a 3´-UTR, which peaked in a homology of over 70 %. The possible intronic distal control regions (DCRis) were named DCRi2a, DCRi2b3´, DCRi2b5´ and DCRi2c (Fig. 4.1).

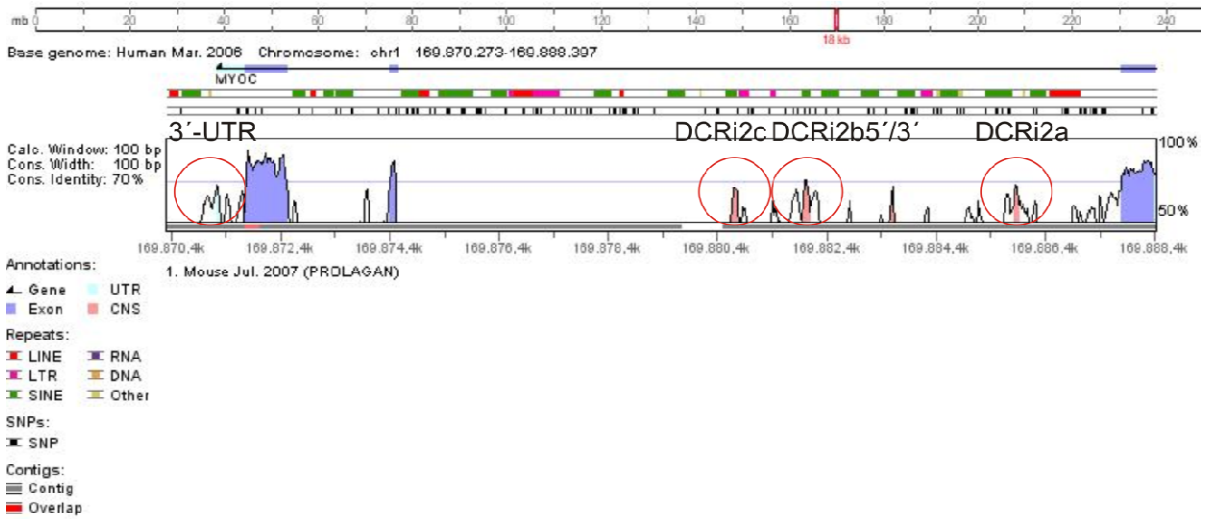

Fig. 4.1: Comparison of human and mouse myocilin genes by using the VISTA Browser 2.0 bioinformatic software for inter-species alignment. Mouse *myoc* is depicted from the right to the left on chromosome one. The heights of the peaks illustrate the degree of homology to human *MYOC* at that nucleotide position. Exons and UTRs are shown in blue and turquoise, respectively. Conserved nc sequences that show a consensus homology of at least 70 % for a length of at least 100 bp are shown in pink. We amplified four intronic homologous regions, possible distal control regions (DCRs), named DCRi2a, DCRi2b5´, DCRi2b3´, DCRi2c, as well a homologous 3´-UTR from human genomic DNA and cloned these in front of the human *MYOC* basal promoter (p313+67) (Fig. 4.2) for Luciferase-reporter assays.

The human *MYOC* basal promoter (p313+67), which extends until the published second in-frame transcriptional start ATG (Nguyen et al., 1998), had already been cloned into Luciferase-reporter constructs by Kirstein et al. (2000) (Fig. 4.2). The designation p313+67 of the 377 bp *MYOC* basal promoter was deduced from the alignment between the human and mouse myocilin genes, where the start ATG of mouse *myoc* (Tomarev et al., 1998) was aligned to match the second possible start ATG of the human gene (Kirstein et al, 2000). The authors showed that p313+67 effectively enhanced reporter gene expression in primary cell cultures of human TM, as well as in the clonal, immortalized and differentiated mouse TM cell line MUTM-NEI/1 (Tamm et al., 1999), when compared to a control vector. To test the above conserved *MYOC* regions (Fig. 4.1) for their capacity to drive reporter gene expression over the level than p313+67 does, and consequently to find out if the conservation plays a functional role in the regulation of *MYOC*, we cloned the four homologous intronic regions DCRi2a, DCRi2b3´, DCRi2b5´, DCRi2c, as well the homologous 3´-UTR, in front of

p313+67 between the restriction enzyme recognition sites *Kpn*I and *Xho*I (Fig. 4.2). Cloned homologous regions, their lengths and positions within *MYOC* are listed in Table 4.1.

Name of region:	**Length (bp):**	**Position in h*myoc*:**
DCRi2a	548	+2207 - (+)2755
DCRi2b3´	1311	+4502 - (+)5813
DCRi2b5´	1690	+5715 - (+)7405
DCRi2c	609	+7459 - (+)8068
3´-UTR	1537	+16896 - (+)18433

Table 4.1: List of conserved, possible regulatory *MYOC* regions that were cloned in front of p313+67 into Luciferase-reporter constructs. The lengths of the regions, as well as their positions within *MYOC*, are shown. The positions refer to the nucleotide positions after the published second possible start ATG (Nguyen et al., 1998).

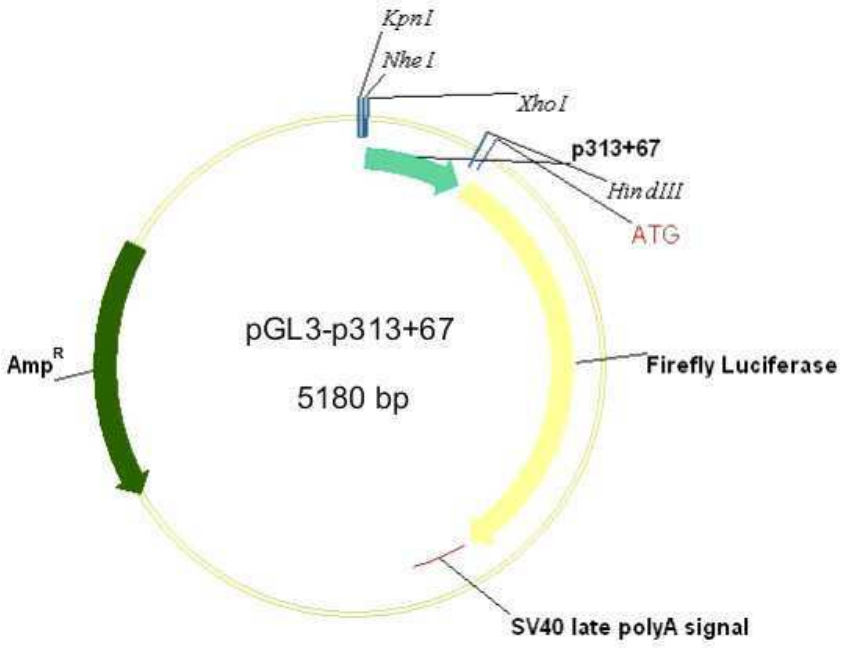

Figure 4.2: Luciferase-reporter construct, where the human *MYOC* basal promoter (p313+67) had been introduced into the MCS between the restriction enzyme overhangs *Xho*I and *Hind*III to drive firefly Luciferase expression, had already been cloned by Kirstein et al. (2000) by using the pGL3-Basic vector from Promega as a backbone. We cloned the conserved *MYOC* regions listed in Table 4.1, as well as the artificial enhancer elements PITX3, FOX, PITX3/FOX and RAREß/PITX3/FOX listed in Table 4.3, in front of p313+67 between the restriction enzyme overhangs *Kpn*I and *Xho*I. The conserved *MYOC* regions listed in Table 4.2, as well as the human *MYOC* E-box listed in Table 4.3, were cloned in front of p313+67 between the restriction enzyme overhangs *Nhe*I and *Xho*I.

The above cloned reporter constructs were transiently transfected into HTM-N cells and the relative light units (RLUs) produced by expressed reporter were measured by Dual-Luciferase® Reporter assays as described in Materials and methods 3.2.5. Repeated assays revealed that DCRi2b5´ and DCRi2c did enhance the expression up to 3.7- and 2.2-fold, respectively, over the basal promoter level. In both cases the capacity to drive reporter expression in comparison to the basal promoter was highly significant ($p = 0.014$ and $p = 0.001$ for DCRi2b5´ and DCRi2c, respectively). The two other conserved intronic regions DCRi2a and DCRi2b3´ did not have any positive effect on gene expression, the effect was rather negative (Fig. 4.3). Also the region 3´-UTR showed rather a negative than a positive effect on gene regulation in these cells (data not shown).

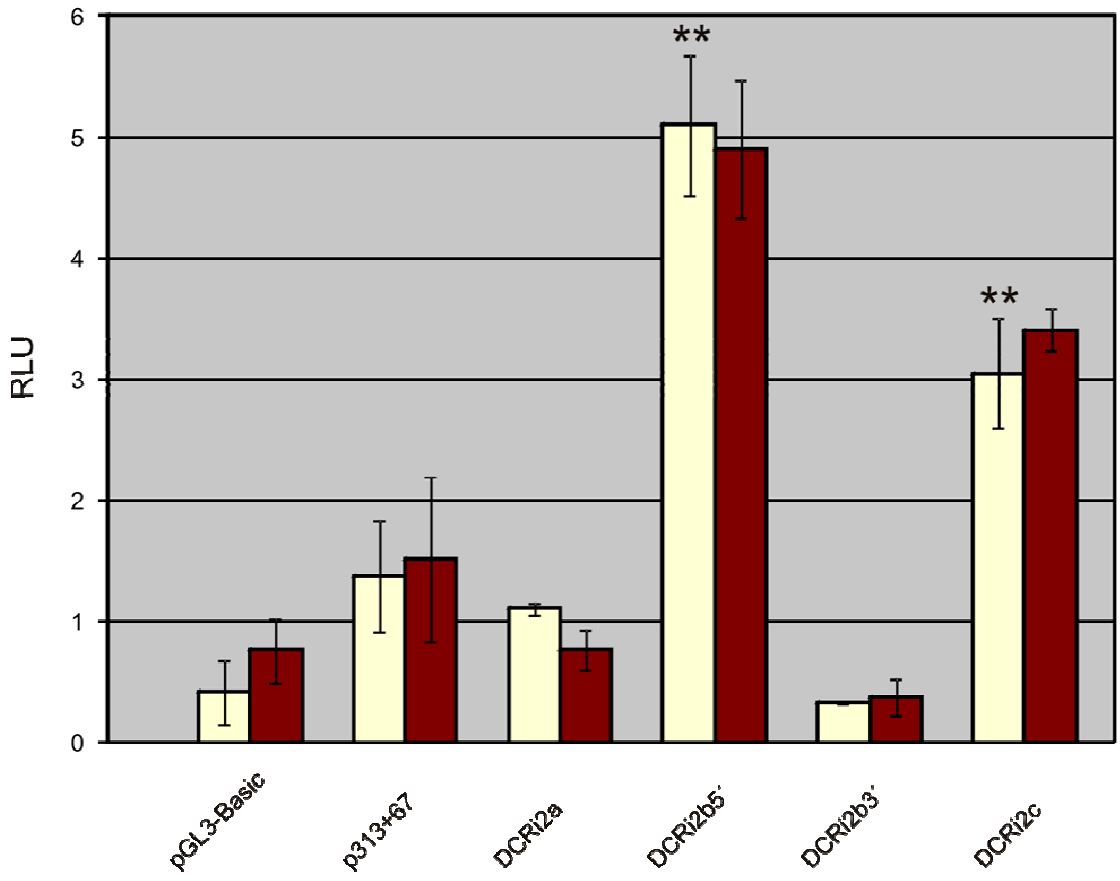

Figure 4.3: Dual-Luciferase® Reporter assay measuring the capacity of conserved intronic *MYOC* regions to regulate reporter gene expression over human basal promoter (p313+67) level in cultured HTM-N cells. Reporter gene expression was measured as relative light units (RLUs) of the experimental reporter to the control reporter. Reporter constructs bearing the conserved intronic *MYOC* regions DCRia, DCRi2b5´, DCRi2b3´and DCRi2c in front of p313+67 were transiently transfected into HTM-N cells and a Dual-Luciferase® Reporter assay was carried out after 72 h of expression. The GC responsiveness of the regions was analyzed by treating the cells with 10^{-7} M of dexamethasone during expression. pGL3-Basic contains no eukaryotic promoter or enhancer sequences and was used as a background control. Repeated assays confirmed that DCRi2b5´ and DCRi2c did enhance reporter gene expression up to 3.7- and 2.2-fold, respectively, over basal promoter level in these cells. The graph shows an individual experiment, where duplicate samples without (yellow bars) and with (wine red bars) dexamethasone treatment were analyzed. Mean standard deviation (± SD) between duplicates are shown. Asterisks mark statistically significant differences of reporter gene activity between basal promoter and DCRi (**$p < 0.02$).

4.1.1.2. Deletion study of conserved intronic and 3´-UTR regions

In order to exactly find out which parts of the conserved intronic and 3´-UTR regions of *MYOC* are responsible for the positive/negative regulation of reporter gene expression in comparison to p313+67, we deleted the outermost parts of above regions to comprise only the highest sharp peaks of homology. By aligning human and mouse DCRia, DCRi2b5´, DCRi2c and 3´-UTR regions by VISTA Browser 2.0, we reduced the lengths of these regions to span only the most conserved parts, to regions that show a homology of 69.2 to 75.8 % throughout their sequence. These shorter new regions of homology range from 87 to 275 bp and were called H3, H4, H5-6 and H7 (H stands for Homology). In fact, H5-6 consists of two sharp homologous peaks residing only 28 bp apart, but because of difficulties in finding appropriate primer pairs for the amplification of H5 and H6 separately, we decided to amplify H5 and H6 in one stretch (Fig. 4.4).

Figure 4.4: Comparison of human and mouse myocilin genes by using the VISTA Browser 2.0 bioinformatic software for inter-species alignment. Mouse *myoc* with surrounding genome landscape on chromosome one is depicted upwards from the right to the left. The heights of the peaks illustrate the degree of homology to human *MYOC* at that nucleotide position. Exons and UTRs are shown in blue and turquoise, respectively. Conserved nc sequences that show a consensus homology of at least 70 % for a length of at least 100 bp are shown in pink. Depicted are the highly conserved intronic and 3´-UTR regions (H3 - H7, small red circles), that were amplified from human genome and cloned into reporter constructs for deletion analysis. For clarity, already tested larger intronic and 3´-UTR regions (DCRi2a, DCRi2b5´/3´, DCRi2c and 3´-UTR) are marked (large orange broken-lined circles). Long-range possible regulatory elements (H1 - H2 and H8 - H10, large red circles) that were amplified from human genome and cloned into reporter constructs in front p313+67 are depicted. The arrow shows the position of the myocilin basal promoter.

H3, H4, H5-6 and H7 were cloned in front of p313+67 into Luciferase-reporter constructs between the restriction enzyme overhangs *Nhe*I and *Xho*I (Fig. 4.2). Because of problems in finding appropriate primer pairs for amplification, the cloned amplicons are a bit longer than the conserved regions themselves. The exact lengths and %-homologies between human and mouse regions H3, H4, H5-6 and H7, as well as their positions within *MYOC* are listed in Table 4.2. The list also summarizes lengths and positions of respective amplicons.

Name of region:	**Length (bp) with % homology to h*myoc*:**	**Position within h*myoc*:**	**Length of Amplicon:**	**Amplicon position within h*myoc*:**
H1	94 (70.0)	+24249 - (+)24343	256	+24190 - (+)24446
H2	102 (70.9)	+22843 - (+)22945	220	+22815 - (+)23035
H1-2	102+94	+22843 - (+)22945; +24249 - (+)24343	1631	+22815 - (+)24446
H3	86 (75.8)	+17104 - (+)17190	281	+17012 - (+)17293
H4	181 (69.5)	+7591 - (+)7772	267	+7562 - (+)7829
H5	133 (72.9)	+6324 - (+)6457	413	6152 - (+)6565
H6	123 (69.2)	+6173 - (+)6296	413	6152 - (+)6565
H7	101 (70.5)	2470 - (+)2571	294	2374 - (+)2668
H8	107 (73.8)	-4961 - (-)4854	288	-5042 - (-)4754
H9	514 (72.0)	-11122 - (-)10608	514	-11122 - (-)10608
H10	1044 (85.0)	-31826 - (-)30782	1178	-31869 - (-)30691

Table 4.2: List of highly conserved, possible regulatory *MYOC* regions, that were cloned in front of p313+67 into Luciferase-reporter constructs. The list summarizes regions analyzed in the deletion study (H3 - H7), as well as tested possible long-range regulatory elements (H1 - 2 and H8 - 10). The lengths of the conserved regions with their %-homology between human and mouse, as well as their positions within *MYOC*, are depicted. The list also summarizes lengths and positions of respective amplicons. The positions refer to the nucleotide positions after the published second possible start ATG of *MYOC* (Nguyen et al., 1998).

To test for the transcriptional enhancer capacity of H3, H4, H5-6 and H7 in comparison to p313+67, and in order to look at which effect a deletion of parts of DCRia, DCRi2b5´, DCRi2c and 3´-UTR has on transcriptional gene regulation, we transiently transfeceted the deletion constructs into HTM-N cells and measured reporter gene expression in comparison to reporter expression in lysates that had been transfected with p313+67 alone. Repeated Dual-

Luciferase® assays as described Materials and methods 3.2.5. showed that the intronic regions H4 and H5-6 had slight, but not statistically significant, positive effects on gene regulation in comparison to p313+67. The effect of H7 on transcriptional gene regulation was also small, though statistically significant (p = 0.028). The effect of H3 was slight negative, but without significance (Fig. 4.5). In conclusion, the deletion analysis showed us that the capacity of DCRi2b5´ and DCRi2c to drive reporter gene expression statistically highly significant above the level than the basal promoter does (Fig. 4.3), went down drastically, when parts of these regions were deleted (Fig. 4.5). In contrast, the rather negative effect on reporter gene expression of the intronic region DCRi2a compared to the effect of p313+67 (Fig. 4.3) turned out into a slight positive effect when parts of it were deleted (Fig. 4.5).

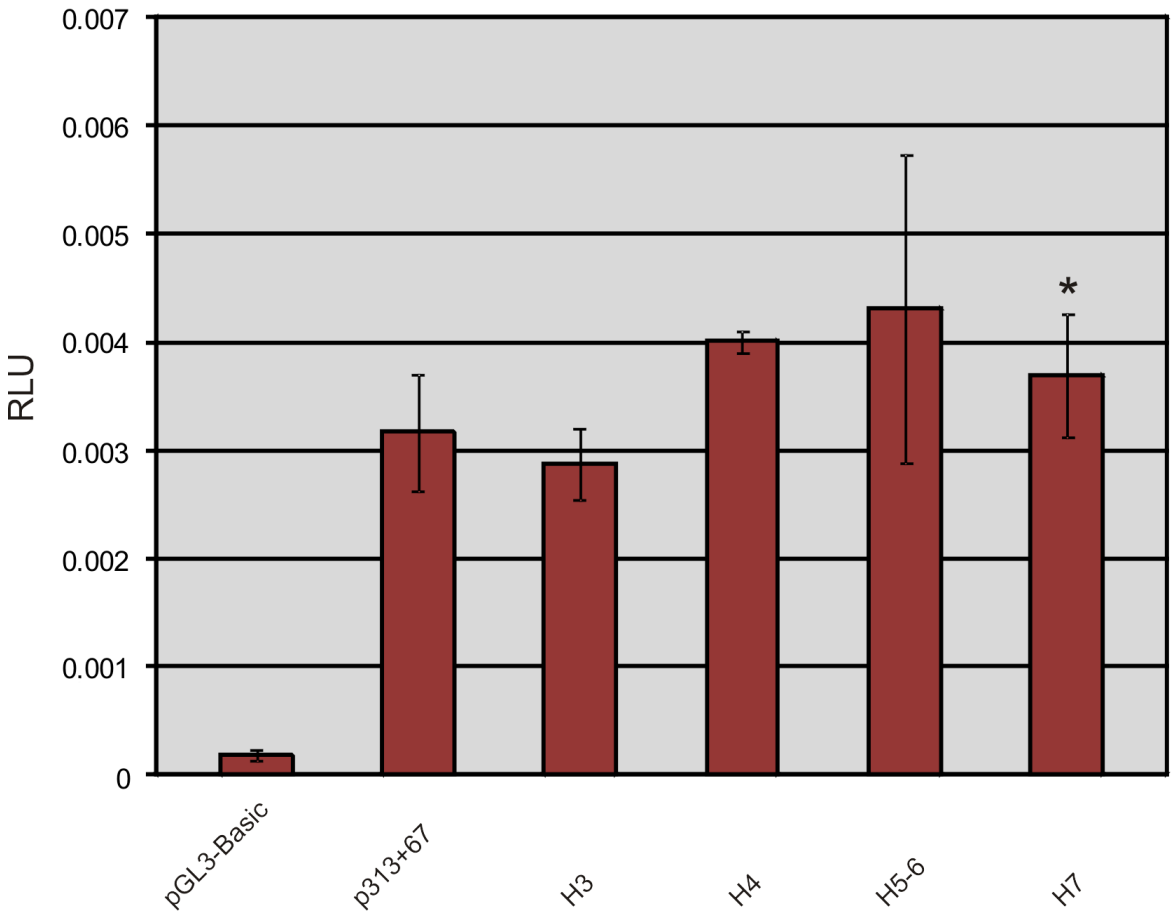

Figure 4.5: Deletion analysis of conserved intronic and 3´-UTR *MYOC* regions by Dual-Luciferase® Reporter assay to analyze their capacity to regulate reporter gene expression in comparison to the *MYOC* basal promoter

(p313+67) in cultured HTM-N cells. H3, H4, H5-6 and H7 are shortened versions of the human intronic regions 3´-UTR, DCRi2c, DCRi2b5´ and DCRi2a, respectively. Reporter constructs bearing the human regions H3, H4, H5-6 and H7 in front of p313+67 were transiently transfected into HTM-N cells and a Dual-Luciferase® Reporter assay was carried out after 72 h of expression. pGL3-Basic contains no eukaryotic promoter or enhancer sequences and was used as a background control. Reporter gene expression was measured as relative light units (RLUs) of the experimental reporter to the control reporter. Repeated assays showed that all intronic regions slightly increased reporter gene expression over basal promoter level, H7 even statistically significant ($p = 0.028$). However, the experiment showed us that a deletion of parts of DCRi2b5´ and DCRi2c results in a dramatic loss of enhancer capacity. In contrast, a deletion of parts of DCRi2a slightly elevated its capacity to drive reporter gene expression over basal promoter level. The graph shows an individual experiment, where duplicate samples were analyzed. Mean standard deviation (± SD) between duplicates are shown. Asterisks mark statistically significant differences of reporter gene activity between p313+67 and H (*$p < 0.05$).

4.1.1.3. Search and analysis of long-range regulatory regions within *MYOC*

We still extended our inter-species comparison between human and mouse myocilin genes to a long-range search for conserved elements far beyond the translated part of *MYOC*. We found three distal 5´-upstream homologous regions (H8 - H10) and two distal 3´-downstream homologous regions (H1 and H2), where the whole sequence showed a homology ranging from 70 - 85 %. These elements varied in lengths from 95 to 1044 bp and resided as far as 31 kb up- and 7 kb downstream, respectively, from the translated part of *MYOC* (Fig. 4.4). H1, H2 and H8 - H10 were cloned in front of p313+67 into Luciferase-reporter constructs between the restriction enzyme overhangs *Nhe*I and *Xho*I (Fig. 4.2). The exact lengths of conserved distal regions, their %-homologies between human and mouse, as well as their positions within *MYOC* are listed in Table 4.2. The list also summarizes the lengths and positions of the true cloned amplicons. In order to compare the transcriptional enhancer capacity of distal conserved regions with the capacity of p313+67 to drive reporter gene expression, we transiently transfeceted the cloned reporter constructs into HTM-N cells and measured reporter gene expression in comparison to reporter gene expression in lysates that had been transfected with p313+67 alone. Repeated Dual-Luciferase® assays as described in Materials and methods 3.2.5. showed that the 3´-downstream conserved regions H1 and H2 enhanced the expression of reporter up to 2.9- and 2.4-fold, respectively, over the level than did p313+67 alone. The capacity of H1 to drive reporter gene expression over the basal

promoter level was significant (p = 0.037). The 5´-upstream conserved regions H8 and H9 showed no effect on transcriptional gene regulation, whereas the most afield residing largest cloned region H10 showed a slight, but negligible, positive effect on reporter gene expression (Fig. 4.6).

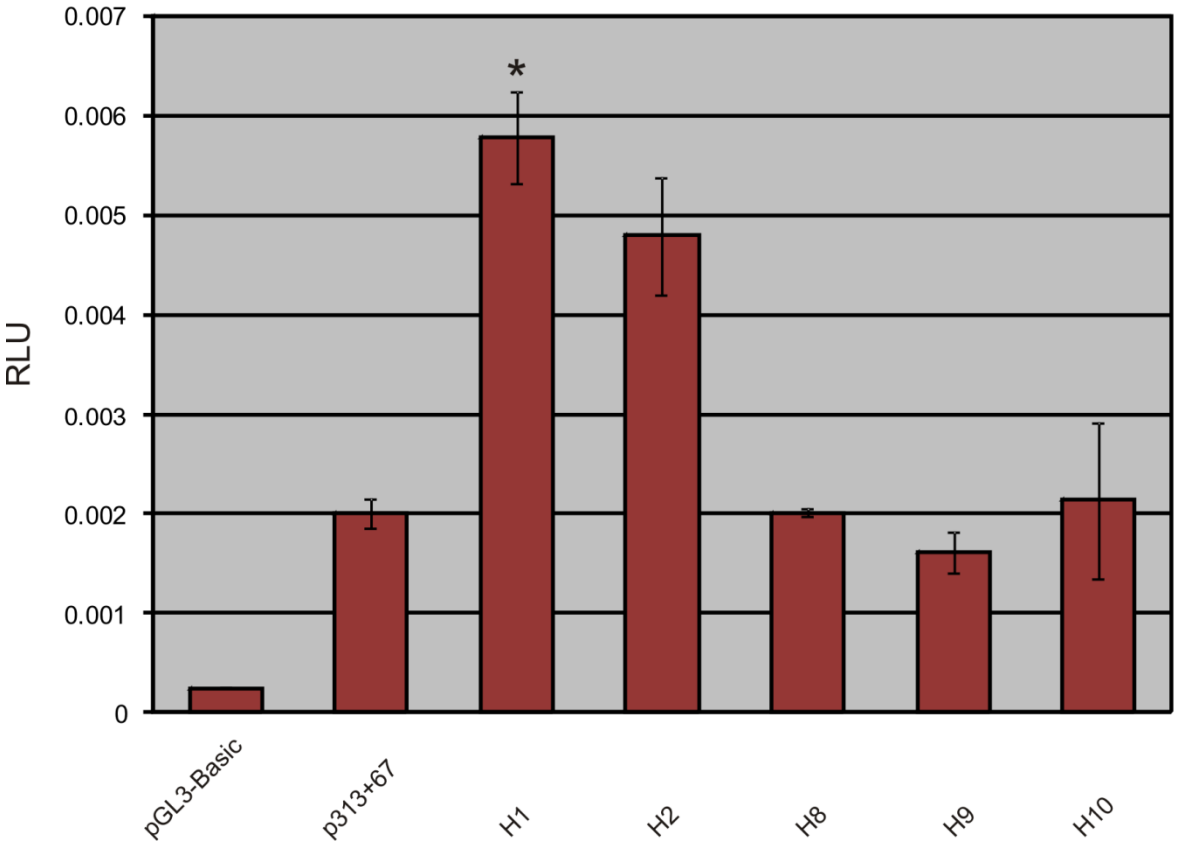

Figure 4.6: Dual-Luciferase® Reporter assay measuring the capacity of conserved long-range *MYOC* elements to regulate reporter gene expression over human basal promoter (p313+67) level in cultured HTM-N cells. Reporter constructs bearing the human 5´-upstream regions H8 - H10, as well as the 3´-downstream regions H1 and H2 in front of p313+67 were transiently transfected into HTM-N cells and a Dual-Luciferase® Reporter assay was carried out after 72 h of expression. pGL3-Basic contains no eukaryotic promoter or enhancer sequences and was used as a background control. Reporter gene expression was measured as relative light units (RLUs) of the experimental reporter to the control reporter. Repeated assays confirmed that the 3´-downstream elements H1 and H2 enhance reporter gene expression up to 2.9- and 2.4-fold, respectively, over the basal promoter level in these cells. The 5´-upstream elements H8 - H10 had no noteworthy effect on gene regulation.

The graph shows an individual experiment, where duplicate samples were analyzed. Mean standard deviation (± SD) between duplicates are shown. Asterisks mark statistically significant differences of reporter gene activity between p313+67 and H (*$p < 0.05$).

4.1.1.4. Expanded analysis of the 3´-UTR region

Many genes are regulated by enhancer elements residing within their 3´-UTRs (Griffin et al., 2002; Sun et al., 1998; Yochum et al., 2008). The discovery of microRNAs (miRNAs) (Chalfie et al, 1981; Ambros et al., 1989) has further corroborated the potential of the 3´-UTR to contribute to the complex network of gene regulation (reviewed by He and Hannon, 2004). Since both H1 and H2 showed a positive effect on reporter gene expression in cultured HTM-N cells (Fig. 4.6), and since these elements both reside within the 3´-UTR of *MYOC*, we expanded our analysis of this region. Inter-species alignment of the 3´-UTR of *MYOC* by VISTA Browser 2.0 revealed that H1 and H2 reside within a larger area of conservation that, when comparing the human and mouse genes, extend as far as 13.5 kb downstream of exon 3. In addition to H1 and H2, this region contains at least four more peaks with a homology of ~ 70 % (Fig. 4.7).

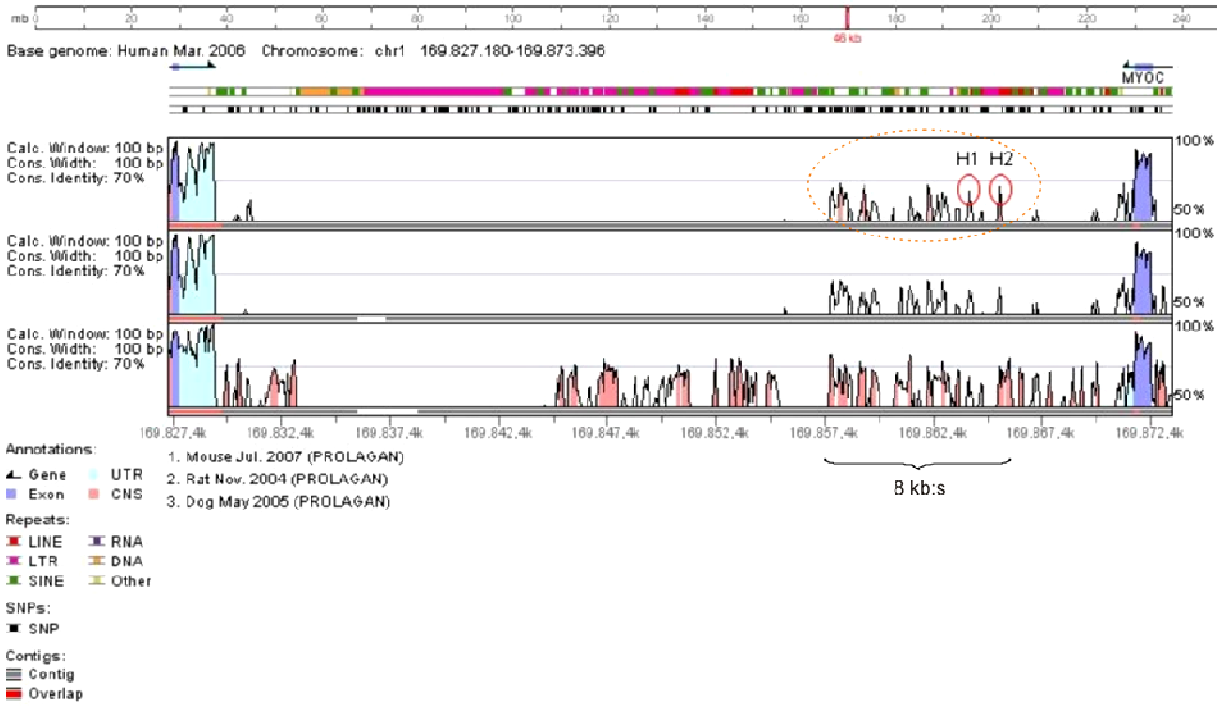

Figure 4.7: Alignment of the 3´-UTR of mouse, rat and dog myocilin genes vs. the human gene by VISTA Browser 2.0 bioinformatic software for inter-species alignment. The 3´-end of *myoc* with its 3´-UTR genomic landscape is depicted from the right to the left. The heights of the peaks illustrate the degree of homology to *MYOC* downstream region at that nucleotide position. Exons and UTRs are shown in blue and turquoise, respectively. Conserved nc sequences that show a consensus homology of at least 70 % for a length of at least 100 bp are shown in pink. The alignment reveals that our already tested positively acting elements H1 and H2 (small red circles) reside within a larger 8 kb evolutionary conserved area (orange broken-lined circle). In order to test if H1 and H2, when coming together, would have a cumulative effect in enhancing reporter gene expression, we amplified H1 and H2 in one stretch and cloned it into a Luciferase-reporter construct in front of p313+67.

We were now interested in, if the wide evolutionary conserved area downstream of *MYOC* as a whole could be important for the positive regulation of the myocilin gene. As a start, we wanted to test if H1 and H2, when coming together, would have a cumulative effect in enhancing reporter gene expression. We amplified H1 and H2 as one 1631 bp amplicon (Table 4.2) and cloned it into a Luciferase-reporter construct in front of p313+67 between the restriction enzyme recognition sites *Nhe*I and *Xho*I (Fig. 4.2). Repeated Dual-Luciferase® assays as described in Materials and methods 3.2.5. confirmed that H1 and H2 did not have a cumulative effect on transcriptional gene regulation (data not shown). Thus, the data do not support our hypothesis of a positive regulatory role of the conserved 3´-UTR of *MYOC*.

4.1.1.5. Analysis of GC responsiveness of conserved nc *MYOC* regions

It has been well documented that myocilin expression is highly up-regulated in TM cells after treating these with the GC dexamethasone (Polansky et al., 1997; Nguyen et al., 1998; Tamm et al., 1999). Sequence analyses of the 5′-promoter region of *MYOC* have revealed that there are many potential functional GREs (Nguyen et al., 1998; Polansky et al., 1997; Adam et al., 1997). However, attempts to analyze the 5′-promoter region of *MYOC* for its direct GC response have been without success (Kirstein et al., 2000), indicating that the GC response of *MYOC* is an indirect secondary response (Shepard et al., 2001). We wanted to expand the search for functional GREs within the *MYOC* locus to encompass also intronic, as well as long-range 5′- and 3′-UTR regions. We transiently transfected HTM-N cells with our cloned reporter constructs containing intronic, as well as distal 5′- and 3′-UTR regions of *MYOC* (Tables 4.1 and 4.2) in front of p313+67 (Fig. 4.2). Dexamethasone treatment (10^{-7} M) during expression did not have any effect on reporter gene expression in any of the samples (data shown only for DCRia, DCRi2b5′, DCRi2b3′and DCRi2c in Fig. 4.3). This indicates that none of our analyzed conserved regions contain functional elements that directly or indirectly are able to respond to dexamethasone.

4.2. Creation of ß-galactosidase overexpression mouse

4.2.1. Search for artificial enhancer elements with strong activity within the TM

In the attempt to better understand the molecular interactions that lie behind an elevated AH outflow resistance in the TM, it would be of great value to be able to direct high expression of interesting, possibly for POAG relevant proteins, into this tissue *in vivo*. The fact that there are additional regions within *MYOC* that contribute to its transcription rate above basal transcription level in cultured TM cells (Figs. 4.3 and 4.6), indicates that the *MYOC* basal promoter alone would not be sufficient to drive protein overexpression in this tissue *in vivo*. We wanted to create and identify an artificial enhancer element that, in combination with p313+67, would drive high protein expression in cultured HTM-N cells. The final aim of the project was to be able to use the identified element to drive overexpression of protein in the TM of a mouse model.

We created a set of artificial enhancer elements that were made up of different combinations of repetitive binding sites for the evolutionary conserved transcription factors PITX (paired-like homeodomain transcription factor) and FOX (forkhead box), known to be pivotal in anterior eye development in human and in mouse (reviewed by Cvekl and Tamm, 2004; Matt et al., 2005). As members of the paired-class of homeodomain proteins, PITX transcription factors can bind the core DNA sequence TAATNN in both the major and minor grooves, where the two last nucleotides of the core sequence are specified by the recognition helix itself (Wilson et al., 1993). Chaney et al. (2005) showed a solution structure of PITX2 protein bound to its consensus DNA site TAATCC. We created an 87 bp element, with three recurring TAATCC PITX binding motives, interspaced by 15 nucleotides (Table 4.3). The FOX family of proteins contain a unique ~ 100 bp conserved winged-helix FOX domain that is essential for DNA binding (Kaestner et al., 2000). It has been shown that the FOX transcription factors can recognize variations of the DNA core motive (T/C)(A/C)AA(C/T)A, and that the less conserved regions of the proteins are able to regulate the DNA binding specificity of the conserved DNA binding regions (Tsai et al., 2006). Pierrou et al. (1995) showed that *in vivo* derived FOXC1 binds the DNA motive GTAAATAAA with high affinity *in vitro*. We created an 87 bp element, with three recurring GTAAATAAA FOX binding

motives, interspaced by 12 nucleotides (Table 4.3). To test for the possibility that a co-effect of both PITX and FOX would lead to a cumulative effect of reporter gene expression, we created an element that combined the repetitive consensus binding motives of PITX and FOX (Table 4.3). RA signalling is thought to control anterior eye development and morphogenesis by regulation of key transcription factors (Matt et al., 2005). The signals affect gene expression by nuclear RAR dimers that bind retinoic acid response elements (RAREs) in the genome. One of these elements, a direct repeat of the nucleotide motif GTTCAC, was originally discovered in the promoter of the mouse RAR*ß*2 gene. The GTTCAC repeat is separated by five nucleotides and is able to confer RA responsiveness via all three RAR subtypes (Sucov et al., 1990). To test for if an element that combines the repetitive binding sites for the transcription factors PITX and FOX, as well as for RAR dimers, would confer overexpression of reporter gene, we created an 150 bp artificial enhancer that combined the RARE GTTCAC repeat with the recognition motives for PITX and FOX transcription factors (Table 4.3). E-boxes (enhancer boxes) with the consensus sequence CANNTG are recognized by helix-loop-helix transcription factors (Funk et al., 1991). Human *MYOC* contains a canonical E-box at the nucleotide position -152-(-146) (the numbers depict the nucleotide position before the by Nguyen et al. (1998) published second possible start ATG). This site was shown to be of prime importance in conferring *MYOC* basal promoter activity by the binding of USF (Kirstein et al., 2000). We created a 32 bp enhancer element of the *MYOC* promoter region -171-(-140) that contains the conserved E-box CACGTG (reviewed by Corre and Galibert 2005) (Table 4.3).

Element:	**Sequence (5´ → 3´) and length:**
PITX3	gtcatggctagcccttgggtaatccagcatgggccttgggtaatccagcatgggccttgggtaatccagcatgggctcgagacgtgt (87 bp)
FOX	gtcatggctagcgccaaaGTAAATAAAcaacaggccaaaGTAAATAAAcaacaggccaaaGTAAATAAAcaacagctcgagacgtgt (87 bp)
PITX3/ FOX	gtcatggctagcccttgggtaatccagcatggggccaaaGTAAATAAAcaacagccttgggtaatccagcatggggccaaaGTAAATAAAcaacagctcgagacgtgt (108 bp)
RAREß/ PITX3/ FOX	gtcatggctagcg**gttcac**cgaaa**gttcac**tcgccttgggtaatccagcatggggccaaaGTAAATAAAcaacagg**gttcac**cgaaa**gttcac**tcgccttgggtaatccagcatggggccaaaGTAAATAAAcaacagctcgagacgtgt (150 bp)
MYOC E-box	gcacagccccacccagcctcacgtggccacct (32 bp)

Table 4.3: List of created artificial enhancer elements that had been cloned in front of p313+67 between the restriction enzyme overhangs *Kpn*I and *Xho*I, or for human *MYOC* E-box between the restriction enzyme overhangs *Nhe*I and *Xho*I, to elicit an overexpression of the reporter gene firefly luciferase (Fig. 4.2). The sequence and the lengths of the elements are indicated. Repetitively ocurring evolutionary conserved binding sites for respective transcription factors are highlighted as underlined, capital letters, in bold and boxed for PITX, FOX, RAR and basic helix-loop-helix proteins, respectively.

To direct the activity of the artificial enhancers PITX3, FOX, PITX3/FOX and RAREß/PITX3/FOX to the TM, they were cloned in front of p313+67 and the reporter firefly luciferase between the restriction enzyme overhangs *Kpn*I and *Xho*I. The *MYOC* E-box was cloned into the same site via the restriction enzyme overhangs *Nhe*I and *Xho*I (Fig. 4.2). To analyze if the artificial elements had the capacity to induce an overexpression of protein in cultured HTM-N cells, we transfected the reporter constructs transiently into HTM-N cells and carried out a Dual-Luciferase® assay as described in Materials and methods 3.2.5. Repeated experiments showed that a combination of the binding sites for RAR, PITX and FOX transcription factors did elevate the expression up to 11.8-fold, highly significant, above the level of basal expression (Fig. 4.8). None of the other tested elements did have an effect on gene expression over *MYOC* basal promoter level (data not shown).

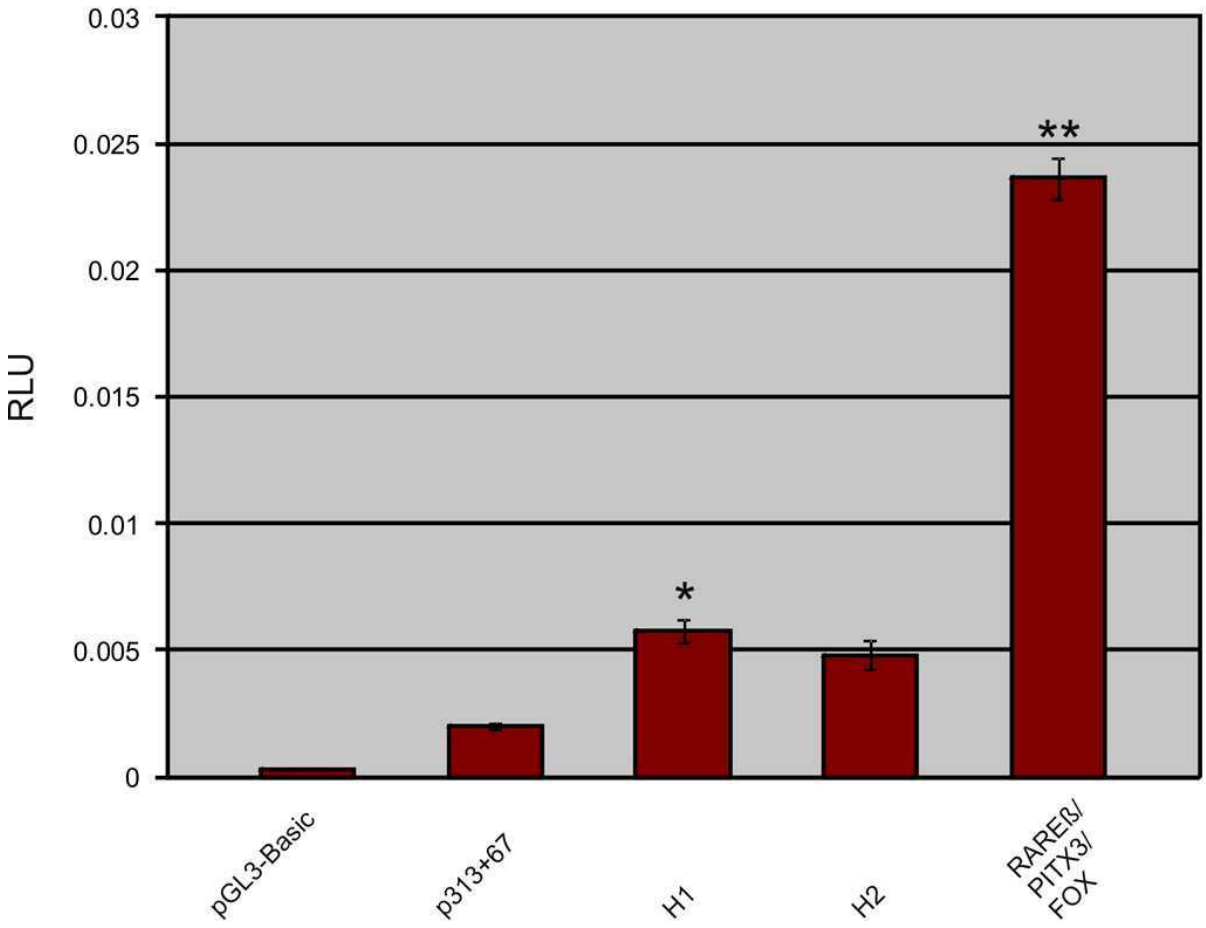

Figure 4.8: Analysis of the capacity of created artificial enhancer elements to, in combination with p313+67, drive high expression of reporter gene in cultured HTM-N cells. Reporter constructs bearing the created artificial enhancer elements listed in Table 4.3 in front of p313+67 were transiently transfected into HTM-N cells and a Dual-Luciferase® Reporter assay was carried out after 72 h of expression. pGL3-Basic contains no eukaryotic promoter or enhancer sequences and was used as a background control. Repeated assays confirmed that a combination of the binding sites for RAR, PITX and FOX transcription factors did elevate the expression up to 11.8-fold, highly significant, above the level of basal expression. As a comparison, the gene expression enhancement by the 3´-UTR genomic *MYOC* regions H1 and H2 are shown. The graph shows an individual experiment, where duplicate samples were analyzed. Mean standard deviation (± SD) between duplicates are shown. Asterisks mark statistically significant differences of reporter gene activity between samples and basal promoter (*$p < 0.05$, **$p < 0.02$).

To investigate if the characteristic of HTM-N cells to activate RAREß/PITX3/FOX-p313+67 to drive a ~ 10-fold elevation of reporter gene expression compared to basal expression level is specific to these cells, we wanted to look at the activity of RAREß/PITX3/FOX-p313+67 in another cell line. We transiently transfected RAREß/PITX3/FOX-p313+67-Firefly Luciferase into HEK-293 cells and analyzed reporter gene expression compared to the expression elicited by p313+67 alone. Repeated Dual-Luciferase® Reporter assays as described in Materials and methods 3.2.5 confirmed that HEK-293 cells do not offer the proper intracellular composition of transcription factors needed for RAREß/PITX3/FOX-p313+67 to activate gene expression (Fig. 4.9). This indicates that the capacity of RAREß/PITX3/FOX-p313+67 to activate reporter gene expression is not a general characteristic of cultured cells. In this regard and when comparing these two cultured cell lines, the capacity of RAREß/PITX3/FOX-p313+67 in activating high reporter gene expression is specific for HTM-N cells.

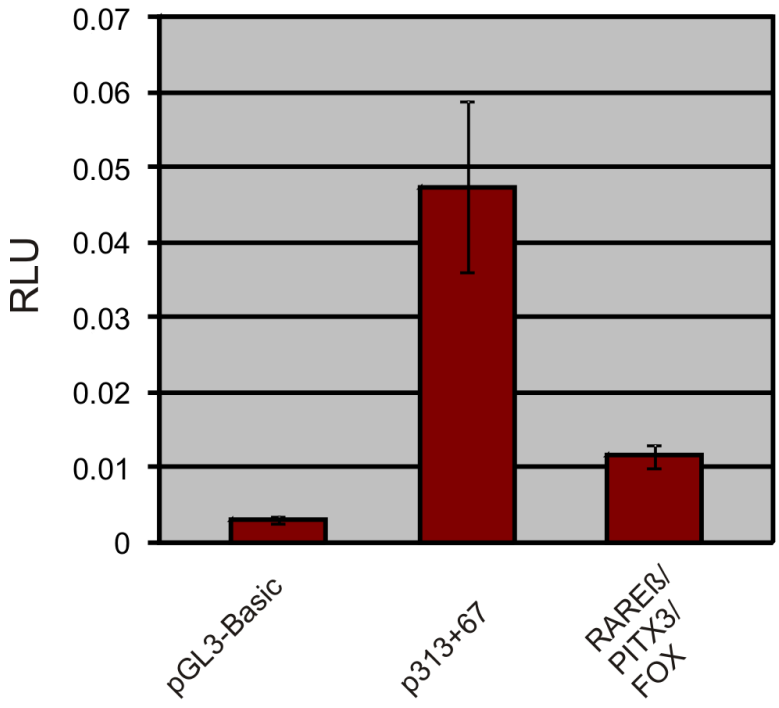

Figure 4.9: Dual-Luciferase® Reporter assay to find out if the activating effect of RAREß/PITX3/FOX-p313+67 on reporter gene expression in cultured HTM-N cells (Fig. 4.8) is a characteristic of these cells. As a comparison, we transiently transfected RAREß/PITX3/FOX-p313+67-Firefly Luciferase into HEK-293 cells and

analyzed reporter gene expression after 72 h of expression. pGL3-Basic contains no eukaryotic promoter or enhancer sequences and was used as a background control. Repeated assays confirmed that RAREß/PITX3/FOX-p313+67 could only confer minimal reporter gene activity in HEK-293 cells. The graph shows an individual experiment, where duplicate samples were analyzed. Mean standard deviation (± SD) between duplicates are shown.

4.2.2. Cloning of ß-galactosidase overexpression construct

Since cultured HTM-N cells had approved to offer the proper molecular machinery needed to activate the enhancer RAREß/PITX3/FOX-p313+67 to drive high reporter gene expression in these cells, we wanted to test if the activity of the element would also be sufficient to drive the expression of the reporter ß-galactosidase. We cloned an overexpression construct, where the gene for ß-galactosidase, *LacZ*, was driven by p313+67, as well as the artificial enhancer RAREß/PITX3/FOX. It has been shown that a reiteration of the SV40 large T-antigen nuclear localization signal (NLS) significantly increases the efficiency of nuclear polypeptide transport in mammalian cells (Fischer-Fantuzzi and Vesco, 1988). To ensure that the mature ß-galactosidase would be effectively imported into the nucleus, a repetitive NLS, 3 X NLS, was cloned in frame with the *LacZ* ORF, just behind the codon for the start ATG (Fig. 4.10).

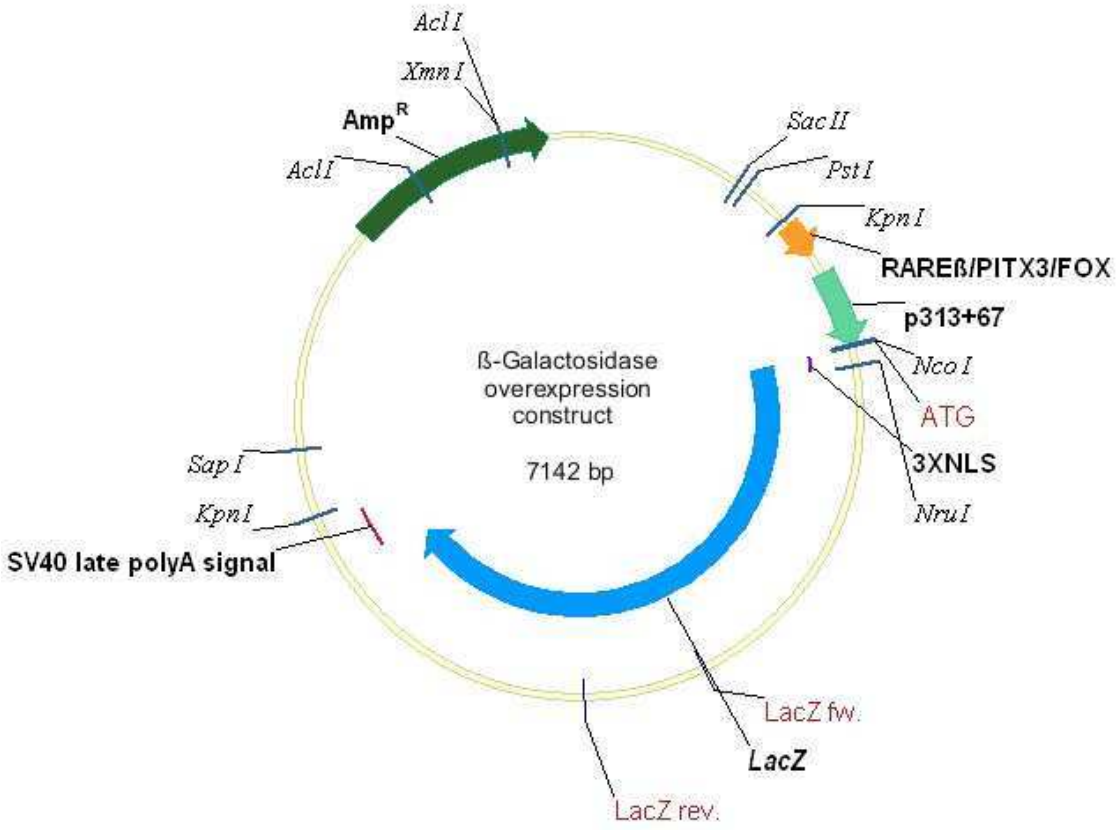

Figure 4.10: Cloned ß-galactosidase overexpression construct, where the gene for ß-galactosidase, *LacZ*, was designed to be driven by the artificial enhancer element RAREß/PITX3/FOX and p313+67. To ensure that the mature ß-galactosidase would be effectively imported into the nucleus, a repetitive nuclear localization signal, 3 X NLS, was cloned in frame with the *LacZ* ORF, just behind the codon for the start ATG. The transgene was cut out from the plasmid by the restriczion enzyme *Kpn*I. Additional restriction enzyme cleavage sites used to degrade the backbone and thus to facilitate separation of the transgene from the rest of the plasmid by agarose gel electrophoresis are depicted. Possible founder animals were screened for by PCR with a primer pair that binds within *LacZ* (LacZ fw./LacZ rev., shown in red) and that produces a 524 bp amplicon. For routine genotyping we used a primer pair that binds within 3 X NLS and *LacZ*, producing a 220 bp amplicon (NLS fw./LacZ rev. 2, not shown).

4.2.3. Testing of functionality of the ß-galactosidase overexpression construct in cultured HTM-N cells

To test for the functionality of our cloned ß-galactosidase overexpression construct in a living system, i.e. to analyze if the activity of the artificial enhancer RAREß/PITX3/FOX and p313+67 is enough to drive visible expression of ß-galactosidase in cell cultures, we transfected the construct into HTM-N cells that had been plated out on object plates. *LacZ* -staining of the cells showed that *LacZ* was transcribed in HTM-N cells *in vitro* and that the reiteration 3 X NLS tagged mature ß-galactosidase effectively into the nucleus in these cells (Fig. 4.11A, B). In contrast, a comparing *LacZ*-staining of HTM-N cells that had been transfected with the same construct devoid of 3 X NLS showed cytocolic, as well as nuclear localization of ß-galactosidase (Fig. 4.11C). The *LacZ*-staining confirmed that our cloned ß-galactosidase overexpression construct was functional in cultured HTM-N cells.

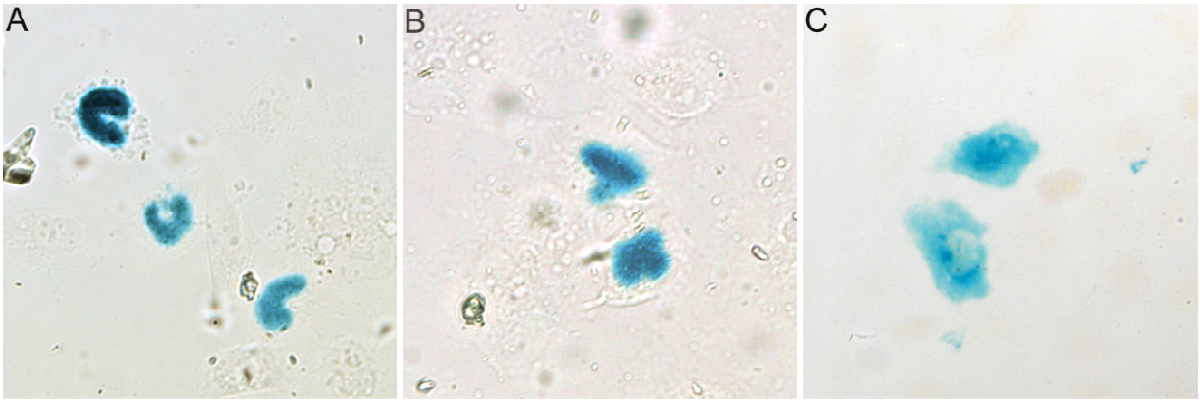

Figure 4.11: Testing of functionality of the ß-galactosidase overexpression construct in cultured HTM-N cells. Cloned ß-galactosidase-expressing construct (Fig. 4.10) was transfected into HTM-N cells that had been plated out on object plates. *LacZ*-staining of the cells showed that RAREß/PITX3/FOX-p313+67 did drive visible ß-galactosidase expression in these cells. The reiteration 3 X NLS tagged mature ß-galactosidase effectively into the nucleus (Fig. 4.11A, B). In contrast, HTM-N cells that had been transfected with the same overexpression construct devoid of 3 X NLS showed cytocolic, as well as nuclear localization (C). Images were made by an Axio Imager Z1 microscope at a 40 X magnification.

4.2.4. Purification of ß-galactosidase overexpression construct for pronuclear injection

Since HTM-N cells proved to have the required molecular machinery to activate RAREß/PITX3/FOX-p313+67 to drive high protein expression in these cells *in vitro* (Fig. 4.8), a characteristic not seemed to be general among cell lines (Fig. 4.9), and since our cloned ß-galactosidase overexpression construct was able to direct expected blue staining into the nuclei of cultured HTM-N cells (Fig. 4.11A, B), we decided to test our ß-galactosidase overexpression construct in an *in vivo* mouse model. We wanted to create a TG mouse line that would express visible RAREß/PITX3/FOX-p313+67-driven ß-galactosidase in the TM. We released the 4041 bp linear transgene from the ß-galactosidase overexpression construct by restriction with *Kpn*I. To facilitate separation of the transgene from the rest of the plasmid by agarose gel electrophoresis, the backbone was further restricted into smaller fragments by the restriction enzymes *Sap*I, *Xmn*I, *Acl*I and *Sac*II (Fig. 4.10). After complete separation of the transgene from the backbone, it was cut out from the gel and purified as described in Materials and methods 3.1.2.2 for mouse male pronuclear injection. 4.45 µg of purified transgene was sent to Max Planck Institute (MPI) for Neurobiology in Martinsried, Münich, for microinjection by standard protocols into male pronuclei of fertilized mouse oocytes of a FVB/N background.

4.2.5. Screening for founder animals

48 tail biopsies from possible founder mice bearing the transgene were sent back to us from MPI. We screened for these biopsies by PCR using a primer pair that binds *LacZ* within the transgene (LacZ fw. and LacZ rev), and that results in an amplicon of 524 bp (Materials and methods 3.3.3. and Fig. 4.10). We identified three animals, animal numbers 8387, 8388 and 8390, that had integrated RAREß/PITX3/FOX-p313+67-3 X NLS-*LacZ* into their genomes (Fig. 4.12).

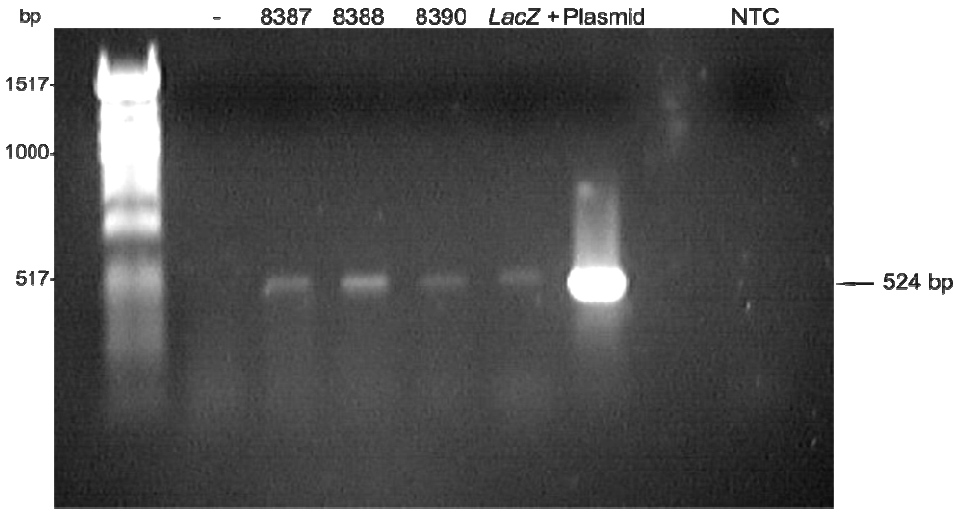

Figure 4.12: Screening for founder animals by PCR with a primer pair that binds and amplifies a 524 bp product from integrated *LacZ* (Fig. 4.10). The image of the agarose gel shows PCR reactions from tail biopsies of three identified founder animals: 8387, 8388 and 8390. PCR reactions from tail biopsies of a negative animal (-) and a known *LacZ*-positive mouse (*LacZ*+), served as negative and positive controls, respectively, for genomic DNA. ß-galactosidase overexpression construct (Plasmid) serves as a general positive control. NTC = no template control.

4.2.6. Establishing of TG mouse lines

In order to establish TG ß-galactisidase overexpression mouse lines, the positive animals 8387 (male), 8388 (male) and 8390 (female) were crossed with a WT animal of the same FVB/N background. The offspring was screened for transgenic animals by PCR as above. After screening of many litters, it appeared that only the lines 8388 and 8390 were able to transfer the transgene to the next generation. The line 8388 produced TG offspring in a normal Mendelian fashion. The mice of this line appeared normal (body size, number of litters etc.). Genotyping of embryos of the line 8390 at E12.5 showed that also this line was able to transfer the transgene to the next generation. Indeed, the born litters of this line were unusually small (only 2 - 5 animals) and did rarely contain TG animals. If a TG animal of this line was born, it was always a female that showed a physically retarded phenotype. It was smaller than normal in body size, the incidence of growth of hair coat was delayed (Fig. 4.13A, B), the incidence of fertility occurred later as usual for mice of the same FVB/N

background and the time span between litters tended to be longer than the normal three weeks. The fact that TG embryos of this line looked normal and existed in a normal Mendelian fashion at E12.5, but were rarely born, indicates that TG embryos of this line died in the uterus at some time point after E12.5. The founder animal of the line 8390 lost its fertility already at an age of 6 months.

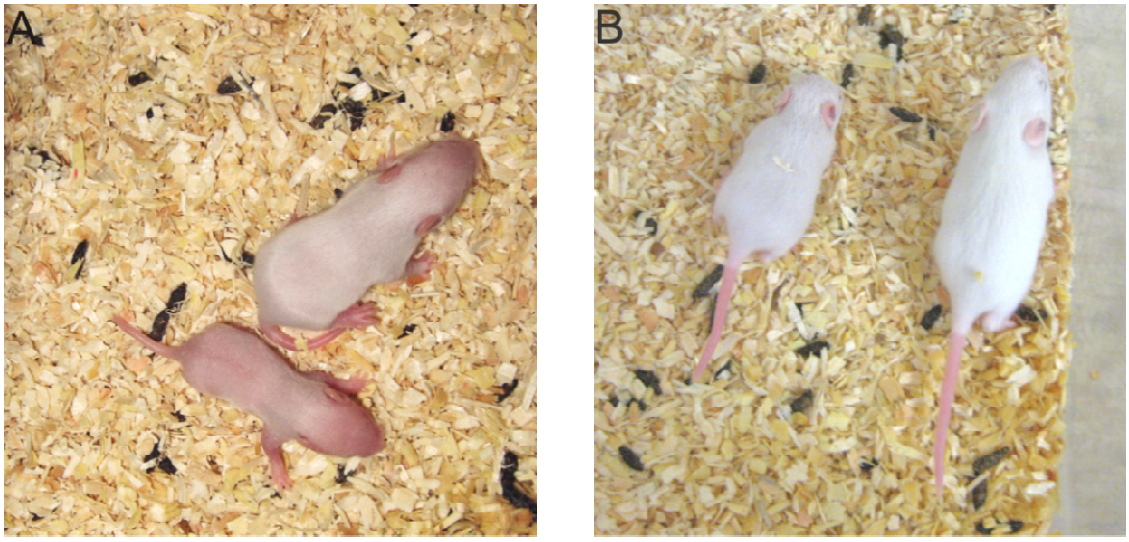

Figure 4.13: A litter of the TG ß-galactosidase overexpression mouse line 8390. The mice of this line transferred the transgene to the next generation in a normal Mendelian fashion. Even though the TG embryos at E12.5 looked normal, TG animals were rarely born. A) 7 d old litters with a TG animal beneath its WT littermate. TG animals were always females and showed a retarded physical development. Note the small size and the delay of the incidence of growth of the hair coat of the TG compared to the WT litter. B) The same animals at an age of 14 d. Even though the TG animal (left) has a hair coat at this age, its body size is still remarkably smaller compared to that of its WT litter (right). The images were taken by a Canon Power Shot A530 digital camera.

Genotyping of many litters of the founder 8387 confirmed that this founder animal was not able to transfer the transgene to the next generation. With respect to these facts, we only had one line, the line 8388 that was stabile in producing TG litters. Due to the rarity of born TG animals of the line 8390, this line could not be considered as stabile.

4.2.7. *LacZ*-staining of adult organs

Since myocilin is expressed in almost every tissue of the adult human and mouse eye (Karali et al., 2000; Knaupp et al., 2004), the adult human and rat sciatic nerve (Ohlmann et al., 2003), and at the RNA level in the human and adult mouse heart (Ortego et al., 1997; Swiderski et al., 1999), we wanted to analyze if RAREß/PITX3/FOX, together with p313+67, would be able to drive and direct visible ß-galactosidase expression into these tissues *in vivo*. Adult eyes, hearts and sciatic nerves from adult TG and WT ß-galactosidase overexpression mice of the lines 8388 and 8390 were *LacZ*-stained as described in Material and methods 3.4.2. Eyes and brain of a Pax6$^{lacZ/+}$-mouse (St. Onge et al., 1997) were stained as positive control. *LacZ*-staining of sectioned organs (for line 8388), as well as of whole organs (for lines 8388 and 8390), did not reveal any expression of ß-galactosidase in TG adult eyes, hearts or sciatic nerves (Fig. 4.14A, B and C). This indicates that RAREß/PITX3/FOX-p313+67 could not be activated to drive visible ß-galactosidase expression in these adult organs.

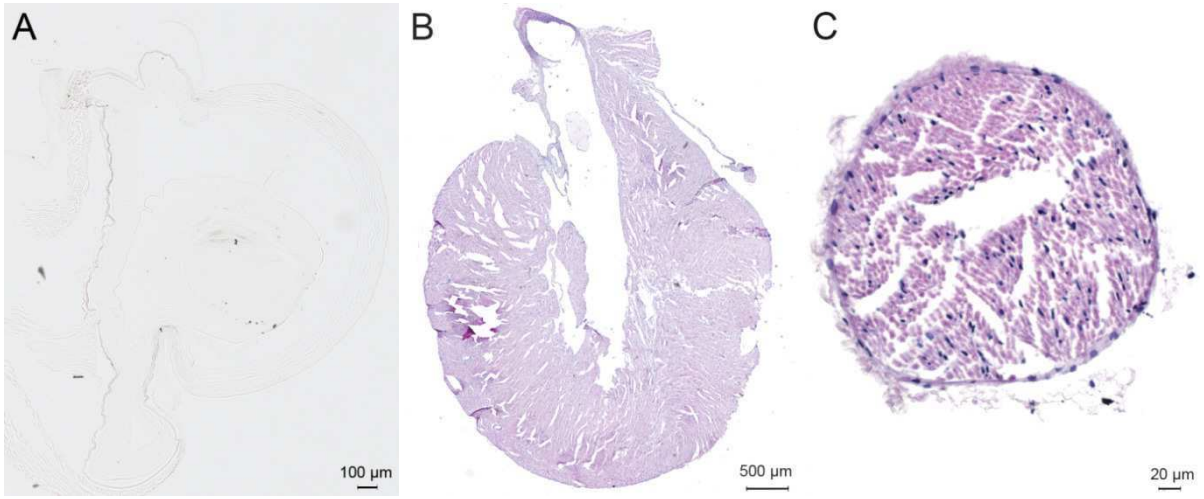

Figure 4.14: *LacZ*-staining of sagittal cryosections of eye (A) and heart (B), as well as a transverse cryosection of sciatic nerve (C) of an adult TG ß-galactosidase overexpression mouse of the line 8388. No *LacZ*-staining was seen in these organs, indicating that RAREß/PITX3/FOX-p313+67 could not be activated to drive visible ß-galactosidase expression in these adult organs. Organs from a $Pax6^{lacZ/+}$-mouse (St. Onge et al., 1997) were stained as a positive control (data not shown). For better visualization of fine structures, sections of heart and sciatic nerve were counterstained by haematoxylin-eosin staining. The images were taken by an Axio Imager Z1 microscope at 5 X and 20 X magnifications for A, B and C, respectively.

4.2.8. *LacZ*-staining of embryos

4.2.8.1 Analaysis of *LacZ*-staining of eyes

As it is known that RA-dimers, PITX- and FOX-transcription factors are pivotal in anterior eye development in human and in mouse at around E12.5 (reviewed by Cvekl and Tamm, 2004; Matt et al., 2005), we wanted to analyze if the artificial enhancer element RAREß/PITX3/FOX, in combination with p313+67, is able to drive visible ß-galactosidase expression in the developing mouse eye at this time point. TG and WT E12.5 embryos of the ß-galactosidase overexpression lines 8388 and 8390 were *LacZ*-stained and analyzed for visible blue staining of the eyes. *LacZ*-stained E12.5 $Pax6^{lacZ/+}$-embryos (St. Onge et al., 1997) served as positive control. Repeated staining experiments showed that RAREß/PITX3/FOX-p313+67 was not activated to drive visible expression of ß-galactosidase in the eyes of TG ß-galactosidase overexpression mice at this time point in either of the TG lines. As in the eye of the WT embryo of line 8390 (Fig. 4.15C), only background staining could be observed in the TG eyes of both lines (Fig. 4.15A and B).

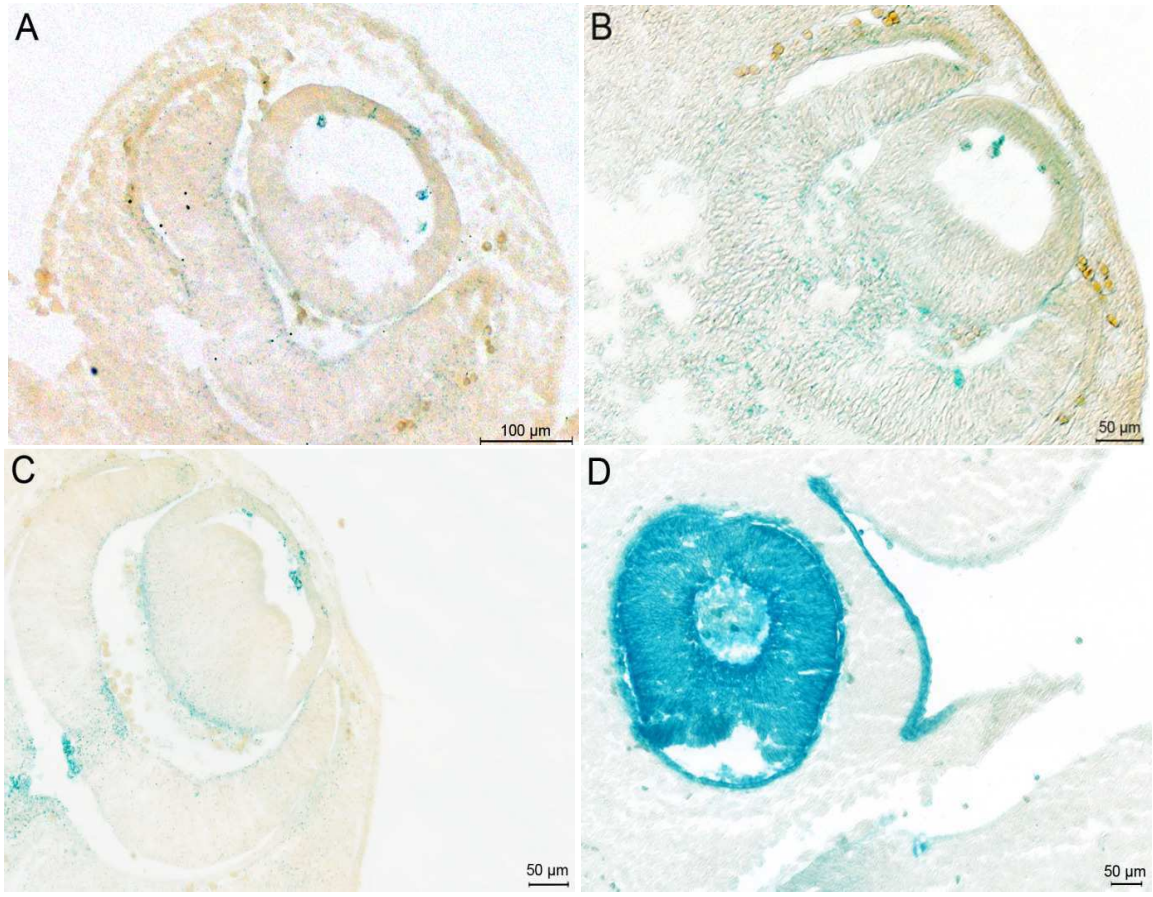

Figure 4.15: *LacZ*-staining of ß-galactosidase overexpression embryos at E12.5. No staining above background level was observed in the eyes of TG embryos of the lines 8388 (A) or 8390 (B). C) A WT littermate of the line 8390 showing background staining. D) Pax6$^{lacZ/+}$-embryos (St. Onge et al., 1997) were stained as positive control. A) and D) show images made by an Axio Imager Z1 microscope at 10 X and 40 X magnifications, respectively, of sagittal cryosections of whole embryos. B) and C) show images made at a 40 X magnification of transverse cryosections of the head.

4.2.8.2 Analaysis of *LacZ*-staining of other embryonic regions

Further investigation of cryosections of *LacZ*-stained E12.5 embryos of the ß-galactosidase overexpression line 8390 revealed that TG embryos had visible staining of ß-galactosidase in

the epithelial layer of cells lining the ventricular system of the brain and the spinal cord (Fig. 4.16A). This ependymal staining could not be detected in WT embryos (Fig. 4.16B).

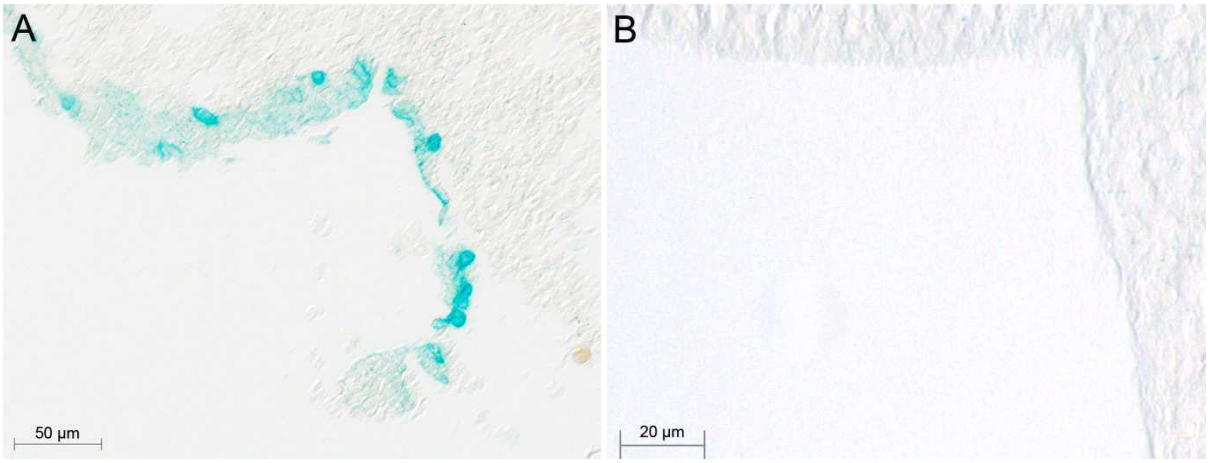

Figure 4.16: Comparison of transverse cryosections of *LacZ*-stained E12.5 embryos of the ß-galactosidase overexpression line 8390. A) The section of the TG littermate shows visible blue staining of the epithelial layer of cells lining the ventricular system of the brain and the spinal cord. B) This ependymal staining could not be detected in a WT littermate. Images were made by an Axio Imager Z1 microscope at a 40 X magnification.

Comparison of lower body parts of cryosections of *LacZ*-stained E12.5 embryos of the ß-galactosidase overexpression line 8390 revealed that TG embryos had visible staining of ß-galactosidase in the epithelial linings of intestinal glands (Fig. 4.17A and B) that could not be detected in WT embryos (data not shown).

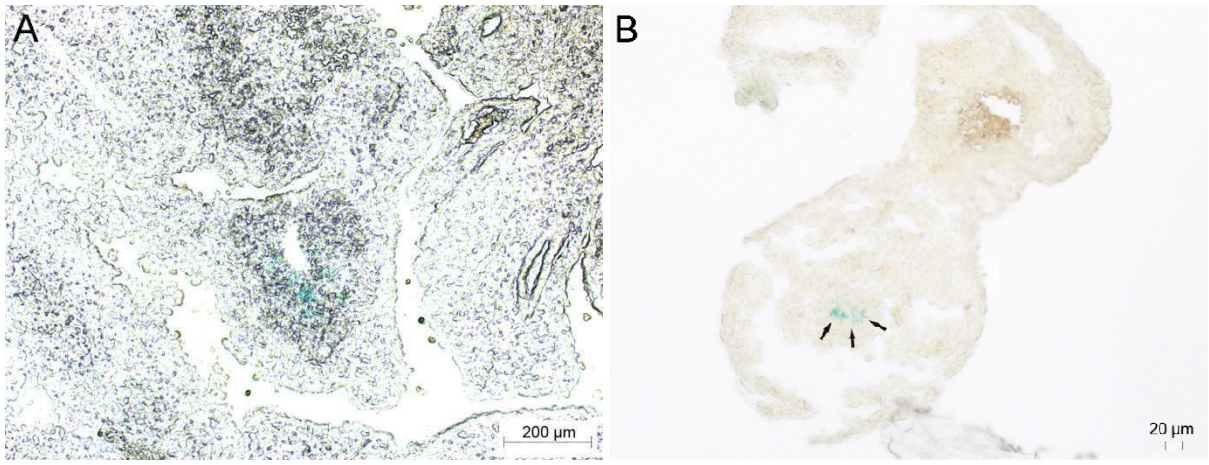

Figure 4.17: Cryosections of *LacZ*-stained TG E12.5 embryos of the ß-galactosidase overexpression line 8390. A) A sagittal section that shows visible staining of ß-galactosidase in the loops of the small intestine. B) A transverse section of a second TG embryo of the same line confirmed that the ß-galactosidase staining seen in A) resided within the epithelial cells of intestinal glands (arrows) B). Images were made by an Axio Imager Z1 microscope at 10 X and 20 X magnifications, respectively, for A) and B).

4.3. Analysis of myocilin expression in mammalian brain

4.3.1. Analysis of myocilin expression in the ependyma and periventricular zone (PVZ) by immunohistochemistry

The fact that the *MYOC* basal promoter, in combination with our constructed artificial enhancer element RAREß/PITX3/FOX, was able to drive unexpected visible ß-galactosidase expression in the ependymal lining of the lateral ventricle in the embryonic mouse brain (Fig. 4.16A), prompted us to investigate the endogenous expression of myocilin in this tissue in mammals by immunohistochemistry. The ependymal lining of the ventricles is continous with the epithelial layer of the choroid plexus (CP), a vascularized structure that produces cerebrospinal fluid (CSF) into the ventricles, and that is responsible for filtration between the blood and the CSF (making up the so called blood-CSF barrier) (Fig. 4.18).

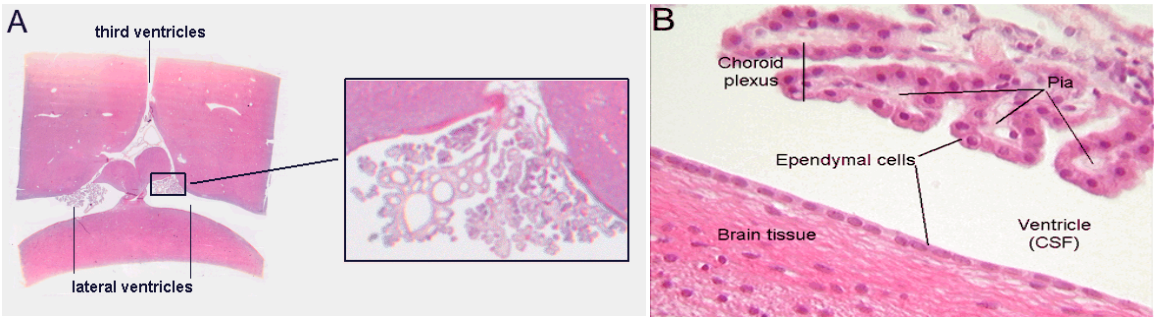

Figure 4.18: Overview of haematoxylin-eosin stained coronal sections showing brain ventricles and ependyma. A) In mammals, the vascular CP can be found within the CSF-filled ventricular system (boxed and shown in higher magnification for the right lateral ventricle). The specialized epithelial lining of the CP secretes CSF into the ventricles and is responsible for filtration of metabolites and waste products between the blood and CSF. B) Despite this specialization, the epithelium is continous with the ependymal lining of the brain tissue. Source: http://neuromedia.neurobio.ucla.edu/campbell/nervous/wp_images%5C199_brain_ependyma.gif.

Various approaches using antibodies against ependymal myocilin in brain sections of newborn mice did not confirm our suggestion about endogenous myocilin expression in this tissue (data not shown). There are generally problems by using anti-myocilin antibodies against mouse myocilin (reviewed by Ezzat et al., 2008), and by experience we know that our available myocilin antibodies may not work well, or may be associated with background staining in mouse tissues. Thus, we wanted to test these antibodies against rat myocilin ependymal cells. Immunohistochemistry of sections of 6 week old rats confirmed our suggestion of endogenous myocilin expression in mammalian ependyma (Fig. 4.19A, C and E).

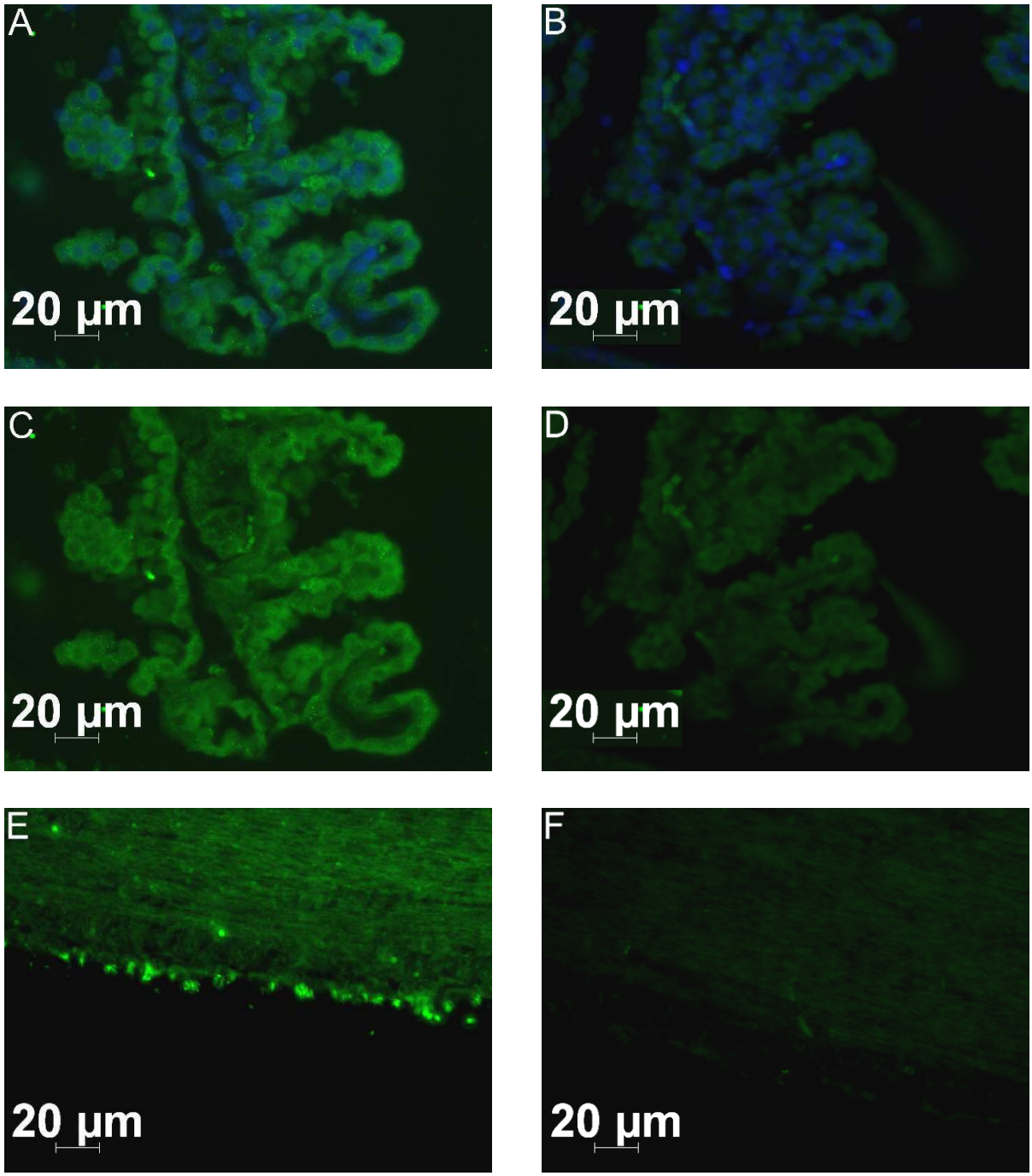

Figure 4.19: Immunohistochemistry of transverse paraffin sections of 6 week old rat brain sections using a rabbit-derived primary antibody against myocilin and a secondary green fluorescent anti-rabbit antibody. The epithelial cells of the CP of the lateral ventricle were distinctively labelled against myocilin (A and C), when compared to the control (B and D). DAPI staining in A and B show the nuclei. The ependymal cells of the ventricular lining are intensively labelled for myocilin (E), whereas only faint background labelling is seen in the control (F). Immunofluorescent images were made by an Axio Imager Z1 fluorescent microscope at a 40 X magnification.

Similarly to neurons and glial cells, ependymal cells originate from the germinal neuroepithelium of the neural tube. Ependymal cells are categorized as glial cells, and they can make contacts to neurons and other glial cells in the adjacent subventricular zone (SVZ) of the PVZ (Gilbert, 2006). The expression of myocilin within the ependymal lining of the lateral ventricle (Fig. 4.19E) prompted us to expand the area of analysis of myocilin expression to the PVZ. Immunohistochemistry of brain sections of 6 week old rats by using an antibody against myocilin showed distinctive endogenous labelling of myocilin within neurons and glial cells of the PVZ of the lateral ventricle. The labelling was located to perikarya and to bundles of axons (Fig. 4.20A and B).

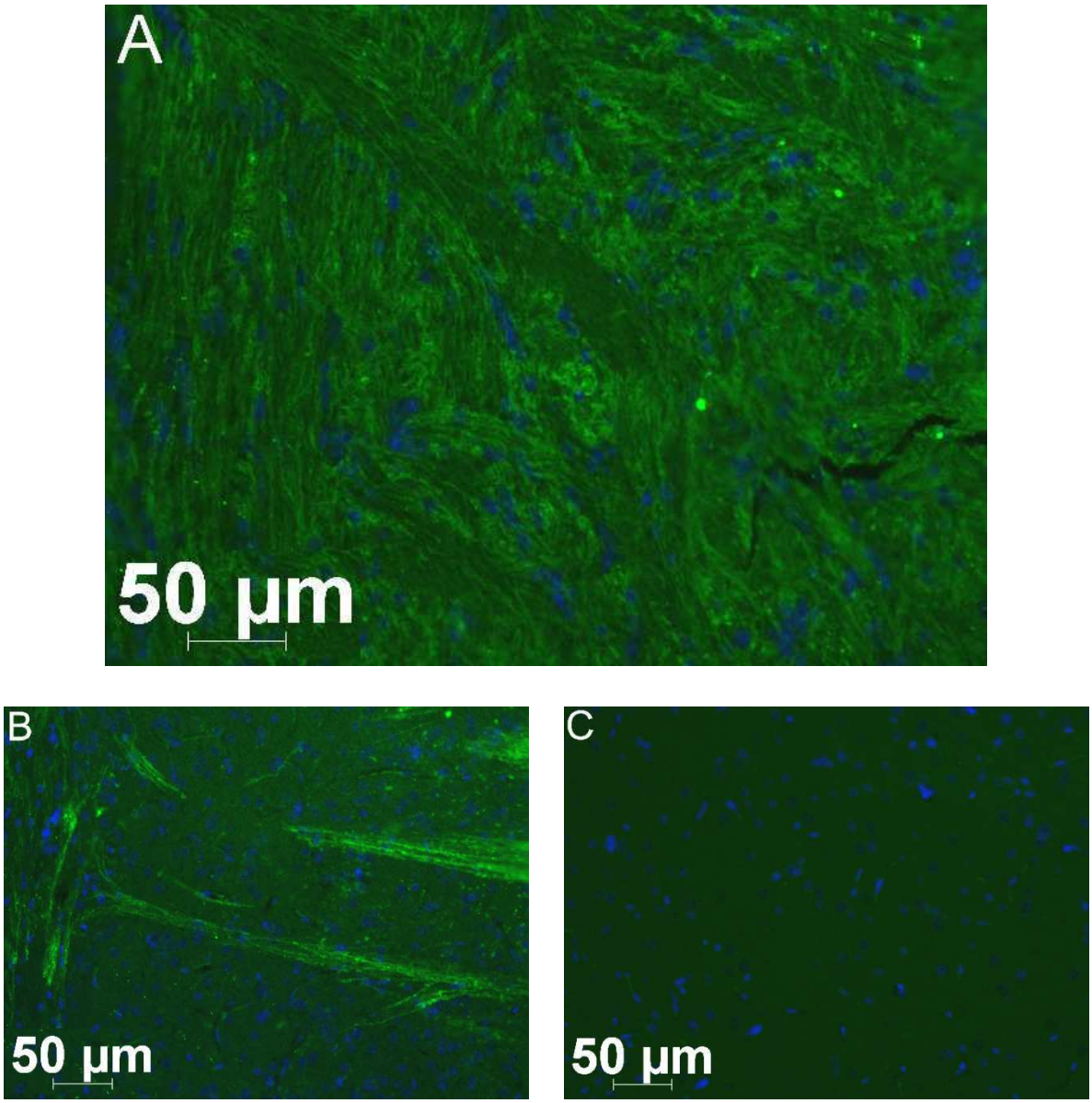

Figure 4.20: Immunohistochemistry of transverse paraffin sections of 6 week old rat brain sections using a rabbit-derived primary antibody against myocilin and a secondary green fluorescent anti-rabbit antibody. Endogenous myocilin expression was observed within neurons and glial cells of the PVZ of the lateral ventricle (A and B), whereas only faint background labelling is seen in the control (C). The positive myocilin labelling locates to perikarya, as well as to bundles of axons as exemplified in B). DAPI staining shows the nuclei (A – C). Immunofluorescent images were made by an Axio Imager Z1 fluorescent microscope at a 20 X magnification.

4.3.2. Analysis of myocilin expression in human CSF by Western blot

Together with the ependymal lining of the ventricles, the ependymal cells of the CP secrete about 450 - 600 ml CSF/day into the ventricles. The CSF offers mechanical protection to and regulates homeostasis of the central nervous system (CNS) (Bob and Bob et al., 2007). Drainage of CSF through the arachnoid granulations into the venous system or directly into the lymphatic vessels clears the CNS from waste products. The rate of secretion into and drainage out of the brain ventricles of CSF thus regulates the intraventricular CSF volume, which in turn regulates intracranial pressure and blood flow perfusion (reviewed by Kapoor et al., 2008).

Since we detected myocilin expression in the ependymal cells of the CP and the lining of the lateral ventricle in rat (Figs. 4.19A and C), we wanted to analyze if myocilin is secreted into the CSF in mammals. As the volume of CSF that can be obtained from rat is limited in comparison to volumes that can be obtained from human patients during lumbar puncture, and since we had access to CSF samples collected from patients during this procedure (PD Dr. med. Andreas Steinbrecher, Department of Neurology, University of Regensburg), we had earlier analyzed the expression of myocilin within human CSF by Western blot. Analysis of CSF samples from 18 patients showed that myocilin is secreted into human CSF. An antibody directed against myocilin detected it as the typical 55 - 57 kD double band (Nguyen et al., 1998; Clark et al., 2001) in most of the samples and, in some samples (4, 7, 8, 10, 19 and 12) as a single ~ 56 kD band. The band intensities varied in intensity between the two bands of the double band, as well as between samples (Fig. 4.21),

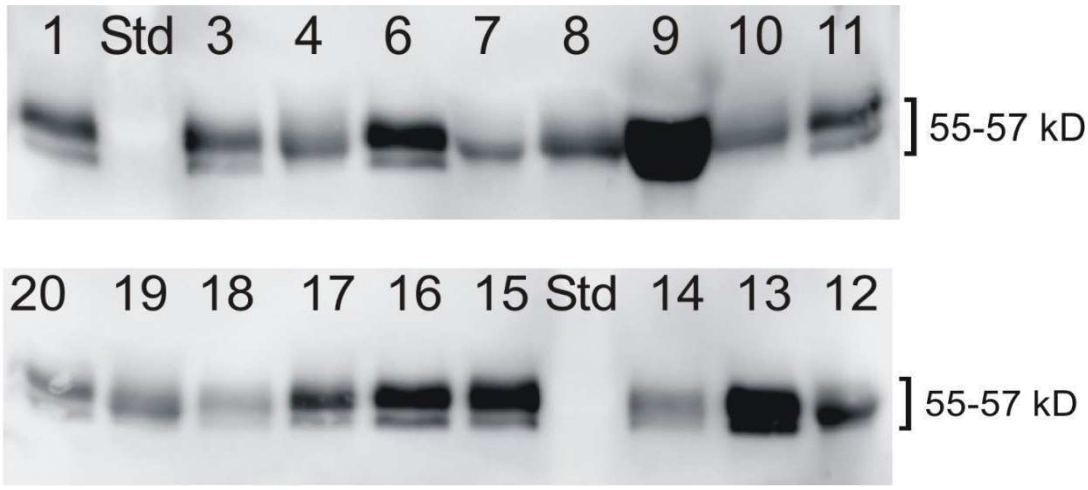

Figure 4.21: Western blot of CSF samples collected from 18 human patients (numbered 1 – 18) during lumbar puncture. 30 µl of CSF was loaded on a polyacrylamide gel, transferred to a nitrocellulose membrane and blotted against myocilin with a goat-derived antibody against myocilin. Visualization of bound primary antibody was carried out by using a chemiluminescent secondary antibody directed against the primary antibody. In most samples myocilin was detected at varying intensity as a 55 – 57 kD double band, whereas it in some samples was detected as a single 56 kD band (samples 4, 7, 8, 10, 19 and 12). Std = standard. Blotting was carried out by Dr. Markus Kröber.

4.4. Creation of *myoc* knock-in mouse line

Since RAREß/PITX3/FOX, in combination with the *MYOC* basal promoter, was not able to drive visible ß-galactosidase expression above background level in mouse TM *in vivo* (Figs. 4.14A and 4.15), we made a second effort to target *in vivo* gene expression into this tissue. Myocilin shows a strong expression at both mRNA and protein level in human and mouse TM (Adam et al., 1997; Karali et al., 2000; Takahashi et al., 1998; Knaupp et al., 2004) and gene expression profiling of human TM confirmed that myocilin is the third most abundant message expressed in this tissue (Tomarev et al., 2003). A conditional knock-out by the Cre/*lox* system (reviewed by Sauer, 1998) in the TM would offer the possibility to study a wide spectrum of molecular interaction and function contexts in this tissue, and should be of immense value in unravelling the mechanisms that build up an elevated IOP. This prompted us to use the endogenous mouse *myoc* promoter to direct the expression of Cre recombinase into the TM of an *in vivo* mouse model.

4.4.1. Cloning of *myoc* knock-in construct

We designed a *myoc* knock-in construct, which would allow the integration of the gene for Cre recombinase in frame at the *myoc* locus by homologous recombination (Tymms and Kola, 2001; Ch. 3). Details to amplification of homologous flanks, as well as to cloning of the construct, are described in Materials and methods 3.1.3.1. Sequencing of amplified 3072 bp homologous 5´-flanks revealed that all screened colonies contained point mutations. The clone of choice carried two mutations: - 1670 G → A and – 897 T → C, where the numbers depict respective nucleotide position before mouse *myoc* start ATG (Tomarev et al., 1998). Sequencing of amplified 2268 bp 3´-homologous flanks revealed that all screened colonies contained point mutations. The clone of choice carried one mutation: + 2129 T → C, where the number depicts the nucleotide position after mouse *myoc* start ATG (Tomarev et al., 1998). Inter-species comparison of the mutated regions did not show conservation, suggesting that the point mutations would not interfere with transcriptional regulation of the construct. The 5´-homologous flank was ligated into the backbone vector pTV-0 between the restriction

enzyme recognition sites *Not*I and *Xho*I. The 3´-homologous flank was ligated into pTV-0-5´-flank between the restriction enzyme recognition sites *Nhe*I and *Sal*I. Finally, the sequenced NLS-Cre-IRES-eGFP was cut out from the pSL1180-backbone vector by *Xho*I and ligated at this recognition site just behind the 5´-homologous flank (Fig. 4.22). The bacterial clones were screened for correct orientation of inserted NLS-Cre-IRES-eGFP by test-cutting their plasmids with appropriate restriction enzymes known to yield fragments of different sizes for either orientation of the insert. The clone bearing the correctly inserted NLS-Cre-IRES-eGFP was still proved for all of its introduced parts by cutting the isolated plasmid DNA with different sets of restriction enzyme combinations, as well as by sequencing over the 5´-flank-NLS-Cre and 3´-flank-Neo edges. The clone bearing the successfully cloned *myoc* knock-in construct was isolated for its plasmid DNA by endonuclease-free Maxi-preparation.

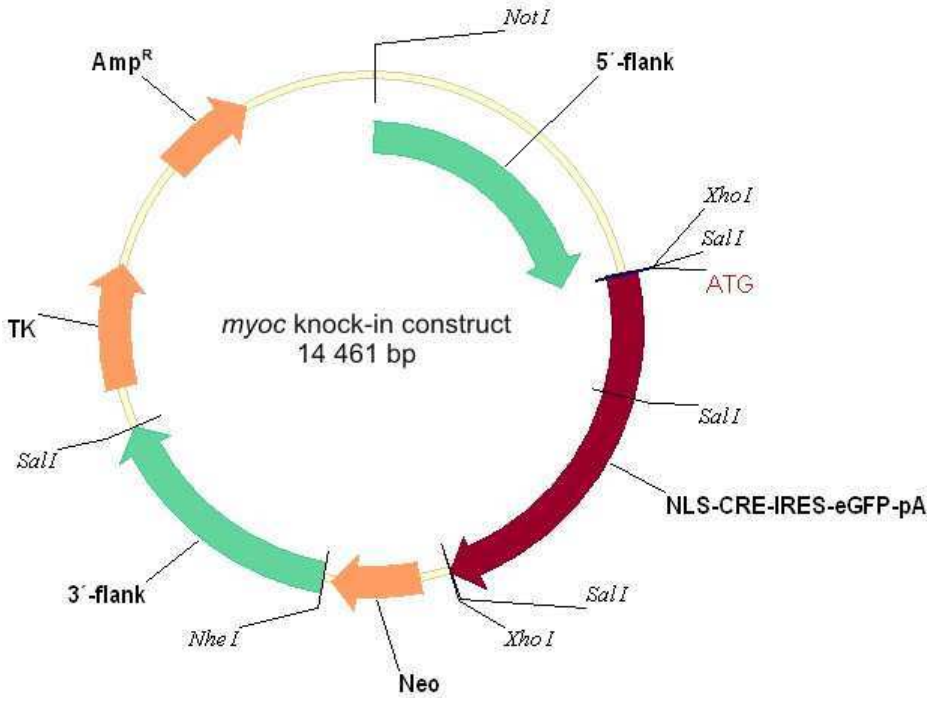

Fig. 4.22: Plasmid map of cloned 14 461 bp *myoc* knock-in construct. The pTV-0 vector, containing the genes for neomycin resistance (Neo) and thymidine kinase (TK) needed for positive and negative selection, respectively, of positive ESCs (Tymms and Kola, 2001; Ch. 3), had been used as a backbone (Fig. 3.5). For electroporation into mouse ESCs, the construct was linearized by restriction with *Not*I and purified by phenol/chloroform/isoamylalcohol extraction.

4.4.2. Linearization and purification of *myoc* knock-in construct for electroporation into mouse ESCs

The *myoc* knock-in construct was linearized by cutting it with *Not*I and purified for electroporation into mouse ESCs by phenol/chloroform/isoamylalcohol extraction as described in Materials and methods 3.1.3.2. 200 µg of linear purified construct was sent to MPI for Neurobiology in Martinsried, Münich, to be electroporated into mouse ESCs of a FVB/N background by standard protocols.

4.4.3. Screening of electroporated ESCs for homologous recombination of the knock-in construct at the *myoc* locus by Southern blot

Clones of electroporated ESCs were positively and negatively selected for the knock-in construct as described in Tymms and Kola 2001; Ch. 3. Clones that had passed this selection were lysed in a 96-well plate by standard methods (Tymms and Kola 2001; Ch. 5). The lysates were screened for proper homologous recombination at both flanks by Southern blot with radioactive probes directed against the *myoc* locus. The Southern blot strategy had been made up in combination with the cloning stategy by carefully choosing restriction enzymes that would cut WT and knock-in alleles differentially and yield fragments with a size difference of at least 1000 bp. Based on database data (Ensembl Genome Browser) for the *myoc* sequence, a restriction with *Xba*I should result in band sizes of 5432 and 7203 bp for WT and knock-in alleles, respectively, after correct homologous recombination of the 5´-end of the construct. After correct homologous recombination of the 3´-end of the construct, a restriction with *Hind*III should result in band sizes of 6743 and 4665 bp for WT and knock-in alleles, respectively (Fig. 4.23).

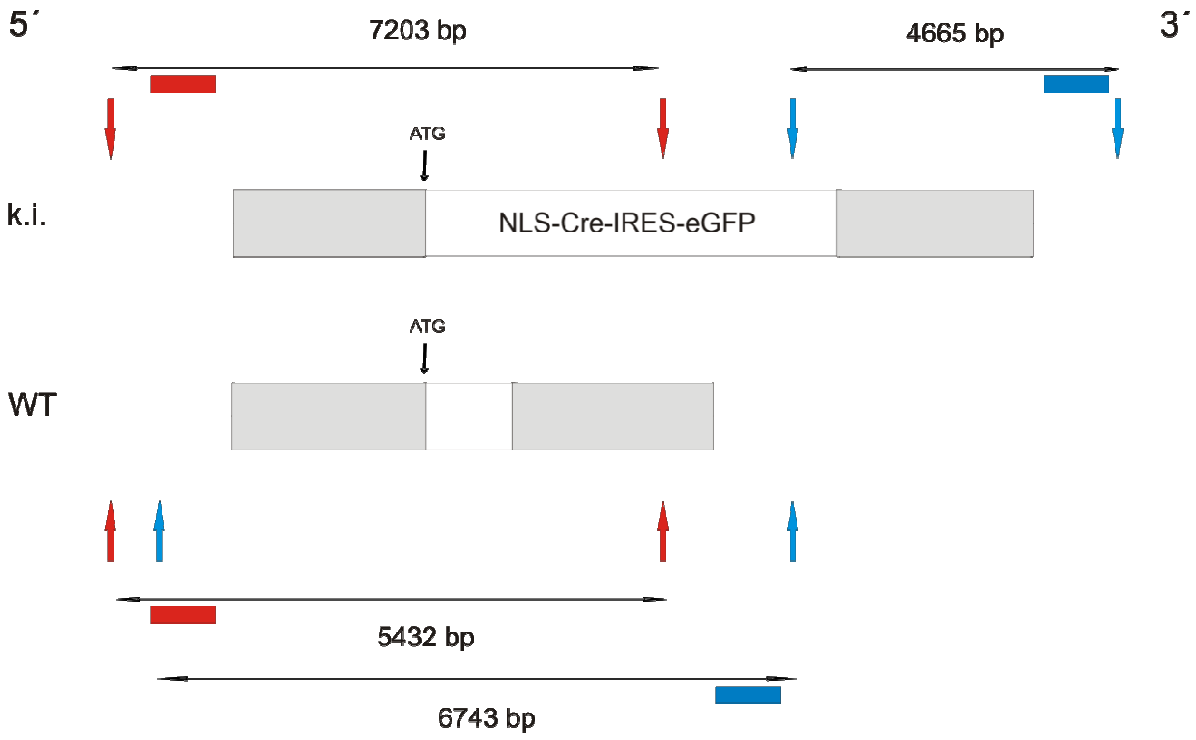

Fig. 4.23: Southern blot strategy for screening of homologous recombination of the knock-in construct at the *myoc* locus. The graphic depicts WT and knock-in (= k.i.) alleles with the 5´- and 3´-homologous flanks in grey. The radioactive probes (red bar for the 5´-probe, blue bar for the 3´-probe) were designed to hybridize with restriction fragments of different size for WT and knock-in alleles, respectively. The 5´-flank was screened for by digestion with *Xba*I to yield WT and knock-in alleles of 5432 and 7203 bp, respectively (red arrows). The 3´-flank was screened for by digestion with *Hind*III to yield WT and knock-in alleles of 6743 and 4665 bp, respectively (blue arrows).

Screening of 420 ESC-clones revealed one colony, where the 3´-homologous flank had recombinated correctly at the *myoc* locus. After restriction with *Hind*III the radioactive probes bound the expected fragments of 6743 and 4665 bp for the WT and knock-in alleles, respectively (Fig. 4.24).

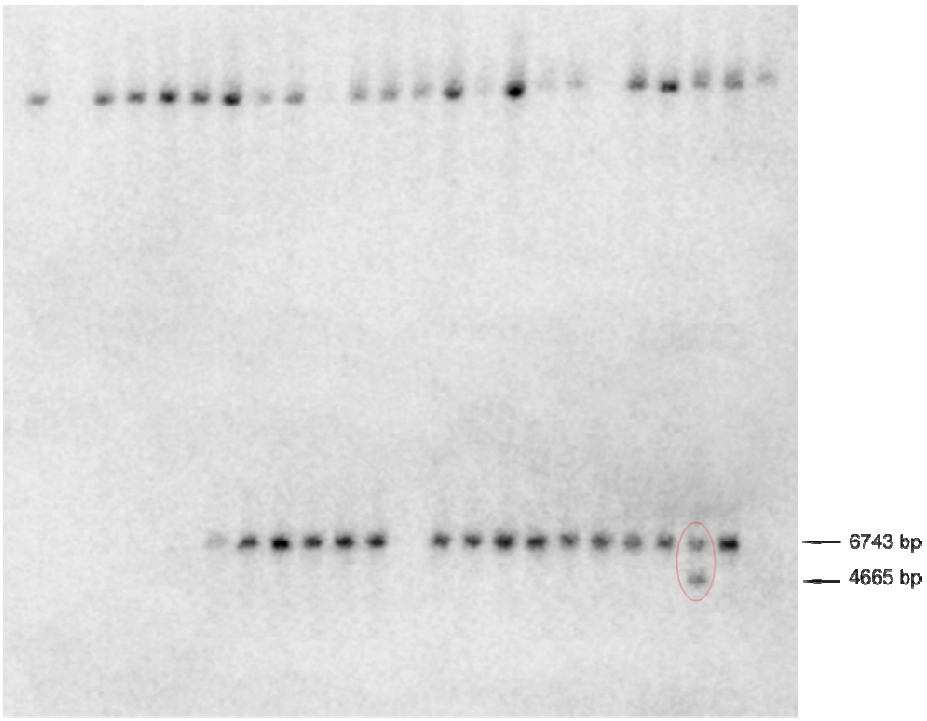

Fig. 4.24: Screening of ESC-clones for homologous recombination of the knock-in construct at the *myoc* locus. Restriction with *Hind*III and Southern blot revealed one clone (red thin circle), where the 3´-homologous flank had recombinated properly. Phosphoimaging of the blot visualized the hybridized radioactive 3´-probe binding to the expected restriction fragments of 6743 and 4665 bp for WT and knock-in alleles, respectively.

To be sure that the whole length of the construct had recombinated properly in the above positive clone, we analyzed the homologous recombination of the 5´-homologous flank by restriction with *Xba*I. Southern blot and phosphoimaging revealed the expected fragment of 5432 bp for the WT allele. The size of the knock-in fragment was not the excepted 7203 bp, it was even smaller than the WT fragment (Fig. 4.25).

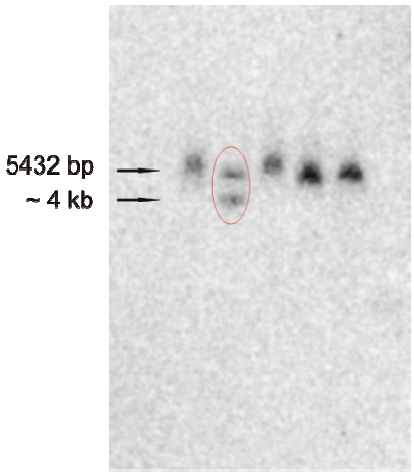

Fig. 4.25: Southern blot and phosphoimaging to analyze the homologous recombination at the *myoc* locus of the 5´-homologous flank of the knock-in construct. Restriction with *Xba*I of genomic DNA from the same clone, where the 3´-flank of the construct had recombinated properly (Fig. 4.20) resulted in the excepted band size of 5432 bp for the WT allel. The band size for the knock-in allel was not the excepted 7203 bp, it was even smaller than the WT band (red thin circle).

To affirm that the unexpected band size was not due to a deletion of a part of the 5´-flank during the recombination process, we tried to amplify the 5´-flank with a primer pair that binds in the genome upstream of the 5´-flank and within NLS-Cre (5´-probe fw /Cre rev. 5). We successfully amplified the correct fragment of 4 kb (data not shown), indicating that no deletions had occurred at the 5´-end of the construct during recombination. Due to contamination problems during ESC culturing, the suggested positive clone did not survive and could not further be analyzed for or prepared for to be injected into a mouse blastocyst.

Since a conditional knock-out in the TM would offer an immense spectrum of possibilities to study the role of molecular effectors thought to be involved in an elevated IOP, we made a second effort in the creation of our knock-in mouse line. Because of the mentioned contamination problems at the MPI, we sent our knock-in construct for electroporation to a biocompany. Future projects beyond this Ph.D. Thesis aim to analyze the Cre knock-in mouse in its ability to conditionally knock out sequences. Crosses with the reporter lines Z/EG (*Lac*Z/EGFP) (Novak et al., 2000) and Z/AP (*Lac*Z/human placental alkaline phosphatase (Lobe et al., 1999) will give an insight into the spatial pattern of Cre activity, whereas analysis of EGFP expression will show the temporal pattern of Cre expression.

4.5. Analysis of corneal gene expression in TGF-ß1 overexpression mice

A second focus in our attempts to investigate gene regulation during pathologic processes in the anterior eye was the fibrotic cornea. Scar formation in the cornea elicits a wound healing process that can lead to inflammation, neovascularisation and ECM accumulation, reducing the transparency of the cornea and impairing vision (reviewed by Fini, 1999). Since activated TGF-ß enhance the fibrotic reactions in the eye, actual efforts to counter this negative side effect of wound healing concentrate on targeting signalling pathways downstream of TGF-ß (reviewed by Saika, 2006; reviewed by Saika et al., 2008). Flügel-Koch et al. (2002) generated a mouse model that overexpress active TGF-ß1 in the lens and that show a fibrotic corneal phenotype including elevated migration and proliferation and of fibroblast-like stromal mesenchyme cells, neovascularisation, as well as abnormal ECM accumulation. To learn more about which corneal gene regulatory networks that are affected upon an overexpression of TGF-ß1, and thus to find out possible genes that may be involved in the loss of corneal transparency in these mice, we carried out gene expression profiling and subsequent quantitative RT-PCR of corneas from TGF-ß1-overexpression mice and compared the data against those of corneas from WT mice.

4.5.1. Selection of genes of interest

In order to get a better understanding of the signalling networks that may lie behind the fibrotic corneal phenotype seen in ßB1-crystalline-TGF-ß1 mice (Flügel-Koch et al., 2002), we earlier compared the corneal gene expression between newborn WT and TGF-ß1-overexpression mice by cDNA microarrays (Affymetrix® 430.0 Mouse Arrays). Comparison of 4 TG and 4 WT animals showed that 98 and 163 genes were at least two-fold up- and down-regulated, respectively in TG corneas. Out of these genes we chose 7 and 5 genes that were up- and down-regulated, respectively, to be confirmed for by quantitative RT-PCR. Criteria for the selection of genes were the presence of mRNA transcript in all arrays, as well as an abundance of transcript that gave a signal of more than 50. Based on the literature, we further selected the genes for those that were known to be regulated by TGF-ß1, or that were

known to be found in the eye or the cornea. Tables 4.4 and 4.5 show the selected genes, their detection *p*-values, as well as their fold change compared to WT animals in the microarrays.

Gene bank:	Gene Symbol:	Gene name:	*p*-Value	Fold change to WT
NM_010118	Egr2	early growth response 2	0.0203	2.811
NM_008046	Fst	Follistatin	0.0184	2.645
NM_008125	Gjb2	gap junction membrane channel protein beta 2	0.0245	2.933
NM_016958	Krt14 (Krt1-14)	keratin complex 1, acidic, gene 14	0.0133	2.656
NM_008484	Lamb3	laminin, beta 3	0.04	2.404
X84014	Lama3	laminin, alpha 3	0.0151	2.356
NM_008607	Mmp13	matrix metallopeptidase 13	0.047	6.156

Table 4.4: Based on our previous microarray data, as well as a profound literature search, the following up-regulated genes were selected to be confirmed for by quantitative RT-PCR.

Gene bank:	Gene Symbol:	Gene name:	*p*-Value	Fold change to WT
NM_008344	Igfbp6	insulin-like growth factor binding protein 6	0.0365	0.42
NM_021879	Oca2 (pink-eyed dilution)	oculocutaneous albinism II	0.0268	0.0916
NM_018752	Trpm1	transient receptor potential cation channel, subfamily M, member 1	0.0261	0.0991
NM_020265	Dkk2	dickkopf homolog 2	0.00479	0.452
NM_008963	Ptgds	prostaglandin D2 synthase	0.0389	0.198

Table 4.5: Based on our previous microarray data, as well as a profound literature search, the following down-regulated genes were selected to be confirmed for by quantitative RT-PCR.

4.5.2. Primer design and testing of reference genes

Primer pairs for quantitative RT-PCR that spanned intron boundaries of the mouse genome were designed by the Universal ProbeLibrary System from Roche (https://www.roche-applied-science.com/sis/rtpcr/upl/index.jsp?id=UP030000) for the selected genes as described in Materials and methods 3.1.4.4. To find the most suitable reference genes with no changes in corneal gene expression between WT and TG animals, we designed primer pairs for the following 6 candidate genes as above (Table 4.6):

Gene name (gene symbol, gene bank):	**Primer sequence:**	**Position in mouse genome:**	**Product size:**
ribosomal protein L32 (Rpl32, NM_172086.2)	fw.: 5´-gctgccatctgttttacgg-3´ rev.: 5´-tgactggtgcctgatgaact-3´	29 - 47 107 - 126	98 bp
glyceraldehyde-3-phosphate dehydrogenase (Gapdh, NM_008084.2)	fw.: 5´-tgtccgtcgtggatctgac-3´ rev.: 5´-cctgcttcaccaccttcttg-3´	763 - 781 818 - 837	75 bp
guanine nucleotide binding protein, beta polypeptide 2 like 1 (Gnb2l1, NM_008143.3)	fw.: 5´-tctgcaagtacacggtccag-3´ rev.: 5´-gagacgatgatagggttgctg-3´	514 - 533 584 - 604	91 bp
ribosomal protein S9 (Rps9, NM_029767.2)	fw.: 5´-atccgccaacgtcacatta-3´ rev.: 5´-tcttcactcggcctggac-3´	437 - 455 555 - 572	136 bp
tubulin, beta 1 (Tubb1, NM_001080971.1)	fw.: 5´-actgtgggacgtctgctctc-3´ rev.: 5´-gcggcacatacttcttaccg-3´	157 - 176 215 - 234	78 bp
hypoxanthine guanine phosphoribosyl transferase 1 (Hprt1, NM_013556.2)	fw.: 5´-tcctcctcagaccgctttt-3´ rev.: 5´-cctggttcatcatcgctaatc-3´	104 - 122 173 - 193	90 bp

Table 4.6: Primer pairs for listed 6 candidate reference genes were designed by the Universal ProbeLibrary System from Roche. The list summarizes the target gene names, primer sequences, positions of the primer binding sites within mouse genome and product sizes.

Comparison of the expression of above candidate reference genes in 4 TG corneas vs. 4 WT corneas in several parallel quantitative RT-PCR experiments confirmed that *Gnb2l1* and *Rpl32* were expressed equally in TG and WT animals (data not shown). These two genes were used as reference genes in all experiments.

4.5.3. Differential gene expression in ßB1-crystalline-TGF-ß1 mouse corneas

Since transgenic TGF-ß1 mRNA levels decrease after day P1 in ßB1-crystallin-TGF-ß1 mouse eyes (Flügel-Koch et al., 2002), and because RNA from P0 mice had been used for the cDNA microarray studies, we chose P0 as the day of preparation of corneal RNA. cDNA was synthesized from RNA and used as template for the quantitative RT-PCR experiments. The gene expression level of the above selected genes was compared between a minimum of 4 WT and 4 TG animals by relating the levels to those of the reference genes. All experiments were assembled by the Gene Study function of the iQ Optical System Software version 2.0. Microarray data showed that in TG corneas *Egr2*, *Fst*, *Gjb2*, *Krt14*, *Lamb3*, *Lama3* and *Mmp13* had fold changes of 2.811, 2.645, 2.933, 2.656, 2.404, 2.356 and 6.156, respectively, when compared to WT corneas (Table 4.4). In our quantitative RT-PCR experiments the expression levels of these genes were 5.68, 3.45, 3.17, 3.04, 2.21, 1.51 and 53.66 times higher in TG corneas than in WT corneas (Figs. 4.26 and 4.27). Thus, we confirmed the previous microarray data that showed that an over-expression of TGF-ß1 in the mouse eye leads to an up-regulation of above genes in the cornea.

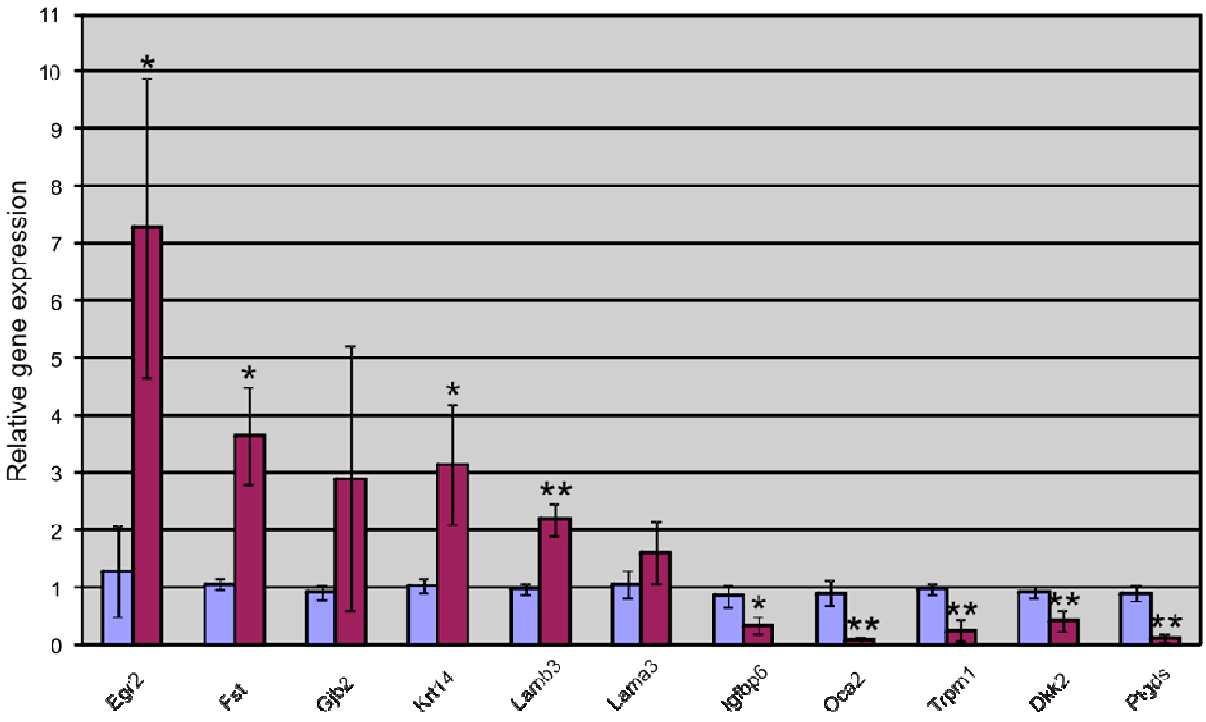

Figure 4.26: Quantitative RT-PCR data comparing the gene expression levels from a minimum of 4 WT and 4 TG corneas. All genes selected for the study confirmed previous microarray data in their being regulated in the cornea upon overexpression of TGF-ß1. Because of the huge up-regulation of MMP13 compared to the other studied genes in TG corneas, the differential regulation of this gene is shown in a separate graph (Fig. 4.23). WT expression is shown in blue, TG expression is shown in wine red. Mean standard deviation (± SD) between samples are shown. Asterisks mark statistically significant differential gene expression in TG vs. WT corneas (*$p < 0.05$; **$p < 0.02$).

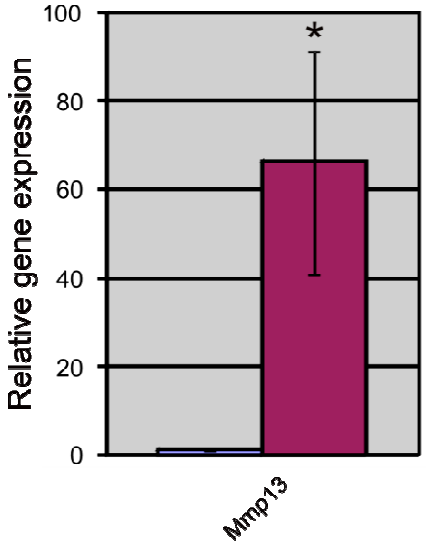

Figure 4.27: Quantitative RT-PCR data comparing the gene expression levels of MMP13 from 4 WT and 4 TG corneas. The data confirmed previous microarray data that showed that MMP13 is regulated in the cornea upon overexpression of TGF-ß1. WT expression is shown in blue, TG expression is shown in wine red. Mean standard deviation (± SD) between samples are shown. Asterisks mark statistically significant differential gene expression in TG vs. WT (*$p < 0.05$; **$p < 0.02$).

Microarray data showed that *Igfbp6*, *Oca2*, *Trpm1*, *Dkk2* and *Ptgds* had fold changes of 0.42, 0.0916, 0.0991, 0.452 and 0.198, respectively, in the corneas from TG mice in comparison to WT corneas (Table 4.5). In our quantitative RT-PCR experiments the expression levels of these genes in TG corneas were 0.38, 0.08, 0.25, 0.46 and 0.13 of that of their expression levels in WT corneas (Fig. 4.26). Thus, we here confirmed the previous microarray data that showed that an over-expression of TGF-ß1 in the mouse eye leads to a down-regulation of these genes in the cornea.

5. Discussion

5.1. Characterization of *MYOC*

Since only few studies focused on the transcriptional regulation of myocilin, and since earlier attempts to characterize *MYOC* are restricted to its near 5´-UTR, resulting in definition of just the immediate proximal promoter that is responsible for myocilin basal transcription (Kirstein et al., 2000), we wanted to characterize human *MYOC* more thoroughly by analysing also intronic and long-range nc regions.

5.1.1. Analysis of conserved nc *MYOC* regions

Being important for protein function, exon coding sequences have been highly conserved between species through evolution. Based on same principle, inter-species alignment can reveal nc sequences that are important for the regulation of a gene over its basal promoter level (reviewed by Visel et al., 2007). We started our characterization of human *MYOC* by searching for possible regulatory sequences within the human *MYOC* transcript, as well as within its immediate 3´-UTR. Inter-species alignment of the myocilin gene, subsequent cloning of conserved regions and reporter gene expression studies revealed that two regions within *MYOC* intron 1, DCRi2b5´ and DCRi2c, induced a 3.7- and 2.3-fold expression (both statistically highly significant) of reporter gene over *MYOC* basal promoter level in TM cells *in vitro*. DCRi2b3´and the 5´-most intronic region DCRi2a had slight inhibitory effects on basal transcription level (Fig. 4.3).

Since we in our deletion studies confirmed that deletion of the flanking sequences of DCRi2b5´ and DCRi2c resulted in only a modest elevation of reporter gene expression over *MYOC* basal promoter level (Fig. 4.5), confirms that the positive effect on reporter gene expression raised by DCRi2b5´ and DCRi2c is not elicited by shorter enhancer elements represented by the sharp homology peaks residing within DCRi2b5´ or DCRi2c (viewed in Fig. 4.4), and suggests that the whole sequences spanned by the intronic regions DCRi2b5´

and DCRi2c are important in the elevation of gene expression over basal transcription level in TM cells.

Interestingly, a deletion of the flanking sequences of the 5′-most intronic region DCRi2a, which had a slightly negative effect on basal transcription (Fig. 4.3), resulted in a significant induction of reporter gene expression over *MYOC* basal promoter level (Fig. 4.5). This could mean that the flanking sequences may in some way repress or inhibit the positive effect that the conserved peak region H7 has on transcriptional regulation. Theoretically, this could occur through binding of an inhibitory factor to the flanking deleted part. Such factors may indirectly repress the action of positively acting factors by e.g. re-organizing chromatin structure to a more packed form that hinders the access of transcription enhancing proteins to neighboring DNA (reviewed by Latchman, 1996). An example of this kind of indirect repression of transcription occurs in *Drosophila melanogaster*, where the Polycomb-group of proteins bind to specific elements of the DNA, thereby inducing heterochromatin formation and inactivating transcription (Zink and Paro, 1995). It illustrates the complexity of regulatory networks present in eukaryotes that allow a fine-tuning of gene regulatory processes to meet the needs of a specific developmental or pathological state.

5.1.2. Analysis of conserved long-range distal elements

To test for the possibility that *MYOC* could be regulated by long-range distal elements, we analysed three and two distal conserved regions within the 5′- and 3′-UTRs of *MYOC*, respectively, for their capacities to regulate gene expression beyond basal promoter level in cultured human TM cells. We confirmed that both distal 3′-UTR regions, H1 and H2, which reside 7 kb downstream of the 3′-end of the transcribed region of *MYOC* (viewed in Fig. 4.4), regulated reporter gene expression 2.9 (statistically significant) and 2.4 fold, respectively, over basal promoter level (Fig. 4.6). Even though these two elements reside only ~ 1600 bp apart from each other, and within a wide 8 kb area of conservation (viewed in Fig. 4.7), our experiments did not confirm a cumulative effect of H1 and H2 on reporter gene expression. However, it does not rule out that other untested elements within the 8 kb conserved 3′-UTR region could participate in the transcriptional regulation of *MYOC*.

The fact that none of the conserved cloned 5´-upstream *MYOC* regions showed any effect on reporter gene expression over basal promoter level in cultured human TM cells (Fig. 4.6), indicate that these regions are not important for the transcriptional regulation of myocilin over basal promoter level. It still raises the question, why these regions (H8 – H10) show such an extent of conservation over such a wide region (in the case of H10 there is 85 % homology for a distance of over 1000 bp between *MYOC* and *Myoc* (Table 4.2). The fact that these regions did not show any effect on transcription efficiency in our human TM culture model, does not rule out that H8 – H10 could be important regions for accessory protein binding *in vivo* or in other tissues where myocilin is normally expressed. Even though our culture model is an established line to be used as a model in the analysis of molecular mechanisms of the TM (Pang et al., 1994), cultured cells are not in contact with neighbouring tissue as in an organism, and thus do not receive extracellular molecular signals. A culture model is thus solely a simplified generalization of the *in vivo* situation. H8 – H10 could therefore be important regions for accessory proteins important for transcriptional regulation *in vivo* or in other tissues, where these factors may be present.

5.1.3. Search for functional GREs within *MYOC*

Myocilin expression is highly activated by GC treatment in TM cell cultures (Polansky et al., 1997; Tamm et al., 1999). Even though there are many putative GREs within 5 kb of the 5´-UTR of *MYOC* (Nguyen et al., 1998), no functional GREs have been found within its close 5´-upstream region (Kirstein et al., 2000; Shepard et al., 2001). Our search for functional GREs within our cloned conserved and analysed *MYOC* intronic and distal 5´- and 3´-UTR regions, did not corroborate that these regions would encompass functional GREs (Fig. 4.3 and data not shown). The fact that myocilin induction by GCs often requires days of treatment (Tamm et al., 1999), has led to a hypothesis that myocilin is a delayed secondary GC responsive gene (Shepard et al., 2001), i.e. a gene that is activated upon binding of another, first to be expressed, primary GC responsive gene. The fact that we did treat our transfected cells with dexamethasone for 3 d, also excludes the possibility that our cloned *MYOC* regions encompass binding sites for factors that are synthesized upon a primary GC response.

Since some authors have shown that high elevation of myocilin expression may not occur until 7 - 10 d of GC treatment (Nguyen et al., 1998), our results do not exclude that the cloned regions could respond to dexamethasone after a longer than 3 d treatment. Available data about GC- induced myocilin expression mainly are derived from experiments using primary TM cell cultures from human or monkey (Nguyen et al., 1998; Tamm et al., 1999; Clark et al., 2001), whereas we used an immortalized human TM cell line (Pang et al., 1994). Since the molecular GC response of a cell usually works by interactions with other accessory proteins present in the cell (e.g. chromatin remodeling factors) (reviewed by Liberman et al., 2007), we can not exclude that our tested *MYOC* regions could respond to GCs in primary lines, tissue culture or *in vivo*.

5.1.4. Future aspects

The fact that there are conserved regions within intron 1 and the 3´-UTR of *MYOC* that elevate reporter gene transcription over *MYOC* basal promoter level, suggests that these regions may be important in pre-mRNA processing, affecting the efficiency of transcription. By using bioinformatic and subsequent biochemichal (e.g. DNase footprinting and chromatin immunoprecipitation) tools it would be interesting to closer analyse the sequences encompassed by DCRi2b5´, DCRi2c, H1 and H2 to find out how and through what accessory factors these regions could be involved in enhancing the transcription of *MYOC*. Since none of our conserved 5´-UTRs did have any effect on transcription level in cultured human TM cells, it could be interesting to look at the effect of these regions in other systems like in astrocyte- or podocyte cell cultures, since myocilin is known to be expressed in these cell types (Obazawa et al., 2004; Goldwich et al., 2005).

It is possible that there are regulatory regions still far beyond those that we analysed above (the farthest analyzed 5´- and 3´-UTR reside 31 and 7 kb, respectively, beyond the transcript coding region of *MYOC*). Examples of genes whose expression is affected by far distal regulatory elements within their 5´- and 3´-UTRs are *Pax6*, *FOXL2* and *Bmp2*. Within *PAX6* a 35 kb long distant regulatory region that is responsible for endogenous Pax6 expression in parts of the brain and the developing eye resides ~ 150 kb downstream of the transcribed region, within the intron of the neighbouring gene *ELP4* (Kleinjan et al., 2006). Long-range

extragenic deletions of wide regions of 5´- and 3´-UTRs of the gene *FOXL2* have been found to be responsible in 14 % of patients suffering from blepharophimosis syndrome (BPES) (Beysen et al., 2005), a rare disease with complex inheritance that is characterized by eyelid malformation and in some cases premature ovarian failure. Bmp2, an important signalling ligand during osteoblast differentiation and bone formation, is transcriptionally regulated by a conserved 656 bp enhancer element that resides 156.3 kb downstream of the Bmp2 promoter (Chandler et al., 2007).

The genomic landscape responsible for the endogenous expression pattern of Pax6 has been resolved by cloning a 420 kb region encompassing the human *PAX6* locus into a yeast artificial chromosome (YAC). Approaches using bacterial artificial chromosomes (BACs) or YACs would make it possible to analyze much wider regions for their participation in the transcriptional regulation of myocilin, as than is possible by simple cloning. Since GCs can exert their transcription enhancing effect not only by binding to GREs or nGREs, but also by affecting and reqruiting accessory protein/transcription or chromatin remodelling factors (reviewed by Liberman et al., 2007), it may be possible that the molecular enhancement of *MYOC* transcription by GCs encompass much wider regions around the *MYOC* transcribed region than tested here. Approaches using BACs or YACs would allow for screening of huge areas at and around the *MYOC* locus for their ability to regulate transcription over basal transcription level, as well as to test for their GC responsiveness, in TM.

5.1.5. The complexity of eukaryotic gene regulation

Classically, basal transcriptional regulation is considered to occur by binding of transcription factors and auxiliary proteins to the 5´-promoter. Binding to far and near enhancer or inhibitory elements by cell- and developmental stage specific factors then can modulate the promoter driven basal transcription (Nelson and Cox, 2001). Critical cell- and developmental stage-specific enhancer or inhibitory elements may reside thousands of kb away from the transcribed region, within other loci (Kleinjan et al., 2006), within introns (Aruga et al., 2007) or even on other chromosomes (reviewed by Bartkuhn and Renkawitz, 2007). Transcriptional regulation in eukaryotes is a complex process that, in addition to the RNA polymerase II complex, is dependent on accessory factors that can bind the complex, as well as the DNA

(reviewed by Hartzog, 2003). In order to enable effective elongation of pre-mRNA transcript, accessory protein- and DNA binding factors are needed for the modulation of the chromatin structure (reviewed by Sunders et al., 2006). Transcriptional regulation is closely interwoven in time and space with pre-mRNA processing and mRNA decay (reviewed by Moore and Proudfoot, 2009). Increasing data show that regulation of gene expression occur both at the DNA and RNA levels. Through complex regulation of the processing of pre-mRNA by RNA binding proteins, a fine-tuning of the repertoire of mRNA species in time and space can be reached (reviewed by Licatalosi and Darnell, 2010). This means that also protein non-coding (nc) regions, like introns and 3´-UTRs, may contain regions that are targets for binding of important RNA processing factors.

5.1.5.1. Possible role of DCRi2b5´and DCRi2c as long ncRNA

The facts that DCRi2b5´and DCRi2c both are able to elicit gene expression highly significant over the human *MYOC* basal promoter level in cultured human TM cells (Fig. 4.3), and that they reside only ~ 50 bp apart (viewed in Fig. 4.1), suggest that they both, as one 2353 bp stretch, may be important for the transcriptional regulation of *MYOC* over basal transcription level. Usually, intronic enhancers have lengths of a few hundred bp, are extremely conserved and have the potential to elevate gene expression considerably over basal level. Examples of such intronic enhancers are the spinal cord-specific enhancer element of *PAX6* (Xu and Saunders, 1998) and the oligodendrocyte-specific enhancer of the myelin gene *Opalin* (Aruga et al., 2007). This raises the possibility that the nc intronic regions DCRi2b5´and DCRi2c, rather than being enhancers, may serve as template(s) for or produce a so called long ncRNA. Usually, ncRNAs are coded by moderately conserved, larger than 200 bp, nc regions of a gene. They may be coded by the sense, antisense (as), or by both strands of the DNA. They can overlap with exons, be interspersed between genes or reside within introns (reviewed by Mercer et al., 2009). They serve various gene regulatory functions e.g. during chromatin remodeling, as exemplified by the long as ncRNA *HOTAIR*, derived from the human homeobox *HOXC* locus, and which recruits the chromatin remodeling complex PRC2 to the *HOXD* locus (Rinn et al., 2007). During transcription, long ncRNAs can modulate the activity of RNA polymerase II or recruit RNA binding regulatory proteins into the transcriptional program (reviewed by Mercer et al., 2009). Post-transcriptional and translational regulation

by long ncRNAs is exemplified by the intronic long ncRNA of the homeobox gene *Zeb2*, that during epithelial-mesenchymal transition masks a splice site on the pre-mRNA, leading to retention of an intronic internal IRES with subsequent efficient translation and expression of *Zeb2* (Beltran et al., 2008). Annealing of long ncRNAs can result in their processing into small interfering (si)RNAs, which then can silence or regulate gene expression (reviewed by Amaral and Mattick, 2007). An example for siRNA induced silencing is X-chromosome inactivation by siRNAs produced from a duplex of the long ncRNA *Xist* (Ogawa et al., 2007).

Transcribed long ncRNAs have been found within genes of many transcription factors that are important for eye development and function. During development, so called natural as transcripts (NATs) are transcribed from 5´-UTR, intronic or 3´-UTR regions of genes like *Pax6*, *Six3*, *Otx2*, *Crx*, *Vax2*, *Six6* and *Rax*. These NATs co-express with, as well as co-localize with the gene they are transcribed from. Since a corresponding NAT expression pattern has been observed in human, it suggests that regulation of important eye development genes by NATs is important in the pathogenesis of developmental eye diseases (Alfano et al., 2005).

In addition to being processed to siRNAs, long ncRNAs may be processed to micro (mi)RNAs, ~ 22 nucleotide ss RNA molecules that bind to target sequences by imperfect base pairing. One miRNA can regulate hundreds of targets, usually in a negative way, by binding of the 3´-UTR of a gene, thus directing mRNA degradation or disturbing the translation process. As other ncRNAs, miRNAs can have a wide variety of other regulatory functions (reviewed by Amaral and Mattick, 2008). In the eye, there is a repertoire of tissue- and cell-specific miRNAs, suggesting that they may be important regulators of gene expression during eye morphogenesis and differentiation (Ryan et al., 2006).

5.1.5.2. Possible role of DCRi2b5´and DCRi2c during pre-mRNA processing

Rather than serving as a template for, or being processed into ncRNA, NAT, si or miRNAs, DCRi2b5´ and DCRi2c could be important for pre-mRNA processing. Since transcription and pre-mRNA processing, as well as termination of transcriptional elongation, are both physically and in time integrated processes, the efficiency of pre-mRNA processing affects

the efficiency of transcription (Pandit et al., 2008). A large number of pre-mRNA processing factors are in contact with the RNA polymerase II complex during elongation in eukaryotic cells (Das et al., 2007) and many of these factors contact the DNA (Listerman et al., 2006; Brès et al., 2004). Such accessory factors can regulate splicing of introns, mRNA surveillance and mRNA export (Moore et al., 2006). DCRi2b5′ and DCRi2c may contain recognition motifs that are important for some accessory factors critical in mRNA processing. Another theory is that these regions encompass motifs that are recognized by accessory factors that aid in resolving transcription bubbles (Li and Manley, 2005), a process that is critical for efficient transcriptional elongation (Pandit et al., 2008), or that are involved in chromatin remodeling.

5.1.5.3. Possible role of H1 and H2

In addition to the possibility that H1 and H2 could act as enhancer elements that bind accessory factors that aid in transcription, elongation and/or internal pre-mRNA processing, these 3′-UTR elements could be important in the termination of *MYOC* transcription. It is known that the immediate 3′-UTR of *MYOC* contains three polyadenylation signals, of which two are used (Nguyen at al., 1998). Classically, cleavage of transcript occurs 10 – 30 bp downstream of a polyadenylation signal, from where the polyadenylation polymerase synthesizes an 80 – 250 bp long poly(A)-tail (Nelson and Cox, 2001). Termination of transcription by RNA polymerase II is coupled to 3′-end and pre-mRNA processing, and is not determined by any conserved site in the 3′-UTR of a gene. Thus, termination can occur a few bp to several kb downstream of the polyadenylation cleavage site (reviewed by Richard and Manley, 2009). This is shown e.g. for the globin genes ß and ε, where transcription continues far downstream of the poly(A) cleavage site, and where cleavage at the poly(A) site is then induced by termination and cleavage at more downstream sites of transcription termination (Dye and Proudfoot, 2001). It is possible that H1 and H2 code for sites that are recognized by factors that facilitate termination of *MYOC* transcription by RNA polymerase II and subsequent cleavage at one of its poly(A) sites. Chromatin remodelling proteins have been shown to associate to genomic regions downstream of the mRNA coding region (Venkataraman et al., 2005), and it is generally thought that chromatin remodelling factors are crucial for effective termination and subsequent cleavage of transcript at the poly(A) site (reviewed by Richard and Manley, 2009). An explanation for the inducing effect on

transcription by H1 and H2 can be that these regions bind important chromatin remodelling factors, which in turn could facilitate the binding of other factors that assist termination and subsequent cleavage of the *MYOC* transcript.

5.1.6. Envisions

Even though an elevated amount of myocilin within the TM has been shown to be related to POAG in some patients (Lütjen-Drecoll et al., 1998; Konz et al., 2009), an overexpression of myocilin in the mouse TM do not result in a phenotype (Gould et al., 2004; Zillig et al., 2005). In contrast to most mice strains, dogs, cats (Brooks, 1990) and horses (Wilcock et al., 1991) do develop secondary glaucoma, and it has been reported that myocilin levels are elevated in the TM (Samuelson et al., 2007), as well as in the AH (MacKay et al., 2008), of glaucomatous dog eyes. Inter-species comparison of the myocilin genes for dog and horse reveals that these genes are much more conserved to human *MYOC* than is mouse *Myoc*. Beyond the sequences that we tested, there are still more peaks of conservation within the introns and the 3´-UTR when comparing human *MYOC* against dog, cat and horse myocilin genes. In the case of intronic conservation, there is eminent conservation within exon 2 that is not found when comparing human *MYOC* with mouse *Myoc* (Fig. 5.1A: grey shaded box). The same is true when looking at the 3´-UTR of *MYOC*. The area of conservation between human, dog, and horse myocilin genes reaches as wide as 28 kb beyond the transcribed region of *MYOC*, while conservation between human *MYOC* and mouse *Myoc* reach only 13 kb beyond the transcribed region (Fig. 5.1B).

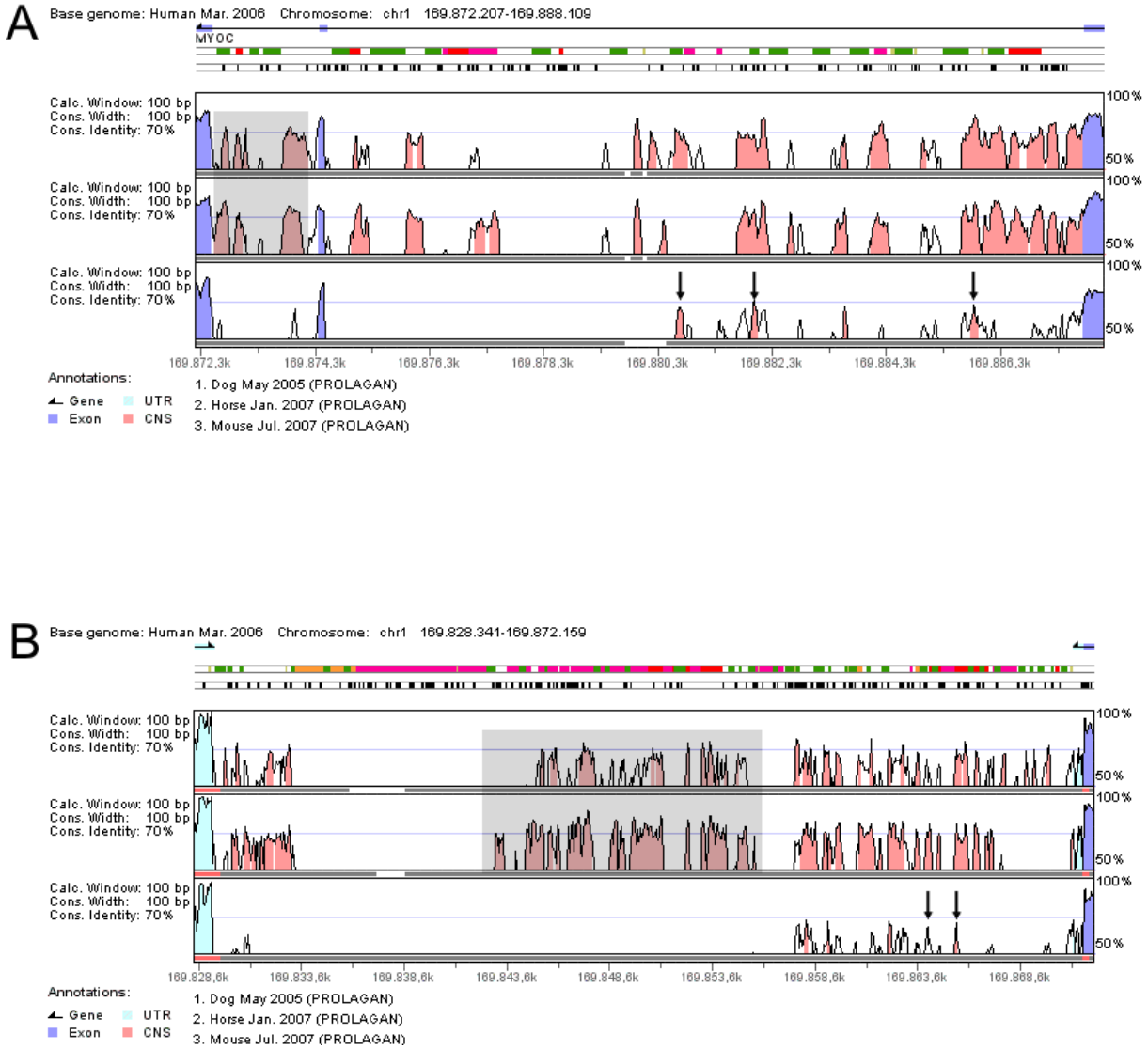

Figure 5.1: Inter-species alignment and comparison of sequence homology of dog, horse and mouse myocilin genes with human *MYOC* by using the VISTA Browser 2.0 bioinformatic software. A) Comparison of intronic nc sequences reveals that dog and horse myocilin genes show many more regions of > 70 % homology to human *MYOC*, as does mouse *Myoc*. Vertical arrows depict our analyzed regions. The grey shaded box highlights conserved regions within intron 2 that are not conserved when comparing human and mouse genes. B) Comparison of 3´-UTR sequences reveals that dog and horse myocilin genes show a much wider region (that reaches as far as 28 kb beyond the transcribed region) of homology to human *MYOC* (grey shaded box), as does mouse *Myoc* (that reaches only 13 kb beyond the transcribed region). Vertical arrows depict our analyzed regions. Exons and proximal UTRs are shown in blue and turquoise, respectively. Conserved nc sequences that show a consensus homology of at least 70 % for a length of at least 100 bp are shown in pink.

Since dog, cat and horse suffer from glaucoma, and since in fact the expression of myocilin is elevated in the eyes of glaucomatous dogs (Samuelson et al., 2007; MacKay et al., 2008), the conservation of wide nc regions between *MYOC* and the myocilin genes for these species may reflect an important role of the transcriptional regulation of myocilin in causing glaucoma in human and in these species. It would be interesting to test the illustrated regions (grey boxes) that are conserved between human, dog, cat and horse for their capacity to regulate transcription in cultured human TM cells.

5.2. Search for and analysis of an artificial enhancer element for TM directed overexpression of protein

5.2.1. Search and testing of a candidate element *in vitro*

So far, there are no glaucoma animal models that show targeted overexpression of protein to the TM, which would be of value in the achievement to better understand the molecular mechanisms that build up an AH outflow resistance too high for the physiology of the eye. Increasing microarray data derived from TM offer a valuable source in the search for potential molecular factors involved in POAG pathology, and may serve as a guideline on which further molecular biological studies can be designed.

We wanted to approach this topic by using the *MYOC* basal promoter (Kirstein et al., 2000) to target expression of protein to the TM. Since it is known that myocilin is one of the most highly expressed protein within TM (Tomarev et al., 2003), whose expression can still be markedly augmented upon GC treatment (Rozsa et al., 2006), and since myocilin is expressed at much lower levels in some tissues outside the, we found the *MYOC* basal promoter to be a good candidate for TM-directed expression of protein. Since our characterization of *MYOC* indicates that the basal proximal promoter alone is not sufficient to drive endogenous myocilin expression (Figs. 4.3; 4.6), we wanted to find an enhancer element that would "boost" the activity of the *MYOC* basal promoter to drive gene expression far beyond basal level in the TM. Since it is known that repetitive binding sites for transcription factors are more effective enhancers of transcription than a single site (Schatt et al., 1990), we had earlier cloned repetitive binding motifs for transcription factors that are known to be pivotal in anterior eye development (Table 4.3) (reviewed by Cvekl and Tamm; Matt et al., 2005), in front of the human *MYOC* basal promoter. The fact that one of our tested cloned artificial enhancer elements, a 150 bp sequence made up of repetitive binding motifs for the transcription factors RAR, PITX and FOX, in combination with the human *MYOC* basal promoter, did elevate reporter gene expression up to 11.8 fold (statistically highly significant) over the level than did the *MYOC* basal promoter alone (Fig. 4.8) in human TM cells in culture, encouraged us to analyze this enhancer further, as a candidate element for directing

expression of protein to the TM *in vivo*. Our data, which confirmed that our artificial enhancer is not a ubiqutous enhancer (Fig. 4.9) prompted us to clone a ß-galactosidase overexpression construct driven by this element and the *MYOC* basal promoter (Fig. 4.10). The ability of our element to drive visible reporter gene expression in TM cells *in vitro* (Fig. 4.11) finally encouraged us to generate a mouse line that would enable the analysis of the capacity of our enhancer to drive and target visible reporter protein expression to the TM *in vivo*.

5.2.2. Creation of a mouse model for the analysis of our candidate element *in vivo*

Since the context of transcriptional regulation *in vitro* may differ significantly from that *in vivo*, a mouse model would confer the most comprehensive information about the usefulness of RAREß/PITX3/FOX as a TM-specific enhancer element. For this purpose, we generated a transgenic mouse line that had integrated a transgene, which would drive ß-galactosidase expression under the control of RAREß/PITX3/FOX and the human *MYOC* basal promoter, into its genome. Screening for founder animals revealed that three animals had integrated the transgene into their genomes (Fig. 4.12). Subsequent genotyping of progeny, affirmed that only two of these founder animals transferred the transgene to the next generation in a Mendelian fashion.

Since DNA synthesis and replication in one-cell stage fertilized mouse oocytes begin already 12 – 14 h after fertilization, it may happen that the microinjected transgene integrates into an already replicated chromosome. If this happens, the developing embryo is a mosaic, where not all cells have integrated the microinjected transgene. In these cases, the transfer of transgene to the next generation is ineffective, i.e. the frequency of transgene transmission is 25 % or less (Pinkert, 2002). This may explain the fact that only two of our three founder animals had TG offspring. Since TG embryos of one of our established lines frequently did not get born, and when, was always a female that showed a physically retarded phenpotype concerning size, incidence of hair coat and fertility (Fig. 4.13), suggests that the transgene had integrated unfavorable into the genome of this line, affecting transcriptional regulation of

other genes (position effect). Due to the rarity of born TG animals of this line, we had difficulties in stabilizing this breed, with the consequence of limited experimental material.

5.2.3. Analaysis of our candidate element *in vivo*

We started our analysis of ß-galactosidase expression by *LacZ*-staining of adult eye, heart and sciatic nerve, since myocilin is known to be expressed in these tissues in adult mouse and human (Karali et al., 2000; Knaupp et al., 2004; Ohlmann et al., 2003; Ortego et al., 1997; Swiderski et al., 1999). Since we did not detect any staining of these organs prepared from TG mice (Fig. 4.14), and since it is known that RAR, PITX and FOX are crucial regulators of embryonic anterior eye development (reviewed by Cvekl and Tamm; Matt et al., 2005), we wanted to analyze ß-galactosidase expression in TG mouse embryos. *LacZ*-staining of whole E12.5 embryos revealed that there was no staining within TG eyes above background level (Fig. 4.15). Since we used standardized protocols for fixation and staining, and since the staining procedure was successful in $Pax6^{LacZ/+}$ embryos (St. Onge et al., 1997), the lack of staining in the eyes of our TG ß-galactosidase overexpression mice could not be due to shortcomings during these procedures.

The fact that our candidate element had proven to be active in human TM cells in culture (Figs. 4.8; 4.11), whereas we could not observe any ß-galactosidase expression in the eyes of adult or embryonic mice (Figs. 4.14A; 4.15), may be explained by the fact that the molecular context involved in gene regulation in the mouse TM may differ from that within human TM. In addition, since the gene regulatory networks *in vivo* are much more complex than those *in vitro*, it is not a rule that a promoter with capacity to drive protein expression in cultured cells will be active also in a living system. Liton et al. (2006) showed that *Ch3L1* (chitinase 3-like), a gene coding for a glycoprotein member of the glycosyl hydrolase 18 family, involved in e.g. inflammation and tissue remodeling (Bernardi et al., 2003; Vind et al., 2003), is one of the few genes that is equally expressed in cultured human TM cells and in TM tissue. In addition, the same authors showed that *Ch3L1* is differentially expressed in TM cells, when compared to SC cells. However, their approach to express visible ß-galactosidase expression in cultured

human TM cells and anterior eye segments under the control of the *Ch3L1* promoter, resulted in ß-galctosidase expression in only a subset of the TM cells, suggesting that the TM may be more complex than earlier thought, being composed of two different cell types (Liton et al., 2005). If the TM really is composed of two different cell types with differing characteristics, and if this is true also for the mouse, it could make it more difficult to observe unambigous expression of reporter in this tissue.

In addition to the explanation that the living TM is, concerning gene regulation, much more complex than cultured cells, the lack of ß-galactosidase expression in mouse eyes *in vivo* could be due to the relative weak enhancer character of RAREß/PITX3/FOX. Even though it has been shown that an enhancer composed of repetitive RAR motifs alone is able to drive ß-galactosidase expression in the eyes of developing mouse embryos (Rossant et al., 1991; Balkan et al., 1992), it can not be presumed that our combination of successive binding motifs for three different transcription factors also should act similarly in a living system. The complexity of our element could lead to unexpected interactions between the transcription factors binding to the element, resulting in a totally different effect on gene regulation than seen *in vitro*. In fact, we observed that RAREß/PITX3/FOX induced ß-galactosidase expression in only a portion of the cultured human TM cells, when compared to positive control cells that had been transfected with a plasmid, where *LacZ* was driven by the cytomegalovirus (CMV) promoter, a known strong promoter used to drive ubiqutous overexpression of protein. Even though we showed that RAREß/PITX3/FOX could elevate reporter gene expression in human TM cell cultures > 11-fold over the level of the *MYOC* basal promoter (Fig. 4.8), our comparison of its activity to that of the CMV promoter in Dual-Luciferase® Reporter assays showed that the CMV promoter was hundreds of thousands of folds more capable in driving reporter gene activity than our candidate element (data not shown). Thus, we had interpreted the small amount of ß-galctosidase expressing cultured cells as a consequence of the relative weak promoter capacity of RAREß/PITX3/FOX, when compared with the CMV promoter. Or, we had explained the few blue cells as being a consequence of low transfection efficiency.

Even though the 377 bp human *MYOC* basal promoter is sufficient in driving reporter gene expression in primary human TM, mouse TM and mouse astrocyte cultures (Kirstein et al.,

2000), as well as in cultured immortalized human TM cultures as seen in our experiments (Figs. 4.3; 4.5; 4.6; 4.8), it may not be capable of driving gene expression in the mouse, since there may be differences between the molecular network active in human vs. mouse TM. Or, the *MYOC* basal promoter may in general be too weak to drive expression *in vivo*. This theory is supported by our *MYOC* promoter studies that showed that even in culture, there are nc elements within *MYOC* that are required for expression of reporter over basal promoter level (Figs. 4.3; 4.6), suggesting that a larger endogenous region of *MYOC* may be needed to drive expression of protein *in vivo* in TM. In fact, Kim et al. (2001) showed that the whole endogenous *Myoc* locus was able to drive visible myocilin mRNA expression in adult mouse TM.

A third explanation to the lack of ß-galactosidase expression within eyes *in vivo*, may be wrong time point of investigation. In the case of the *MYOC* basal promoter, there is no doubt that our decision to analyze adult eyes would not be appropriate, since myocilin mRNA and protein can be detected within the mouse eye already at P9 (whole eye) and P12 – 14 (TM), respectively (Knaupp et al., 2004). The decision to analyze ß-galactosidase expression in mouse embryos was based on the fact that RAR, PITX and FOX are known to be pivotal regulators of anterior eye development, concretely this can be observed in the range of ASDs, which rely on mutations in PITX and FOX (reviewed by Cvekl and Tamm, 2004; Matt et al., 2005). Matt et al. (2005) confirmed that in the developing mouse eye the target of action of RA is the NC crest-derived anterior eye mesenchyme, from which also the CB stroma, TM and SC are derived (reviewed by Cvekl and Tamm, 2004). Based on these facts, there is no doubt that these transcription factors are present and active at our embryonic stages of analysis. As mentioned above, the complex design of our element may lead to unexpected interactions between the binding transcription factors, resulting in a totally different effect on gene regulation *in vivo* than observed *in vitro*. Moreover, the facts that the binding transcription factors are predominantly active at embryonic stages, exemplified by the fact that overall RARE-driven ß-galactosidase expression decreases in later embryonic stages (Rossant et al., 1991), and that the *Myoc* basal promoter is not active in the anterior mouse eye until P10 (Knaupp et al., 2004), may rise the possibility that the enhancer and promoter can not co-operate in the anterior eye at the same time point.

5.2.3.1. Unexpected expression of ß-galactosidase outside the eye

Unexpectedly, we observed ß-galactosidase expression within the ependymal lining of the lateral ventricle (Fig. 4.16) and within epithelial cells of intestinal glands (Fig. 4.17) in TG embryos of our instabile transgenic line. Due to limited material from this line, we only had the opportunity to analyze two TG embryos. Both TG embryos showed staining within the intestinal glands, whereas the ependymal staining was observed only in one of the TG animals. The positive staining within the ependyma could be observed in the transverse cut embryo, but not in the other embryo that was cut sagittal. It can be, that staining within the ependymal lining of the lateral ventricles can be better detected in transverse sections, whereas the plane of a sagittal section could affect detection of ependymal staining. Another theory is, as already discussed, that our used enhancer may not be strong enough to invariably drive expression of *LacZ* to an extent that turns cells blue. In fact, our observed staining was rather turquise that deep blue (Fig. 4.16), which was true also for the expression colour in our transfected culltured TM cells (Fig. 4.11). The probably too weak character of RAREß/PITX3/FOX to drive uniform reporter gene expression *in vivo*, may thus explain why we did not observe any *in vivo* expression within the complex eye.

The ependymal ß-galactosiadse expression correlates with the fact that components of the RA signalling pathway, RAR-ß and the RA acid synthesis facilitating cellular retinol binding protein type I, are both expressed in developing neural structures in mouse, including the neuroepithelium of the neural tube, as well as in the from neuroepithelium originating ependymal lining and CP, suggesting that RA-signalling is important in the development of these structures (Ruberte et al., 1993). In fact, improper concentrations of RA has been shown to result in congenital hydrocephalus in human infants (Lammer and Armstrong, 1992) and in calves (Okamoto et al., 1962), reflecting the role of RA in the developing ependymal lining and CP, the sites that secrete CSF.

PITX and FOX proteins are likewise involved in the regulation of brain CNS development. Pitx2 is expressed in the developing mouse neuroepithelium, where it controls differentiation of neural progenitors into differentiated neuronal phenotypes (Martin et al., 2002).

Homozygous mutations in *PITX3* may affect CNS development in humans (Bidinost et al., 2006). It is also interesting to note that mutations in *Mf1*, the mouse homologue to *FOXC1*, leads to congenital lethal hydrocephalus in mice, suggesting that this gene may be involved in the regulation of CSF secretion or filtration (Hong et al., 1999). In fact, human patients that suffer from Axenfeld-Rieger syndrome, a subtype of ASD that relies on mutations or deletions in the ocular mesenchyme-derived transcription factors *FOXC1* and *PITX2* (reviewed by Cvekl and Tamm, 2004), also may show pehotypes that affect the CNS, including hydrocephalus (Maclean et al., 2005; Moog, 1998). All these facts indicate that RAR, PITX and FOX isoforms may be active in the developing ependyma of the lateral ventricle, explaining the visible ependymal ß-galactosidase expression observed in our embryonic TG mice (Fig. 4.16).

ß-galctosidase expression within the epithelial cells of intestinal gland (Fig. 4.17) in TG mice of the same instabile ß-galactosidase overexpression line, correlates with the fact that RA-synthesizing enzymes are present differentially in time and space within the outer mesenchyme, lamina propria and epithelial layers of the developing mouse intestine (Niederreither et al., 2001), suggesting that regualted RA expression in these tissues is important for differentiation of the different layers of the intestinal mucosa. Due to limited material of TG mice of this line, we could not closer analyze in which parts of the mucosa ß-galactosidase was present. Since the epithelial expression of ß-galactosidase in our experiments is only based on visual interpretion of our sections, the observed blue colour may likewise be expression within the whole mucosal layer, including the outer mesenchyme, lamina propria and epithelial layer.

Differential expression of *Pitx2* within the mesenchyme of the embryonic mouse small intestine affects protein expression in a way that results in asymmetries of the ECM and cell-cell adhesion throughout the mesentery, resulting in correct looping of the intestine (Kurpios et al., 2008). Also forkhead transcription factors have been shown to be involved in the development of the intestine. *FOXC1* cDNA has been derived from intestine (NCBI UniGene). Subfamilies of FOX-proteins usually show overlapping functions during embryogenesis, whereas they may have diverse specific functions in the adult (Cirillo and Barton, 2008). FOXC2, which belongs to the same subclass as the eye mesenchyme-derived

FOXC1, is expressed in the intestinal mesenchyme adjacent to the developing epithelium. From here, it regulates morphological changes of the becoming overlying intestinal epithelium, including the definition of the zone occupied by crypts of Lieberkühn and the lengths of the villi (Kaestner et al., 1997). The above facts that describe expression of RAR, PITX and FOX isoforms within the embryonic intestine thus may explain the visible intestinal ß-galactosidase expression observed in our embryonic TG mice (Fig. 4.17).

If the observed intestinal ß-galctosidase expression is due to the activity of the *MYOC* basal promoter, the data would correlate with the fact that Fingert et al. (1998) showed that *MYOC* mRNA is found within intestine at comparable amounts as within skeletal muscle and heart. Since also other genes that code for olfactomedin-domain containing proteins have been shown to be expressed within the human intestine, it suggests that olfactomedin-related glycoproteins in general may have a role in regulating the extracellular environment of mucus-lined tissue (Kulkami et al., 2000). Interesting is also that the intestinal mucosal cells, together with the protruding tubular crypts of Lieberkühn, akin to the CB and TM, are involved in secretion and absorption/drainage, respectively. If myocilin is expressed within the intestine, the attempt to clarify its function within this organ will be a topic of future research.

The answer to the question why ß-galactosidase expression was observed only in one of our two transgenic lines, may be the fact that this line has more copies of the transgene inserted into its genome, a possibility that we never tested. Another explanation may be a positional effect, where our transgene may have integrated into a position in the genome that favors expression, e.g. into a site that is affected by a nearby promoter or enhancers. Since this line was the one that had proven to be instabile, we already discussed the possibility of a positional effect in this line (see section 5.2.2 for discussion).

5.3. Analysis of myocilin expression in mammalian brain

5.3.1. Expression of myocilin within the ependymal lining of the CP and the lateral ventricle

The fact that the *MYOC* basal promoter, in combination with our constructed artificial enhancer element RAREß/PITX3/FOX, directed visible ß-galactosidase expression to the ependymal lining of the lateral ventricle in the embryonic mouse brain (Fig. 4.16A), prompted us to investigate if myocilin is endogenously expressed at protein level in this tissue in mammals. Swiderski et al. (1999) already showed that myocilin mRNA is expressed in widespread regions of the adult mouse brain, including the ependymal lining of the third and fourth ventricles and the CP, and within regions that are involved in vision, hearing, olfaction, regulation of visceral activity, salt-water balance and emotional behaviour.

Our immunohistochemical data for the first time showed that myocilin protein is endogenously expressed in the ependymal lining of the lateral ventricle (Fig. 4.19E) and the CP (Figs. 4.19A, B). Since the ventricles in mammals are connected, and since Swiderski et al. (1999) showed that myocilin mRNA is expressed in the ependymal lining of the third and fourth ventricles, suggests that myocilin is endogenously expressed within the ependymal lining of the whole inner ventricular system in mammals.

5.3.2. Expression of myocilin within the CSF

Together with the ependymal lining of the ventricles, the ependymal cells of the CP secrete about 450 - 600 ml CSF/day into the ventricles, making up the so called blood-CSF barrier. Normally, CSF is clear, containing tiny amounts of protein (15 – 45 mg/dl within the lumbar region and even lower levels within the ventricles, which corresponds to ca 1 % of the concentration in blood), glucose and lymphocytes (Bob and Bob, 2007). CSF offers

mechanical protection to, and regulates homeostasis of, the CNS (Bob and Bob, 2007). The fact that myocilin is expressed in CSF secreting epithelial ependymal cells of the CP and the lining of the ventricular system in mammals (Fig. 4.19), prompted us to analyze if myocilin is also secreted into the CSF. As the volume of CSF that can be obtained from rodents is limited in comparison to volumes that can be obtained from human patients during lumbar puncture, and since we had access to CSF samples collected from patients during this procedure (PD Dr. med. Andreas Steinbrecher, Department of Neurology, University of Regensburg), we had earlier analyzed the expression of myocilin within human CSF by Western blot. The fact that all 18 analyzed human CSF samples expressed myocilin (Fig. 4.21) confirmed our suggestion that myocilin is secreted from ependymal cells into the CSF in mammals.

5.4. Pathology and architecture of the ventricular ependyma

Improper functioning of the CP due to atrophy of the ependyma, thickening of the basement membrane and decrease in enzymatic activity, often seen during ageing, reduce CSF secretion rate up to 50 %, affecting brain activity (reviewed by Serit et al., 2003). The process may impair the blood-brain barrier and result in pathological states like neurological and infectious disorders, as well as tumours. Multiple sclerosis, a neuroimmunological disease where the immune system attacks the myelin sheath of the CNS, is caused by entry of lymphocytes into the normally, due to the blood-CSF barrier, immune privileged CSF/CNS. Infections are triggered by viruses or bacteria that invade the CNS via the fenestrated vessels of the CP, where they activate cytokines, resulting in damage of the ependyma. Concerning prion diseases, it has been shown that the scrapie agent can escape the blood-CSF barrier (Banks et al., 2004). In Alzheimer´s disease neurotoxic plaques of the fibrous insoluble amyloid-ß, as well as tangles of neurofibrils and so called Bondi rings, accumulate within the CP ependyma (reviewed by Wolburg and Paulus, 2010). One theory to the accumulation of amyloid-ß in the brain is that the CP produces and secretes substances into the CSF that bind and sequester amyloid-ß (Choi et al., 2007). Ischemia in neighbouring tissue may impair blood flow to the CP, resulting in disruption of the blood-CSF barrier and subsequent neuronal death (Ennis et al., 2006). Following ischemia, there is an increase in the expression and release of

vasopressin from the CP, which may affect vascular resistance and induce edema formation (reviewed by Kozniewska and Romaniuk, 2008).

The ependymal lining of the ventricles is continous with the epithelial layer of the CP and it is, similarly to the ependymal lining of the central canal of the spinal cord, of neuroectodermal origin. Since the ependymal epithelial cells are non-neuronal cells of the brain, they are classified as a type of macroglial cells. The CP is the primary source of CSF secretion. It consists of ependymal epithelial cells, fenestrated arterial blood vessels and an ECM-rich stroma. In the CP, the CSF is produced by the ependymal cells from blood that leaks through the fenestrated blood vessels, and which then is transported to the ventricular space by a combination of passive diffusion and active transport (reviewed by Wolburg und Paulus, 2010). The epithelial ependymal cells are ciliated. It has generally been assumed that these motile cilia circulate CSF through the ventricular spaces, though more up to date studies show that the ependymal cilia can act as sensitive chemosensors to regulate CSF production (Narita et al., 2009). The ependymal cilia are of the motile primary type. Other cilia of the primary type are the ciliated photoreceptors of the retina and the cilia of principal cells of the kidney nephron. Defects in primary cilia in the ependyma, the photoreceptor and nephron (called primary ciliary dyskinesia), cause diseases like hydrocephalus (Ibanez-Tallon et al., 2004), retinitis pigmentosa and cystic kidney (reviewed by Eley et al., 2005), respectively.

5.4.1. Possible ependymal role of myocilin

Our finding that myocilin is expressed within ciliated ependymal cells of the CP and the ventricular lining (Fig. 4.19), correlates with the fact that myocilin is expressed in the connecting cilia of the axoneme, which connects the outer and inner segments of photoreceptors (Kubota et al., 1997). By assisting in molecular turnover and by transporting molecules between the diverse segments, the microtubular connecting cilium in the photoreceptor axoneme participates in morhogenesis and maintenance of the diverse segments (reviewed by Insinna and Besharse, 2008). Topics of future research are to find out, where exact within the ependymal cells myocilin is expressed, and to then analyze, if myocilin also

in these cells has a role in the maintenence of morphology and proper function of the ependymal cells. Such an analysis would be of great value in deciphering the molecular mechanisms that help maintain the normal function of ependymal cells. Since many neurological and infectious diseases, as well as CP tumours, are generally thought to rely on dysfunction of the CP epedyma, and since ischemia may result in dysfunction of the barrier capacity of the CP (reviewed by Wolburg and Paulus, 2010), a charachterization of the molecular mechanisms that maintain normal function of the ependyma would be of clinical relevance.

5.4.2. Possible correlation between amount of and extent of post-translational modification of myocilin and disease

CSF collection by lumbar puncture is routinely used to detect different forms of inflammation, like meningitis, or disease, like multiple sclerosis, of the brain and spinal cord. An interesting observation was that the overall myocilin expression between CSF samples varied significantly (Fig. 4.21). This may reflect differing pathological conditions of the patients at the time of CSF collection, and suggests that myocilin may be present in different amounts depending on disease or a pathological state thereof. Thus, the amount of myocilin within CSF may be relevant in the pathology of a certain disease. To clear this, it would be informative to get data about the disease, and pathological state thereof, that respective patient suffered from at the time point of lumbar puncture.

In most samples myocilin was detected as the typical 55 - 57 kD double band (Nguyen et al., 1998; Clark et al., 2001), of which the two bands are thought to be a result of post-translational modifications like glycosylation (Nguyen at al., 1998; Fingert et al., 1998). Normally, the two bands of the double band appear at same intensity. Our results showed different expression of the two myocilin isoforms, whereby the heavier 57 kD isoform was more abundant than the light 55 kD form. Appropriate glycosylation of a protein is important for correct folding, quality control, stability, enzymatic activity and molecular interactions. It is a general fact that aberrant glycosylation of a protein is involved in disease. Since myocilin

contain many putative glycosylation sites (Nguyen et al., 1988), and since it is known that the glycosylation status of a protein regulates its function, as exemplified for integrins and cadherins (reviewed by Zhao et al., 2008), the higher expression of the heavier 57 kD myocilin isoforms relative to the lighter 55 kD form in CSF samples from patients, may indicate that a higher degree of glycosylation of myocilin could be responsible for the respective pathologies.

5.4.3. A general function for myocilin in regulating drainage of fluid?

After circulation of CSF through the ventricles, most of it is drained through the arachnoid granulations into the venous system. The drainage of CSF through this so called CSF-blood barrier clears the CNS from waste products. Minor CSF volumes are thought to escape the ventricles through lymphatic capillaries, as well as the ependymal lining. The rate of CSF secretion into, and drainage out of, the brain ventricles thus regulates the intraventricular CSF volume, which in turn regulates intracranial pressure and blood flow perfusion. As already discussed, failure of the CSF secretory-drainage system may lead to hydrocephalus, or neurological and infectious diseases, as well as tumours of the CNS. Failure of the secretory-drainage system can also be induced by ischemia (reviewed by Wolburg and Paulus, 2010; reviewed by Kapoor et al., 2008).

In the same way as the balance between secretion and drainage of CSF in the CNS is important for the proper functioning of the CNS, the balance and proper interplay between secretion of AH by the CB and subsequent drainage through the TM is crucial in maintaining a physiological IOP (reviewed by Coca-Prados and Escribano, 2007). The secretion-drainage system between ependyma and the arachnoid granulations closely resembles that of the CB and TM in the following aspects. 1) Both secreting tissues, the ependyma and the CB, are of neuroectodermal origin. 2) Both the ependyma and the CB express myocilin. 3) Myocilin is found in both secretes, the AH and the CSF. 4) In both systems a balance between inward secretion and outward drainage are important for respective physiological intraocular and intracranial pressures. 5) Defects in both systems are associated with disease.

The facts that both the ependyma and CB express myocilin suggests that myocilin may be involved in the maintenance of structure and/or proper function of these neuroectodermal tissues, or in the secretion process itself. Concerning CNS this would link myocilin to neurological and infectious diseases, CNS tumours and hydrocephalus. Future studies are needed to clarify if myocilin is involved in the secretion process, or in the maintenance and function of both CB and ependyma. Very interesting is that both the ependyma and the CB secrete myocilin. Even though the function of myocilin within the AH is unknown, there are data that support that bacterially expressed recombinant myocilin accumulate in the TM, thereby increasing outflow resistance and IOP, when perfused through human anterior eye segments. Perfusion with high concentrations of various control proteins corroborated that the observed effect on outflow resistance and IOP is not due to the amount of overall protein, but rather due to a specific property of myocilin (Fautsch et al., 2000). These data were specified by the same experiment using recombinant eukaryotically expressed myocilin, which confirmed that an increase in outflow resistance and IOP occurs only when myocilin is first incubated with AH. Interaction studies showed that myocilin formed a complex with another unknown protein in the AH. At maximum outflow resistance, myocilin located to the JCT (Fautsch et al., 2006), the region within TM that is responsible for the generation of most of the AH resistance (reviewed by Johnson, 2006). The different data between these studies indicate that post-translational modifications, which are possible only in eukaryotic systems, may alter the ability of myocilin to interact with other proteins within the AH and the TM, thus affecting changes in hydrodynamics. In fact, it was already shown that AH is able to obstruct filter pores with diameters corresponding to the smallest flow dimensions in the JCT (Johnson et al., 1986). Later, it was shown that AH myocilin is able to block filters with pores of the same diameter. Most AH myocilin had a molecular weight of ~ 66 kD, suggesting post-translational modifications, most probably glycosylation (Russell et al., 2001).

Interestingly, our experiments showed that within human CSF the higher MW 57 kD myocilin isoform predominated over the 55 kD form (Fig. 4.21), suggesting that there may be more of glycosylated than non-glycosylated forms of myocilin within human CSF. This resembles the data from Russell et al. (2001), where AH myocilin was mostly found in its glycosylated form, and may indicate that a possibly glycosylated form of myocilin, as within the TM, may affect drainage hydrodynamics within the arachnoid granulations. The fact that the amount of myocilin varied between CSF samples from patients in our experiment (Fig. 3.21), may

indicate that the amount of myocilin within the CSF affected CSF drainage and pathology in these patients. Thus, in addition to being involved in the elevation of AH outflow resistance and IOP in the eye, which leads to glaucoma, myocilin may have a role in the regulation of CSF drainage out of the CNS. All these data suggest that myocilin may be involved in diseases caused by an inappropriate function of CSF secretion and drainage structures, as seen in neurological or infectious diseases, CNS tumours and hydrocephalus (reviewed by Kapoor et al., 2008), or after ischemia (Ennis et al., 2006).

5.4.4. Expression of myocilin within nerve cells of the PVZ

Adjacent to the ependymal layer is the SVZ of the PVZ, which separates the ependyma from the caudate nucleus that is involved in memory and learning. The SVZ is made up of a layer of mainly astrocytes, neuronal progenitor cells, as well as of a layer of myelinated fibers (reviewed by Curtis et al., 2007). During brain development, most of the neurons are generated from the SVZ and recent findings about populations of cells within the SVZ that can serve as adult neuronal stem cells (reviewed by Chojnacki et al., 2009), have given this tissue much clinical interest. In fact, during neurodegenerative diseases like Alzheimer´s or Parkinson´s disease there is a down-regulation of proliferative cells within the SVZ (reviewed by Curtis et al., 2007).

The observation that myocilin was, in addition to the ependyma, also expressed within axons and perikarya of nerve cells of the PVZ of 6 week old rat brain (Fig. 3.20) correlates with data that show that myocilin is expressed in astrocytes of adult rat brain (Jurynec et al., 2003), in ONH astrocytes, retinal perikarya and axons in human (Karali et al., 2000), as well as within the oligodendrocyte myelin sheath of human and primate optic nerve axons (Ricard et al., 2001). Myocilin expression within the peripheral nervous system has been observed in the Schwann cell myelin sheath of rat sciatic nerve (Ohlmann et al., 2003). The function of myocilin within nerve cells is unclear, though since the commence of expression within the myelin sheaths of optic nerve axons in human fetuses (Ricard et al., 2001), as well as of rat sciatic nerve (Ohlmann et al., 2003), correlate with respective time points of myelin sheath

formation, it is thought that myocilin may have a supporting role in the formation and/or maintenance of the myelin sheath of neurons. A supporting maintaining neuronal function of myocilin is supported by the fact that the expression of *MYOC* mRNA and protein decreased in glaucomatous human and monkey ONHs, when compared to controls (Ricard et al., 2001). In contrast to primates, elevation of IOP in rats resulted in an increase of ONH *Myoc* mRNA (Ahmed et al., 2001), suggesting that myocilin may be differentially regulated between primates and rodents.

Injury to the CNS induces a response that activates astrocytes, resulting in a so called glial scar, a characteristic of neurological diseases (Eng et al., 2000). The activation of astrocytes induces expression of specific glycosylated ECM proteins that inhibit regeneration of the CNS, including axonal regeneration (Fitch and Silver, 1999: Bradbury et al., 2002). It has been documented that myocilin is upregulated in activated astrocytes of glial scars *in vivo*, whereby the glycosylated 66 kD form predominated (Jurynec et al., 2003). As a possible extracellular matricellular protein, myocilin may be secreted and bind to other molecules needed for regeneration/maintenance of the CNS, thereby inhibiting their function. *In vitro*, myocilin interacts physically with flotillin-1 (but not when mutated) (Joe et al., 2005), a lipid-raft protein that is found within the same fraction of bovine CNS myelin sheath as the cytoskeletal proteins actin and tubulin, as well as the plasma membrane protein caveolin (Arvanitis et al., 2005). Also within the peripheral nervous system myocilin was expressed within regions of the myelin sheath that is enriched in proteins having structural and/or signalling roles (Ohlmann et al., 2003). Thus, myocilin might support neuronal function structurally and/or through signalling, thereby maintaining proper myelin sheath characteristics and/or interacations. Since astrocytes, the most common and largest glial cell of the CNS, akin to oligodendrocytes are supportive nerve cells, the increase of myocilin expression in glial scar may indicate a response to restore structure and function of the astrocyte. Thus, myocilin could have a general role in maintaining structure and function of glial cells.

4.4.5. Possible periventricular role of myocilin

Since we did not label our brain sections, we can not exactly define the area of the PVZ where myocilin expression was present. If it is the adjacent SVZ, the expression of myocilin is an interesting fact, since this area is the origin of most neurons in development, and it maintains a pool of progenitor cells, which replace neurons in the olfactory bulb in adulthood. In neurological diseases, like Alzheimer´s, Huntington´s or Parkinson´s, the regulation of progenitor cell proliferation is disturbed (reviewed by Curtis et al., 2007). There has been debate about the identity of the SVZ progenitor cells, which may be of ependymal, astocytic or of neural stem cell origin (reviewed by Chojnacki et al., 2009). If future experiments show that myocilin is expressed within the SVZ, it would bring our ependymal myocilin expression data (Fig. 4.19) into a new light, regarding a possible role of myocilin in the differentiation of e.g. myelinating oligodendrocytes. If the myocilin expression turns out to reside within a more distal site of the PVZ, myocilin anyhow seems to have some neuronal supporting role in that it seems to generally be expressed within nerve cells (Fig. 4.20A), most probably glial cells and neuronal axons (Fig. 4.20B). Concerning neurons, the role could be a cytoskeletal role, as seen within the connecting cilium of photoreceptors (Kubota et al., 1997). The role of myocilin in glial cells suggests an involvement in myelination and/or in the support and maintenance of the myelin sheath (Ricard et al., 2001; Ohlmann et al., 2003), as well as a supporting role in the function of astrocytes, as exemplified by the fact that the expression of myocilin is increased during glial scar formation (Jurynec et al., 2003), probably in an attempt to restore astrocyte function. As a matricellular protein myocilin may be secreted by glial cells to the ECM, thereby affecting ECM interactions and function of the nervous system.

5.5. Outcome

In summary, our attempt to target protein expression into the TM *in vivo* opened totally new aspects concerning the function of myocilin. Our results have brought more evidence for a neuronal supporting function of myocilin, which is in accordance with its assumed role as a matricellular protein, since these proteins do not by themselves show to have any specific

functional role, in contrast, matricellular proteins act by modulating other proteins (reviewed by Bornstein et al., 2000). In fact, astrocytes are known to secrete matricellular proteins that regulate developmental processes, as well as CNS repair after injury in adulthood. In concordance with matricellular proteins in general, knock-out within the CNS do not evoke any observable phenotype (reviewed by Eroglu, 2009), which matches the fact that myocilin knock-out mice seem to be normal (Kim et al., 2001). Despite the absence of an obvious phenotype, there is however evidence that deletion of CNS matricellular proteins modulate synaptic transmission (Eroglu, 2009). In addition to showing evidence for a suggested general function in supporting and/or modulating the function of nerve cells, our data suggest a possible role of myocilin in the drainage of CSF in the brain, which also in this context links myocilin to new areas of clinical interest.

5.4. Creation of an animal model that would allow a TM directed conditional knock-out

The Cre/*lox* system is the most widely used (and perhaps the most effective) system by which a conditional gene knock-out can be achieved in mammals. A mouse line that expresses Cre recombinase in a tissue-specific manner allows this mouse line to be used as a tool to generate a conditional tissue-specific knock-out of a desired gene in TG offspring. This is of huge advantage, since classical germ-line knock-outs usually may be associated with embryonic lethality (reviewed by Sauer, 1998).

Whereas there have been many attempts to conditionally knock-out genes in the posterior eye, only few reports involve the anterior eye (reviewed by Kao, 2006). TM-directed expression of Cre would open the possibility to study the effect that deletion of a desired gene has on the hydrodynamics of AH outflow, without the need to create a germ-line knock-out line for every gene of interest. The growing microarray data from normal, glaucomatous and dexamethasone-treated TM (Tomarev et al., 2003; Rozsa et al., 2006; Vittal et al., 2005; Diskin et al., 2006) makes it necessary to create a straightforward strategy to analyze potential candidate glaucoma genes. To approach this topic, we wanted to create a mouse-line that drives the expression of Cre specifically in the TM. Since myocilin is abundantly expressed at both mRNA and protein levels in adult mouse TM (Takahashi et al., 1998; Knaupp et al., 2004), and since Kim et al. (2002) already showed that the endogenous *Myoc* locus can be targeted by homologous recombination, and that this knock-out of the myocilin gene did not have any effect on the viability or phenotype, we wanted to use the endogenous *Myoc* promoter to drive the expression of Cre in the TM. Our data that showed that the *MYOC* basal promoter, even though acting in combination with an enhancer element, was too weak to drive gene expression *in vivo* (Fig. 4.15), further prompted us to this time use the whole endogenous myocilin promoter for expression of protein in the living TM.

We designed and cloned a knock-in construct that would be able to integrate at the *Myoc* locus by homologous recombination in mouse ESCs, and that as well would later enable for screening of properly integrated ESCs by Southern blot. (Chapter 4.4.1; Figs. 4.22, 4.23). Linearization, purification and electroporation of the knock-in construct into mouse ESCs

resulted in > 600 clones expressing our construct. Screening of these colonies for correct homologous recombination at the *Myoc* locus by Southern blot revealed that one of the clones had integrated the 3´-flank of the knock-in construct correctly at the *Myoc* locus (Fig. 4.24). Screening for the 5´-flank of the construct revealed that also this flank had integrated, however, the expected band size after restriction digestion did not show the calculated size (Fig. 4.25). Since the ESC lysate was limited, we could not repeat the experiment. Since the band was smaller than the expected 7203 bp, showing a size of ~ 4 kb, we first thought about a possible deletion that may have occurred during the recombination process. To exclude this, we amplified the whole 5´-flank, beginning from the 5´-upstream region of the genome and ending downstream of the flank within the gene for Cre (data not shown). This indicates that the whole 5´-flank promoter region was present but, since we did not further clone and sequence the amplified region, we can´t exclude that the amplicon was an artefact.

If a deletion of a part of the 5´-flank had occurred, it probably arose during the meiotic homologous recombination process, which may be affected by processes like gene conversion (whereby a part of a recombinating sequence do not recombinate, but retains the sequence from the other strand, resulting in two identical alleles) or some of the DNA proof-reading mechanisms that inhibit crossing-over of e.g. improperly aligned homologous sequences (Alberts, 2004). Since we by sequencing detected that we only had two point mutations in our amplified 3072 bp 5´-homologous flank (Chapter 4.4.1), it is though unlikely that improper alignment of the 5´-flank sequences would have, due to non-complementarity, interrupted the recombination event at this end of the construct. The unexpected too short size resulting from our 5´-end restriction could theoretically be a consequence of a novel restriction enzyme site due to a naturally occurring small nuclear polymorphism in the 5´-homologous region, or due to a nucleotide exchange during amplification. However, based on our sequencing data, this theory seems to be unlikely. A third theory concerning the restriction, and which could have resulted in the unexpected restriction pattern, may be star activity of our enzyme.

Contamination problems in the ESC facility finally resulted in the death of our analyzed clone, thus we could not proof this clone further for it possibly having a correct integration of our knock-in construct at the *Myoc* locus. Further attempts by a biocompany to target the *Myoc* locus of ESCs, destined to become germ-line cells, by our knock-in construct failed,

indicating that the *Myoc* locus in general may not be easy to manipulate. This correlates with the fact that we earlier had to screen over 600 colonies until we detected possibly one positive clone. Even though Kim et al. (2001) targeted the *Myoc* locus successfully, they did not mention how many ES clones they screened for. Homologous recombination is a rare process, occurring once per 10^5 – 10^7 electroporated cells (Sargent and Wilson, 1998), whereby the propability of a crossing over increases proportionally with the lengths of the homologous flanks (Hasty et al., 1991). Since a conditional knock-out in the TM would offer an immense spectrum of possibilities to study the role of molecular factors thought to be involved in an elevated IOP, we at the moment are in the process of elongating our homologous flanks, aiming later to send our elongated knock-in construct for electroporation. Future projects beyond this Ph.D. Thesis aim to analyze the Cre knock-in mouse in its ability to conditionally knock out sequences in the TM. Crosses with reporter lines like Z/EG (*Lac*Z/EGFP) (Novak et al., 2000) and Z/AP (*Lac*Z/human placental alkaline phosphatase (Lobe et al., 1999) will give an insight into the spatial pattern of Cre activity, whereas analysis of eGFP expression will show the temporal pattern of Cre expression. Then, our Cre mouse line can be crossed with lines that carry *loxP*-flanked genes to generate double TG progeny with knock-out in a Cre expression pattern dependent fashion.

5.5. Analysis of corneal gene expression in TGF-ß1 overexpression mice

Earlier microarray analysis of our TGF-ß1 overexpression mice, which have eye defects like a thick opaque cornea, due to a stroma with undifferentiated and excessively proliferated mesenchyme cells, vascularisation and an unorganized ECM, and which show an up- and downregulation of fibronectin, perlecan, α-smooth muscle actin and type VI collagen expression, respectively (Flügel-Koch et al., 2002), revealed that there were 98 and 163 genes that were differentially up- and down-regulated, respectively, in the corneas of these mice (not yet published). Since the corneal defects in these mice in many aspects resemble a fibrotic corneal phenotype, knowledge of the TGF-ß1-induced differential gene expression may be of clinical relevance, not at least in finding out which genes that may be responsible in maintaining the transparency of this tissue. Thus, we wanted to extend our earlier microarray data to be validated for 12 genes that are known, based on literature, to be regulated by TGF-ß1 or to be expressed in the cornea, by RT real-time PCR.

The microarray data showed that the expression of many genes that are important for the maintenance of normal characteristics of the cornea was altered in response to an overexpression of TGF-ß1 (Tables 4.4; 4.5). Cytoskeletal and ECM proteins, and their interplay via integrins, are pivotal in the maintenance of an ordered cell-ECM architecture, a criterion that is crucial for the for transparency responsive corneal stroma (Maurice, 1957). Proteins that serve as connectors and communicators between cells (e.g. junction-forming proteins) are important for tissue integrity, not at least for the as barriers functioning epithelium and endothelium (reviewed by Lu et al., 2001). Enzymes and signalling molecules are finally the ones that maintain basic metabolic functions and regulate growth, migration and differentiation during development or disease. In addition, high expression of some general enzymes are thought to also have a second crystallin role in the corneal stroma (reviewed by Jester, 2008). Our microarray data showed that the expression of proteins from all above described classes were affected in TG corneas, indicating that the observed phenotype in these mice is a result of a complex alteration in protein expression and molecular signalling that affect both intra- and extracellular molecular mechanisms. Changes in gene expression of cytoskeletal, extracellular and junction-forming proteins, as well as of

enzymes and signalling molecules can also generally be observed during wound healing, making our study relevant also in this aspect.

5.5.1. Differential expression of genes coding for ECM proteins

Our real time PCR data confirmed that the genes for the extracellular Mmp13, as well as the basal lamina proteins Lama3 and Lamb3 were up-regulated in TG corneas, indicating a remodelling of ECM and cell-matrix contacts. MMP13, a secreted proteinase with a wide substrate specificity ranging from various collagens to adhesion molecules like tenascin C and fibronectin (Knäuper et al., 1997), was originally cloned from human breast carcinoma tissue (Freije et al., 1994), and is a critical regulator of cartilage formation and ossification during development (Inada et al., 2004). MMPs are generally known to be involved in ocular surface diseases like corneal wound healing (Ye et al., 2000), corneal erosions (Dursun et al., 2001), corneal ulcers (Fini et al., 1998) and corneal inflammation and neovascularisation (Kvanta et al., 2000), though the regulation of the MMPs in these diseases are unclear. The expression of MM13 was induced in neovascularized rabbit corneas (Huang et al., 2001), which correlates with the fact that our TGF-ß1 overexpressing mice showed a vascularised corneal stroma. MMP13 expression is up-regulated in keratoconus human corneas (Mackiewicz et al., 2006). Even though keratonus corneas are thinner than normal, in contrast to the too thick than normal corneas of our TG mice, it may not exclude that Mmp13 may be involved, through remodelling of the ECM, in the regulation of corneal thickness. MMP13 was shown to be active in embryonic chick corneal stroma, where it by degrading ECM facilitated NC cell migration (Huh et al., 2007). The increased cellularity of our TG corneas may be, in addition due to an increased proliferation, due to an increased migration of NC-derived mesenchyme cells into the stromal space during development. Migration of cells is dependent on adhesive ECM molecules, like fibronectin, on which to migrate (reviewed by Perris and Perrissinotto, 2000), and Mmp13 may facilitate this migration by digesting excess ECM. Up-regulation of MMP13 in wounded rat corneas (Ye et al., 2000) and its role in mediating fibrosis and inflammation in hepatic stellate cells (Uchinami et el., 2006), finally shows that our TG mice show fibrotic characteristics also at the gene expression level, underscoring that these mice may be a good model to study fibrotic molecular mechanisms.

Since MMP13 was originally found to be a protease that digests fibrillar collagens (Freije et al., 1994), and since the corneal transparency is dependent on a highly ordered structure of abundant fibrillar collagens (Maurice, 1957), the opaque corneas of our TG mice may be due to digestion of the stromal fibrous collagens by Mmp13, resulting in disturbances of both homeostasis and the ordered architecture normally present in a healthy cornea. Since MMP13 has a central role in the network of MMPs and their inhibitors tissue inhibitor of matrix metalloproteinases (TIMPs), in that it activates and is activated by many of them, the high expression of MMP13 in our analyzed TG corneas is likely to be accompanied by a differential expression of also other MMPs and TIMPs.

MMP13 is differentially regulated by various signalling cascades, depending on cellular environment and developmental or pathological state. Even though *MMP13* contains a TGF-ß inhibitory element in its promoter (Pendas et al., 1997), its mRNA and protein levels, as well as its activity, can be increased by TGF-ß1 treatment, from barely detectable levels under normal conditions (Li et al., 2003), in a dose-dependent manner in cultured human corneal epithelial cells (Kim et al., 2004), indicating that the inhibitory element is not used in the cornea. This correlates with the fact that our TGF-ß1 overexpressing mice showed a 6.156 and > 53-fold elevation in *Mmp13* expression in the microarray and real-time PCR (highly significant), respectively, when compared to WT corneas (Table 4.4, Fig. 4.27), and reflects the fact that our TGF-ß1 overexpression mice showed a high, > 7-fold over that of WT eyes, expression of TGF-ß1 mRNA at P0, the time point of preparation of our analyzed corneas, as well as an effective translation of the TGF-ß1 mRNA into protein (Flügel-Koch et al., 2002). Since TGF-ß can, in addition to via Smad2/3, signal via different arms of the MAPK pathway (reviewed by Saika, 2006), and since it has been shown that MMP13 is activated via p38 MAPK upon TGF-ß1 treatment in transformed human keratinocytes (Johansson et al., 2000), *Mmp13* could be activated by TGF-ß1 via the MAPK signalling pathway also in our TG corneas. Since all MAPKs, MAPK, JNK and p38, are able to phosphorylate Smad2/3 (reviewed by Saika, 2006), a TGF-ß1 induced activation of MAPKs could result in a positive-feedback loop of TGF-ß1 expression.

Basal lamina proteins are synthesized by the cells that rest on it, i.e. in the case of the cornea by the epithelium and endothelium. These proteins bind integrin, as well as other ECM

molecules, thus connecting the cytoskeleton of a cell to the ECM. Thus, they are involved in structural organization of both intra- and extracellular architecture, cell migration during development and wound healing, as well as in cell signalling via integrins. The basal lamina multidomain adhesive glycoprotein laminin is one of the first ECM proteins synthesized in a developing embryo (Alberts et al., 2004). Lama3 and Lamb3 are subunits of laminin 5 and normally expressed in the basal lamina (Bowman´s membrane) of the corneal epithelium, whereas they in diseased corneas are also expressed in the corneal stroma (Byström et al., 2007). In wounded rat corneas TGF-ß and its receptors were induced in the regenerating epithelium, as well as in the stroma, which showed hypercellularity and fibrotic characteristics. The expression of laminin and fibronectin were as well up-regulated in the stroma. The authors suggest that TGF-ß may be responsible for the stromal ECM formation and cell reqruitment (Mita et al., 1997). *In vitro* data confirmed that TGF-ß1 physically interacts with laminin (Kumar et al., 1995), and that the *Lama3* promoter contains a TGF-ß1 responsive element that is responsible for reporter gene expression in keratinocytes (Virolle et al., 1998). These data correlate with the fact that the expression of *Lama3* and *Lamb3* was up-regulated (for *Lamb3* highly significant) in corneas of TGF-ß1 overexpressing mice (Fig. 4.26). Since TGF-ß1 is known to regulate the expression of both integrin and laminin subunits in rat alveolar cells, indicating that TGF-ß1 is involved in differentiation of this tissue through the regulated expression of these proteins (Kumar et al., 1995), the TGF-ß1 induction of *Lama3* and *Lamb3* in our analyzed TG corneas may have influenced the differentiation and/or migration of mesenchyme cells into the stroma in these mice. Or, as basal lamina proteins are known, together with integrins, to co-ordinate incoming extracellular signalling (Alberts et al., 2004), Lama3 and Lamb3 may have structurally been involved in accumulating extracellular growth signalling at the cell surface, leading to the excess proliferation of stromal mesenchyme cells seen in our TG mice. It would be interesting to analyze if also integrins are differentially expressed in the corneas of our TGF-ß1 overexpressing mice.

5.5.2. Effect of TGF-ß1 on the cytoskeleton

Krt14 makes up intermediate filaments (IFs) of the cytoskeleton primarily in the epidermis, where it in its mutated form is associated with skin fragility and blistering diseases

(Coulombe et al., 1991). Our data that showed that *Krt14* was up-regulated significantly upon TGF-ß1 overexpression in mouse corneas (Fig. 4.26) correlate with earlier data that showed that TGF-ß1 induces the expression of Krt14 in cultured human keratinocytes and cutaneous wounds in mice (Jiang et al., 1995; Werner et al., 2000). Embryonic mouse corneal epithelial cells express Krt14, whereas it in adult is limited to mitotically active basal cells (Kurpakus et al., 1994). The facts that Krt14 is thus considered a marker for mitotically active basal cells, and that *Krt14* was up-regulated in our TG corneas, correlates with the observed excessive cellular proliferation of the corneal stroma in these mice (Flügel-Koch et al., 2002). The fact that there is normally a switch from the keratin pair Krt5/Krt14 to Krt3/Krt12 as the cornea differentiates (Schermer et al., 1986) correlates with the fact that the corneas of our TGF-ß1 overexpression mice had an immature character (Flügel-Koch et al., 2002).

During wound-healing, activated cells alter their composition and architecture of IFs, which may alter their viscoelastic properties, facilitating proliferation and migration (reviewed by DePianto and Coulombe, 2004). In addition, IFs are able to bind and modulate the activities of receptors, enzymes, and adaptor molecules, whereby they organize and assemble activities of the cell to maintain proper metabolism and homeostasis (reviewed by Green et al., 2005). It is also known that IFs can sequester regulators of signalling pathways, resulting in changes in cell size, migration and survival (reviewed by Pallari and Eriksson, 2006). Thus, in addition to contributing to changes in viscoelastic properties of the cells of the corneal stroma in our TG mice, which could have affected the excessive migration of mesenchyme cells into the stroma (Flügel-Koch et al., 2002), the up-regulation of *Krt14* could have affected growth signals in a positive way to enhance proliferation of these cells. Patients with posterior polymorphous endothelial dystrophy show abnormalities of the corneal endothelium and the Descemet´s membrane, including opacities. Jirsova et al. (2007) showed novel expression of Krt14 in the diseased endothelium of these patients, indicating that there is an epithelialization of this tissue. Interestingly, our analyzed TGF-ß1 overexpression mice do not either have a defined normal corneal endothelium. The fact that the corneas of these mice are opaque (Flügel-Koch et al., 2002), also suggests that there may be an epithelialization of this tissue. In fact, the microarray data showed that also other epidermal-specific keratins were up-regulated in the microarray, including *Krt16* and *Krt23* (data not shown).

5.5.3. Changes in cell-cell communication and cation permeability

Gjb2 is an epithelial integral membrane protein of the connexin proteinfamily, it also called connexin 26. Connexins build up a connexon and connexons from adjacent cells form gap junctions (Alberts et al., 2004). Mutations in GJB2 cause keratitis-ichthyosis-deafness syndrome, a disease that depending on mutation may cause deafness, thickening of the epidermis and corneal defects, incuding opacity, scarring, inflammation, neovascularisation and absence of sensation (Bale et al., 1999; Richard et al., 2002, Sonoda et al., 2004). Connexins show a spatially regulated pattern of expression in the cornea, suggesting that they have important roles in proliferation, differentiation and maintenance of this tissue. Gjb2 was found in epithelial basal and intermediate cells, as well as between endothelial cells in rat cornea (Laux-fenton et al., 2003). *In vitro* data showed that GJB2 mediates gap junction communication in well differentiated human corneal epithelial cells, whereas undifferentiated cells were uncoupled, and that mutant GJB2 was not capable of forming gap junctions in these cells (Shurman et al., 2005). These data show that a proper expression of GJB2 is inevitable for proper development and function of the cornea, and may indicate that the observed up-regulation of *Gjb2* in our TG corneas (Fig. 4.26) may have disturbed normal communication between the cells.

Also for this gene there is a parallel to the wound healing process, since Gjb2 has shown to be transiently up-regulated and to re-locate in wounded rabbit corneas, indicating that cell-cell communication is important during corneal wound healing (Ratkay-Traub et al., 2001). Epidermal wounding also up-regulated Gjb2 in hyperproliferative cells proximal to the wound, and these cells showed an altered intercellular communication (Goliger and Paul, 1995). This correlates with the fact that stromal cells of our analyzed TG corneas showed hyperproliferation (Flügel-Koch et al., 2002). Interstingly, connexin 43, which is the most prevalent connexin within the cornea (Shurman et al., 2005) directed embryonic NC cell migration in the heart and the proliferation of neighbouring non-NC tissue (Huang et al., 1998). Even though it has not yet been shown that Gjb2 can do the same, it is interesting that our TG corneas also had an increase of NC migration into the corneal stroma (Flügel-Koch et al., 2002). The facts that FGF-2 up-regulated TGF-ß1 and *GJB2* in human ESCs, suggesting that *GJB2* was induced by TGF-ß1 (Greber et al., 2007), and that TGF-ß1 up-regulated

connexin expression in cultured bovine aortic endothelial cells, correlate with our microarray and real-time PCR data. On the other hand, Flügel-Koch et al. (2002) assumed that TGF-ß1 would indirectly act via FGF-2 to cause the phenotype seen in our analyzed TGF-ß1 corneas. Thus, *Gjb2* could have been either directly by TGF-ß1 or indirectly via FGF-2 up-regulated in our analyzed TG corneas.

Trpm1, which was highly significant down-regulated in our real-time PCR experiments (Fig. 4.26), codes for a transient receptor potential cation channel protein, originally discovered in benign metastatic melanomas, where its expression inversely correlated with tumour thickness (Duncan et al., 1998; 2001) and thus is regarded as a possible tumour suppressor. Since transient receptor potential cation channel proteins are permeable for e.g. Ca^{2+} and Mg^{2+}, and thus involved in the regulation of intracellular Ca^{2+} and Mg^{2+} levels that in turn regulate signalling and stabilization of enzymes (Stryer, 1995; Wolf and Cittadini, 1999), respectively, dysfunction in these proteins can affect proliferation, differentiation and growth. These channel proteins are reported to be associated with a diverse spectrum of diseases called channelopathies, including systemic diseases like asthma, pulmonary disease and neurodegenrative disorders (reviewed by Nilius et al., 2007). The facts that cations like Ca^{2+} and Mg^{2+} are important in maintaining the health of the corneal epithelium (Bachman and Wilson, 1985), that the chelation of Ca^{2+} and Mg^{2+} by sodium citrate reduces corneal ulceration after injury in rabbit eyes (Haddox et al., 1996), and that these cations decreased bovine stromal swelling (Hogan et al., 2008), indicate that proper regulation of intra- and extracellular Ca^{2+} and Mg^{2+} concentrations are important for corneal homeostasis. In fact, improper Ca^{2+} homeostasis in the cornea may lead to band keratopathy, a disease where calcium deposits in the cornea and which may be accompanied by inflammation and impairment of vision (Galor et al., 2008). The down-regulation of *Trpm1* in our experiments could thus, due to an abnormal cation homeostasis, have resulted in the corneal phenotype observed in our analyzed TG mice. Or, the reduced amount of *Trpm1* transcript could be a result of the immature character of the cornea in these mice, i.e. be a consequence rather than cause of the phenotype. It is interesting to note that *TRPM1* is a direct target for micropthalmia-associated transcription factor (MITF) in diverse human melanoma cell lines, and its mRNA location corresponds to that of *MITF* in the mouse eye (Miller et al., 2004), suggesting that it is a downstream target of MITF. This correlates with the fact that *Mitf* was 2.6-fold down-regulated in our analyzed TG corneas compared to WT corneas (data not

shown) and suggests that the down-regulation of *Trpm1* in our experiments may be a result of TGF-ß1 induced down-regulated *Mitf*.

5.5.4. Differential regulation of enzymes/transporters

Oca2, or pink-eyed dilution, is a melanosomal transmembrane protein involved in the processing and trafficking of tyrosinase in the melanogenesis process (Chen et al., 2002), and/or it mediates neutralization of melanosomal pH, which favors melanogenesis (Ancans et al., 2001). Mutations in *OCA2* cause oculocutaneous albinism type 2, a disease that show a phenotype that results from defects in melanogenesis, i.e. hypopigmentation of skin, hair and the pigmented parts of the eye (Rinchik et al., 1993). Mutations in *OCA2* may cause symptoms like nystagmus, foveal dysplasia, as well as affect vision (reviewed by Grønskov et al., 2007). Since only the pigmented part of the retina and the iris contain melanosomes, the role of OCA2 within the cornea suggests another, not with melanogenesis associated function. Since the exact function of OCA2 in the melanogenesis process is not defined, and since Oca2 has been suggested to act as an ion transporter (Puri et al., 2000) and been shown to modulate glutathione metabolism (Staleva et al., 2002), the role of Oca2 in the cornea may be to generally maintain homeostasis by e.g. ion transport or detoxification. If Oca2 has a general homeostatic role, the highly significant down-regulation of this gene in our analyzed TG corneas (Fig. 4.26) could have affected normal development of these corneas by generally disturbing e.g. homeostasis or protein folding. It is interesting that *Oca2* is mutated in the cavefish Astynax, whose eye primordia degenerate by apoptosis of the lens (Jeffery, 2009). In fact, the lenses of our TG mice were apoptotic (Flügel-Koch et al., 2002). Even though the severe phenotype seen in the cavefish relies on mutations that cause total loss of function of Oca2, as well as due to additional mutated genes (reviewed by Jeffery, 2009), it suggests that this protein could have an important eye developmental function.

The down-regulation of *Mitf* in our microarray of corneas from TGF-ß1 overexpressing mice (data not shown) correlates with data where TGF-ß1 was shown to down-regulate MITF and melanin synthesis in cultured mouse melanocytes via a delayed activation of ERK MAPK signalling (Kim et al., 2004). Since MITF is known to regulate melanogenesis associated

genes (Cheli et al., 2010), the down-regulation of *Oca2* in our experiments could thus be a consequence of by TGF-ß1 down-regulated *Mitf*.

Another gene that showed a highly significant down-regulation in TG vs. WT corneas was the gene coding for dual function brain protein Ptgds (Fig. 4.26). Intracellularly Ptgds acts as an enzyme that converts prostaglandin H2 (PGH2) to prostaglandin D2 (PGD2), a potent endogenous somnogen, nociceptive modulator, anti-coagulant, vasodilator, bronchoconstrictor and allergic and anti-inflammatory mediator, whereas it extracellularly acts as a lipophilic ligand binding protein (rewiewed by Urade and Hayaishi, 2000). The down-regulation of *Ptgds* due to an overexpression of TGF-ß1 in our experiments correlates with data that show that TGF-ß1 can modulate the expression of cyclooxygenase, the enzyme that converts arachidonic acid to the prostaglandin precursor PGH2, in human bronchial epithelial cells in a time- (Liu et al., 2007) and in neurons and astrocytes of rat CNS in a dose-dependent manner (Luo et al., 1998), respectively. *PTGDS* was shown to be the most abundant transcript in human corneal endothelium (Sakai et al., 2002) and PGD2 is a major prostanoid in ocular tissues. However, is the enzymatic activity of PTGDS in the cornea negligible (Goh et al., 1987), suggesting that this protein may have another than an enzymatic role in this tissue. Indeed, since rat and human PTGDS bind RA and retinaldehyde, as well as RA and retinal, respectively, with high affinity (Tanaka et al, 1997; reviewed by Urade and Hayaishi, 2000), PTGDS could have a role in the transport of RA and its derivatives throughout the cornea. During mouse development NC cells of the ocular mesenchyme are target for RA signalling (Matt et al., 2005), which affects other important (including Pitx- and Fox-mediated) signalling pathways, resulting in the required determination of the conjunctiva-corneal border (Gage et al., 2008). Thus, indirectly, RA signalling is involved in directing cues for the establishment of corneal transparency, and a possible disturbed RA transport, due to a down-regulation of *Ptgds*, could have resulted in the observed corneal phenotype of our analyzed TG corneas.

Cultured bovine keratocytes were shown to express Ptgds as a keratan sulphate proteoglycan (KSPG) (Berryhill et al., 2001), the type of post-translationally modified ECM proteoglycans that, in addition to collagens, are important for the maintenance of corneal transparency (Michelacci, 2003). This is evidenced by the facts that there is an increase in corneal KSPG

content during development, which correlates with the time point of acquisition of transparency (Coulombre and Coulombre, 1958), and that KSPGs are absent in opaque corneal scars (Hassell et al., 1983). If PTGDS has a role in conferring transparency, the down-regulation of *Ptgds* in our analyzed TG corneas could thus be one of the reasons that lead to corneal opacity in these mice. It is a general fact that abundantly occurring enzymes involved in basal metabolism can have a second crystalline role, conferring transparency, in the cornea. Such enzymes are e.g. aldehyde dehydrogenase 1A1 and transketolase (reviewed by Jester, 2008). In fact, transketolase was down-regulated in our analyzed TG corneas in the microarrays (data not shown). It is tempting to speculate that Ptgds would also, in addition to its enzymatic role, have a crystallin transparency conferring function in the cornea.

5.5.5. Modulation of signalling pathways

Egr2, or Krox-20 which was significantly up-regulated in our real-time PCR experiments (Fig. 4.26), codes for a zink finger immediate-early transcription factor. *Egr-2* is up-regulated early, without *de novo* protein synthesis, and transiently in the G_0/G_1 transition of the cell cycle (Chavrier et al., 1988). Egr-2 activates *Hox* genes, necessary for the morphological segmentation of the hindbrain (Seitanidou et al., 1997). In mouse, Egr2 is also involved in the myelination of PNS (peripheral nervous system) Schwann cells, where it activates genes necessary for proper myelination (Topilko et al., 1994). In human, mutations in *EGR* lead to sensory neuropathies including axonal atrophy and disability, as well as defects in axonal transport (reviewed by Berger et al., 2006). *Egr*-2 expression increases as development proceeds in chick corneas (Conrad et al., 2009). EGR-2 could thus have a role in the myelination of nerves also in the cornea. The facts that only the peripheral/limbal corneal stroma contains myelinated nerves, whereas the central and transparent corneal stroma only contains unmyelinated nerve fibers (Müller et al., 1996), may be a sign of conjunctivalization of our analyzed TG corneas. This suggestion is supported by the fact that *Dkk2* was highly significant down-regulated in our experiments (Fig. 4.26) (discussed later in this chapter), which in turn suggests an up-regulation of Wnt signalling. Data from Gage et al. (2008) showed that down-regulation of the Wnt signalling in the central cornea is necessary for the development of corneal over conjuctival fates, including the acquisition of transparency.

In embryonic and adult wounds *Egr-2* was rapidly and transiently up-regulated, suggesting that it is involved in the initiation of the wound healing process by activating other genes (Grose et al., 2002). Our data that showed that TGF-ß1 overexpression induced the expression of *Egr-2* in mouse corneas correlate with earlier data where TGF-ß1 induced an almost five-fold up-regulation of *Egr-2* in primary mouse embryonic maxillary mesenchyme cells (Pisano et al., 2003). TGF-ß1 also induced the expression of *Egr2* in both mouse fibroblast and epithelial cells, which were growth-stimulated and growth-inhibited by the treatment, respectively (Koskinen et al., 1991). This is interesting, since our analyzed TG corneas had proliferation of the stroma, whereas the epithelium was degenerated, covering only a part of the stroma (Flügel-Koch et al., 2002).

Fst, which codes for a secreted ubiquitous autocrine glycoprotein that originally was identified as a follicle-stimulating hormone suppressing protein (Ueno et al., 1987), was significantly up-regulated in our real-time experiments (Fig. 4.26). Fst binds and inhibits downstream signalling of the TGF-ß superfamily members activin in rat ovary (Nakamura et al., 1990), as well as BMP4 (Fainsod et al., 1997) and myostatin (Amthor et al., 2004) in the embryonic frog and chick mesoderm, respectively. Activin is also known to be an embryonic morphogen, determining cell fate in a concentration dependent manner (Alberts et al., 2004). You and Kruse (2002) showed that activin and its receptors are transcribed in human corneal fibroblasts, and that activin mediates differentiation of cultured human keratocytes. The fact that the activin mediated effect on differentiation was inhibited by Fst in these cells indicates that the activin-Fst system may be present in the cornea. This correlates with the up-regulation of *Fst* in (Fig. 4.26), as well as the disturbance of keratocyte differentiation of (Flügel-Koch et al., 2002), our analyzed TG corneas. *In vivo*, in the rabbit cornea, Fst was shown to have an angiogenic effect. The angiogenic effect of Fst was increased sharply in combination with FGF-2 (Kozian et al., 1997). Thus, since Flügel-Koch et al. (2002) proposed that FGF-2 may be up-regulated by TGF-ß1 overexpression in the eyes of our analyzed TG mice, and since these mice show neovascularisation, the up-regulation of *Fst* in these mice could act in concert with FGF to induce the observed neovascularisation.

The activin-Fst system is important in regulation of fibrosis during wound healing, and an overexpression of activin reduced scar formation in mice in a concentration dependent

manner (Bamberger et al., 2005). An Fst-mediated inhibition of activin could thus be responsible for the fibrotic phenotype observed in our analyzed TG corneas. TGF-ß1 activates activin in embryonic mesoderm and endothelial cultures (van der Kruijssen et al., 1993), and activin is known to induce, via Smad2/3 signalling, the expression of *Fst* both at mRNA and protein levels in liver cell cultures, suggesting a negative feedback of Fst on activin signalling (Bartholin et al., 2002). Thus, TGF-ß1 may have induced the expression of activin in the eyes of our TG mice, which then could have activated *Fst* via Smad2/3. Or, since Fst can be activated via Smad2/3, as shown by Bartholin et al. (2002), and since TGF-ß1 also signals via these proteins, TGF-ß1 could have directly activated *Fst*.

BMP4, which can be inhibited by Fst during frog mesodermal development (Fainsod et al., 1997), is expressed at the protein level in all cell types of fresh frozen human cornea. In addition, mRNA for BMP receptors were found to be expressed in cultured human corneal cells, and further analysis showed that BMP4 regulated keratocyte proliferation and apoptosis (Mohan et al., 1998). Thus, the significant up-regulation of *Fst* in our analyzed TG corneas may have had an impact on BMP4-mediated signalling, resulting in observed stromal cell proliferation and/or lens epithelial apoptosis, and/or in apoptosis of peripheral corneal epithelium (Flügel-Koch et al., 2002). Keratoconus corneas are thinner than normal, probably due to apoptosis of keratocytes (Wilson et al., 1996). Interestingly, *BMP4* was shown to be up-regulated in human keratoconus fibroblasts, suggesting that this protein mediates keratocyte apoptosis during keratoconous (Lee et al., 2009). Thus, the up-regulation of *Fst*, and possible subsequent inhibition of Bmp4, in our analyzed TG corneas could have led to the observed excess proliferation of corneal stromal cells, causing the three-fold than normal thick cornea (Flügel-Koch et al., 2002). Moreover, deletions of *BMP4* resulted in congenital corneal opacity in a human patient (Hayashi et al., 2008) and haploinsufficient *Bmp4*-null mice showed corneal defects including neovascularisation, irregular collagen bundle architechture of the stromal ECM, scarring, scleralization and opacity (Chang et al., 2001). Most of these corneal phenotypes were also observed in our analyzed TG mice (Flügel-Koch et al., 2002), suggesting that overexpression of TGF-ß1 may have resulted in defect Bmp4 signalling, possibly via the up-regulation of *Fst*.

Igfb6, significantly down-regulated in our real-time PCR experiments (Fig. 4.26), codes for an extracellular protein which preferentially binds the insulin-like growth factor II (IGF-II), over IGF-I, with high affinity, (Kiefer et al., 1992), thus inhibiting IGF-II mediated downstream signalling normally involved in cell survival, cell metabolism and cell proliferation (Alberts et al., 2004). There is also some evidence that IGFBP6 may have IGF-independent activity in cell growth or apoptosis, or as an intracrine effector modulating transcriptional activity after nuclear entry (reviewed by Bach, 2005), and Fu et al. (2007) showed that IGFBP6 was independently able to induce migration of colon cancer cells via phosphorylation and activation of the p38 MAPK. It is possible that the down-regulation of *Igfbp6* in our experiments could have elevated IGF-II mediated signalling, resulting in e.g. the observed excess proliferation of TG corneal stromal cells or, if acting in an IGF independent way, resulting in modulation of e.g. transcriptional regulation or migration. The fact that other proteins that also modulate IGF signalling, i.e. IGFBP3 and IGFBP5, have been shown to be significantly differentially regulated in keratoconus keratocytes (Ha et al., 2004), suggests that proper regulation of IGF signalling, possibly also by Igfbp6, may be important for the regulation of stromal thickness. The fact that IGF-II is present in bovine corneal stroma, where it activates keratocytes to proliferate *in vitro* and counteracts TGF-ß-induced gene expression changes that affect corneal transparency (Musselmann et al., 2008), further indicates that proper regulation of IGF-II signalling is important in regulating stromal development and differentiation. IGF signalling has been shown to stimulate the expression of collagens in cultured keratocytes (Lelbach et al., 2005; Hassell et al., 2008) and neonatal mouse keratocytes were shown to express high amounts of IGF-I/II and collagens (Kane et al., 2009). Thus, the possible elevated IGF signalling, due to down-regulation of *Igfbp6*, in our analyzed TG corneas may have influenced development of the abnormal ECM structure observed in these mice (Flügel-Koch et al., 2002). The fact that TGF-ß1 down-regulated *Igfbp6* in our analyzed TG corneas correlates with earlier data that showed that TGF-ß1 is able to down-regulate the expression of *IGFBP6* in fibroblast cultures (Nik et al., 2007) and in rat osteoblasts (Gabbitas and Canalis, 1997).

Dkk2, which was highly significant down-regulated in our real-time experiments (Fig. 4.26), codes for a secreted glycoprotein that belongs to an evolutionary conserved ancient protein family, originally discovered to being responsive for head induction in *Xenopus* by antagonizing Wnt signalling (Glinka et al., 1998). Dkk proteins are expressed throughout

development in a tissue- and stage-specific manner in tissues where epithelial-mesenchymal interactions occur (Monaghan et al., 1999), and where they modulate Wnt-signalling mediated developmental processes like cell fate, polarity and proliferation. Dkk2 binds to the frizzled co-receptor LDL-receptor related protein 6 (LPR6) with high affinity and, depending on cell context, the binding either promote or inhibit downstream canonical Wnt signalling. If the transmembrane receptor protein Kremen 2 also binds LRP6, the effect of Dkk on Wnt signalling will be negative (Mao et al., 2002). *Dkk2* mRNA showed a strong expression in the developing murine cornea at E11.5 (Monaghan et al., 1999), whereas *DKK2* was not found to be expressed in the mature human cornea (Turner et al., 2007), indicating that this gene is important for corneal development. As a modulator of Wnt-signalling through ß-catenin, Dkk2 may alter NC induction and cell differentiation, as well as NC cell migration, since ß-catenin, in addition to translocating to the nucleus affecting gene expression, also can affect cytoskeletal architecture, cell shape and cell adhesion via binding to α-catenin and E-cadherin (reviewed by Jamora and Fuchs, 2002). In fact, Dkk2 down-regulates Wnt signalling in the NC-derived stroma and overlying surface ectoderm-derived corneal epithelium in the mouse. RA-signals originating from the retina activate *Pitx2* in the developing stroma (Kumar and Duester, 2010). Here, Pitx2 activates Dkk2 which, via down-regulation of Wnt- signalling, can down-regulate *Pitx2*. Thus, Dkk2 is an integration-node between RA- and Wnt signalling in the developing ocular mesenchyme. The down-regulation of *Dkk2* in our TG corneas could thus have led to an excess Wnt signalling, which could have led to the observed defects in corneal stromal architecture, including the abnormal shape of the cells and the irregular ECM, as well as to observed excessive proliferation and/or migration of NC-derived stromal mesenchyme cells (Flügel-Koch et al., 2002).

The crucial role of Dkk2 in the developing cornea could be observed in *Dkk2*-deficient mice, which showed a phenotype with hypomorphic eyes, ectopic eyelashes, abnormally thick corneal epithelium, irregular stromal ECM, immature stellate-shaped keratocytes, ectopic corneal stromal blood vessels, conjunctivalization of the corneal ectoderm, as well as epidermal characteristics of the conjunctiva/limbus. In another study *Dkk2*$^{-/-}$ mice showed a phenotype where the cornea was opaque and where the corneal epithelium and conjunctiva showed characteristics of epidermis, including expression of epidermal-specific differentiation markers, hair growth, sebaceous glands and pigment granules. In both of these studies, the absence of Dkk2 led to an up-regulation of Wnt-signalling in ocular mesenchyme

(Gage et al., 2008; Mukhopadhyay et al., 2006). Many of the above mentioned corneal defects resemble the defects seen in our analyzed TG corneas, including hypomorphic eyes, opacity, irregular stromal ECM, immature stellate-shaped keratocytes and ectopic blood vessels (Flügel-Koch et al., 2002). Additionally, our microarray data showed that there was an up-regulation of many epidermal-specific keratins in our analyzed TG corneas (discussed in Chapter 4.5.2). Down-regulation of *Dkk2* in our analyzed TG corneas could thus be, via an up-regulation of Wnt-signalling, responsible for some of the observed corneal defects. Gage et al. (2008) suppose that NC-derived stromal RA and Pitx2 activated Dkk2 is needed to fine-tune Wnt signalling in the stroma, as well as in the overlying epithelium. Wnt signalling is known to be high in conjunctival epithelium, whereas it is down-regulated in the developing corneal ectoderm (Liu et al., 2003). Thus, Wnt signalling could be important in the determination of corneal vs. conjunctival fate of ocular ectoderm. Since our analyzed TG corneas were opaque, and since *Dkk2* in these corneas was highly significant down-regulated, Wnt signalling could be a factor that is involved in the development of corneal opacity in these mice.

6. Conclusion

Since the normal and pathologic function of myocilin is unknown, we aimed to characterize *MYOC*, and thus to learn more about the way the gene is regulated, a topic of clinical interest, since myocilin expression has been found to be elevated in glaucoma patients (Lütjen-Drecoll et al., 1998; Konz et al., 2009). In addition, characterization of *MYOC* may give insight into the molecular networks that are linked to myocilin, thus enhancing the understanding of its function. The fact that we found elements within near nc regions of *MYOC* that enhanced gene expression over the level of the known *MYOC* basal promoter (Kirstein et al., 2000), indicates that *MYOC* may be subject of extensive pre-mRNA processing. Since these elements yet did not elevate gene expression level more than up to 3.7-fold over basal transcription level, there may be more important regions residing far beyond those analyzed. Future biochemical studies will be required to learn more about the mechanisms that are involved in pre-mRNA processing of *MYOC* and to find out what functional role and consequence an eventual processing of *MYOC* mRNA has on the molecular networks active in TM.

Our aim to create a TM-specific enhancer element for targeted protein expression in this tissue, an aim that also is of clinical relevance in the attempt to treat POAG, gave unexpected novel information about the possible functions of myocilin in the brain. Unexpected and novel *in vivo* expression in the ependymal lining of the ventricular system, CP and CSF suggest that myocilin may have a function in the drainage of CSF, possibly in the way it acts in the CB and TM. Unexpected and novel myocilin expression within nerve cells of the CNS, suggesting a supporting, maintaining and/or modulating role, accentuates the known role of myocilin as a matricellular protein. Future molecular biological and histological studies aim to learn more about the function and possible clinically relevant role of myocilin within the CNS.

Our project that aimed to create a mouse line that would able conditional knock-out of genes within the TM, which would help to resolve the molecular networks that are active in maintaining normal TM homeostasis and architecture, and thus a normal AH outflow

resistance, is still going on and intend to elongate the homologous flanks required for homologous recombination. Future projects aim to analyze the usefulness of the *Myoc* knock-in mouse in its ability to conditionally knock out genes in the TM.

Our aim to find genes that are differentially regulated upon TGF-ß1 overexpression in the mouse cornea intended to get an insight into the molecular networks that are active in corneal scar formation, and thus to find possible candidate genes that are responsible for corneal transparency, a clinically relevant area of interest, since corneal scar formation affects vision. Our analysis revealed that excess TGF-ß1 affects corneal development and integrity by affecting both extra- and intracellular molecular mechanism. Differential expression of genes coding for proteases, junction- and channel-forming proteins, cytoskeletal proteins, enzymes and transporters was observed in TG corneas. Additionally, several genes coding for proteins that affect elemental signalling pathways important in growth and differentiation were differentially regulated. Our findings might be of value for designing further future experiments that intend to resolve the molecular mechanisms that are active in scar formation, as well as intend to learn more about the molecular basis that maintain corneal transparency.

7. Summary

The main focus of the thesis was set on approaches that aim to clarify molecular mechanisms that are responsible for an elevated aqueous humour (AH) outflow resistance in the trabecular meshwork (TM), leading to an elevated intraocular pressure (IOP) and primary open-angle glaucoma (POAG), an optic neuropathy that if uncured leads to blindness. Myocilin is, when mutated, responsible for autosomal dominant forms of POAG, which account for about 3 % of all cases. In addition, there is evidence that patients with other forms of POAG may express higher than normal amounts of TM myocilin. The normal and pathological function of how myocilin affects AH outflow resistance is unknown. By characterizing the human myocilin gene (*MYOC*) by reporter gene analysis, we wanted to get knowledge about how myocilin expression is regulated, and thus which elements within *MYOC* are responsible for its higher than normal expression in POAG cases. Our results indicate that intronic, as well as non-coding (nc) 3´-downstream regions, are important for effective expression of myocilin, probably by being important during pre-mRNA processing.

In a second animal model approach, we aimed to generate an artificial enhancer element for *in vivo* TM-directed protein expression. For this approach, we combined the *MYOC* basal promoter, since myocilin is abundantly and primarily expressed in the TM in human, with a tested artificial enhancer element that had been shown to drive effective reporter gene expression in TM cells *in vitro*. Unexpected activity of this combination in the tissues that regulate secretion and drainage of cerebrospinal fluid (CSF) in a mouse model, as well as expression of myocilin in these tissues and in CSF in rat and human, respectively, opened totally new insights about the function of myocilin, and confirmed that myocilin may have a function in regulating CSF secretion and drainage in the central nervous system (CNS) in mammals, much like it is involved in the drainage of AH in anterior eye in human. Expression of myocilin in nerve cells of rat CNS further confirmed earlier data about a neuronal function of myocilin.

The third approach concerning POAG aimed to create a mouse model that would allow for conditional knock-out of genes in the TM by the Cre/*loxP* system, and which thus would offer immense possibilities in analyzing the effect that candidate POAG-causing genes has on AH

drainage resistance through the TM. For this purpose we successfully cloned a knock-in construct that would enable Cre recombinase to be expressed under the control of the endogenous myocilin promoter after homologous recombination at the *Myoc* locus in mouse embryonic stem cells (ESCs), and which thus would offer the possibility to generate a mouse-line that would express Cre recombinase highly in the TM.

Another focus was set on clarifying molecular mechanisms that are active during corneal wound healing, a process that may lead to loss of transparency of this tissue and thus impairment of vision. As a model for our analysis we used a mouse model that, due to an overexpression of the key wound healing processes regulator transforming growth factor (TGF)-ß1 in the lens, shows a phenotype that resembles corneal fibrosis, including corneal opacity. Microarray and real-time PCR data of transgenic (TG) corneas confirmed that TGF-ß1 induces differential regulation of several genes that code for proteins that regulate extra- and intracellular homeostasis and integrity, as well as code for proteins that modulate signalling cascades that are pivotal in growth and differentiation. The identified genes may be candidate genes that are important in maintaining corneal transparency. Our data serve as a basis on which further experiments concerning corneal scar formation and corneal transparency can be designed.

8. References:

Acott T.S.: Biochemistry of aqueous humor outflow. *Glaucoma* 7:1.47-1.78. Mosby London, 1991.

Acott T.S., Kelley M.J.: Extracellular matrix in the trabecular meshwork. *Exp. Eye Res.* 86(4):543-61. Review, 2008.

Adam M.F., Belmouden A., Binisti P., Brézin A.P., Valtot F., Béchetoille A., Dascotte J.C., Copin B., Gomez L., Chaventré A., Bach J.F., Garchon H.J.: Recurrent mutations in a single exon encoding the evolutionarily conserved olfactomedin-homology domain of TIGR in familial open-angle glaucoma. *Hum. Mol. Genet.* 6(12):2091-7, 1997.

Adatia F.A., Damji K.F.: Chronic open-angle glaucoma. Review for primary care physicians. *Can. Fam. Physician* 51:1229-37. Review, 2005.

Ahmed F., Torrado M., Johnson E., Morrison J., Tomarev S.I.: Changes in mRNA levels of the Myoc/Tigr gene in the rat eye after experimental elevation of intraocular pressure or optic nerve transection. *Invest. Ophthalmol. Vis. Sci.* 42(13):3165-72, 2001.

Alberts B., Johnson A., Lewis J., Raff M., Roberts K., Walter P., Jaenicke L.: *Molekularbiologie der Zelle* 4. Auflage, Kapitel 5.5: Allgemeine Rekombination; 15.3: Signalisierung über Enzym gekoppelte Zelloberflächen-Rezeptoren; 19.1: Zell/Zell-Verbindung; 19.3: Die extracelluläre Matrix von Tieren; en; 21.1: Allgemeine Mechanismen tierischer Entwicklung. WILEY-VCH Verlag GmbH & Co. KgaA, Weinheim, 2004.

Alfano G., Vitiello C., Caccioppoli C., Caramico T., Carola A., Szego M.J., McInnes R.R., Auricchio A., Banfi S.: Natural antisense transcripts associated with genes involved in eye development. *Hum. Mol. Genet.* 14(7):913-23, 2005.

Alward W.L., Fingert J.H., Coote M.A., Johnson A.T., Lerner S.F., Junqua D., Durcan F.J., McCartney P.J., Mackey D.A., Sheffield V.C., Stone E.M.: Clinical features associated with mutations in the chromosome 1 open-angle glaucoma gene (GLC1A). *N. Engl. J. Med.* 338(15):1022-7, 1998.

Alward W.L., Kwon Y.H., Khanna C.L., Johnson A.T., Hayreh S.S., Zimmerman M.B., Narkiewicz J., Andorf J.L., Moore P.A., Fingert J.H., Sheffield V.C., Stone E.M.: Variations in the myocilin gene in patients with open-angle glaucoma. *Arch. Ophthalmol.* 120(9):1189-97, 2002.

Amaral P.P., Mattick J.S.: Noncoding RNA in development. *Mamm. Genome* 19(7-8):454-92, 2008.

Ambros V.: A hierarchy of regulatory genes controls a larva-to-adult developmental switch in *C. elegans*. *Cell* 57(1):49-57, 1989.

Amini Nik S., Ebrahim R.P., Van Dam K., Cassiman J.J., Tejpar S.: TGF-beta modulates beta-Catenin stability and signaling in mesenchymal proliferations. *Exp. Cell Res.* 313(13):2887-95, 2007 .

Amthor H., Nicholas G., McKinnell I., Kemp C.F., Sharma M., Kambadur R., Patel K.: Follistatin complexes Myostatin and antagonises Myostatin-mediated inhibition of myogenesis. *Dev. Biol.* 270(1):19-30, 2004.

Anand A., Negi S., Khokhar S., Kumar H., Gupta S.K., Murthy G.V., Sharma T.K.: Role of early trabeculectomy in primary open-angle glaucoma in the developing world. *Eye* (Lond). 21(1):40-5, 2007.

Ancans J., Hoogduijn M.J., Thody A.J.: Melanosomal pH, pink locus protein and their roles in melanogenesis. *J. Invest. Dermatol.* 117(1):158-9, 2001.

Armaly M.F.: Effect of corticosteroids on intraocular pressure and fluid dynamics. II. The effect of dexamethasone in the glaucomatous eye. *Arch. Ophthalmol.* 70:492-9, 1963.

Armaly M.F.: Inheritance of dexamethasone hypertension and glaucoma. *Arch. Ophthalmol.* 77(6):747-51, 1967.

Armaly M.F.: Statistical attributes of the steroid hypertensive response in the clinically normal eye. I. The demonstration of three levels of response. *Invest. Ophthalmol.* 4:187-97, 1965.

Armstrong R.A., Smith S.N.: The genetics of glaucoma. *Optometry Today* Nov. 16, 2001.

Aroca-Aguilar J.D., Sánchez-Sánchez F., Ghosh S., Coca-Prados M., Escribano J.: Myocilin mutations causing glaucoma inhibit the intracellular endoproteolytic cleavage of myocilin between amino acids Arg226 and Ile227. *J. Biol. Chem.* 280(22):21043-51, 2005.

Aruga J., Yoshikawa F., Nozaki Y., Sakaki Y., Toyoda A., Furuichi T.: An oligodendrocyte enhancer in a phylogenetically conserved intron region of the mammalian myelin gene Opalin. *J. Neurochem.* 102(5):1533-47, 2007.

Avidor-Reiss T., Maer A.M., Koundakjian E., Polyanovsky A., Keil T., Subramaniam S., Zuker C.S.: Decoding cilia function: defining specialized genes required for compartmentalized cilia biogenesis. *Cell* 117:527–539, 2004.

Bach L.A.: IGFBP-6 five years on; not so 'forgotten'? *Growth Horm IGF Res.* 15(3):185-92. Review, 2005.

Bachman W.G., Wilson G.: Essential ions for maintenance of the corneal epithelial surface. *Invest. Ophthalmol. Vis. Sci.* 26(11):1484-8, 1985.

Bahler C.K., Howell K.G., Hann C.R., Fautsch M.P., Johnson D.H.: Prostaglandins increase trabecular meshwork outflow facility in cultured human anterior segments. *Am. J. Ophthalmol.* 145(1):114-9, 2008.

Bale S.J., White T.W., Munro C., Taylor A.E.M., Richard G.: Functional defects of Cx26 due to mutations in two families with dominant palmoplantar keratoderma and deafness. *J. Invest. Dermatol.* 112:A550, 1999.

Balkan W., Colbert M., Bock C., Linney E.: Transgenic indicator mice for studying activated retinoic acid receptors during development. *Proc. Natl. Acad. Sci. U S A* 89(8):3347-51, 1992.

Bamberger C., Schärer A., Antsiferova M., Tychsen B., Pankow S., Müller M., Rülicke T., Paus R., Werner S.: Activin controls skin morphogenesis and wound repair predominantly via stromal cells and in a concentration-dependent manner via keratinocytes. *Am. J. Pathol.* 167(3):733-47, 2005.

Banks W.A., Niehoff M.L., Adessi C., Soto C.: Passage of murine scrapie prion protein across the mouse vascular blood–brain barrier. *Biochem. Biophys. Res. Commun.* 318:125–1, 2004.

Bartholin L., Maguer-Satta V., Hayette S., Martel S., Gadoux M., Corbo L., Magaud J.P., Rimokh R.: Transcription activation of FLRG and follistatin by activin A, through Smad proteins, participates in a negative feedback loop to modulate activin A function. *Oncogene* 21(14):2227-35, 2002.

Baulmann D.C., Ohlmann A., Flügel-Koch C., Goswami S., Cvekl A., Tamm E.R.: Pax6 heterozygous eyes show defects in chamber angle differentiation that are associated with a wide spectrum of other anterior eye segment abnormalities. *Mech. Dev.* 118(1-2):3-17, 2002.

Becker B.: Intraocular pressure response to topical corticosteroids. *Invest. Ophthalmol.* 4:198-205, 1965.

Becker B., Kolker A.E., Roth F.D.: Glaucoma family study. *Am. J. Ophthalmol.* 50:557-67, 1960.

Beltran M., Puig I., Peña C., García J.M., Alvarez A.B., Peña R., Bonilla F., de Herreros A.G.: A natural antisense transcript regulates Zeb2/Sip1 gene expression during Snail1-induced epithelial-mesenchymal transition. *Genes Dev.* 22(6):756-69, 2008.

Benedek G.B.: Theory of transparency of the eye. *Applied Optics* 10(3):459-473, 1971.

Berger P., Niemann A., Suter U.: Schwann cells and the pathogenesis of inherited motor and sensory neuropathies (Charcot-Marie-Tooth disease). *Glia* 54(4):243-57. Review, 2006.

Bernardi D., Podswiadek M., Zaninotto M., Punzi L., Plebani M.: YKL-40 as a marker of joint involvement in inflammatory bowel disease. *Clin. Chem.* 49(10):1685-8, 2003.

Bernstein P., Ross J.: Poly(A), poly(A) binding protein and the regulation of mRNA stability. *Trends Biochem. Sci.* 14(9):373-7. Review, 1989.

Berryhill B.L., Beales M.P., Hassell J.R.: Production of prostaglandin D synthase as a keratan sulfate proteoglycan by cultured bovine keratocytes. *Invest. Ophthalmol. Vis. Sci.* 42(6):1201-7, 2001.

Beysen D., Raes J., Leroy B.P., Lucassen A., Yates J.R., Clayton-Smith J., Ilyina H., Brooks S.S., Christin-Maitre S., Fellous M., Fryns J.P., Kim J.R., Lapunzina P., Lemyre E., Meire F., Messiaen L.M., Oley C., Splitt M., Thomson J., Van de Peer Y., Veitia R.A., De Paepe A., De Baere E.: Deletions involving long-range conserved nongenic sequences upstream and downstream of FOXL2 as a novel disease-causing mechanism in blepharophimosis syndrome. *Am. J. Hum. Genet.* 77(2):205-18, 2005.

Bidinost C., Matsumoto M., Chung D., Salem N., Zhang K., Stockton D.W., Khoury A., Megarbane A., Bejjani B.A., Traboulsi E.I.: Heterozygous and homozygous mutations in PITX3 in a large Lebanese family with posterior polar cataracts and neurodevelopmental abnormalities. *Invest. Ophthalmol. Vis. Sci.* 47(4):1274-80, 2006.

Bob A., Bob K.: *Anatomie*: Kapitel 1.3: Hüllen des ZNS (Meningen) und Liquorsystem. Georg Thieme Verlag, 2007.

Bornstein P.: Matricellular proteins: an overview. *Matrix Biology* 19(7):555-556, 2000.

Bradbury E.J., Moon L.D., Popat R.J., King V.R., Bennett G.S., Patel P.N., Fawcett J.W., McMahon S.B.: Chondroitinase ABC promotes functional recovery after spinal cord injury. *Nature* 416, 636–640, 2002.

Bres V., Gomes N., Pickle L., Jones K.A.: A human splicing factor, SKIP, associates with P-TEFb and enhances transcription elongation by HIV-1 Tat. *Genes Dev.* 19:1211–1226, 2005.

Brooks D.E.: Glaucoma in the dog and cat. *Vet. Clin. North Am. Small Anim. Pract.* 20(3):775-97, 1990.

Byström B., Virtanen I., Rousselle P., Miyazaki K., Lindén C., Pedrosa Domellöf F.: Laminins in normal, keratoconus, bullous keratopathy and scarred human corneas. *Histochem. Cell Biol.* 127(6):657-67, 2007.

Caballero M., Rowlette L.L., Borrás T.: Altered secretion of a TIGR/MYOC mutant lacking the olfactomedin domain. *Biochim. Biophys. Acta* 1502(3):447-60, 2000.

Chalasani M.L., Balasubramanian D., Swarup G.: Focus on molecules: optineurin. *Exp. Eye Res.* 87(1):1-2, 2008.

Chalfie M., Horvitz H.R., Sulston J.E.: Mutations that lead to reiterations in the cell lineages of *C. elegans*. *Cell* 24(1):59-69, 1981

Challa P.: Glaucoma genetics. *Int. Ophthalmol. Clin.* 48(4):73-94. Review, 2008.

Chandler R.L., Chandler K.J., McFarland K.A., Mortlock D.P.: Bmp2 transcription in osteoblast progenitors is regulated by a distant 3' enhancer located 156.3 kilobases from the promoter. *Mol. Cell. Biol.* 27(8):2934-51, 2007.

Chaney B.A., Clark-Baldwin K., Dave V., Ma J., Rance M.: Solution structure of the K50 class homeodomain PITX2 bound to DNA and implications for mutations that cause Rieger syndrome. *Biochemistry* 44(20):7497-511, 2005.

Chang B., Smith R.S., Peters M., Savinova O.V, Hawes N.L., Zabaleta A., Nusinowitz S., Martin J.E., Davisson M.L., Cepko C.L., Hogan B.L., John S.W.: Haploinsufficient Bmp4 ocular phenotypes include anterior segment dysgenesis with elevated intraocular pressure. *BMC Genet.* 2:18, 2001.

Chavrier P., Zerial M., Lemaire P., Almendral J., Bravo R., Charnay P.: A gene encoding a protein with zinc fingers is activated during G0/G1 transition in cultured cells. *EMBO J.* 7(1):29–35, 1988.

Cheli Y., Ohanna M., Ballotti R., Bertolotto C.: Fifteen-year quest for microphthalmia-associated transcription factor target genes. *Pigment Cell Melanoma Res.* 23(1):27-40, 2010.

Chen K., Manga P., Orlow S.J.: Pink-eyed dilution protein controls the processing of tyrosinase. *Mol. Biol. Cell* 13(6):1953-64, 2002.

Choi S.H., Leight S.N., Lee V.M., Li T., Wong P.C., Johnson J.A., Saraiva M.J., Sisodia S.S.: Accelerated Abeta deposition in APPswe/PS1deltaE9 mice with hemizygous deletions of TTR (transthyretin). *J. Neurosci.* 27(26):7006-10, 2007.

Chojnacki A.K., Mak G.K., Weiss S.: Identity crisis for adult periventricular neural stem cells: subventricular zone astrocytes, ependymal cells or both? *Nat. Rev. Neurosci.* 10(2):153-63, 2009.

Cirillo L.A., Barton M.C.: Many forkheads in the road to regulation. Symposium on forkhead transcription factor networks in development, signalling and disease. *EMBO Rep.* 9(8):721-4, 2008.

Civan M.: *The eye´s aqueous humour*, ed. 2, Chapter 1: Formation of the aqueous humour: Transport components and their integration, Elsevier Inc. 2008.

Clark A.F., Steely H.T., Dickerson J.E. Jr., English-Wright S., Stropki K., McCartney M.D., Jacobson N., Shepard A.R., Clark J.I., Matsushima H., Peskind E.R., Leverenz J.B., Wilkinson C.W., Swiderski R.E., Fingert J.H., Sheffield V.C., Stone E.M.: Glucocorticoid induction of the glaucoma gene MYOC in human and monkey trabecular meshwork cells and tissues. *Invest. Ophthalmol. Vis. Sci.* 42(8):1769-80, 2001.

Clark A.F., Wilson K., McCartney M.D., Miggans S.T., Kunkle M., Howe W.: Glucocorticoid-induced formation of cross-linked actin networks in cultured human trabecular meshwork cells. *Invest. Ophthalmol. Vis. Sci.* 35(1):281-94, 1994.

Coakes R.: Laser trabeculoplasty. *Br. J. Ophthalmol.* 76(10):624-6. Review, 1992.

Coca-Prados M., Escribano J.: New perspectives in aqueous humor secretion and in glaucoma: the ciliary body as a multifunctional neuroendocrine gland. *Prog. Retin. Eye Res.* 26(3):239-62. Review, 2007.

Collinson J.M., Quinn J.C., Hill R.E., West JD.: The roles of Pax6 in the cornea, retina, and olfactory epithelium of the developing mouse embryo. *Dev. Biol.* 255(2):303-12, 2003.

Conrad A.H., Albrecht M., Pettit-Scott M., Conrad G.W.: Embryonic corneal Schwann cells express some Schwann cell marker mRNAs, but no mature Schwann cell marker proteins. *Invest. Ophthalmol. Vis. Sci.* 50(9):4173-84, 2009.

Corre S., Galibert M.D.: Upstream stimulating factors: highly versatile stress-responsive transcription factors. *Pigment Cell Res.* 18(5):337-48. Review, 2005.

Costagliola C., dell'Omo R., Romano M.R., Rinaldi M., Zeppa L., Parmeggiani F.: Pharmacotherapy of intraocular pressure: part I. Parasympathomimetic, sympathomimetic and sympatholytics. *Expert. Opin Pharmacother.* 10(16):2663-7, 2009.

Coulombe P.A., Hutton M.E., Letai A., Hebert A., Paller A.S., Fuchs E.: Point mutations in human keratin 14 genes of epidermolysis bullosa simplex patients: genetic and functional analyses. *Cell* 66(6):1301-11, 1991.

Coulombre A.J., Coulombre J.L.: Corneal development, I: corneal transparency. *J. Cell. Comp. Physiol.* 51:1–11, 1958.

Curtis M.A., Faull R.L., Eriksson P.S. : The effect of neurodegenerative diseases on the subventricular zone. *Nat. Rev. Neurosci.* 8(9):712-23. Review, 2007.

Cvekl A., Tamm E.R.: Anterior eye development and ocular mesenchyme: new insights from mouse models and human diseases. *Bioessays* 26(4):374-86. Review, 2004.

Das R., Yu J., Zhang Z., Gygi M.P., Krainer A.R., Gygi S.P., Reed R.: SR proteins function in coupling RNAP II transcription to pre-mRNA splicing. *Mol. Cell* 26:867–881, 2007.

Davis E.E., Brueckner M., Katsanis N.: The emerging complexity of the vertebrate cilium: new functional roles for an ancient organelle. *Dev. Cell* 11:9–19, 2006.

DePianto D., Coulombe P.A.: Intermediate filaments and tissue repair. *Exp. Cell Res*. 301(1):68-76. Review, 2004.

de Thé H., Vivanco-Ruiz M.M., Tiollais P., Stunnenberg H., Dejean A.: Identification of a retinoic acid responsive element in the retinoic acid receptor beta gene. *Nature* 343(6254): 177-80, 1990.

Dickerson J.E. Jr., Steely H.T. Jr., English-Wright S.L., Clark A.F.: The effect of dexamethasone on integrin and laminin expression in cultured human trabecular meshwork cells. *Exp. Eye Res.* 66(6):731-8, 1998.

Dimasi D.P., Burdon K.P., Craig J.E.: The genetics of central corneal thickness. *Br. J. Ophthalmol.* Jun 24 [Epub ahead of print], 2009.

Diskin S., Kumar J., Cao Z., Schuman J.S., Gilmartin T., Head S.R., Panjwani N.: Detection of differentially expressed glycogenes in trabecular meshwork of eyes with primary open-angle glaucoma. *Invest. Ophthalmol. Vis. Sci.* 47(4):1491-9, 2006.

Doward W., Perveen R., Lloyd I.C., Ridgway A.E., Wilson L., Black G.C.: A mutation in the RIEG1 gene associated with Peters' anomaly. *J. Med. Genet.* 36:152–155, 1999.

Duncan L.M., Deeds J., Cronin F.E., Donovan M., Sober A.J., Kauffman M., McCarthy J.J.: Melastatin expression and prognosis in cutaneous malignant melanoma. *J. Clin. Oncol.* 19(2):568-76, 2001.

Duncan L.M., Deeds J., Hunter J., Shao J., Holmgren L.M., Woolf E.A., Tepper R.I., Shyjan A.W.: Down-regulation of the novel gene melastatin correlates with potential for melanoma metastasis. *Cancer Res.* 58(7):1515-20, 1998.

Dursun D., Kim M.C., Solomon A., Pflugfelder S.C.: Treatment of recalcitrant recurrent corneal erosions with inhibitors of matrix metalloproteinase-9, doxycycline and corticosteroids. *Am. J. Ophthalmol.* 132:8–13, 2001.

Dye M.J., Proudfoot N.J.: Multiple transcript cleavage precedes polymerase release in termination by RNA polymerase II. *Cell* 105(5):669-81, 2001.

Eley L., Yates L.M., Goodship J.A.: Cilia and disease. *Curr. Opin. Genet. Dev.* 15(3):308-14, 2005.

Ennis S.R., Keep R.F.: The effects of cerebral ischemia on the rat choroid plexus. *J. Cereb. Blood Flow Metab.* 26:675–683, 2006.

Enwright J.F. 3rd, Grainger R.M.: Altered retinoid signaling in the heads of small eye mouse embryos. *Dev. Biol.* 221(1):10-22, 2000.

Eroglu C.: The role of astrocyte-secreted matricellular proteins in central nervous system development and function. *J. Cell. Commun. Signal.* Nov 11, 2009 [Epub ahead of print].

Ethier C.R.: The inner wall of Schlemm's canal. *Exp. Eye Res.* 74(2):161-72, 2002.

Ezzat M.K., Howell K.G., Bahler C.K., Beito T.G., Loewen N., Poeschla E.M., Fautsch M.P.: Characterization of monoclonal antibodies against the glaucoma-associated protein myocilin. *Exp. Eye Res.* 87(4):376-84, 2008.

Fainsod A., Deissler K., Yelin R., Marom K., Epstein M., Pillemer G., Steinbeisser H., Blum M.: The dorsalizing and neural inducing gene follistatin is an antagonist of BMP-4. *Mech. Dev.* 63(1):39-50, 1997.

Fares F.: The role of O-linked and N-linked oligosaccharides on the structure-function of glycoprotein hormones: development of agonists and antagonists. *Biochim. Biophys. Acta.* 1760(4):560-7. Review, 2006.

Farrell R.E. Jr.: *RNA methodologies*: A laboratory guide for isolation and characterization. Chapter 8: Electrophoresis of RNA. Academic Press, Inc., 1993.

Fautsch M.P., Bahler C.K., Jewison D.J., Johnson D.H.: Recombinant TIGR/MYOC increases outflow resistance in the human anterior segment. *Invest. Ophthalmol. Vis. Sci.* 41(13):4163-8, 2000.

Fautsch M.P., Bahler C.K., Vrabel A.M., Howell K.G., Loewen N., Teo W.L., Poeschla E.M., Johnson D.H.: Perfusion of His-tagged eukaryotic myocilin increases outflow resistance in human anterior segments in the presence of aqueous humor. *Invest. Ophthalmol. Vis. Sci.* 47(1):213-21, 2006.

Fautsch M.P., Johnson D.H.: Characterization of myocilin-myocilin interactions. *Invest. Ophthalmol. Vis. Sci.* 42:2324-31, 2001.

Fautsch M.P., Vrabel A.M., Johnson D.H.: Characterization of the Felix domesticus (cat) glaucoma-associated protein myocilin. *Exp. Eye Res.* 82:1037–1045, 2006.

Fautsch M.P., Vrabel A.M., Johnson D.H.: The identification of myocilin-associated proteins in the human trabecular meshwork. *Exp. Eye Res.* 82(6):1046-52, 2006.

Fautsch M.P., Vrabel A.M., Peterson S.L., Johnson D.H.: In vitro and in vivo characterization of disulfide bond use in myocilin complex formation. *Mol. Vis.* 10:417–425, 2004.

Felgner P.L., Gadek T.R., Holm M., Roman R., Chan H.W., Wenz M., Northrop J.P., Ringold G.M., Danielsen M.: Lipofection: a highly efficient, lipid-mediated DNA-transfection procedure. *Proc. Natl. Acad. Sci. U S A* 84:7413-7417, 1987.

Fingert J.H., Clark A.F., Craig J.E., Alward W.L., Snibson G.R., McLaughlin M., Tuttle L., Mackey D.A., Sheffield V.C., Stone EM.: Evaluation of the myocilin (MYOC) glaucoma gene in monkey and human steroid-induced ocular hypertension. *Invest. Ophthalmol. Vis. Sci.* 42(1):145-52, 2001.

Fingert J.H., Ying L., Swiderski R.E., Nystuen A.M., Arbour N.C., Alward W.L., Sheffield V.C., Stone E.M.: Characterization and comparison of the human and mouse GLC1A glaucoma genes. *Genome Res.* 8(4):377-84, 1998.

Fini M.E.: Keratocyte and fibroblast phenotypes in the repairing cornea. *Prog. Retin. Eye Res.* 18(4):529-51. Review, 1999.

Fini M.E., Cook J.R., Mohan R.: Proteolytic mechanisms in corneal ulceration and repair. *Arch. Dermatol. Res.* 290:S12–S23, 1998.

Fischbarg J., Lim J.J.: Role of cations, anions and carbonic anhydrase in fluid transport across rabbit corneal endothelium. *J. Physiol.* 241(3):647-75, 1974.

Fischer-Fantuzzi L., Vesco C.: Cell-dependent efficiency of reiterated nuclear signals in a mutant simian virus 40 oncoprotein targeted to the nucleus. *Mol. Cell. Biol.* 8(12):5495-503, 1988.

Fitch M.T., Silver J.: Beyond the glial scar: cellular and molecular mechanisms by which glial cells contribute to CNS regenerative failure. *CNS Regeneration: Basic Science and Clinical Advances*, Academic Press, New York, pp. 55–88, 1999.

Floege J., Johnson R.J., Gordon K., Iida H., Pritzl P., Yoshimura A., Campbell C., Alpers C.E., Couser W.G.: Increased synthesis of extracellular matrix in mesangial proliferative nephritis. *Kidney Int.* 40(3):477-88, 1991.

Flügel-Koch C., Ohlmann A., Fuchshofer R., Welge-Lüssen U., Tamm E.R.: Thrombospondin-1 in the trabecular meshwork: localization in normal and glaucomatous eyes, and induction by TGF-beta1 and dexamethasone in vitro. *Exp. Eye Res.* 79:649–663, 2004.

Flügel-Koch C., Ohlmann A., Piatigorsky J., Tamm E.R.: Disruption of anterior segment development by TGF-beta1 overexpression in the eyes of transgenic mice. *Dev. Dyn.* 225(2):111-25, 2002.

Frazer K.A., Pachter L., Poliakov A., Rubin E.M., Dubchak I.: VISTA: computational tools for comparative genomics. *Nucleic Acids Res*. 32(Web Server issue):W273-9., 2004.

Freije J.M.P., Díez-Itza I., Balbín M., Sánchez L.M., Blasco R., Tovilia J., and López-Otín C.: Molecular cloning and expression of collagenase-3, a novel human matrix metalloproteinase produced by breast carcinomas. *J. Biol. Chem.* 269: 16766–73, 1994.

Fu P., Thompson J.A., Bach L.A.: Promotion of cancer cell migration: an insulin-like growth factor (IGF)-independent action of IGF-binding protein-6. *J. Biol. Chem.* 282(31):22298-306, 2007.

Funk W.D., Ouellette M., Wright W.E.: Molecular biology of myogenic regulatory factors. *Mol. Biol. Med.* 8:185-195. Review, 1991.

Gabbitas B., Canalis E.: Growth factor regulation of insulin-like growth factor binding protein-6 expression in osteoblasts. *J. Cell. Biochem.* 66(1):77-86, 1997.

Gage P.J., Qian M., Wu D., Rosenberg K.I.: The canonical Wnt signaling antagonist DKK2 is an essential effector of PITX2 function during normal eye development. *Dev. Biol.* 317(1):310-24, 2008.

Gage P.J., Suh H., Camper S.A.: Dosage requirement of Pitx2 for development of multiple organs. *Development* 126:4643–4651, 1999.

Galor A., Leder H.A., Thorne J.E., Dunn J.P.: Transient band keratopathy associated with ocular inflammation and systemic hypercalcemia. *Clin. Ophthalmol.* 2(3):645-7, 2008.

Gilbert S.F: *Developmental Biology*, 8th Ed., Sinauer associates Inc., 2006.

Giménez E., Montoliu L.: A simple polymerase chain reaction assay for genotyping the retinal degeneration mutation ($Pdeb^{rd1}$) in FVB/N-derived transgenic mice. *Lab. Anim.* 35(2):153-6, 2001.

Girard J-P., Springer T.A.: Modulation of Endothelial Cell Adhesion by Hevin, an Acidic Protein Associated with High Endothelial Venules. *J. Biol. Chem.* 271(8):4511-7, 1996.

Glinka A., Wu W., Delius H., Monaghan A.P., Blumenstock C., Niehrs C.: Dickkopf-1 is a member of a new family of secreted proteins and functions in head induction. *Nature* 391(6665):357-62, 1998.

Goh Y., Urade Y., Fujimoto N., Hayaishi O.: Content and formation of prostaglandins and distribution of prostaglandin-related enzyme activities in the rat ocular system. *Biochim. Biophys. Acta.* 921(2):302-11, 1987.

Goldwich A., Baulmann D.C., Ohlmann A., Flügel-Koch C., Schöcklmann H., Tamm E.R.: Myocilin is expressed in the glomerulus of the kidney and induced in mesangioproliferative glomerulonephritis. *Kidney Int.* 67(1):140-51, 2005.

Goldwich A., Ethier C.R., Chan D.W., Tamm E.R.: Perfusion with the olfactomedin domain of myocilin does not affect outflow facility. *Invest. Ophthalmol. Vis. Sci.* 44(5):1953-61, 2003.

Goldwich A., Scholz M., Tamm E.R.: Myocilin promotes substrate adhesion, spreading and formation of focal contacts in podocytes and mesangial cells. *Histochem. Cell Biol.* 131:167–180, 2009.

Goliger J.A., Paul D.L.: Wounding alters epidermal connexin expression and gap junction-mediated intercellular communication. *Mol. Biol. Cell.* 6(11):1491-501, 1995.

Gordon M.O., Beiser J.A., Brandt J.D., Heuer D.K., Higginbotham E.J., Johnson C.A., Keltner J.L., Miller J.P., Parrish R.K. 2nd, Wilson M.R., Kass M.A.: The Ocular Hypertension Treatment Study: baseline factors that predict the onset of primary open-angle glaucoma. *Arch. Ophthalmol.* 120(6):714-20; discussion 829-30, 2002.

Gould D.B., Miceli-Libby L., Savinova O.V., Torrado M., Tomarev S.I., Smith R.S., John S.W.: Genetically increasing Myoc expression supports a necessary pathologic role of abnormal proteins in glaucoma. *Mol. Cell. Biol.* 24(20):9019-25, 2004.

Gould D.B., Reedy M., Wilson L.A., Smith R.S., Johnson R.L., John S.W.: Mutant myocilin nonsecretion in vivo is not sufficient to cause glaucoma. *Mol. Cell. Biol.* 26(22):8427-36, 2006.

Graham F.L., Smiley J., Russell W.C., Nairn R.: Characteristics of a human cell line transformed by DNA from human adenovirus type 5. *J. Gen. Virol.* 36 (1):59–74, 1977.

Greber B., Lehrach H., Adjaye J.: Fibroblast growth factor 2 modulates transforming growth factor beta signaling in mouse embryonic fibroblasts and human ESCs (hESCs) to support hESC self-renewal. *Stem Cells* 25(2):455-64, 2007.

Green KJ, Böhringer M, Gocken T, Jones JC.: Intermediate filament associated proteins. Adv. Protein Chem. 70:143-202, 2005.

Griffin C., Kleinjan D.A., Doe B., van Heyningen V.: New 3' elements control Pax6 expression in the developing pretectum, neural retina and olfactory region. *Mech. Dev.* 112(1-2):89-100, 2002.

Grose R., Harris B.S., Cooper L., Topilko P., Martin P.: Immediate early genes krox-24 and krox-20 are rapidly up-regulated after wounding in the embryonic and adult mouse. *Dev. Dyn.* 223(3):371-8, 2002.

Gruber H., Ingram J., Hanley E. Jr.: Cellular immunohistochemical localization of the matricellular protein myocilin in the intervertebral disc. *Biotechnic & Histochemistry* 81(4-6): 119-124, 2006.

Grønskov K., Ek J., Brondum-Nielsen K.: Oculocutaneous albinism. *Orphanet J. Rare Dis.* 2:43. Review, 2007.

Ha N.T., Nakayasu K., Murakami A., Ishidoh K., Kanai A.: Microarray analysis identified differentially expressed genes in keratocytes from keratoconus patients. *Curr. Eye Res.* 28(6):373-9, 2004.

Haddox J.L., Pfister R.R., Slaughter S.E.: An excess of topical calcium and magnesium reverses the therapeutic effect of citrate on the development of corneal ulcers after alkali injury. *Cornea* 15(2):191-5, 1996.

Hale F: Pigs born without eyeballs. *J. Hered.* 24:105-127, 1933.

Hart H., Samuelson D.A., Tajwar H., MacKay E.O., Lewis P.A., Kallberg M., Gelatt K.N.: Immunolocalization of myocilin protein in the anterior eye of normal and primary open-angle glaucomatous dogs. *Vet. Ophthalmol.* 1:28-37, 2007.

Hartzog G.A.: Transcription elongation by RNA polymerase II. *Curr. Opin. Genet. Dev.* 13(2):119-26. Review, 2003.

Hassell J.R., Cintron C., Kublin C., Newsome D.A.: Proteoglycan changes during restoration of transparency in corneal scars. *Arch. Biochem. Biophys.* 222:362–369, 1983.

Hassell J.R., Kane B.P., Etheredge L.T., Valkov N., Birk D.E.: Increased stromal extracellular matrix synthesis and assembly by insulin activated bovine keratocytes cultured under agarose. *Exp. Eye Res.* 87:604–611, 2008.

Hasty P., Rivera-Pérez J., Bradley A.: The length of homology required for gene targeting in embryonic stem cells. *Mol. Cell. Biol.* 11(11):5586-91, 1991.

Hayashi S., Okamoto N., Makita Y., Hata A., Imoto I., Inazawa J.: Heterozygous deletion at 14q22.1-q22.3 including the BMP4 gene in a patient with psychomotor retardation, congenital corneal opacity and feet polysyndactyly. *Am. J. Med. Genet. A.* 146A(22):2905-10, 2008.

He L., Hannon G.J.: MicroRNAs: small RNAs with a big role in gene regulation. *Nat. Rev. Genet.* 5(7):522-31. Review, 2004.

He Y., Leung K.W., Zhuo Y.H., Ge J.: Pro370Leu mutant myocilin impairs mitochondrial functions in human trabecular meshwork cells. *Mol. Vis.* 15:815-25, 2009.

Hogan Z.S., Brown K.L., Ishola A., Gatimu J., Flucker L., Huff J.W.: Effects of divalent cations on bovine corneal stromal swelling rates. *Curr. Eye Res.* 33(8):677-82, 2008.

Hong H.K., Lass J.H., Chakravarti A.: Pleiotropic skeletal and ocular phenotypes of the mouse mutation congenital hydrocephalus (*ch*/*Mfl*) arise from a winged helix/forkhead transcription factor gene. *Hum. Mol. Genet.* 8(4):625-37, 1999.

Honkanen R.A., Nishimura D.Y., Swiderski R.E., Bennett S.R., Hong S., Kwon Y.H., Stone E.M., Sheffield V.C., Alward W.L.: A family with Axenfeld-Rieger syndrome and Peters Anomaly caused by a point mutation (Phe112Ser) in the FOXC1 gene. *Am. J. Ophthalmol.* 135:368–375, 2003.

Horwitz J.: α-crystallin can function as a molecular chaperone. *Proc. Natl. Acad. Sci. U S A.* 89(21):10449-53, 1992.

Howe A.K.: Regulation of actin-based cell migration by cAMP/PKA. *Biochim. Biophys. Acta.* 1692(2-3):159-74. Review, 2004.

Huang A.J.W., Li D.Q., Shang T.Y., Dursun D.: ARVO Abstract 661, 2001.

Huang G.Y., Cooper E.S., Waldo K., Kirby M.L., Gilula N.B., Lo C.W.: Gap junction–mediated cell–cell communication modulates mouse neural crest migration. *J. Cell Biol.* 143(6):1725–1734, 1998.

Huh M.I., Kim Y.H., Park J.H., Bae S.W., Kim M.H., Chang Y., Kim S.J., Lee S.R., Lee Y.S., Jin E.J., Sonn J.K., Kang S.S., Jung J.C.: Distribution of TGF-beta isoforms and signaling intermediates in corneal fibrotic wound repair. *J. Cell. Biochem.* 108(2):476-88, 2009.

Huh M.I., Lee Y.M., Seo S.K., Kang B.S., Chang Y., Lee Y.S., Fini M.E., Kang S.S., Jung J.C.: Roles of MMP/TIMP in regulating matrix swelling and cell migration during chick corneal development. *J. Cell. Biochem.* 101(5):1222-37, 2007.

Hurst H.C.: *Leucine Zippers*: *Transcription Factors*, 3rd ed. 1–72, San Diego, CA: Academic Press, Inc., 1996.

Hynes R.O.: *Fibronectins*. New York: Springer-Verlag, 1990.

Ibanez-Tallon I., Pagenstecher A., Fliegauf M., Olbrich H., Kispert A., Ketelsen U.P., North A., Heintz N., Omran H.: Dysfunction of axonemal dynein heavy chain Mdnah5 inhibits ependymal flow and reveals a novel mechanism for hydrocephalus formation. *Hum. Mol. Genet.* 13:2133–2141, 2004.

Inada M., Wang Y., Byrne M.H., Rahman M.U., Miyaura C., López-Otín C., Krane S.M.: Critical roles for collagenase-3 (Mmp13) in development of growth plate cartilage and in endochondral ossification. *Proc. Natl. Acad. Sci. U S A.* 101(49):17192-7, 2004.

Insinna C., Besharse J.C.: Intraflagellar transport and the sensory outer segment of vertebrate photoreceptors. *Dev. Dyn.* 237(8):1982-92. Review, 2008.

Jacobson N., Andrews M., Shepard A.R., Nishimura D., Searby C., Fingert J.H., Hageman G., Mullins R., Davidson B.L., Kwon Y.H., Alward W.L., Stone E.M., Clark A.F., Sheffield VC.: Non-secretion of mutant proteins of the glaucoma gene myocilin in cultured trabecular meshwork cells and in aqueous humor. *Hum. Mol. Genet.* 10(2):117-25, 2001.

Jamora C., Fuchs E.: Intercellular adhesion, signalling and the cytoskeleton. *Nat. Cell Biol.* 4(4):E101-8. Review, 2002Jang S.K., Kräusslich H.G., Nicklin M.J., Duke G.M., Palmenberg A.C., Wimmer E.: A segment of the 5' nontranslated region of encephalomyocarditis virus RNA directs internal entry of ribosomes during *in vitro* translation. *J. Virol.* 62:2636–2643, 1988.

Jeffery W.R.: Chapter 8. Evolution and development in the cavefish Astyanax. *Curr. Top. Dev. Biol.* 86:191-221, 2009.

Jeffery W.R.: Regressive evolution in Astyanax cavefish. *Annu. Rev. Genet.* 43:25-47. Review, 2009.

Jester J.V.: Corneal crystallins and the development of cellular transparency. *Semin. Cell Dev. Biol.* 19(2):82–93. Review, 2008.

Jiang C.K., Tomić-Canić M., Lucas D.J., Simon M., Blumenberg M.: TGF beta promotes the basal phenotype of epidermal keratinocytes: transcriptional induction of K#5 and K#14 keratin genes. *Growth Factors* 12(2):87-97, 1995.

Jirsova K., Merjava S., Martincova R., Gwilliam R., Ebenezer N.D., Liskova P., Filipec M.: Immunohistochemical characterization of cytokeratins in the abnormal corneal endothelium of posterior polymorphous corneal dystrophy patients. *Exp. Eye Res.* 84(4):680-6, 2007.

Joe M.K., Sohn S., Choi Y.R., Park H., Kee C.: Identification of flotillin-1 as a protein interacting with myocilin: implications for the pathogenesis of primary open-angle glaucoma. *Biochem. Biophys. Res. Commun.* 336(4):1201-6, 2005.

Joe M.K., Sohn S., Hur W., Moon Y., Choi Y.R., Kee C.: Accumulation of mutant myocilins in ER leads to ER stress and potential cytotoxicity in human trabecular meshwork cells. *Biochem. Biophys. Res. Commun.* 312(3):592-600, 2003.

Johansson N., Ala-aho R., Uitto V., Grénman R., Fusenig N.E., López-Otín C., Kähäri V.M.: Expression of collagenase-3 (MMP-13) and collagenase-1 (MMP-1) by transformed keratinocytes is dependent on the activity of p38 mitogen-activated protein kinase. *J. Cell Sci.* 113(Pt 2):227-35, 2000.

Johnson D.H., Bradley J.M., Acott T.S.: The effect of dexamethasone on glycosaminoglycans of human trabecular meshwork in perfusion organ culture. *Invest. Ophthalmol. Vis. Sci.* 31(12):2568-71, 1990.

Johnson M., Erickson K.: Mechanisms and routes of aqueous humor drainage. *Principles and Practice of Ophthalmology.* Philadelphia: W. B. Saunders Co. 2577-2595, 2000.

Johnson M., Ethier C.R., Kamm R.D., Grant W.M., Epstein D.L., Gaasterland D.: The flow of aqueous humor through micro-porous filters. *Invest. Ophthalmol. Vis. Sci.* 27(1):92-7, 1986.

Jones G.E., Arumugham R.G., Tanzer M.L.: Fibronectin glycosylation modulates fibroblast adhesion and spreading. *J. Cell Biol.* 103(5):1663-70, 1986.

Jurynec M.J., Riley C.P., Gupta D.K., Nguyen T.D., McKeon R.J., Buck C.R.: TIGR is upregulated in the chronic glial scar in response to central nervous system injury and inhibits neurite outgrowth. *Mol. Cell. Neurosci.* 23(1):69-80, 2003.

Kaestner K.H., Knochel W., Martinez D.E.: *Genes. Dev.* 14:142-146, 2000.

Kalderon D., Roberts B.L., Richardson W.D., Smith A.E.: A short amino acid sequence able to specify nuclear location. *Cell* 39:499-509, 1984.

Kane B-P., Jester J.V., Huang J., Wahlert A., Hassell J.R.: IGF-II and collagen expression by keratocytes during postnatal development. *Exp. Eye Res.* 89(2):218-23, 2009.

Kao W.W.: Ocular surface tissue morphogenesis in normal and disease states revealed by genetically modified mice. *Cornea* 25(10 Suppl 1):S7-S19. Review, 2006.

Kapoor K.G., Katz S.E., Grzybowski D.M., Lubow M.: Cerebrospinal fluid outflow: an evolving perspective. *Brain Res. Bull.* 77(6):327-34, 2008.

Karali A., Russell P., Stefani F.H., Tamm E.R.: Localization of myocilin/trabecular meshwork--inducible glucocorticoid response protein in the human eye. *Invest. Ophthalmol. Vis. Sci.* 41(3):729-40, 2000.

Kaufmann B., Muller S., Hanisch F.G., Hartmann U., Paulsson M., Maurer P., Zaucke F.: Structural variability of BM-40/SPARC/osteonectin glycosylation: implications for collagen affinity. *Glycobiology* 14:609–619, 2004.

Kellerman L., Posner A.: The value of heredity in the detection and study of glaucoma. *Am. J. Ophthalmol.* 40(5 Part 1):681-5, 1955.

Kiefer M.C., Schmid C., Waldvogel M., Schläpfer I., Futo E., Masiarz F.R., Green K., Barr P.J., Zapf J.: Characterization of recombinant human insulin-like growth factor binding proteins 4, 5, and 6 produced in yeast. *J. Biol. Chem.* 267(18):12692-9, 1992.

Kim B.S., Savinova O.V., Reedy M.V., Martin J., Lun Y., Gan L., Smith R.S., Tomarev S.I., John S.W., Johnson R.L.: Targeted disruption of the myocilin Gene (Myoc) suggests that human glaucoma-causing mutations are gain of function. *Mol. Cell. Biol.* 21(22):7707-13, 2001.

Kim D.S., Park S.H., Park K.C.: Transforming growth factor-beta1 decreases melanin synthesis via delayed extracellular signal-regulated kinase activation. *Int. J. Biochem. Cell Biol.* 36(8):1482-91, 2004.

Kim H.S., Shang T., Chen Z., Pflugfelder S.C., Li D.Q. : TGF-beta1 stimulates production of gelatinase (MMP-9), collagenases (MMP-1, -13) and stromelysins (MMP-3, -10, -11) by human corneal epithelial cells. *Exp. Eye Res.* 79(2):263-74, 2004.

Kirstein L., Cvekl A., Chauhan B.K., Tamm E.R.: Regulation of human myocilin/TIGR gene transcription in trabecular meshwork cells and astrocytes: role of upstream stimulatory factor. *Genes Cells* 5(8):661-76, 2000.

Kleinjan D.A., Seawright A., Mella S., Carr C.B., Tyas D.A., Simpson T.I., Mason J.O., Price D.J., van Heyningen V.: Long-range downstream enhancers are essential for Pax6 expression. *Dev. Biol.* 299(2):563-81, 2006.

Klenow H. and Henningsen I.: Selective elimination of the exonuclease activity of the deoxyribonucleic acid polymerase from *Escherichia coli* B by limited proteolysis. *Proc. Natl. Acad. Sci. U S A* 65(1):168–175. 1970.

Knaupp C., Flügel-Koch C., Goldwich A., Ohlmann A., Tamm E.R.: The expression of myocilin during murine eye development. *Graefe´s Arch. Clin. Exp. Ophthalmol.* 242(4):339-45, 2004.

Knäuper V., Cowell S., Smith B., López-Otin C., O'Shea M., Morris H., Zardi L., Murphy G.: The role of the C-terminal domain of human collagenase-3 (MMP-13) in the activation of procollagenase-3, substrate specificity, and tissue inhibitor of metalloproteinase interaction. *J. Biol. Chem.* 272(12):7608-16, 1997.

Konz D.D., Flügel-Koch C., Ohlmann A., Tamm E.R.: Myocilin in the trabecular meshwork of eyes with primary open-angle glaucoma. *Graefes Arch. Clin. Exp. Ophthalmol.* 247(12):1643-9, 2009.

Koskinen P.J., Sistonen L., Bravo R., Alitalo K.: Immediate early gene responses of NIH 3T3 fibroblasts and NMuMG epithelial cells to TGF beta-1. *Growth Factors* 5(4):283-93, 1991.

Kozian D.H., Ziche M., Augustin H.G.: The activin-binding protein follistatin regulates autocrine endothelial cell activity and induces angiogenesis. *Lab. Invest.* 76(2):267-76, 1997.

Kozniewska E., Romaniuk K.: Vasopressin in vascular regulation and water homeostasis in the brain. *J. Physiol. Pharmacol.* 59(8):109-16. Review, 2008.

Krachmer J.H., Mannis M.J., Holland E.J.: *Cornea* Elsevier Mosby, New York, 2005.

Kubota R., Noda S., Wang Y., Minoshima S., Asakawa S., Kudoh J., Mashima Y., Oguchi Y., Shimizu N.: A novel myosin-like protein (myocilin) expressed in the connecting cilium of the photoreceptor: molecular cloning, tissue expression, and chromosomal mapping. *Genomics*. 41(3):360-9, 1997.

Kulkarni N.H., Karavanich C.A., Atchley W.R., Anholt R.R.: Characterization and differential expression of a human gene family of olfactomedin-related proteins. *Genet. Res.* 76(1):41-50, 2000.

Kumar N.M., Sigurdson S.L., Sheppard D., Lwebuga-Mukasa J.S.: Differential modulation of integrin receptors and extracellular matrix laminin by transforming growth factor-beta 1 in rat alveolar epithelial cells. *Exp. Cell Res.* 221(2):385-94, 1995.

Kumar S., Duester G.: Retinoic acid signaling in perioptic mesenchyme represses Wnt signaling via induction of Pitx2 and Dkk2. *Dev. Biol.* Feb 1, 2010 [Epub ahead of print].

Kupfer C., Kaiser-Kupfer M.I.: New hypothesis of developmental anomalies of the anterior chamber associated with glaucoma. *Trans. Ophthalmol. Soc. U. K.* 98:213–215, 1978.

Kupfer C., Kaiser-Kupfer M.I.: Observations on the development of the anterior chamber angle with reference to the pathogenesis of congenital glaucomas. *Am. J. Ophthalmol.* 88(3 Pt 1):424-6, 1979.

Kurpakus M.A., Maniaci M.T., Esco M.: Expression of keratins K12, K4 and K14 during development of ocular surface epithelium. *Curr. Eye Res.* 13(11):805-14, 1994.

Kurpios N.A., Ibañes M., Davis N.M., Lui W., Katz T., Martin J.F., Izpisúa Belmonte J.C., Tabin C.J.: The direction of gut looping is established by changes in the extracellular matrix and in cell:cell adhesion. *Proc. Natl. Acad. Sci. U S A* 105(25):8499-506, 2008.

Kvanta A., Sarman S., Fagerholm P., Seregard S., Steen B.: Expression of matrix metalloproteinase-2 (MMP-2) and vascular endothelial growth factor (VEGF) in inflammation-associated corneal neovascularization. *Exp. Eye Res.* 70:419–428, 2000.

Kwon H.S., Lee H.S., Ji Y., Rubin J.S., Tomarev S.I.: Myocilin is a modulator of Wnt signaling. *Mol. Cell. Biol.* 29(8):2139-54, 2009.

Lam D.S., Leung Y.F., Chua J.K., Baum L., Fan D.S., Choy K.W., Pang C.P.: Truncations in the TIGR gene in individuals with and without primary open-angle glaucoma. *Invest. Ophthalmol. Vis. Sci.* 41(6):1386-91, 2000.

Lammer, E.J. Armstrong D.L.: Malformations of hindbrain structures among humans exposed to isotretinoin (13-*cis*-retinoic acid) during early embryogenesis. In: *Retinoids in Normal Development and Teratogenesis*: 281-295. Oxford University Press, 1992.

Land M.F., Fernald R.D.: The evolution of eyes. *Annu. Rev. Neurosci.* 15:1–29, 1992.

Larson D.M., Wrobleski M.J., Sagar G.D., Westphale E.M., Beyer E.C.: Differential regulation of connexin43 and connexin37 in endothelial cells by cell density, growth, and TGF-beta1. *Am. J. Physiol.* 272(2 Pt 1):C405-15, 1997.

Latchman D.S.: Inhibitory transcription factors. *Int. J. Biochem. Cell Biol.* 28(9):965-74. Review, 1996.

Laux-Fenton W.T., Donaldson P.J., Kistler J., Green C.R.: Connexin expression patterns in the rat cornea: molecular evidence for communication compartments. *Cornea* 22(5):457-64, 2003.

Le Y., Gagneten S., Tombaccini D., Bethke B., Sauer B.: Nuclear targeting determinants of the phage P1 cre DNA recombinase. *Nucleic Acids Research* 27(24):4703-4709, 1999.

Lee J.E., Oum B.S., Choi H.Y., Lee S.U., Lee J.S.: Evaluation of differentially expressed genes identified in keratoconus. *Mol. Vis.* 15:2480-7, 2009.

Lelbach A., Muzes G., Feher J.: The insulin-like growth factor system: IGFs, IGF-binding proteins and IGFBP-proteases. *Acta Physiol. Hung.* 92:97–107, 2005.

Leske M.C.: Open-angle glaucoma - an epidemiologic overview. *Ophthalmic Epidemiol.* 14(4):166-72. Review, 2007.

Li D.Q., Shang T.Y., Kim H.S., Solomon A., Lokeshwar B.L., Pflugfelder S.C.: Regulated expression of collagenases MMP-1, -8, and -13 and stromelysins MMP-3, -10, and -11 by human corneal epithelial cells. *Invest. Ophthalmol. Vis. Sci.* 44(7):2928-36, 2003.

Li H.S., Yang J.M., Jacobson R.D., Pasko D., Sundin O.: Pax-6 is first expressed in a region of ectoderm anterior to the early neural plate: implications for stepwise determination of the lens. *Dev. Biol.* 162(1):181-94, 1994.

Li X., Manley J.L.: Inactivation of the SR protein splicing factor ASF/SF2 results in genomic instability. *Cell* 122(3):365-78, 2005.

Li Y., Aroca-Aguilar J.D., Ghosh S., Sánchez-Sánchez F., Escribano J., Coca-Prados M.: Interaction of myocilin with the C-terminal region of hevin. *Biochem. Biophys. Res. Commun.* 339(3):797-804, 2006.

Liberman A.C., Druker J., Perone M.J., Arzt E.: Glucocorticoids in the regulation of transcription factors that control cytokine synthesis. *Cytokine Growth Factor Rev.* 18(1-2):45-56, 2007.

Licatalosi D.D., Darnell R.B.: RNA processing and its regulation: global insights into biological networks. *Nat. Rev. Genet.* 11(1):75-87. Review, 2010.

Listerman I., Sapra A.K., Neugebauer K.M.: Cotranscriptional coupling of splicing factor recruitment and precursor messenger RNA splicing in mammalian cells. *Nat. Struct. Mol. Biol.* 13:815–822, 2006.

Liton P.B., Liu X., Stamer W.D., Challa P., Epstein D.L., Gonzalez P.: Specific targeting of gene expression to a subset of human trabecular meshwork cells using the chitinase 3-like 1 promoter. *Invest. Ophthalmol. Vis. Sci.* 46(1):183-90, 2005.

Liton P.B., Luna C., Challa P., Epstein D.L., Gonzalez P.: Genome-wide expression profile of human trabecular meshwork cultured cells, nonglaucomatous and primary open angle glaucoma tissue. *Mol. Vis.* 12:774-90, 2006.

Liu H., Mohamed O., Dufort D., Wallace V.A.: Characterization of Wnt signaling components and activation of the Wnt canonical pathway in the murine retina. *Dev. Dyn.* 227(3):323-34, 2003.

Liu Y., Vollrath D.: Reversal of mutant myocilin non-secretion and cell killing: implications for glaucoma. *Hum. Mol. Genet.* 13(11):1193-204, 2004.

Livak K.J., Schmittgen T.D.: Analysis of relative gene expression data using real-time quantitative PCR and the $2^{-\Delta\Delta C}$T method. *Methods* 25:402-408, 2001.

Lobe C.G., Koop K.E., Kreppner W., Lomeli H., Gertsenstein M., Nagy A.: Z/AP, a double reporter for cre-mediated recombination. *Dev. Biol.* 208(2):281-92, 1999.

Lottspeich F., Zorbas H.: *Bioanalytik* Kap. 23.4.3 Nichtradioaktive Systeme: S. 665-666. Spektrum Akademischer Verlag: Heidelberg, 1998.

Lu L., Reinach P.S., Kao W.W.: Corneal epithelial wound healing. *Exp. Biol. Med.* 226(7):653-64. Review, 2001.

Lütjen-Drecoll, E.: Conventional and uveoscleral routes. *Glaucoma in the 21st century*. Hartcourt Health Communications, Mosby International Ltd., London, UK. 95-102, 2000.

Lütjen-Drecoll E., Futa R., Rohen J.W.: Ultrahistochemical studies on tangential sections of the trabecular meshwork in normal and glaucomatous eyes. *Invest. Ophthalmol. Vis. Sci.* 21(4):563-73, 1981.

Lütjen-Drecoll E., May C.A., Polansky J.R., Johnson D.H., Bloemendal H., Nguyen T.D.: Localization of the stress proteins αB-crystallin and trabecular meshwork inducible glucocorticoid response protein in normal and glaucomatous trabecular meshwork. *Invest. Ophthalmol. Vis. Sci.* 39(3):517-25, 1998.

MacKay E.O., Kallberg M.E., Barrie K.P., Miller W., Sapienza J.S., Denis H., Ollivier F.J., Plummer C., Rinkoski T., Scotty N., Gelatt K.N.: Myocilin protein levels in the aqueous humor of the glaucomas in selected canine breeds. *Vet. Ophthalmol.* 11(4): 234–241, 2008.

Mackiewicz Z., Määttä M., Stenman M., Konttinen L., Tervo T., Konttinen Y.T. : Collagenolytic proteinases in keratoconus. *Cornea* 25(5):603-10, 2006.

Maclean K., Smith J., St Heaps L., Chia N., Williams R., Peters G.B., Onikul E., McCrossin T., Lehmann O.J., Adès L.C.: Axenfeld-Rieger malformation and distinctive facial features: Clues to a recognizable 6p25 microdeletion syndrome. *Am. J. Med. Genet.* 132(4):381-5. Review, 2005.

Makashova N.V., Kiseleva T.N., Ronzina I.A., Vasil'eva A.E.: Effect of vasoactive drugs on visual functions and ocular hemodynamics in patients with primary open-angle glaucoma. *Vestn. Oftalmol.* 124(5):55-9, 2008.

Mao B., Wu W., Davidson G., Marhold J., Li M., Mechler B.M., Delius H., Hoppe D., Stannek P., Walter C., Glinka A., Niehrs C.: Kremen proteins are Dickkopf receptors that regulate Wnt/beta-catenin signalling. *Nature* 417(6889):664-7, 2002.

Martin D.M., Skidmore J.M., Fox S.E., Gage P.J., Camper S.A.: Pitx2 distinguishes subtypes of terminally differentiated neurons in the developing mouse neuroepithelium. *Dev. Biol.* 252(1):84-99, 2002.

Mastrobattista J.M., Luntz M.: Ciliary body ablation: where are we and how did we get here? *Surv. Ophthalmol.* 41(3):193-213. Review, 1996.

Matt N., Dupé V., Garnier J.M., Dennefeld C., Chambon P., Mark M., Ghyselinck N.B.: Retinoic acid-dependent eye morphogenesis is orchestrated by neural crest cells. *Development* 132(21):4789-800, 2005.

Matthews, J.C., Hori K. and Cormier M.J.: Purification and properties of *Renilla* reniformisluciferase. *Biochemistry* 16:85-91, 1977.

Maurice D.M.: The location of the fluid pump in the cornea. *J. Physiol.* 221(1):43-54, 1972.

Maurice D.M.: The structure and transparency of the cornea. *J. Physiol.* 136(2):263-86 Review, 1957.

Mercer T.R., Dinger M.E., Mattick J.S.: Long non-coding RNAs: insights into functions. *Nat. Rev. Genet.* 10(3):155-9. Review, 2009.

Michelacci Y.M.: Collagens and proteoglycans of the corneal extracellular matrix. *Braz. J. Med. Biol. Res.* 36(8):1037-46, 2003.

Mita T., Yamashita H., Kaji Y., Obata H., Yamada H., Kato M., Hanyu A., Suzuki M., Tobari I.: Effects of transforming growth factor beta on corneal epithelial and stromal cell function in a rat wound healing model after excimer laser keratectomy. *Graefes Arch. Clin. Exp. Ophthalmol*. 236(11):834-4, 1998.

Mohan R.R., Kim W.J., Mohan R.R., Chen L., Wilson S.E.: Bone morphogenic proteins 2 and 4 and their receptors in the adult human cornea. *Invest. Ophthalmol. Vis. Sci.* 39(13):2626-36, 1998.

Molotkov A., Molotkova N., Duester G.: Retinoic acid guides eye morphogenetic movements via paracrine signaling but is unnecessary for retinal dorsoventral patterning. *Development* 133:1901–1910, 2006.

Monaghan A.P., Kioschis P., Wu W., Zuniga A., Bock D., Poustka A., Delius H., Niehrs C.: Dickkopf genes are co-ordinately expressed in mesodermal lineages. *Mech. Dev.* 87(1-2):45-56, 1999.

Moog U., Bleeker-Wagemakers E.M., Crobach P., Vles J.S., Schrander-Stumpel C.T.: Sibs with Axenfeld-Rieger anomaly, hydrocephalus, and leptomeningeal calcifications: a new autosomal recessive syndrome? *Am. J. Med. Genet.* 78(3):263-6, 1998.

Moore D., Harris A., Wudunn D., Kheradiya N., Siesky B.: Dysfunctional regulation of ocular blood flow: A risk factor for glaucoma? *Clin. Ophthalmol.* 2(4):849-61, 2008.

Moore M.J., Proudfoot N.J.: Pre-mRNA processing reaches back to transcription and ahead to translation. *Cell* 136(4):688-700, 2009.

Morise H., Shimomura O., Johnson F.H., Winant J.: Intermolecular energy transfer in the bioluminescent system of *Aequorea*. *Biochemistry* 13:2656–2662, 1974.

Mukhopadhyay M., Gorivodsky M., Shtrom S., Grinberg A., Niehrs C., Morasso M.I., Westphal H.: Dkk2 plays an essential role in the corneal fate of the ocular surface epithelium. *Development* 133(11):2149-54, 2006.

Musselmann K., Kane B.P., Alexandrou B., Hassell J.R.: IGF-II is present in bovine corneal stroma and activates keratocytes to proliferate in vitro. *Exp. Eye Res.* 86(3):506-11, 2008.

Müller L.J., Pels L., Vrensen G.F.: Ultrastructural organization of human corneal nerves. *Invest. Ophthalmol. Vis. Sci.* 37(4):476-88, 1996.

Nagy A., Gertsenstein M., Vintersten K. and Behringer R.: *Manipulating the Mouse Embryo: A Laboratory Manual, 3rd edn.* Ch. 3: Production of transgenic animals. Cold Spring Harbor Laboratory Press, 2002.

Nagy I., Trexler M., Patthy L.: Expression and characterization of the olfactomedin domain of human myocilin. *Biochem. Biophys. Res. Commun.* 302(3):554-61, 2003.

Nakamura T., Takio K., Eto Y., Shibai H., Titani K., Sugino H.: Activin-binding protein from rat ovary is follistatin. *Science* 247(4944):836-8, 1990.

Narita K., Kawate T., Kakinuma N., Takeda S.: Multiple primary cilia modulate the fluid transcytosis in choroid plexus epithelium. *Traffic* 11(2):287-301, 2010.

Nelson and Cox: *Lehninger Biochemie* 3. Auflage: Kapitel: 26.2: RNA-Processing; 28.3: Regulation der Genexpression bei Eukaryoten. Springer-Verlag Berlin, Heidelberg, 2001.

Nguyen T.D., Chen P., Huang W.D., Chen H., Johnson D., Polansky J.R.: Gene structure and properties of TIGR, an olfactomedin-related glycoprotein cloned from glucocorticoid-induced trabecular meshwork cells. *J. Biol. Chem.* 273(11):6341-50, 1998.

Niederreither K., Fraulob V., Garnier J.M., Chambon P., Dollé P.: Differential expression of retinoic acid-synthesizing (RALDH) enzymes during fetal development and organ differentiation in the mouse. *Mech. Dev.* 110(1-2):165-71, 2002.

Nilius B., Owsianik G., Voets T., Peters J.A.: Transient receptor potential cation channels in disease. *Physiol. Rev.* 87(1):165-217. Review, 2007.

Nobrega M.A., Ovcharenko I., Afzal V., Rubin E.M.: Scanning human gene deserts for long-range enhancers. *Science* 302(5644):413, 2003.

Novak A., Guo C., Yang W., Nagy A., Lobe C.G.: *Z*/EG, a double reporter mouse line that expresses enhanced green fluorescent protein upon Cre-mediated excision. *Genesis* 28(3-4):147-55, 2000.

Obazawa M, Mashima Y, Sanuki N, Noda S, Kudoh J, Shimizu N, Oguchi Y, Tanaka Y, Iwata T. Analysis of porcine optineurin and myocilin expression in trabecular meshwork cells and astrocytes from optic nerve head. *Invest. Ophthalmol. Vis. Sci.* 45(8):2652-9, 2004.

O'Brien E.T., Ren X., Wang Y.: Localization of myocilin to the golgi apparatus in Schlemm's canal cells. *Invest. Ophthalmol. Vis. Sci.* 41(12):3842-9, 2000.

Ogawa Y., Sun B.K., Lee J.T.: Intersection of the RNAi and X-inactivation pathways. *Science* 320(5881):1336–1341, 2008.

Ohlmann A., Goldwich A., Flügel-Koch C., Fuchs A.V., Schwager K., Tamm E.R.: Secreted glycoprotein myocilin is a component of the myelin sheath in peripheral nerves. *Glia* 43(2): 128-40, 2003.

Okamoto M., Bitman J., Cecil H.C., Connolly M.R., Miller R.W., Wrem T.R.: Replacement and absorption of cerebrospinal fluid in normal and vitamin A deficient calves. *J. Dairy Sci.* 45:882-885, 1962.

Ormestad M., Blixt A., Churchill A., Martinsson T., Enerback S., Carlsson P.: Foxe3 haploinsufficiency in mice: a model for Peters' anomaly. *Invest. Ophthalmol. Vis. Sci.* 43:1350–1357, 2002.

Ortego J., Escribano J., Coca-Prados M.: Cloning and characterization of subtracted cDNAs from a human ciliary body library encoding TIGR, a protein involved in juvenile open angle glaucoma with homology to myosin and olfactomedin. *FEBS Lett.* 413(2):349-53, 1997.

Pallari H.M., Eriksson J.E.: Intermediate filaments as signaling platforms. *Sci. STKE.* 366:pe53. Review, 2006.

Pandit S., Wang D., Fu X-D.: Functional Integration of Transcriptional and RNA Processing Machineries. *Curr. Opin. Cell Biol*. 20(3):260–265, 2008.

Pang I.H., Shade D.L., Clark A.F., Steely H.T., DeSantis L.: Preliminary characterization of a transformed cell strain derived from human trabecular meshwork.. *Curr. Eye Res.* 13(1):51-63, 1994.

Park B-C., Tibudan M., Samaraweera M., Shen X., Yue B.Y.: Interaction between two glaucoma genes, optineurin and myocilin. *Genes to Cells* 12:969–979, 2007.

Pearson B., Wolf P.L., Vazquez J.: A comparative study of a series of new indolyl compounds to localize ß-galactosidase in tissues. *Lab. Invest.* 12:1249-59, 1963.

Pelletier J., Sonenberg N.: Internal initiation of translation of eukaryotic mRNA directed by a sequence derived from poliovirus RNA. *Nature* 334:320–325, 1988.

Pendas A.M., Balbín M., Llano E., Jiménez M.G., López-Otín C.: Structural analysis and promoter characterisation of the human collagenase-3 gene (MMP-13). *Genomics* 40: 222–33, 1997.

Perris R., Perissinotto D.: Role of the extracellular matrix during neural crest cell migration. *Mech. Dev.* 95(1-2):3-21. Review, 2000.

Peters D.M., Herbert K., Biddick B., Peterson J.A.: Myocilin binding to Hep II domain of fibronectin inhibits cell spreading and incorporation of paxillin into focal adhesions. *Exp. Cell Res.* 303(2):218-28, 2005.

Pierrou S., Enerbäck S., Carlsson P.: Selection of high-affinity binding sites for sequence-specific, DNA binding proteins from random sequence oligonucleotides. *Anal. Biochem.* 229(1):99-105, 1995.

Pinkert C.A.: *Transgenic Animal Technology: A Laboratory Handbook*: Part 2, chapter 3: Factors affecting transgenic animal production. Elsevier Science (USA), 1994.

Pisano M.M., Mukhopadhyay P., Greene R.M.: Molecular fingerprinting of TGFbeta-treated embryonic maxillary mesenchymal cells. *Orthod. Craniofac. Res.* 6(4):194-209, 2003.

Plaza S., Dozier C., Langlois M.C., Saule S.: Identification and characterization of a neuroretina-specific enhancer element in the quail *Pax-6* (*Pax-QNR*) gene. *Mol. Cell. Biol.* 15(2):892–903, 1995.

Polansky J.R., Fauss D.J., Chen P., Chen H., Lütjen-Drecoll E., Johnson D., Kurtz R.M., Ma Z.D., Bloom E., Nguyen T.D.: Cellular pharmacology and molecular biology of the trabecular meshwork inducible glucocorticoid response gene product. *Ophthalmologica* 211(3):126-39, 1997.

Puri N., Gardner J.M., Brilliant M.H.: Aberrant pH of melanosomes in pink-eyed dilution (*p*) mutant melanocytes. *J. Invest. Dermatol.* 115(4):607-13, 2000.

Qazi Y., Wong G., Monson B., Stringham J., Ambati B.K.: Corneal transparency: Genesis, maintenance and dysfunction. *Brain Res. Bull*. 81(2-3):198-210. Review, 2010.

Ratkay-Traub I., Hopp B., Bor Z., Dux L., Becker D.L., Krenacs T.: Regeneration of rabbit cornea following excimer laser photorefractive keratectomy: a study on gap junctions, epithelial junctions and epidermal growth factor receptor expression in correlation with cell proliferation. *Exp. Eye Res.* 73:291–302, 2001.

Ray K., Mukhopadhyay A., Acharya M.: Recent advances in molecular genetics of glaucoma. *Mol. Cell. Biochem.* 253(1-2):223-31. Review, 2003.

Reneker L.W., Silversides D.W., Xu L., Overbeek P.A.: Formation of corneal endothelium is essential for anterior segment development - a transgenic mouse model of anterior segment dysgenesis. *Development* 127(3):533-42, 2000.

Resch Z.T., Fautsch M.P.: Glaucoma-associated myocilin: A better understanding but much more to learn. *Exp. Eye Res.* 88(4):704-12, 2009.

Rhee D.J., Fariss R.N., Brekken R., Sage E.H., Russell P.: The matricellular protein SPARC is expressed in human trabecular meshwork. *Exp. Eye Res.* 77:601–607, 2003.

Ricard C.S., Agapova O.A., Salvador-Silva M., Kaufman P.L., Hernandez M.R.: Expression of myocilin/TIGR in normal and glaucomatous primate optic nerves. *Exp. Eye Res.* 73(4):433-47, 2001.

Ricard C.S., Mukherjee A., Silver F-L., Wagenknecht P.L.: Canine myocilin is associated with lipid modified by palmitic acid. *Mol. Vis.* 12:1427-36, 2006.

Richard G**.**, Rouan F**.**, Willoughby C**.**E**.**, Brown N**.**, Chung P**.**, Ryynänen M**.**, Jabs E**.**W**.**, Bale S**.**J**.**, DiGiovanna J**.**J**.**, Uitto J**.**, Russell L.: Missense mutations in GJB2 encoding connexin-26 cause the ectodermal dysplasia keratitis-ichthyosis-deafness syndrome. *Am. J. Hum. Genet.* 70(5):1341-8, 2002.

Richard P., Manley J.L.: Transcription termination by nuclear RNA polymerases. *Genes Dev.* 23(11):1247-69, 2009.

Rinchik E.M., Bultman S.J., Horsthemke B., Lee S.T., Strunk K.M., Spritz R.A., Avidano K.M., Jong M.T., Nicholls R.D.: A gene for the mouse pink-eyed dilution locus and for human type II oculocutaneous albinism. *Nature* 361(6407):72-6, 1993.

Rinn J.L., Kertesz M., Wang J.K., Squazzo S.L., Xu X., Brugmann S.A., Goodnough L.H., Helms J.A., Farnham P.J., Segal E., Chang H.Y.: Functional demarcation of active and silent chromatin domains in human HOX loci by noncoding RNAs. *Cell* 129(7):1311-23, 2007.

Rohen, J.W., Lütjen E., Bárány E.: The relation between the ciliary muscle and the trabecular meshwork and its importance for the effect of miotics on aqueous outflow resistance. A study in two contrasting monkey species, Macacairus and Cercopithecus aethiops. *Albrecht Von Graefes Arch. Klin. Exp. Ophthalmol.* 172:23–47, 1967.

Rohen J.W., Lütjen-Drecoll E., Flügel C., Meyer M., Grierson I.: Ultrastructure of the trabecular meshwork in untreated cases of primary open-angle glaucoma (POAG). *Exp. Eye Res.* 56(6):683-92, 1993.

Rossant J., Zirngibl R., Cado D., Shago M., Giguère V.: Expression of a retinoic acid response element-hsplacZ transgene defines specific domains of transcriptional activity during mouse embryogenesis. *Genes Dev.* 5(8):1333-44, 1991.

Rozsa F.W., Reed D.M., Scott K.M., Pawar H., Moroi S.E., Kijek T.G., Krafchak C.M., Othman M.I., Vollrath D., Elner V.M., Richards J.E.: Gene expression profile of human trabecular meshwork cells in response to long-term dexamethasone exposure. *Mol. Vis.* 12:125-41, 2006.

Ruberte E., Friederich V., Chambon P., Morriss-Kay G.: Retinoic acid receptors and cellular retinoid binding proteins III. Their differential transcript distribution during mouse nervous system development. *Development* 118:267-282, 1993.

Russell P., Tamm E.R., Grehn F.J., Picht G., Johnson M.: The presence and properties of myocilin in the aqueous humor. *Invest. Ophthalmol. Vis. Sci.* 42(5):983-6, 2001.

Ryan D.G., Oliveira-Fernandes M., Lavker R.M.: MicroRNAs of the mammalian eye display distinct and overlapping tissue specificity. *Mol. Vis.* 12:1175-84, 2006.

Sachs A.: The role of poly(A) in the translation and stability of mRNA. *Curr. Opin. Cell Biol.* 2(6):1092-8. Review, 1990.

Saha M.S., Spann C.L., Grainger R.M.: Embryonic lens induction: More than meets the optic vesicle. *Cell Diff. Dev.* 28:153–172. Review, 1989.

Saika S.: TGFbeta pathobiology in the eye. *Lab. Invest.* 86(2):106-15. Review, 2006.

Saika S., Yamanaka O., Sumioka T., Miyamoto T., Miyazaki K., Okada Y., Kitano A., Shirai K., Tanaka S., Ikeda K.: Fibrotic disorders in the eye: targets of gene therapy. Prog. *Retin. Eye Res.* 27(2):177-96. Review, 2008.

Sakai R., Kinouchi T., Kawamoto S., Dana M.R., Hamamoto T., Tsuru T., Okubo K., Yamagami S.: Construction of human corneal endothelial cDNA library and identification of novel active genes. *Invest. Ophthalmol. Vis. Sci.* 43(6):1749-56, 2002.

Sánchez-Sánchez F., Martínez-Redondo F., Aroca-Aguilar J.D., Coca-Prados M., Escribano J.: Characterization of the intracellular proteolytic cleavage of myocilin and identification of calpain II as a myocilin-processing protease. *J. Biol. Chem.* 282(38):27810-24, 2007.

Sanford L.P., Ormsby I., Gittenberger-de Groot A.C., Sariola H., Friedman R., Boivin G.P., Cardell E.L., Doetschman T.: TGFbeta2 knockout mice have multiple developmental defects that are non-overlapping with other TGFbeta knockout phenotypes. *Development* 124(13):2659-70, 1997.

Sargent R.G., Wilson J.H.: Recombination and gene targeting in mammalian cells. *Curr. Res. Mol. Ther.* 1, 584–692, 1998.

Sauer B.: Inducible gene targeting in mice using the Cre/lox system. *Methods* 14(4):381-92. Review, 1998.

Saunders A., Core L.J., Lis J.T.: Breaking barriers to transcription elongation. *Nat. Rev. Mol. Cell Biol.* 7(8):557-67, 2006.

Schatt M.D., Rusconi S., Schaffner W.: A single DNA-binding transcription factor is sufficient for activation from a distant enhancer and/or from a promoter position. *EMBO J.* 9(2):481-7, 1990.

Schermer A., Galvin S., Sun T.T.: Differentiation-related expression of a major 64K corneal keratin in vivo and in culture suggests limbal location of corneal epithelial stem cells. *J. Cell Biol.* 103(1):49-62, 1986.

Semina E.V., Brownell I., Mintz-Hittner H.A., Murray J.C., Jamrich M.: Mutations in the human forkhead transcription factor FOXE3 associated with anterior segment ocular dysgenesis and cataracts. *Hum. Mol. Genet.* 10:231–236, 2001.

Semina E.V., Ferrell R.E., Mintz-Hittner H.A., Bitoun P., Alward W.L., Reiter R.S., Funkhauser C., Daack-Hirsch S., Murray J.C.: A novel homeobox gene PITX3 is mutated in families with autosomal-dominant cataracts and ASMD. *Nat. Genet.* 19:167–170, 1998.

Semina E.V., Murray J.C., Reiter R., Hrstka R.F., Graw J.: Deletion in the promoter region and altered expression of Pitx3 homeobox gene in aphakia mice. *Hum. Mol. Genet.* 9:1575–1585, 2000.

Serot J.M., Béné M.C., Faure G.C.: Choroid plexus, aging of the brain, and Alzheimer's disease. *Front. Biosci.* 8:515-21. Review, 2003.

Sheffield V.C., Stone E.M., Alward W.L., Drack A.V., Johnson A.T., Streb L.M., Nichols B.E.: Genetic linkage of familial open angle glaucoma to chromosome 1q21-q31. *Nat. Genet.* 4(1):47-50, 1993.

Shen X., Koga T., Park B.C., SundarRaj N., Yue B.Y.: Rho GTPase and cAMP/protein kinase A signaling mediates myocilin-induced alterations in cultured human trabecular meshwork cells. *J. Biol. Chem.* 283(1):603-12, 2008.

Shepard A.R., Jacobson N., Fingert J.H., Stone E.M., Sheffield V.C., Clark A.F.: Delayed secondary glucocorticoid responsiveness of MYOC in human trabecular meshwork cells *Invest. Ophthalmol. Vis. Sci.* 42(13):3173-81, 2001.

Shepard A.R., Jacobson N., Sui R., Steely H.T., Lotery A.J., Stone E.M., Clark A.F.: Characterization of rabbit myocilin: Implications for human myocilin glycosylation and signal peptide usage. *BMC Genetics* 2(4):5, 2003.

Shimizu S., Lichter P.R., Johnson A.T., Zhou Z., Higashi M., Gottfredsdottir M., Othman M., Moroi S.E., Rozsa F.W., Schertzer R.M., Clarke M.S., Schwartz A.L., Downs C.A., Vollrath D., Richards J.E.: Age-dependent prevalence of mutations at the GLC1A locus in primary open-angle glaucoma. *Am. J. Ophthalmol.* 130(2):165-77, 2000.

Shurman D.L., Glazewski L., Gumpert A., Zieske J.D., Richard G.: In vivo and in vitro expression of connexins in the human corneal epithelium. *Invest. Ophthalmol. Vis. Sci.* 46(6):1957-65, 2005.

Smith R.S., Zabaleta A., Kume T., Savinova O.V., Kidson S.H., Martin J.E., Nishimura D.Y., Alward W.L., Hogan B.L., John S.W.: Haploinsufficiency of the transcription factors FOXC1 and FOXC2 results in aberrant ocular development. *Hum. Mol. Genet.* 9:1021–1032, 2000.

Sohn S., Hur W., Joe M.K., Kim J.H., Lee Z.W., Ha K.S., Kee C.: Expression of wild-type and truncated myocilins in trabecular meshwork cells: their subcellular localizations and cytotoxicities. *Invest. Ophthalmol. Vis. Sci.* 43(12):3680-5, 2002.

Sonoda S., Uchino E., Sonoda K.H., Yotsumoto S., Uchio E., Isashiki Y., Sakamoto T.: Two patients with severe corneal disease in KID syndrome. *Am. J. Ophthalmol.* 137(1):181-3, 2004.

Southern E.M.: Detection of specific sequences among DNA fragments separated by gel electrophoresis. *J. Mol. Biol.* 98(3):503-17, 1975.

Staleva L., Manga P., Orlow S.J.: Pink-eyed dilution protein modulates arsenic sensitivity and intracellular glutathione metabolism. *Mol. Biol. Cell.* 13(12):4206–4220, 2002.

Stamer W.D., Perkumas K.M., Hoffman E.A., Roberts B.C., Epstein D.L., McKay B.S.: Coiled-coil targeting of myocilin to intracellular membranes. *Exp. Eye Res.* 83(6):1386-95, 2006.

St-Onge L., Sosa-Pineda B., Chowdhury K., Mansouri A., Gruss P.: Pax6 is required for differentiation of glucagon-producing alpha-cells in mouse pancreas. *Nature* 387(6631):406-9, 1997.

Stramer B.M., Zieske J.D., Jung J.C., Austin J.S., Fini M.E.: Molecular mechanisms controlling the fibrotic repair phenotype in cornea: Implications for surgical outcomes. *Invest. Ophthalmol Vis. Sci.* 44:4237–4246, 2003.

Stryer L.: *Biochemistry*, 4 th ed. Chapter 13: Signal transduction cascades. W.H. Freeman & Company, 1995.

Sucov H.M., Murakami K.K., Evans R.M.: Characterization of an autoregulated response element in the mouse retinoic acid receptor type beta gene. *Proc. Natl. Acad. Sci. U S A.* 87(14):5392-6, 1990.

Sun Y., Jan L.Y., Jan Y.N.: Transcriptional regulation of atonal during development of the Drosophila peripheral nervous system *Development* 125(18):3731-40, 1998.

Swiderski R.E., Ying L., Cassell M.D., Alward W.L., Stone E.M., Sheffield V.C.: Expression pattern and in situ localization of the mouse homologue of the human MYOC (GLC1A) gene in adult brain. *Brain Res. Mol. Brain Res.* 68(1-2):64-72, 1999.

Taguchi M., Kanno H., Kubota R., Miwa S., Shishiba Y., Ozawa Y.: Molecular cloning and expression profile of rat myocilin. *Mol. Genet. Metab.* 70(1):75-80, 2000.

Takahashi H., Noda S., Imamura Y., Nagasawa A., Kubota R., Mashima Y., Kudoh J., Oguchi Y., Shimizu N.: Mouse myocilin (Myoc) gene expression in ocular tissues. *Biochem. Biophys. Res. Commun.* 248(1):104-9, 1998.

Taketo M., Schroeder A.C., Mobraaten L.E., Gunning K.B., Hanten G., Fox R.R., Roderick T.H., Stewart C.L., Lilly F., Hansen C.T., Overbeek P.A.: FVB/N: an inbred mouse strain preferable for transgenic analyses. *Proc. Natl. Acad. Sci. U S A* 88(6):2065-9, 1991.

Tamm E.R.: Myocilin and glaucoma: facts and ideas. *Prog. Retin. Eye Res.* 21(4):395-428. Review, 2002.

Tamm E.R., Flügel C., Stefani F.H., Rohen J.W.: Contractile cells in the human scleral spur. *Exp. Eye Res.* 54:531–543, 1992.

Tamm E.R., Koch T.A., Mayer B., Stefani F.H., Lütjen-Drecoll E.: Innervation of myofibroblast-like scleral spur cells in human and monkey eyes. *Investig. Ophthalmol. Vis. Sci.* 36:1633–1644, 1995.

Tamm E.R., Russell P., Epstein D.L., Johnson D.H., Piatigorsky J.: Modulation of myocilin/TIGR expression in human trabecular meshwork. *Invest. Ophthalmol. Vis. Sci.* 40(11):2577-82, 1999.

Tamm E.R., Russell P., Piatigorsky J.: Development of characterization of a immortal and differentiated murine trabecular meshwork cell line. *Invest. Ophthalmol. Vis. Sci.* 40(7):1392-403, 1999.

Tanaka T., Urade Y., Kimura H., Eguchi N., Nishikawa A., Hayaishi O.: Lipocalin-type prostaglandin D synthase (beta-trace) is a newly recognized type of retinoid transporter. *J. Biol. Chem.* 272(25):15789-95, 1997.

Taniguchi F., Suzuki Y., Kurihara H., Kurihara Y., Kasai H., Shirato S., Araie M.: Molecular cloning of the bovine MYOC and induction of its expression in trabecular meshwork cells. *Invest. Ophthalmol. Vis. Sci.* 41(8):2070-5, 2000.

Tawara A., Okada Y., Kubota T., Suzuki Y., Taniguchi F., Shirato S., Nguyen T.D., Ohnishi Y.: Immunohistochemical localization of MYOC/TIGR protein in the trabecular tissue of normal and glaucomatous eyes. *Curr. Eye Res.* 21(6):934-43, 2000.

Tian B., Geiger B., Epstein D.L., Kaufman P.L.: Cytoskeletal involvement in the regulation of aqueous humor outflow. *Invest. Ophthalmol. Vis. Sci.* 41(3):619-23, 2000.

Tomarev S.I., Nakaya N.: Olfactomedin domain-containing proteins: possible mechanisms of action and functions in normal development and pathology. *Mol. Neurobiol.* 40(2):122-38, 2009.

Tomarev S.I., Tamm E.R., Chang B.: Characterization of the mouse Myoc/Tigr gene *Biochem. Biophys. Res. Commun.* 245(3):887-93, 1998.

Tomarev S.I., Wistow G., Raymond V., Dubois S., Malyukova I.: Gene expression profile of the human trabecular meshwork: NEIBank sequence tag analysis. *Invest. Ophthalmol. Vis. Sci.* 44(6):2588-96, 2003.

Topilko P., Schneider-Manoury S., Levi G., Baron-Van Evercooren A., Chennoufi A.B.Y., Seitanidou T., Babinet C., Charnay P.: Krox-20 controls myelination in the peripheral nervous system. *Nature* 371:796–799, 1994.

Torrado M., Trivedi R., Zinovieva R., Karavanova I., Tomarev S.I.: Optimedin: a novel olfactomedin-related protein that interacts with myocilin. *Hum. Mol. Genet.* 11(11):1291-301, 2002.

Tsai K.L., Huang C.Y., Chang C.H., Sun Y.J., Chuang W.J., Hsiao C.D.: Crystal structure of the human FOXK1a-DNA complex and its implications on the diverse binding specificity of winged helix/forkhead proteins. *J. Biol. Chem.* 281(25):17400-9, 2006.

Turner H.C., Budak M.T., Akinci M.A., Wolosin J.M.: Comparative analysis of human conjunctival and corneal epithelial gene expression with oligonucleotide microarrays. *Invest. Ophthalmol. Vis. Sci.* 48(5):2050-61, 2007.

Tymms M.J., Kola I.: *Gene knockout protocols* (Methods in Molecular Biology vol. 158): Chapter 3: Gene targeting in ES cells, Chapter 5: Gene targeting in a centralized facility. Human Press Inc, 2001.

Uchikawa M., Takemoto T., Kamachi Y., Kondoh H.: Efficient identification of regulatory sequences in the chicken genome by a powerful combination of embryo electroporation and genome comparison. *Mech. Dev.* 121:1145-1158, 2004.

Uchinami H., Seki E., Brenner D.A., D'Armiento J.: Loss of MMP 13 attenuates murine hepatic injury and fibrosis during cholestasis. *Hepatology* 44(2):420-9, 2006.

Ueda J., Wentz-Hunter K.K., Cheng E.L., Fukuchi T., Abe H., Yue B.Y.: Ultrastructural localization of myocilin in human trabecular meshwork cells and tissues. *J. Histochem. Cytochem.* 48:1321–1330, 2000.

Ueda J., Wentz-Hunter K..K., Yue B.Y.: Distribution of myocilin and extracellular matrix components in the juxtacanalicular tissue of human eyes. *Invest. Ophthalmol. Vis. Sci.* 43(4):1068-76, 2002.

Ueno N., Ling N., Ying S.Y., Esch F., Shimasaki S., Guillemin R.: Isolation and partial characterization of follistatin: a single-chain Mr 35,000 monomeric protein that inhibits the release of follicle-stimulating hormone. *Proc. Natl. Acad. Sci. U S A* 84(23):8282-6, 1987.

Urade Y., Hayaishi O.: Biochemical, structural, genetic, physiological, and pathophysiological features of lipocalin-type prostaglandin D synthase. *Biochim. Biophys. Acta* 1482(1-2):259-71. Review, 2000.

van der Kruijssen C.M., Feijen A., Huylebroeck D., van den Eijnden-van Raaij A.J.: Modulation of activin expression by type beta transforming growth factors. *Exp. Cell Res.* 207(2):407-12, 1993.

Vasiliou V., Gonzalez F.J.: Role of CYP1B1 in glaucoma. *Annu. Rev. Pharmacol. Toxicol.* 48:333-58. Review, 2008.

Vind I., Johansen J.S., Price P.A., Munkholm P.: Serum YKL-40, a potential new marker of disease activity in patients with inflammatory bowel disease. *Scand. J. Gastroenterol.* 38(6):599-605, 2003.

Virolle T., Monthouel M.N., Djabari Z., Ortonne J.P., Meneguzzi G., Aberdam D.: Three activator protein-1-binding sites bound by the Fra-2.JunD complex cooperate for the regulation of murine laminin alpha3A (lama3A) promoter activity by transforming growth factor-beta. *J. Biol. Chem.* 273(28):17318-25, 1998.

Visel A., Minovitsky S., Dubchak I., Pennacchio L.A.: VISTA Enhancer Browser-a database of tissue-specific human enhancers. *Nucleic Acids Res.* 35(Database issue):D88-92; 2007.

Vittal V., Rose A., Gregory K.E., Kelley M.J., Acott TS.: Changes in gene expression by trabecular meshwork cells in response to mechanical stretching. *Invest. Ophthalmol. Vis. Sci.* 46(8):2857-68, 2005.

Vitzthum F., Geiger G., Bisswanger H., Brunner H., Bernhagen J.: A quantitative fluorescence-based microplate assay for the determination of double-stranded DNA using SYBR Green I and a standard ultraviolet transilluminator gel imaging system. *Analytical Biochemistry* 276:59–64, 1999.

Wentz-Hunter K., Ueda J., Shimizu N., Yue B.Y.: Myocilin is associated with mitochondria in human trabecular meshwork cells. *J. Cell. Physiol.* 190(1):46-53, 2002.

Wentz–Hunter K., Ueda J., Yue B.Y.: Protein Interactions with Myocilin. *Invest. Ophthalmol. Vis. Sci.* 43:176-182, 2002.

Werner S., Munz B.: Suppression of keratin 15 expression by transforming growth factor beta in vitro and by cutaneous injury in vivo. *Exp. Cell Res.* 254(1):80-90, 2000.

Wiggs J.L., Vollrath D.: Molecular and clinical evaluation of a patient hemizygous for TIGR/MYOC. *Arch. Ophthalmol.* 119(11):1674-8, 2001.

Wilcock B.P., Brooks D.E., Latimer C.A.: Glaucoma in horses. *Vet. Pathol.* 28(1):74-8, 1991.

Wilson D., Sheng G., Lecuit T., Dostatni N., Desplan C.: Cooperative dimerization of paired class homeo domains on DNA. *Genes. Dev.* 7(11):2120-34, 1993.

Wilson S.E., He Y.G., Weng J., Li Q., McDowall A.W., Vital M., Chwang E.L.: Epithelial injury induces keratocyte apoptosis: Hypothesized role for the interleukin-1 system in the modulation of corneal tissue organization. *Exp. Eye Res.* 62:325–7, 1996.

Wirtz M.K., Samples J.R., Xu H., Severson T., Acott T.S.: Expression profile and genome location of cDNA clones from an infant human trabecular meshwork cell library. *Invest. Ophthalmol. Vis. Sci.* 43(12):3698-704, 2002.

Wolburg H., Paulus W.: Choroid plexus: biology and pathology. *Acta Neuropathol.* 119(1):75-88, 2010.

Wolf F.I., Cittadini A.: Magnesium in cell proliferation and differentiation. *Front. Biosci.* 4:D607-17. Review, 1999.

Wordinger R.J., Clark A.F.: Effects of glucocorticoids on the trabecular meshwork: towards a better understanding of glaucoma. *Prog. Retin. Eye Res.* 18(5):629-67. Review, 1999.

Xu Z.P., Saunders G.F.: PAX6 intronic sequence targets expression to the spinal cord. *Dev. Genet.* 23(4):259-63, 1998.

Yam G.H., Gaplovska-Kysela K., Zuber C., Roth J.: Sodium 4-phenylbutyrate acts as a chemical chaperone on misfolded myocilin to rescue cells from endoplasmic reticulum stress and apoptosis. *Invest. Ophthalmol. Vis. Sci.* 48:1683-1690, 2007.

Ye H.Q., Maeda M., Yu F.S., Azar D.T.: Differential expression of MT1-MMP (MMP-14) and collagenase III (MMP-13) genes in normal and wounded rat corneas. *Invest. Ophthalmol. Vis. Sci.* 41:2894–2899, 2000.

Yochum G.S., Cleland R., Goodman R.H.: A genome-wide screen for beta-catenin binding sites identifies a

downstream enhancer element that controls c-Myc gene expression. *Mol. Cell. Biol.* 28(24):7368-79, 2008.

Yokozeki M., Moriyama K., Shimokawa H., Kuroda T.: Transforming growth factor-beta 1 modulates myofibroblastic phenotype of rat palatal fibroblasts in vitro. *Exp. Cell Res.* 231(2):328-36, 1997.

Zernicka-Goetz M., Pines J., McLean Hunter S., Dixon J.P., Siemering K.R., Haseloff J., Evans M.J.: Following cell fate in the living mouse embryo. *Development* 124(6):1133-7, 1997.

Zhao Y., Sato Y., Isaji T., Fukuda T., Matsumoto A., Miyoshi E., Gu J., Taniguchi N.: Branched N-glycans regulate the biological functions of integrins and cadherins. *FEBS J.* 275(9):1939-48, 2008.

Zillig M., Wurm A., Grehn F.J., Russell P., Tamm E.R.: Overexpression and properties of wild-type and Tyr437His mutated myocilin in the eyes of transgenic mice. *Invest. Ophthalmol. Vis. Sci.* 46(1):223-34, 2005.

Zink D., Paro R.: Drosophila Polycomb-group regulated chromatin inhibits the accessibility of a trans-activator to its target DNA. *EMBO J.* 14(22):5660–5671, 1995.

9. Appendix

9.1. Recipes for buffers, solutions and media

10 X annealing buffer:

Ingredient:	Final concentration:
$MgCl_2$	10 mM
Tris-HCl, pH 8.0	200 mM

Fill up with nuclease-free H_20.

Denaturation solution:

Ingredient:	Final concentration:
NaOH	0.5 M
NaCl	1.5 M

Fill up with H_20 and autoclave.

50 X Denhardt´s solution:

Ingredient:	Final concentration:
BSA	10 mg/ml
Ficoll 400	10 mg/ml
PVP K-30	10 mg/ml

Fill up with H_20, filter sterilize and store proper aliquots at – 20 °C.

HEK-293-medium:

DMEM + GlutaMAX-™ -II + 4.5 g/l D-Glucose, - Pyruvate containing from Invitrogen. Addition of 10 % (final concentration) sterile FCS.

High-salt buffer (500 ml):

NaCl	29.22 g
Tris-base	1.21 g
0.5 M EDTA, pH 8.0	1 ml

Adjust pH to 7.4, fill up with H_20 to 500 ml and filter sterilize.

HTM-N-medium:

DMEM + GlutaMAX-™ -II + 4.5 g/l D-Glucose, - Pyruvate from Invitrogen.

Addition of 10 % (final concentration) sterile fetal calf serum (FCS) and 1 % (final concentration) sterile penicillin (10 000U/ml)/streptomycin (10 mg/ml)-mix.

Injection buffer (100 ml):

Tris-base	0.121 g
0.5 M EDTA, pH 8.0	40 µl

Adjust to pH 7.5, fill up with ultrapure H_20 to 100 ml and filter sterilize.

LacZ-fixation buffer (50 ml):

Ingredient:	**Stock solution:**	**ml/50 ml buffer:**
Glutaraldehyde	25 %	0.4 ml
EGTA, pH 7.3	0.25 M	1.0 ml
$MgCl_2$	1 M	0.1 ml

Fill up to 50 ml with 0.1 M $NaPO_4$ buffer.

LacZ-staining solution 50 ml):

Ingredient:	**Add:**	**Final concentration:**
X-gal (dissolved in DMF)	2 ml (25 mg/ml in DMSO)	1 mg/ml
Potassium ferrocyanide	106 mg	5 mM
Potassium ferricyanide	82 mg	5 mM

Fill up volume to 50 ml with *LacZ*-wash buffer.

LacZ-wash buffer (500 ml):

Ingredient:	Stock solution:	ml/500 ml buffer:
$MgCl_2$	1 M	1 ml
Sodium deoxycholate	1 %	5 ml
Nonidet-P40	2 %	5 ml

Fill up volume with 0.1 M $NaPO_4$ buffer.

LB (lysogeny broth)-medium and agar plates (1 l):

NaCl	10 g
Bacto tryptone	10 g
Bacto yeast extract	5 g

Adjust to pH 7.0, fill up with H_20 to 1 l, autoclave and store at + 4 °C. For agar plates, let LB-medium cool down to ~ 55 °C after autoclaving and add antibiotic for selection. In case of blue/white screening add also X-gal (5-bromo-4-chloro-3-indolyl-beta-D-galactopyranoside) and IPTG (isopropyl-ß-D-thiogalactopyranoside). Pour plates and store at + 4 °C.

Additives to LB-medium and LB-agar plates:

Antibiotic:	Stock solution:	ml/1 l LB-medium:
Ampicillin	100 µg/ml	1 ml
Kanamycin	50 µg/ml	1 ml

Additives for blue/white screening:

Additive:	Stock solution:	ml/1 l LB-medium:
IPTG	23.83 mg/ml	1 ml
X-gal	20 mg/ml in dimethylformamide	1 ml

Low-salt buffer (500 ml):

NaCl	5.84 g
Tris-base	1.21 g
0.5 M EDTA, pH 8.0	1 ml

Adjust pH to 7.4, fill up with H_20 to 500 ml and filter sterilize.

0.1 M $NaPO_4$ buffer (500 ml):

1 M NaH_2PO_4	11.5 ml
1 M Na_2HPO_4	38.5 ml
H_20	450 ml

Adjust to pH 7.3.

Neutralization solution:

Ingredient:	**Final concentration:**
Tris-HCl	0.5 M
NaCl	1.5 M

Fill up with H_20, adjust to pH 7.4 and autoclave.

(Pre-)hybridization solution (~ 20 ml):

Formamide	10 ml
20 X SSC	5 ml
50 X Denhadt´s solution	2 ml
15 % SDS	2 ml
Sheared salmon sperm (10 mg/ml)	200 µl

Use this total of 19.2 ml for pre-hybridization. Just before hybridization, add 2 ml of 50 % dextransulphate (dissolved in H_20), as well as the radioactively labelled probe to the pre-hybridization solution (end volume 21.25 ml).

Proteinase K lysis buffer:

Ingredient:	Final concentration:
KCl	50 mM
Tris-HCl, pH 8.3	10 mM
$MgCl_2$	2 mM
Gelatine	0.1 mg/ml
Nonidet P-40	0.45 %
Tween-20	0.45 %

Store at – 20 °C. Tie up just before use and add 50 µl/ml of Proteinase K (stock concentration 10 mg/ml).

20 X SSC (saline-sodium citrate) (1 l):

NaCl	175.3 g
Sodium citrate	88.2 g

Adjust to pH 7.0, fill up with H_20 to 1 l and autoclave.

50 X TAE (Tris-acetate-EDTA (1 l):

Tris base	242 g
Acetic acid	57.1 ml
0.5 M EDTA, pH 8.0	100 ml

Fill up with H_20 to 1 l and filter sterilize.

10 X TBE (Tris-borate-EDTA (1 l):

Tris base	108 g
Boric acid	55 g
0.5 M EDTA pH 8.0	40 ml

Fill up to 1 l with H_20, autoclave.

9.2. Oligonucleotides

Tables 9.1A – D summarize primers used in the creation of a *myoc* knock-in mouse line (Materials and methods 3.1.3 and Results 4.4.1).

Primer:	**Sequence (5´→ 3´):**
Cre fw 1	GCTGGTTCCCACACTTCTC
Cre fw 2	GGAGACAATGGTTGTCAACAGAG
Cre fw 3	GGCGCTCTTGAAGAAGTCGTG
Cre rev. 1	AATGGCCATGGGACGTCGACCTG
Cre rev. 2	CTGCCACGACCAAGTGACAG
Cre rev. 3	AGTGAAACAGGGGCAATGGTG
Cre rev. 4	GCCTCGGTGCACATGCTTTAC

Table 9.1A: Primers and their 5´ → 3´ sequences used for sequential sequencing of NLS-Cre-IRES-eGFP.

*Not*I- 5´-flank fw	GCGGCCGCAGCTTGGGAATCAGGTTTTCC
*Xho*I- 5´-flank rev.	CTCGAGCTTGGGACCACAGCTGCAG
5´-flank fw 1	CAGGAACCAGGAAGAGAGCAG
5´-flank fw 2	CCTGCAGAAGCCAAGTAGTCC
5´-flank fw 3	GACTTGCCAGGCAAGAGTGG
5´-flank fw 4	CAGGTGAACGCAGATGCACAC
5´-flank fw 5	GTACTTGGTTCTCCTGCTTGG
5´-flank rev. 1	CGTCCTGTAGCAGAGACGAAG

Table 9.1B: Primers and their 5´ → 3´ sequences used for amplification of, and sequencing through, the 5´-homologous flank. The restriction enzyme recognition sites for cloning are underlined. Primers used for the amplification of template for radioactive 5´-probe used in Southern blot are listed.

*Nhe*I- 3´-flank fw	GCTAGCAGCATCCAGCATGCAGACC
*Sal*I- 3´-flank rev.	GTCGACGGACCAGCAATCTCTCTGG
5´-probe fw	GAGTCTCTGTGTCCAGAAATCC
5´-probe rev.	CAGCCAAGTCAGAGAAACTACC
3´-probe fw	GTCAGCAGTATTCTGAGGGTC
3´-probe rev.	TGGTCTCTTGCCTTCTTGCTC

Table 9.1C: Primers and their 5´ → 3´ sequences used for amplification of, and sequencing through, the 3´-homologous flank. The restriction enzyme recognition sites for cloning are underlined. Primers used for the amplification of template for radioactive 3´-probe used in Southern blot are listed.

5´-flank-NLS-Cre fw	CTCTTGCTGGCAGTGTGAGTG
3´-flank-Neo rev.	TCCAGATCCCTGGTTTGGGTC
Cre rev. 5	CCTGTTTTGCACGTTCACCG

Table 9.1D: Primers and their 5´ → 3´ sequences used to check the integrity of the *myoc* knock-in construct. Cre rev. 5 was, together with 5´-probe fw. (Table 9.1C), used to check that no deletion of the 5´-flank had occured during homologous recombination.

Tables 9.2A and B summarize primers that are used in the creation of a ß-galactosidase overexpression mouse (Materials and methods 3.1.2.1 and Results 4.2.2), as well as in screening of founder animals (Materials and methods 3.3.3 and Results 4.2.5).

*Pst*I- RAREß fw	CTGCAGGGTACGGGAGGTACTTGG
*Nco*I- p313+67 rev.	CCATGGTGCAGAGGCTTGGTGAGG
LacZ rev. 3	CACCAACGTAACCTATCCCATT

Table 9.2A: Primers and their 5´ → 3´sequences used for amplification of RAREß/PITX3/FOX-p313+67 from the Firefly Luciferase-reporter construct, as well as for proving for correct annealing of long 3 X NLS oligos. Restriction enzyme recognition sites for cloning are underlined.

LacZ fw	ATTATTTGCCCGATGTACGC
LacZ rev.	ACATCCAGAGGCACTTCACC
NLS fw	GATCCAAAAAAGAAGAGAAAGG
LacZ rev. 2	CTGCGCAACTGTTGGGAAG

Table 9.2B: Primers and their 5´ → 3´ sequences used for screening of ß-galactosidase overexpression founder animals, as well as for routine genotyping of TG animals.

*Nhe*I-H1 fw	GCTAGCGTGCCGTGCTTACATAGTGG
*Xho*I-H1 rev.	CTCGAGTGCTTCAGCCTAGGCAACAG
*Nhe*I-H2 fw	GCTAGCTCCTTGAATGCACCAGGCAC
*Xho*I-H2 rev.	CTCGAGTTACAGGGCCCATGCAAGTC
*Nhe*I-H3 fw	GCTAGCGTTACATGGTTACCACAAGCC
*Xho*I-H3 rev.	CTCGAGCTGCAATCACATCTCCCAACC
*Nhe*I-H4 fw	GCTAGCCAGCATACATGGGAGGGTG
*Xho*I-H4 rev.	CTCGAGGTACTGTGCTGGGTGCTTG
*Nhe*I-H5-6 fw	GCTAGCACTATCTGACACAGTACAGCC
*Xho*I-H5-6 rev.	CTCGAGTTCTTCTAGGTCATGTCAGCC
*Nhe*I-H7 fw	GCTAGCCATGTGTGTATGTGGGTGTGG
*Xho*I-H7 rev.	CTCGAGGCTCATTAGGTCCCTTTCCAG
*Nhe*I-H8 fw	GCTAGCAATGCCAGGAGAGCAAATAATG
*Xho*I-H8 rev.	CTCGAGTAACATGACCTTCCTGAACTTG
*Nhe*I-H9 fw	GCTAGCCTGGACCAGAACTATAACCAC
*Xho*I-H9 rev.	CTCGAGGAGGGATTTCATGACTGGAAC
*Nhe*I-H10 fw	GCTAGCCAACAGCCATGGTGAGAGG
*Xho*I-H10 rev.	CTCGAGACCACAGGCTTCTTGCCTG

Table 9.3: Primers and their 5′ → 3′ sequences used for amplification of conserved *MYOC* regions. Restriction enzyme recognition sites for cloning are underlined.

9.3. DNA standards

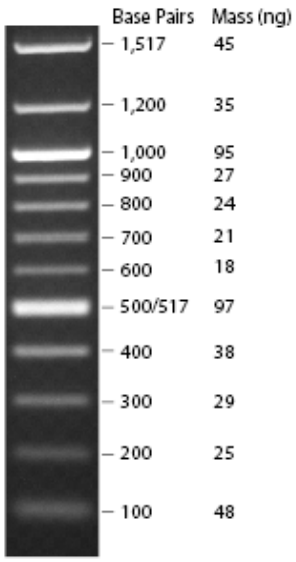

Fig. 9.1: 100 bp DNA ladder. 0.5 µg of 100 bp DNA ladder run on a 1.3 % agarose gel and visualized by EtBr staining (source: New England Biolabs).

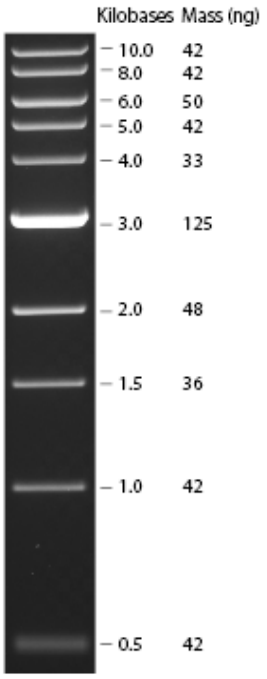

Fig. 9.2: 1 kb DNA ladder. 0.5 µg of 1 kb DNA ladder run on a 0.8 % agarose gel and visualized by EtBr (source: New England Biolabs).

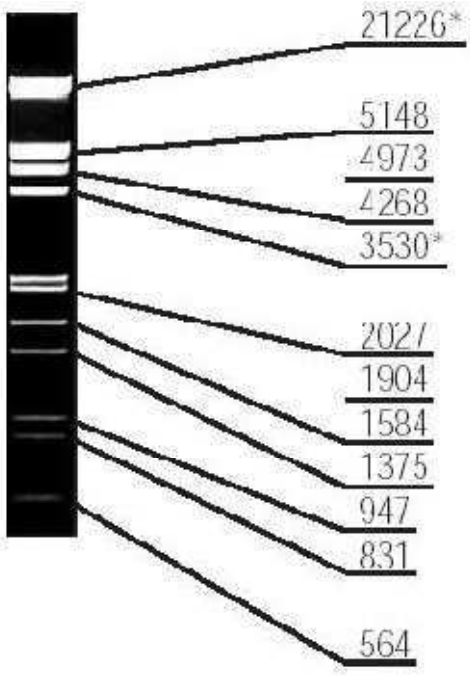

Fig. 9.3: 1 µg of λ DNA marker, EcoRI/HindIII digest run on a 1 % agarose gel (source: New England Biolabs).

9.4. Laboratory supplies

9.4.1. Bacteria, reagents and kits used for molecular biology

In all reactions nuclease-free H_20 of HPLC grade was used (ROTH). All used chemical substances were of p.A. quality or designated as "extra pure" and purchased from Merck or Roth. Buffers and enzymes for restriction digestion were purchased from New England Biolabs or Fermentas.

Supply:	**Source:**
Ampicillin	ROTH
Antibody H130 anti-myocilin	Santa Cruz Biotechnology
BSA	ROTH
Competent one shot® TOP10 *E. coli* cells	Invitrogen
100 mM d(A/C/G/T/)P	Qiagen
[α-^{32}P]dCTP	HARTMANN ANALYTIC GmbH
DMSO	ROTH
EndoFree Plasmid Maxi Kit	Qiagen
Fluorescein	Qiagen
Gel Loading Dye, blue (6 X)	New England Biolabs
GoTaq® Green Master Mix	Promega
IPTG	ROTH
iScript™ cDNA Synthesis Kit	Bio-Rad Laboratories
Kanamycin	ROTH
25 mM $MgCl_2$	Qiagen
Mini Quick Spin™ Column	Roche
NucleoSpin® Extract II	Macherey-Nagel
NucleoSpin® Plasmid	Macherey-Nagel
10 X PCR Buffer	Qiagen
PCR Cloning kit	Qiagen
Proteinase K	Fermentas
PureYield™ Plasmid Midiprep System	Promega
QIAfilter Plasmid Maxi Kit	Qiagen
Random Primers DNA Labeling System	Invitrogen
Secondary antibody Alexa Fluor® 488	Invitrogen
SYBR-Green I	Qiagen
Taq DNA Polymerase	Qiagen
TRIzol® Reagent	Invitrogen

9.4.2. Kits and reagents used for cell culture techniques

Supply:	Source:
CASY®ton	Roche Innovatis AG
Dexamethasone	Sigma
Dual-Luciferase® Reporter Assay System	Promega
FCS	Invitrogen
Lipofectamine™ 2000	Invitrogen
1 X PBS	Invitrogen
Penicillin/Streptomycin-mix	Invitrogen
Plus™ Reagent	Invitrogen
Trypsin	Invitrogen

9.4.3. Reagents and media used for histological techniques

Supply:	Source:
DePeX mounting medium	SERVA Electrophoresis GmbH
Diethyl ether	ROTH
EGTA	ROTH
Glutaraldehyde 25%	SERVA Electrophoresis GmbH
Nonidet™ P-40	Sigma
Potassium ferricyanide	Merck
Potassium ferrocyanide	Merck
Sodium deoxycholate	Roth
Tissue-Tek®	Sakura Finetek Europe B.V.
VECTASHIELD® Mounting Medium with DAPI	Vector Laboratories
X-gal	ROTH

9.4.4. Labware

Supply:	Source:
BAS-MS 2025 imaging plate	FUJIFILM Germany
Cell culture plate, 24-well	Sarstedt
Chamber slide (1.8 cm^2)	Nunc

Coverslips, 24 x 60 mm	VWR
Dialysis tubular membrane and clips	ROTH
EasYFlask™ Nunclon™ Δ (75 cm^2)	Nunc
Elutip-d® Purification Minicolumn	Schleicher & Schuell
Eppendorf tube (1.7 ml/2.0 ml)	ROTH
Falcon tube (15 ml/50 ml)	Sarstedt
(Filter) pipette tips	Sarstedt
Hybridization bottle and caps with seals	Biometra
iCycler iQ™ PCR Real-Time PCR Plate, 96 well	BioRad
Injection canulae	HEILAND
Luminometer vials (5 ml)	Sarstedt
Microseal® "B" Adhesive Seal	BioRad
Nylon membrane, positively charged	Roche
Parafilm® M Barrier Film	Pechiney Plastic Packaging, Inc.
Phase Lock Gel™ (light) tube (2.0 ml)	Eppendorf
Single-use syringe (1/2/5/10/50 ml)	HEILAND
Sterile plastic pipette (1/2/5/10/25/50 ml)	Sarstedt
Sterilization filter, 0.22 µm	ROTH
SuperFrost Ultra Plus® microscope slide	MENZEL-GLÄSER
UV-Cuvette	PLASTIBRAND®
Whatman®-Blotting paper	NeoLab
X-ray cassette	Rego X-ray GmbH

9.4.5. Laboratory equipment

Equipment:	**Source:**
Agarose gel electrophoresis system	PEQLAB Biotechnologie GMBH
Analytical balance	Kern & Sohn GmbH
AutoLumat LB 953	Berthold Technologies
Axio Imager Z1 microscope	Zeiss
Axioskop 40 microscope	Zeiss
Axiovert 40 CFL microscope	Zeiss
CASY® Cell Counter	Roche Innovatis AG
Centrifuge Biofuge 13	Heraeus
Centrifuge (models: 5415D, 5415R, 5804R and 5810R)	Eppendorf
Centro XS^3 LB 960 microplate luminometer	Berthold Technologies
Crosslinker CL-1	Herolab GmbH
Eraser	Raytest GmbH
HB-1000 hybridization oven	UVP Laboratory Products
HERAcell 150 incubator	Heraeus

HERAsafe® safety cabinet	Heraeus
Hybridization oven for isotopes	Bachofer
IDA Gel Documentation System	Raytest GmbH
IKAMAG® heating magnetic stirrer	IKA®Werke GmbH
Innova® 4200 Incubator Shaker	New Brunswick Scientific
inoLab®-pH Meter	WTW GmbH
iQ™5 Multicolor Real-time PCR Detection System + iCycler	BioRad
Julabo SW water-bath	Julabo Labortechnik GmbH
LB 124 contamination monitor	Berthold Technologies
Mastercycler Gradient	Eppendorf
Mastercycler Personal	Eppendorf
Memmert water-bath	Memmert GmbH
Mettler AE163 analytical balance	Mettler-Toledo
Microcome HM 500OM cryostat	Microm International
Microtome Supercut 2050	Reichert-Jung
OV3 hybridization oven	Biometra
Phosphoimager Fujifilm FLA-5000	FUJIFILM Germany
PIPETMAN® Concept electronic pipettes	Gilson International
Promax 1020 platform shaker	Heidolph Instruments GmbH
Research pipettes	Eppendorf
Spectrophotometer	Eppendorf
Sprout™ minicentrifuge	Biozym Scientific GmbH
Stemi 2000 CS + KL 1500 LCD stereomicroscope	Zeiss
Systec V-75 autoclave	Systec GmbH
Thermoblock	Bioblock Scientific
Thermomixer	Eppendorf
Vortex-Genie 2	Scientific Industries, Inc.

9.5. Software

Software:	**Provider/Source:**
Adobe® Photoshop®	Adobe
Aida Image Analyzer V.3.28	Fuji
BLAST	Source: http://blast.ncbi.nlm.nih.gov/Blast.cgi
CorelDRAW®	Corel Corporation
Corel PHOTO-PAINT®	Corel Corporation
iQ™5 Optical System Software Version 2.0	Bio-Rad
Microsoft® Excel	Microsoft

Microsoft® PowerPoint	Microsoft
Microsoft® Word	Microsoft
MicroWin 2000	Berthold Technologies
Primo Pro 3.4: PCR Primer Design	Chang Bioscience
Universal ProbeLibrary System	Roche
Vector NTI®	Invitrogen
VISTA Browser	Source: http://pipeline.lbl.gov/cgi-bin/gateway2

10. Acknowledgements

I would like to thank Prof. Dr. med. Ernst Tamm for giving me the opportunity to focus on anterior eye pathology by such a spectrum of various attempts and methodologies. I would like to thank the post-docs Dr. Markus Kröber, Dr. Andreas Ohlmann and Dr. Barbara Braunger for advice and help in questions during my investigation concerning myocilin and POAG, as well as Dr. Rudolf Fuchshofer for excellent expertise during my research concerning corneal wound healing. I would like to thank the technical assistance personnel Elke Stauber and Margit Schimmel for help and assistance in our histology lab, Katharina Fizia for assistance in the animal facility, as well as Angelika Pach and Tina Steil for help and assistance in our molecular biology lab. I would like to thank Prof. Weber for the use of their sequencing facility, Prof. Witzgall for the use of their isotope lab and Dr. Dr. Todorov for the use of their microplate luminometer, as well as for expertise concerning reporter gene expression studies. I would like to thank Antje Zenker for graphical help, Dr. Markus Kröber for the CSF-Western blots and artificial enhancer element constructs, and Dr. Maximilian Lenhardt for the microarray data. Finally, I want to thank the whole VKL-people for a friendly atmosphere during my 4.5 years of Ph. D. studies and my dear family for support and flexibility in the practical everyday life that made it possible for me to full concentrate on my research.